Serviceability and Ultimate Performance of Steel and Chopped Glass Fibre Reinforced Concrete Flexural Members: Experimental and Analytical Study

by

Helmi Ali Saleh Al-Guhi

A thesis submitted in partial fulfillment of the requirements for the degree of

Doctor of Philosophy

in

STRUCTURAL ENGINEERING

Department of Civil and Environmental Engineering

University of Alberta

ABSTRACT

Fibre reinforcement in concrete mitigates cracking, significantly enhancing peak, post-cracking, and toughness responses. The versatile applications of Fibre-reinforced Concrete (FRC) encompass parking lots, taxiways, runways, ground slabs, tunnels, barriers, railway tracks, site access road bridges, and culverts, showcasing its adaptability across diverse infrastructure projects, from transportation networks to structural foundations. A profound understanding of FRC's compressive and flexural behaviour holds paramount importance in designing structural elements such as beams, slabs, columns, piers, and compressive struts of beams. Commonly, Steel fibres (SFs) and glass fibres (GF) are often added to concrete to enhance toughness, durability, and post-cracking response, affecting the flexural and cracking behaviour of Fiber Reinforced Concrete (FRC). Understanding this is important because fibres increase moment resistance and stiffness.

The investigation initiates with the optimization of mixture designs for FRC, examining the impact of fibre type (SF, GF, and/or a combination to evaluate the benefits of non-corrosive and deformable GF with higher stiffness SF), aspect ratios (55 for SF and 67 for GF), lengths (50 mm for SF and 36 mm for GF) and dosage (0.5, 1.0, and 1.5% by volume fraction). The findings reveal substantial reductions in slump with increased fibre content, offering nuanced insights crucial for concrete mixture designers and structural engineers. Moving to the compressive behaviour of FRC, the study examines the effects of incorporating SF and/or GF on critical parameters such as compressive strength, modulus of elasticity, Poisson’s ratio, and toughness index. A simplified model is proposed to understand how adding fibres changes the stress-strain relationship in concrete.

Subsequently, the research delves into the flexural and cracking behaviour of FRC prisms, employing a combination of experimental and analytical methods. The outcomes introduce

proposed design-oriented expressions for equivalent stress block parameters, refining our understanding of FRC's structural response. Addressing a notable gap in the literature, the thesis employs Finite Element Analysis (FEA) to model large-scale Steel Reinforced (SR)-FRC and Glass Fibre-Reinforced Polymer (GFRP)-FRC beams. This analysis extends beyond conventional load-displacement considerations to encompass parameters like crack width and reinforcement strain. The findings show the viability of FEA predictions for both steel and GFRP reinforced concrete beams response, indicating a potentially cost-effective alternative to extensive experimental programs.

The recent update in one-way shear provisions for steel-reinforced concrete by the American Concrete Institute prompts consideration for similar provisions in Fibre-Reinforced Polymer (FRP) Reinforced Concrete (FRP-RC). The lower shear strength of FRP-RC, particularly GFRP, is attributed to its considerably lower modulus of elasticity compared to steel. This research evaluates existing design provisions for one-way shear in FRP-reinforced concrete, offering recommendations based on an analysis of 147 tests documented in the literature. The CSA S806-12 standard is considered the most consistent at predicting shear strength.

Lastly, this study used the numerical database from FEA to develop service and ultimate design equations for FRC with SR and GFRP bars. The flexural and shear strength models demonstrated precision. Short-term deflection and reinforcement strain were obtained by deriving an effective moment of inertia for FRC. The FEA underestimates deflection because it often assumes ideal and perfect conditions. The analytical model accurately predicts reinforcement strain, aligning closely with FEA results. These findings significantly advance our understanding of FRC structures, guiding future research and practical applications in structural engineering.

PREFACE

This thesis is an original work of Helmi Ali Saleh Al-Guhi. The recognition and design of the research program were accomplished with the supervision of Dr. Douglas Tomlinson at the University of Alberta, and three journal papers and two conference papers related to this thesis have been published or submitted, as listed below.

Journals:

1. **Helmi Alguhi and Douglas Tomlinson.** " Experimental and Analytical Study of Steel and Chopped Glass Fibre Reinforced, *Journal of Contraction and Building Materials,* Science Direct [Published February 2024]. *(Chapter 3)*
2. **Helmi Alguhi and Douglas Tomlinson.** " Crack Behaviour and Flexural Response of Steel and Chopped Glass Fibre-Reinforced Concrete: Experimental and Analytical Study." *Journal of Building Engineering,* Science Direct [Published May 2023]. *(Chapter 4)*
3. **Helmi Alguhi and Douglas Tomlinson.** " One-Way Shear Strength of FRP Reinforced Concrete Members without Stirrups: Design Provision Review" Journal of Composites for Construction, ASCE [Published March 2021]. *(Chapter 6)*

Conferences:

1. **Helmi Alguhi and Douglas Tomlinson.** " Evaluation of proposed Steel Fibre Reinforced Concrete Beams under Ultimate and Serviceability Limit States" Canadian Society of Civil Engineering Conference, Laval City, Montréal, 2019. *(Appendix A)*
2. **Helmi Alguhi and Douglas Tomlinson.**" Chopped Fibre Dosage and Material Effects on The Fresh Properties of Normal Strength and Density Concrete" Canadian Society of Civil Engineering Conference, Whistler, British Columbia, 2022. *(Appendix B)*

DEDICATION

Firstly, Praise Be to Allah for Giving Me the Strength and Patience to Complete This Work and Peace Be Upon His Final Prophet and Messenger, Mohammed.

I Dedicate This Work to My Mother (Fatima) and late father (Ali), Allah blesses his soul for Continuous Encouragement, for Their Exhortation, Coaching, Nonstop Help, and Efforts.

Finally, I Dedicate This thesis to My Lovely Wife (Shroq), My kids (Hasan, Hussain, Jana), My Brothers, Sisters and All My Relatives.

ACKNOWLEDGEMENTS

The author expresses profound gratitude to GOD ALMIGHTY, the source of knowledge, wisdom, and all goodness. Without the grace and countless blessings bestowed by the Almighty, the author and their work would not have existed. Embarking on graduate studies, particularly a Ph.D., necessitates support, guidance, and considerable patience throughout the long-term academic journey. My Ph.D. thesis is a heartfelt expression of gratitude to everyone who loved, supported, and assisted me during the nearly six years dedicated to pursuing my doctoral degree.

Firstly, I want to thank my supervisor sincerely, Dr. Tomlinson. I am thankful for the opportunity you gave to a civil engineering graduate from the heart of the Arabian Desert. Your guidance and mentorship during my Ph.D. have been precious. Reflecting on the initial research document I presented to you highlights my significant progress, and examining my thesis is a constant reminder of my gratitude towards you. I want to thank my committee members Dr. Carlos A. Cruz-Noguez (El-Lobo), Dr. Samer Adeeb, and Dr. Yong Li, for their valuable comments and feedback.

My mother and late father provided unwavering support, allowing me to dedicate my time and effort to education. I want to genuinely apologize for my absence and lack of support, as no words can adequately convey my gratitude for everything. All my love to my wonderful wife and family; I'm sorry for the challenges brought about by my busy study schedule and am deeply thankful to my brothers and sisters for their enduring love, support, and advice. Heartfelt thanks and love to my friends and colleagues who stood by me during the challenging moments throughout this journey.

My journey through graduate studies has been made possible through the unwavering support and encouragement of Shaikh Abdullah Bugshan. I am deeply grateful for his limitless support.

Additionally, I extend my heartfelt thanks to the Hadhramout Foundation for granting me the scholarship that facilitated my Ph.D. pursuits.

TABLE OF CONTENTS

LIST OF TABLES

LIST OF FIGURES

LIST OF ACRONYMS AND SYMBOLS

The following acronyms and symbols are used in this thesis.

Acronyms	Definition
CFRC	Chopped fibre-reinforced concrete (*Appendix B*)
CoV	Coefficient of variation
FRC	Fibre-reinforced concrete
FRP	Fibre-reinforced polymer
GFRP	Glass fibre-reinforced polymer
GF	Glass fibres
HF	Hybrid fibres (combined steel and glass)
MCFT	Modified compression field theory
pc	Plain concrete
RC	Concrete reinforced with discrete reinforcement (rebar)
SD	Standard deviation
SF	Steel fibres
SR	Steel rebar reinforced concrete

Symbols	Definition
A_b	Area of tension reinforcement bar, mm^2
A_s	Total area of tension steel reinforcement bar, mm^2
A_f	Area of FRP flexural tension reinforcement, mm^2 *(chapter 6)*
A_{rv}	Area of stirrup reinforcement, mm^2
a	shear span, mm
a_g	Nominal maximum aggregate size, mm
a/d	Shear span to effective depth
b	Beam width, mm
b_w	Member effective shear width (mm) *(chapter 6)*
C_c	Compression force, N

c	Neutral-axis depth for a cracked transformed section, mm *(chapter 6)*
c_f	Plastic neutral axis for fibre-reinforced concrete
c_{pc}	Plastic neutral axis for plain concrete
d	Effective depth to the centroid of tensile reinforcement, mm
d_{Gf}	Glass fibre diameter, mm
d_{Sf}	Steel fibre diameter, mm
D_{Gf}	Glass fibre diameter, mm *(chapter 4)*
D_{Sf}	Steel fibre diameter, mm *(chapter 4)*
d_f/l_f	Fibre aspect ratio
D_f/L_f	Fibre aspect ratio *(chapter 4)*
d_v	Effective shear depth, mm
E_c	Compression modulus of elasticity, Mpa
E_t	Tension modulus of elasticity, MPa
E_f	GFRP modulus of elasticity, MPa
E_s	Steel modulus of elasticity
E_{sh}	Steel strain hardening modulus of elasticity
f_b	Reinforcement bar stress, MPa
$f_c^{'}$	Cylinder compressive strength of concrete, MPa
f_{cr}	Concrete cracking strength, MPa
f_{fu}	GFRP ultimate stress, MPa
f_{sy}	Steel yield stress, MPa
f_r	Modulus of rupture, MPa
f_{rv}	Stirrup yield stress, MPa
h	Overall member thickness, mm
$I_{e\,fib}$	Effective moment of inertia for FRC, mm^4
$I_{cr\,fib}$	Cracked moment of inertia of FRC, mm^4
$I_{cr\,pc}$	Cracked moment of inertia of plain concrete, mm^4
I_t	Moment of inertia of transformed section, mm^4
k	Ratio between the depth of the neutral axis of the cracked transformed section and the tensile reinforcement effective depth, d. *(chapter 6)*

k_f	FRC modification factor
k_{fib}	Ratio of elastic, cracked neutral axis depth to for effective depth fibre-reinforced concrete
k_m	Moment-shear interaction factor
k_{pc}	Ratio of elastic, cracked neutral axis depth to effective depth for plain concrete
k_r	Reinforcement stiffness factor
k_s	Size effect factor
l	Beam span, mm
l_a	Distance from the nearest support, mm
l_{Gf}	Glass fibre length, mm
l_{Sf}	Steel fibre length, mm
L_{Gf}	Glass fibre length, mm *(chapter 4)*
L_{Sf}	Steel fibre length, mm *(chapter 4)*
M_{cr}	Cracking moment, kNm
M_f	Factored moment, Nmm
M_{fib}	Moment resistance for FRC flexural members, kNm
$M_{fib\ A}$	Analytical moment resistance for FRC flexural members, kNm
$M_{fib\ num.}$	Numerical moment resistance for FRC flexural members, kNm
$M_{fib\ pre.}$	Predicted moment resistance for FRC flexural members, kNm
M_{pc}	Flexure capacity of a cracked section without fibres, kNm
$M_{s\ fib}$	Flexure capacity of a cracked section with fibres, kNm
M_u	Factored moment, kN.m *(chapter 6)*
n	Modular ratio
n_f	Ratio of modulus of elasticity of FRP bars to modulus of elasticity of concrete
s_z	Smaller of d and the maximum spacing between longitudinal reinforcement layers, mm
s_{ze}	Effective crack spacing
T_b	Tension force in reinforcement bar, N
T_{fib}	Tension force induced from FRC, N
V_c	Shear strength from concrete contribution, kN

V_c	One-way shear resistance provided by concrete and FRP flexural reinforcement, kN
$V_{c.fib}$	Shear strength from fibre contribution, kN
V_f	Fibre volume fraction
$V_{exp.}$	Experimental shear strength, kN *(chapter 6)*
V_{fs}	Factored shear, N
$V_{predicted}$	Predicted shear strength, kN *(chapter 6)*
V_s	Shear strength from stirrups contribution, kN
V_u	Shear strength, kN
V_u	Factored shear, N *(chapter 6)*
$V_{u\ num.}$	Numerical shear strength, kN
$V_{u\ pre.}$	Predicted shear strength, kN
y_t	Distance from centroid to extreme tension face, mm
P_s	Total concentrated load at service, , kN
α	Inclination angle of principle compressive stresses to the horizontal line, degrees
β	Factor that accounts for the shear resistance of cracked concrete
β_d	Size effect factor (The Japanese Society of Civil Engineering)
β_p	Axial stiffness factor (The Japanese Society of Civil Engineering)
β_{ts}	Tension stiffening factor
α_1 and β_1	Concrete compression stress block modification factors
α_{1t} and β_{1t}	Concrete tension stress block modification factors
γ	Hybrid mixture ratio
γ_b	Member safety factor
γ_d	Size effect factor
ΔM_{fib}	Additional moment carried by fibres, kN
$\Delta\varphi_{fib}$	Curvature that fibres can resist, m^{-1}
$\Delta\varphi'_{max}$	The different between $\Delta\varphi_{max}$ and $\Delta\varphi_{fib}$, m^{-1}
$\Delta\varphi_{max}$	Maximum tension stiffening curvature at first cracking, m^{-1}

$\delta_{max.num.}$	Numerical maximum service deflection
$\delta_{max.pre}$	Predicted maximum service deflection
ε_{fu}	GFRP ultimate strain
ε_{c0}	Concrete compressive strain at peak stress
ε_{cu}	Concrete compressive strain at ultimate
ε_{cy}	Concrete compressive strain at yield
ε_{su}	Steel ultimate strain
$\varepsilon_{t\ cr}$	Concrete cracking tensile strain
$\varepsilon_{t\ res}$	Concrete residual tensile strain
ε_x	Longitudinal strain at mid-depth of the cross section
θ_c	Inclined crack angle in the compression zone, degree
λ	Concrete density factor
ξ	Combined size and slenderness factor
ρ	Tension longitudinal reinforcement ratio
ρ_f	Longitudinal FRP reinforcement ratio
σ_{c0}	Peak compressive stress, MPa
$\bar{\sigma}_{ct}$	Compression zone stress, MPa
σ_{cy}	Yield compressive stresses, MPa
σ_{res}	Residual compressive stresses, MPa
σ_{t0}	Concrete peak tensile stress
$\sigma_{t\ res}$	Concrete residual tensile stresses
τ_{Rd}	Design shear stress, MPa
φ	Member curvature, m^{-1}
ϕ_c	Material reduction factor for concrete

CHAPTER 1

INTRODUCTION

1.1 Background

In North America, the restoration and maintenance of deteriorating infrastructure has become a major concern. Beyond the economic concerns, which point to billions of dollars of lost economic activity (Joseph, 2017) and infrastructure funding deficits (Mirza, 2007) each year, there are safety concerns and potentially catastrophic loss of life worries with crumbling infrastructure. The choice of materials and construction methods primarily relies on technical performance criteria, with a particular emphasis on factors like durability and service life (Edvardsen, 2010). One of the most promising materials that have emerged for prolonging the life of structures is Fibre Reinforced Concrete (FRC). This is due to a substantial factor contributing to the durability of FRC, which is the crack control mechanism. This mechanism limits the infiltration rate of detrimental substances like water, chlorides, and carbon dioxide into structural elements, playing a crucial role in effectively extending the structure's service life (Paul et al., 2020).

Fibres play a substantial role in the context of Ultimate Limit State (ULS) criteria by enhancing the resistance of RC elements, potentially increasing their load-carrying capacity and reducing the risk of brittle failure modes. Additionally, including fibres often promotes ductility in Reinforced Concrete (RC) structures, which is particularly advantageous for buildings exposed to extreme loading conditions, allowing for controlled failure modes and improved safety measures. Furthermore, fibres can also replace the contribution of stirrups in both shear and torsional responses. The substantial impact of fibres on ULS criteria underscores their importance in designing and evaluating RC elements, especially when addressing ULS considerations.

In the context of Serviceability Limit State (SLS) criteria, a significant role is played by fibres, as they render reinforced RC elements stiffer and more durable, mitigating concerns such as excessive deflection and deformation, which are the focal points of attention in SLS. The reinforcement of resistance to cracking and deformation is facilitated by fibres, ensuring that structures remain robust and functional, especially when subjected to prolonged or repetitive loads. Consequently, when contemplating the influence of fibres on SLS, their indispensability for strengthening and extending the lifespan of RC structures is evident, thereby underlining their significance when addressing SLS concerns.

This comprehensive study evaluates the impact of material (steel and/or glass) and dosage (0.5, 1.0, and 1.5% by volume fraction) on mechanical properties, such as compressive and tensile responses. The results lead to the proposal of a simplified design compressive and tensile stress-strain model that accounts for fibre effects, demonstrating applicability in engineering practice. Moreover, the study explores the combination of non-corrosive glass fibres with stiffer steel fibres to enhance mechanical properties while reducing costs. The research introduces Digital Image Correlation (DIC) for crack measurement, and a validated inverse analysis approach generates a more general model for FRC that is adaptable for practical engineering use. The investigation extends to large-scale RC beams, utilizing finite element analysis (FEA) to assess structural benefits and performance under various parameters, including shear span, size effect, and reinforcement ratios.

Additionally, the study evaluates the one-way shear strength of fibre-reinforced concrete (FRP-RC) members, presenting an experimental database and comparing results to existing design guides and codes. This highlights the need for diverse data in ultimate and serviceability design equations, addressing limitations in existing models derived from a constrained dataset. Using a numerical database of 720 beams, the study develops models for predicting ultimate flexural and shear strength, serviceability, short-term deflection, and reinforcement strain. The models consider parameters such as beam heights, reinforcement ratios, and different fibre types and dosages. Overall, this research provides a comprehensive understanding of the structural benefits of using FRC in various applications, connecting experimental findings with numerical analyses to advance the current state of knowledge in the field.

1.2 Problem Statement

This thesis addresses critical gaps in the existing FRC literature, focusing on investigating key problem areas that warrant substantial attention. The initial challenges revolve around evaluating the performance of Glass Fibres (GF) and combinations of Steel Fibres (SF) and GF on fresh and hardened concrete properties. Moreover, the scarcity of investigations evaluating the effects of GFs and combinations of SF and GF on compressive parameters accentuates the need for focused inquiries to enrich our comprehension in this pivotal area. The subsequent set of challenges pertains to the flexural impact of SF and GF in Normal Strength Concrete (NSC). The limited research in this domain prompts a thorough exploration into integrating non-corrosive and deformable GF with higher stiffness SF. This exploration not only seeks to advance our understanding of compressive and flexural behaviour but also holds the potential to contribute to the reduction of production and construction costs.

Additionally, the study extends to gaps in applying inverse analysis in FRC studies, the SLS performance of FRP in combination with FRC, and the shear strength of large-scale FRP-FRC members. The thesis also tackles the absence of comprehensive numerical models for large-scale SR and GFRP beams combined with FRC, emphasizing the necessity for further exploration in SLS and ULS performance domains.

Moreover, several design provisions of codes and guidelines such as ACI 318-19, fib 2013, ACI 544.4R-18 and CSA S6:19 have been developed to predict the ultimate capacity of FRC members over the years that are based on conventional design methods modified by special procedures to account for contributions of the fibres. However, these provisions have been applied only for SF or with conventional SR bars. There are no design provisions specifically for FRP-FRC members; therefore, this study provided design provisions for members with different fibres. This research endeavours to fill gaps in designing FRC beams, considering diverse fibre types and combinations, shear span-to-depth ratios, and other primary reinforcements for both SR and GFRP flexural members. Through these investigations, the thesis seeks to make a substantial contribution to the advancement of knowledge in the field of Fibre-Reinforced Concrete.

1.3 Research Objectives

After concluding the literature review to identify research gaps **(Chapter 2)** and obtaining favourable results from the pilot study **(Appendix A)**, the primary objectives of this research program are delineated based on goals for both experimental and analytical programs.

1.3.1 Experimental programme objective

Evaluate the influence of chopped fibre types (steel, glass, and a blend of the two) and dosages on normal to medium concrete's fresh and hardened properties. **(Chapters 3, 4, and Appendix B).**

The following experimental-specific tasks have been identified to achieve this primary objective.

1. Design mixtures using the ACI Absolute Volume mix design method, then optimize mixtures for FRC using trial batches. **(Appendix B)**

2. Batch and cast specimens for each trial mixture for compression, tension, and flexural testing. **(Appendix B)**
3. Run a series of small-scale experimental tests (material properties test) following ASTM standards on FRC-RC reinforced with different chopped fibres, including compression, split cylinder, modulus of elasticity, and flexural tests. **(Chapters 3 and 4)**
4. Use Digital Image Correlation to evaluate the crack formation and propagation on FRC flexural prisms. **(Chapter 4).**

1.3.2 Analytical programme objectives

1. Develop a constitutive model for FRC materials similar to those developed in the experimental program. **(Chapters 3 and 4).**
2. Evaluate the impact of FRC on a large-scale (FEA) model. **(Chapter 5).**
3. Determine the best performance shear strength provision for FRP members (**Chapter 6).**
4. Develop design provisions for evaluating the serviceability and ultimate response of RC-FRC. **(Chapter 7).**

The following analytical-specific tasks have been identified to achieve these primary objectives.

1. Collect experimental data from FRC small-scale tests from the experimental program and develop a constitutive model for these FRC concrete beams and those from the experimental program in the previous objective using Inverse Analysis. This model can be used to characterize FRC material. (**Chapters 3 and 4).**
2. Create an FEA model of RC-FRC concrete beams using VecTor2® and validate this model against experimental data load-displacement responses and crack patterns. (**Chapter 5).**

3. Collect experimental data of FRP-RC members available in the literature and compare these results to predictions from models, codes, and guidelines to assess their ability to predict the one-way shear strength of FRP-RC beams, ,identifying the best code/model then using that provision as a foundation for a new design provision of RC-FRC. (**Chapter 6).**
4. Generate data from FEA to recommend the serviceability and ultimate design equations for RC-FRC beams and verify these equations based on collected experimental data available in the literature. (**Chapter 7).**

1.4 Scope and Limitations

This study is limited to studying the performance of RC-FRC members under pseudo-static mechanical loading. Only instantaneous responses were considered (i.e., effects of creep/shrinkage not considered). The tension softening response associated with normal to medium strength concrete was considered (i.e., strain hardening responses were not considered). Moreover, this work focused on simply supporting members with medium SF and GF dosages.

Furthermore, the research operates under the assumption of a uniform distribution of fibres, neglecting considerations for nuanced factors such as flow direction that could potentially impact performance.

1.5 Research Methodology

This research is broken into two programs: experimental and analytical. Each one is divided into phases and sub-phases to achieve the objectives of this study, as shown in Figure 1-1.

I: Literature Review:

This section includes a state-of-the-art review of various aspects of the performance of the RC-FRC beam in SLS and ULS. This review considers previous studies to determine research gaps, the study's objectives, problem statement, scope, and methodology.

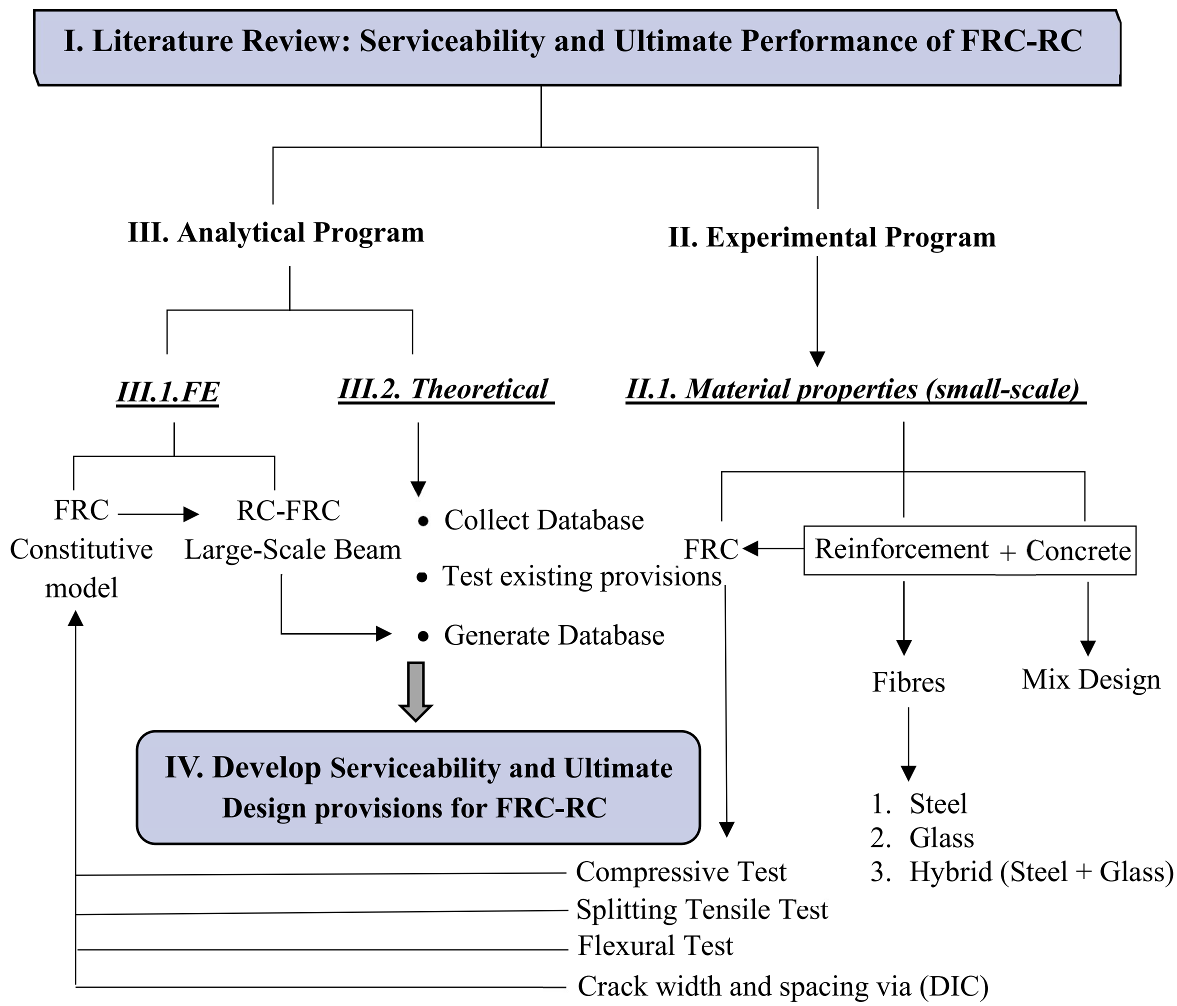

Figure 1-1: Methodology flow chart of research

II: Experimental Program.

This program aims to determine the material properties of FRC (small scale) and study the effect of fibres on the mechanical properties of normal concrete. This phase aims to determine the constitutive model of FRC based on its material properties. The flowchart in Figure 1-1 shows the primary sequence of the first phase in the experimental program. The work in this phase was divided into three sub-phases, as shown in Figure 1-2.

II.1 Material

Different materials, such as binders, aggregate, superplasticizer, and chopped fibres, were collected during this sub-phase.

II.1.1 Binders

The primary binder used is Type GU cement (70%), and the supplementary binder was fly ash (30%); the cement specifications are according to CSA A3000 and ASTM C150. General-purpose cement is suitable for all uses for which the special properties of other types of Portland cement are not required. Fly ash type F was used to increase the strength without reducing the workability of cementitious paste, an extremely fine powder with spherical particles less than 50 microns in size. Fly ash is one of the construction industry's most commonly used pozzolans. Class F fly ash is designated in ASTM C 618 and originates from anthracite and bituminous coals.

II.1.2 Admixtures

Sika® ViscoCrete® 1000 was used as a superplasticizer in all mixes. It is a high-range water reducer utilizing the combination of Sika® ViscoCrete® and Sika® ViscoFlow® Technology, and its unique formulation is based on polycarboxylate technology.

II.1.3 Aggregate

Two aggregate types, coarse and fine aggregate, were used in this study, with both being typical aggregates available in the Edmonton area. Coarse aggregate properties will determine a concrete batch's final quality and strength. The size, grading, shape, strength and water absorption of aggregates influence the final concrete mix in various ways, so this work needs to control these variables. Angular coarse aggregate requires more water and cement because they have a higher surface area. This aggregate angularity can make a concrete batch more expensive, stronger (aggregate interlock), and more durable. The maximum size of the coarse aggregate used in this study is 20 mm because the aggregate interlock plays the main role in increasing the shear strength of normal-strength concrete; the larger the aggregate size, the higher the shear strength. Aggregate gradation, absorption, and specific gravity tests were performed per ASTM C136, ASTM C127, and ASTM C128, respectively.

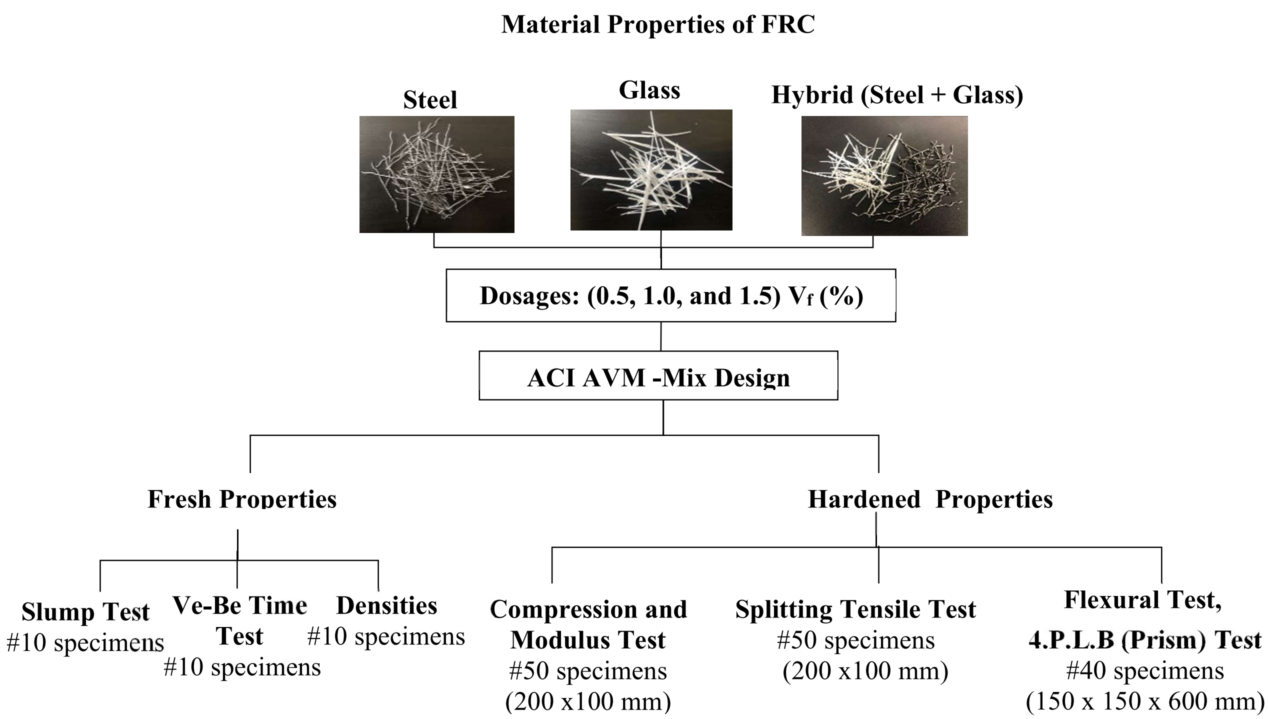

Figure 1-2: Material properties (small scale) tests flow chart.

II.1.4 Fibres

Fibres are the main contributor to preventing cracks from causing splitting failure. In this study, different chopped fibres were used: steel, glass and hybrid (steel and glass) fibres; these fibres have high tensile strength (1200-1000) and (3000-3500) MPa, respectively. The specific gravity and modulus of elasticity of steel and glass fibres are 7.75 and 2.68 and (200 and 72) GPa, respectively, with three fibre contents (0.5,1.0, and 1.5%) and (1.0% of hybrid fibres), the 1.0 % of hybrid fibre was also be contained of three dosages (0.75% steel + 0.25% glass), (0.50% steel + 0.50% glass), and (0.25% steel + 0.75% glass). The steel fibres were used in this study as reference fibre since they have been investigated comprehensively.

II.2. Preparation

In this sub-phase, the ACI Absolute Volume method (ACI 211.1-91 1991) is used to design the concrete mix. This method is widely used in North America; it is generally accepted and is convenient for normal concrete (ACI 211.1-91 1991). Ten mixes were designed with a total volume of 0.08 m3 per batch, one control mix and nine FRC mixes of two chopped fibres as steel, glass, and hybrid (steel and glass). The optimum volumetric percentage of FRC dosages should be in the range of between 0.5% to 1.5%. Dosages larger than 1.5% are ineffective since there are physical difficulties in providing a homogenous FRC, leading to a decrease in compressive strength compared with plain concrete (Altun et al. 2007).

II.3 Experimental measurements

ll.3.1 Fresh concrete measurements

Workability was measured using the slump test according to ASTM C143/C143M-15 and the Ve-Be time test according to ASTM C1170/C1170M-14 of all control concrete and FRC mixes. Since adding chopped fibres to the RC matrix would reduce the workability (Han et al. 2019; Liao et al. 2020), a minimum slump of 150 mm for plain concrete was targeted to provide adequate workability after the addition of chopped fibres (slump > 50 mm).

The bulk fresh, one-day dry, and 28-day dry densities were obtained using ASTM C138/C138M - 17a of an average of 10 cylinders for each mix.

ll.3.2 Hardened concrete measurements

The compressive strength of FRC was obtained by testing 50 cylinders of 100 x 200 mm in size as per ASTM C39/C39M-19. The concrete modulus of elasticity and complete stress-strain relationship were obtained from these tests using a compressometer and following ASTM C469/C469M-19. The tensile strength was measured by testing 50 cylinders of size 100 x 200 mm as per ASTM C 496.

Forty prismatic beams with dimensions of 150 × 150 × 600 mm were prepared in this study, according to ASTM C1609, which is recommended for high levels of crack control and post-crack flexural capacity is expected from fibres for FRC beams (ACI 544.4R-18 2018). The DIC was used to study the crack width and failure model.

III: Analytical Program

III.2. FEA of RC-FRC

A large-scale test program was initially planned but cut out due to constraints caused by the combination of the COVID-19 pandemic and construction delays from the Morrison Structures Lab expansion. These tests were replaced with FEA divided into two sub-phases: sub-phase one, where the constitutive model of FRC will be developed using inverse analysis of closed-form approach proposed by Soranakom and Mobasher (Soranakom and Mobasher 2008) (see section 4.5). This material model was used in a large-scale FE model in sub-phase two to run a parametric study and generate a database. Experimental test program results from the literature were used to verify numerical results at this stage. 2D (VecTor2®) FEA software was used to reduce the computational time of the analysis compared to 3D software. Since VecTor2® was specifically developed to assess reinforced concrete structures and contains the constitutive models and optimized approaches to simulate reinforced concrete, it was selected for this program.

III.1. Theoretical approach to predict the shear strength of FRP-RC beams

This quantitative approach collected a database of 147 beams published in the literature and prepared for statistical analysis. Fourteen existing and proposed design provisions for calculating the one-way shear strength of FRP-RC members without stirrups were presented. The effect of changing design parameters (concrete strength, size effect, reinforcement ratio, shear span to effective depth ratio, and fibre modulus of elasticity) was assessed using a trial beam. These provisions were then compared to results from the database. In this sub-phase, the all-around best performance provision for the shear strength of FRP-RC was determined, and then this provision was used with the effect of the fibres to provide the shear design equation for FRP-FRC members.

IV. Develop Better Serviceability and Ultimate Design provisions of RC-FRC

Based on experimental testing and the verified FEA database, design provisions for RC-FRC SLS and ULS performance were generated and compared with other databases in the literature. These design provisions were mainly based on the most appropriate SLS and ULS design equations and account for fibre as an additional force, T_{fib}, to the sectional analysis for SLS (see section 7.4.1), and as internal tensile force transferred across the diagonal crack for ULS (see sections 7.3.1 and 7.3.2). T_{fib}, force was induced from the tri-linear tensile constitutive stress-strain model; this tensile model was generated using inverse analysis (see section 4.5).

1.6 Thesis Structure

The thesis is separated into eight chapters:

- **Chapter 1** introduces the research study and contains its problem statement, objectives, scope, methodology and thesis structure.
- **Chapter 2** includes a literature review of fibres, FRC fresh and hardened properties, reinforcement, serviceability, and ultimate behaviour of RC-FRC reinforced beams, FRC application, pervious studies, and research gaps.
- **Chapter 3** addresses the first part of experimental objective (1) by testing 50 cylinders of control (without fibre) and FRC to investigate the compressive response of FRC. Additionally, this chapter provides an analytical compressive model for FRC, aligning with the first part of the analytical objective (1).
- **Chapter 4** introduces the second part of experimental objective (1) by conducting a flexural test on 40 prisms and a splitting tensile test on 50 cylinders to investigate the tensile response. An analytical tensile model for FRC is also presented, aligning with the second part of the analytical objective (1).
- **Chapter 5** addresses analytical objective (2) by presenting a FEA model of 720 RC-FRC beams using the FE program VecTor2.
- **Chapter 6** addresses analytical objective (3) by presenting the assembly database of FRP with and without stirrups and evaluating this database regarding codes, guidelines and models available in the literature.
- **Chapter 7** addresses analytical objective (4) by developing serviceability and ultimate design equations for RC-FRC flexural members.
- **Chapter 8** outlines the conclusions and recommendations based on Chapters 3, 4, 5, 6, and 7.

CHAPTER 2

LITERATURE REVIEW

2.1 General

This chapter provides an overview of fibres, Fibre-Reinforced Concrete (FRC), Fibre-Reinforced Polymers (FRP), and the serviceability and ultimate behaviour of Reinforced Concrete (RC)-FRC reinforced beams. Additionally, it includes reviews of previous studies on experimental and Finite Element Analysis (FEA) of RC-FRC beams. Later chapters of this thesis present more focused literature reviews on the content presented in those chapters.

2.2 Fibres

Fibres have served as reinforcement throughout history and have experienced significant technological advancements over time. In ancient times, mud bricks were crafted using straw and mortar, with horsehair used for reinforcement. The evolution of fibre technology saw the introduction of asbestos fibres as reinforcement in cement (Asbestos-cement) by the late 19th century. During World War II, asbestos cement gained widespread adoption, facilitating the construction of easily assembled, robust, and cost-effective structures for military purposes. In the mid-20th century, researchers explored the use of composite materials for concrete reinforcement, leading to the replacement of asbestos fibres with materials like steel, glass, and synthetic fibres. This shift was prompted by the direct association between asbestos exposure and various life-threatening diseases, as noted in studies such as (Campopiano et al., 2009). There are many types of fibres, such as metal fibres (steel), chemical fibres (e.g. polypropylene, polyethylene), mineral fibres (e.g. glass and basalt), carbon fibres, and natural fibres (e.g. flax and kenaf) that have been successfully used in the concrete matrix.

2.2.1 Glass fibre

Glass fibre (GF) has a higher modulus of elasticity, tensile strength, density and lower water absorption than synthetic and natural fibres (Madhkhan and Katirai 2019). These properties improve the mechanical behaviour of normal-strength concrete (NSC) reinforced with GF. GF contributes more to the durability performance of high alkalinity concretes (D'Antino and Pisani, 2019; Holubová et al., 2017). GFs, as shown in Figure 2-1, have attracted attention as they offer beneficial improvements to plain concrete, such as crack control, impact resistance, fatigue resistance, and abrasion resistance (Madhkhan and Katirai, 2019).

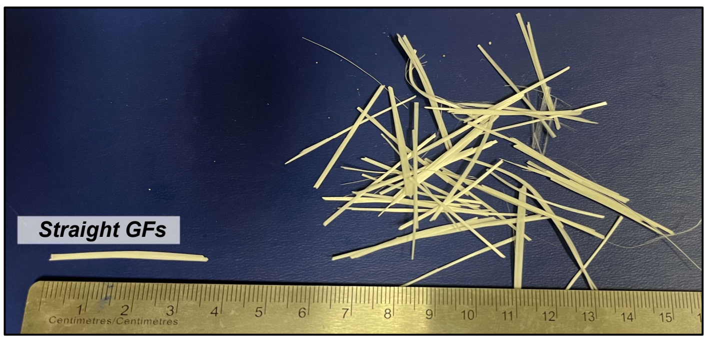

Figure 2-1: Photo of plain GF used in the test program.

2.2.2 Steel fibre

Steel fibre (SF) serves as a metallic reinforcement in concrete. It is characterized as short, distinct SF lengths with aspect ratios (length to diameter ratio) ranging from approximately 20 to 100 (Behbahani et al., 2011) featuring diverse shapes, as in Figure 2-2. Double hooked-end SFs exhibit superior anchorage to straight SF (Abdallah, Fan, and Rees, 2016; Abdallah, Fan, Zhou, et al., 2016). These fibres are small enough to be randomly dispersed in an unhardened concrete mixture through standard mixing procedures (Behbahani et al., 2011). SF are categorized into five groups: cold-drawn wire, cut sheet, melt-extracted, shaved cold-drawn wire, and milled from blocks. Adding SF to concrete improves its physical properties, making it more resistant to cracking, impact, fatigue, bending, tenacity, durability, and other essential factors (Abbas et al. 2014; Alguhi and Tomlinson 2019; Ding et al. 2011; Minelli et al. 2014).

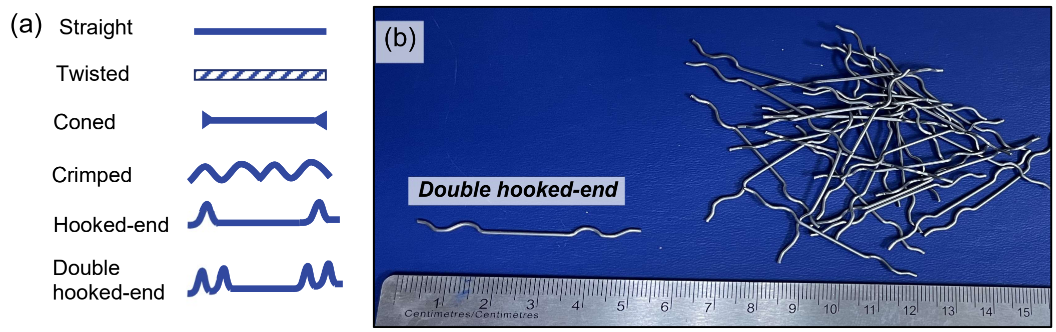

Figure 2-2: (a) SFs shapes (b) photo of double hooked-end SFs used in the test program.

2.2.3 Hybrid fibres

In this thesis, the term "hybrid" denotes the combination of more than one fibre type. Numerous researchers have observed enhancements in mechanical and fracture properties through the utilization of various fibre combinations (Almusallam et al., 2016; Babaie et al., 2020; Banthia and Sappakittipakorn, 2007; Chasioti and Vecchio, 2017; Pereira et al., 2012; Sivakumar, 2011). However, limited studies examine the impact of incorporating steel and GF in NSC, particularly concerning longer fibre lengths and larger dosages.

2.3 FRC

Fibre Reinforced Concrete (FRC) is defined as a composite material consisting of mixtures of cement, mortar or concrete and discontinuous, discrete, uniformly dispersed suitable fibres. Adding fibres into the concrete allows tension to cross cracks; thus, the fracture process zone (FPZ), which consists of the zone within FRC where fibres intersect the single major crack and micro-cracks (minute cracks situated closer to the crack tip), increases. The traction-free area (i.e., part of the crack where there is no bridging between crack faces) decreases, as shown in Figure 2-3. The size of the fracture process zone determines the toughness of the concrete. The larger the fracture process zone, the larger the concrete's toughness. The tensile strength of concrete increases using fibres, and this is happening by delaying the growth of cracks and transmitting stress across a cracked section, leading to better service performance and aggregate interlock resistance in shear at ultimate limit states (Huber et al., 2019).

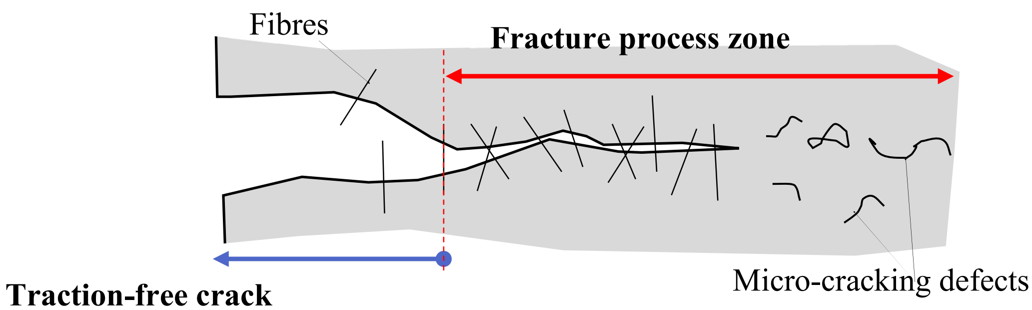

Figure 2-3: Fracture mechanism of FRC

Concrete has a low tensile strength compared to its compressive strength. This is a particular disadvantage when the material is used for a member with lower flexural stiffness, such as in glass fibre-reinforced polymer (GFRP)-RC beams. It is accepted that the performance of concrete mixtures can be improved by adding fibres such as steel fibre into the concrete to increase shear strength (Abbas et al. 2014; Alguhi and Tomlinson 2019; Ding et al. 2011; Minelli et al. 2014), improve post cracking behaviour (Alguhi and Tomlinson 2019; Cucchiara et al. 2004), and increase the ductility of steel RC flexural members (Abbas et al. 2014; Alguhi and Tomlinson 2019; Minelli et al. 2014). SF can change failure modes from brittle shear failure to more ductile flexural failure (Abbas et al. 2014; Alguhi and Tomlinson 2019; Cucchiara et al. 2004).

2.3.1 Material Characterization

This section briefly explores the characterizations of FRC, categorizing them into fresh and hardened properties.

1.1.1.1 Fresh concrete properties

Fresh properties encompass the state and behaviour of FRC in its recently mixed form including aspects such as workability, consistency, and setting time. Even though there are various improvements in the mechanical properties of hardened concrete when using fibres, the use of fibres reduces the flowability of fresh concrete (Abdelrazik and Khayat, 2020; Abousnina et al., 2021; Alguhi and Tomlinson, 2022; Carroll and Helminger, 2016; Gültekin et al., 2022), which causes a negative impact on concrete's workability. In particular, these effects may cause challenges with fresh concrete mixing, handling, pouring, compaction, and finishing. Nevertheless, studies are scarce assessing the influence of glass fibres and combinations of steel and glass fibres on fresh concrete properties.

1.1.1.2 Hardened concrete properties

Hardened properties delve into the enduring qualities of FRC after the concrete has cured, exploring attributes like compressive, tensile, and flexural response.

The structural design of elements under compression, such as columns, piers, and the compressive struts of beams, relies significantly on the compressive characteristics of FRC, including compressive strength, modulus of elasticity, Poisson's ratio and toughness.

Several studies have explored FRC with diverse fibres, including metal, synthetic, and mineral fibres, each possessing distinct properties. Noteworthy investigations (Altun et al., 2007; Mebarkia and Vipulanandan, 1992; Neves and Fernandes de Almeida, 2005; Sun et al., 2018) delved into the compressive response of SF, GF, and polyvinyl alcohol fibres, revealing increased compressive strength with larger fibre dosage. Conversely, conflicting findings exist, with some studies suggesting that SF has a negligible impact on compressive strength (Bencardino et al., 2008; Chasioti and Vecchio, 2017). Additionally, certain researchers observed a slight reduction in the modulus of elasticity when using steel fibres (Lee et al., 2015; Suksawang et al., 2018)and GFs (Mebarkia and Vipulanandan, 1992), while others reported almost no effect on the modulus of elasticity with the addition of steel fibres (Sun et al., 2018). The addition of fibres results in a reduction in Poisson's ratio compared to the control mix (Chu et al., 2018). This reduction is attributed to the lateral confinement effect imparted by the fibres.

The tensile response of FRC composites can be estimated by either stress-strain ($\boldsymbol{\sigma}$-ε) or stress-crack open month displacement ($\boldsymbol{\sigma}$-*w*), and this response can be classified as either "strain-softening" or "strain-hardening". In the "strain-softening" case, which is a primarily linear elastic ascending tensile stress-strain curve up to the same point representing both the first cracking and peak stress, followed by a reduction in stress as strain increases (ACI-544-16, 2016) (see Figure 2-4). Localization occurs immediately after the first cracking, and with increasing elongation, the stress after the first cracking decreases from the stress at the first cracking. In the "strain-hardening" case, which is a primarily linear elastic ascending tensile stress-strain curve up to first cracking, microcracks coalescence, and a post-cracking portion characterized by an increase in the stress with a much lower effective stiffness (representing tension stiffening) up to a maximum stress (ACI-544-16, 2016) (see Figure 2-4).

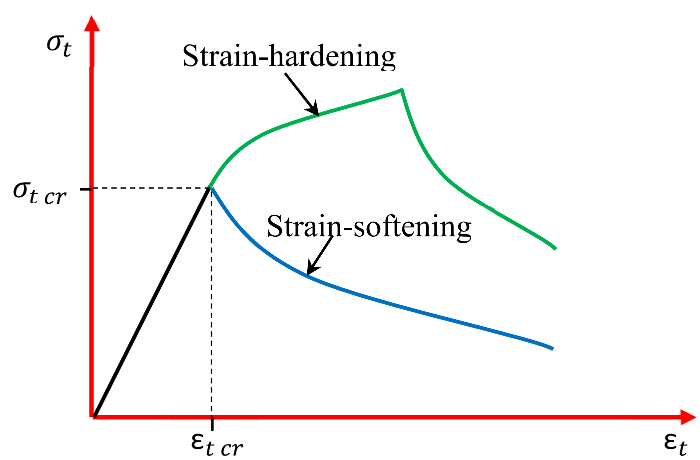

Figure 2-4: Strain-softening and strain-hardening of FRC

Uniaxial direct tensile tests are a means to characterize the constitutive properties of FRC under tension, yet they are characterized by high variability and challenges in controlling crack location and propagation. There are challenges in establishing a gripping arrangement that avoids specimen cracking at the grips with this test method (Chao et al., 2016). While the flexural response outcomes obtained from the ASTM C1609 (ASTM C1609/C1609M-10, 2010) bending test better represent the behaviour of members under both uni- and bi-axial bending (Chao et al., 2016).

Recent studies have assessed the flexural response of FRC using various fibres, including metal, synthetic, and mineral fibres. For instance, (Babaie et al., 2020; Branston et al., 2016; Jiang et al., 2014; Shafiq et al., 2016a; Simões et al., 2017; Yoo et al., 2015) investigated the use of steel, glass, basalt, polymer, and polyvinyl alcohol (PVA) fibres in concrete and found that flexural strength and post-cracking performance increased with fibre dosage. However, others reported that PVA did not significantly affect flexural strength; PVA and basalt fibres did not contribute to the post-cracking behaviour (Shafiq et al., 2016). Adding fibres such as glass and basalt increases flexural strength and fracture energy (Arslan, 2016; Kizilkanat et al., 2015).

2.3.2 FRC constitutive model

Several techniques have been proposed to model FRC's tensile stress-strain (σ-ε) relationship; however, most techniques were developed for Steel Fibre Reinforced Concrete (SFRC). Lim et al. (1987) developed tensile σ-ε relationships using laws of mixture and results from SF pullout tests. The limitation of the laws of the mixture method is that not all of the fibres are effective because of their random orientation in concrete. Only fibres parallel or nearly parallel to the tensile stress effectively control cracks. The quantity of effective fibres is of concern when modelling FRC structures, and correction factors are often introduced to estimate the number of effective SF. RILEM TC 162-TDF and Barros et al. (Barros and Figueiras 2001) suggested a tensile σ-ε relationship based on fracture energy that uses results from a deformation-controlled beam-bending test to determine the peak and post-cracking stresses. The main concern is the accuracy and objectivity of calculating horizontal strains using vertical deflections (Kooiman and Walraven 2000).

The process of inverse analysis to get FRC constitutive properties is gaining the attention of researchers (Alguhi and Elsaigh 2016; Elsaigh et al. 2004; Hemmy 2002; Kohoutkova et al. 2004; Labib 2008; Tlemat et al. 2006). Moreover, inverse analysis is being considered for the latest Canadian bridge code (CSA S6-2019), and the ACI adopts inverse analysis in the ACI-544.8R-16 report, which is based on a closed-form approach derived by Soranakom and Mobasher (2008). The advantage of inverse analysis is that the flexural response of FRC can be obtained with minimal complexities compared to procedures requiring results from direct tensile tests. The disadvantage is that this method is numerically demanding. However, the solution capabilities of available computer programs can be used to perform the analysis without substantial time or effort.

2.4 Reinforcing bars

Steel rebars are the most common reinforcing bars used in reinforced concrete, with FRP bars being a distant second. Steel and FRP have their own distinct features. Steel reinforcement is renowned for its high stiffness and ductility, among other assets, making it a traditional and widely used choice in construction. FRP bars, comprised of fibres, resin, interface, and additives, are used in a variety of applications where steel may have issues with corrosion or magnetic disturbance. FRP bars have advantages in mechanical properties compared to steel, including higher strength, lower density, corrosion resistance, lower thermal conductivity, lack of electrical conductivity, electromagnetically inert, better impact-resistance, and low lifecycle costs (ACI 440, 2015). However, FRP bars tend to have a much lower elastic modulus than steel and have a brittle failure mode. Three fibre types are commonly used in structural engineering applications: carbon, glass, and basalt (CFRP, GFRP, and BFRP). The typical tensile strengths and the stress-strain relationship of FRP bars relative to typical grade 400 steel reinforcement are shown in Figure 2-5.

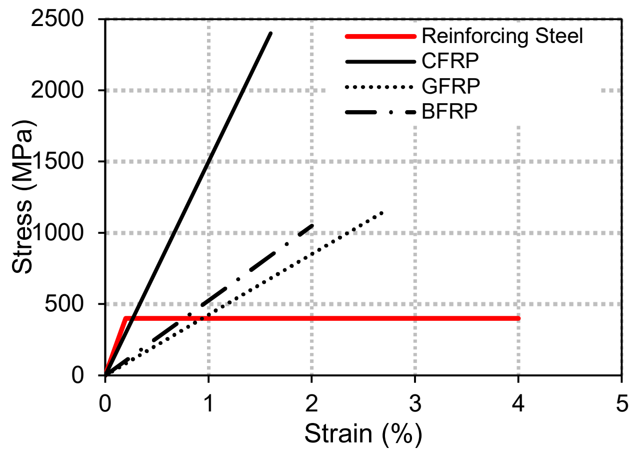

Figure 2-5: Typical FRP and steel stress-strain relationships.

Typical commercially available GFRP bars have elastic moduli around 40 to 60 GPa. The lower elastic modulus of these bars relative to steel, which has an elastic modulus around 200 GPa (Figure 2-5), leads to GFRP-RC members developing wider and deeper cracks than steel-RC members with the same reinforcement ratio under equivalent loading (Barris et al. 2017). Consequently, GFRP-RC members are often controlled by serviceability limits such as crack and deflection control (Barris Peña 2011; El Refai et al. 2015; Machial et al. 2012; Silva et al. 2020). Therefore, adding fibres together with FRP bars to create FRP-FRC structures is considered a practical solution to overcome serviceability problems seen in purely FRP-RC structures. Wider and deeper cracks in FRP-RC reduce the compression zone depth, aggregate interlock, and tensile stresses transferred across inclined cracks. The shear resistance of concrete, V_c, is proportional to the axial stiffness of the longitudinal reinforcing bars. The lower the reinforcing bars' reinforcement ratio or modulus of elasticity, the lower the expected shear strength (El-Sayed et al. 2006; Tureyen and Frosch 2002). To account for the reduced modulus of GFRP compared to steel, some design provisions modified expressions for steel-RC by including a term reflecting the ratio between the FRP and steel moduli of elasticity (ISIS 2007, JSCE 1997 and BISE 1999) though more recent work, such as the ACI 440.11 code for GFRP bars in concrete is leading to FRP-specific expressions (ACI 2022).

2.5 Bar-reinforced concrete with FRC.

Adding fibres into concrete reinforced with discrete reinforcement (e.g., rebar) enhances flexural and shear strength by increasing post-cracking tensile strength, as observed in literature (Amin and Foster, 2016; Cuenca et al., 2018; Dinh et al., 2011; Issa et al., 2016; Marì Bernat et al., 2020; F. Minelli et al., 2014). Consequently, SF can potentially reduce or eliminate the need for shear reinforcement, which mitigates reinforcement congestion, particularly in slender members, and reduces installation costs, lowering labour expenses (S. Foster, 2010; F. Minelli and Plizzari, 2010). Fibres can also improve service parameters such as deflection, crack width, and reinforcement strain due to reducing early-age cracking (particularly shrinkage cracking). Previous work has shown that fibres can increase the possible limiting service moment by 60% (Barros et al., 2017).

2.6 FRC Design Equation

2.6.1 Ultimate response

Numerous models have been created to forecast the flexural strength of steel FRC members (Henager et al., 1975; Imam et al., 1995; Mobasher et al., 2015). These models are based on cross-sectional analysis, incorporating fibre effects as an additional tensile force which enhances moment resistance. Other models for flexural strength are based on fracture mechanics principles (Carmona et al., 2022). All of these models account for fibres' residual or post-cracking strength contribution.

Several models have been proposed for predicting the shear strength of FRC, primarily relying on regression of test data (Ashour et al., 1992; Kwak et al., 2002; Mansur et al., 1986; RILEM TC 162-TDF, 2000; Sharma, 1986;Ashour et al., 1992; Kwak et al., 2002; Mansur et al., 1986; RILEM TC 162-TDF, 2000; Sharma, 1986), while others are based on fracture mechanics (Gastebled and May, 2001; K. S. Kim et al., 2012; Nguyen-Minh and Rovňák, 2011). However, all of these models are tailored for SF and consider only a few parameters, such as fibre dosage and profile shape. There is a noticeable lack of models that evaluate shear strength across different shear spans to effective depth, a/d ratios, fibre types, combinations of fibres, and sizes.

2.6.2 Serviceability response

SF effectively controls the formation of splitting cracks, leading to substantial enhancements in the tension stiffening of RC elements (Abrishami and Mitchell, 1997). Alsayed (1993) developed an equation for predicting FRC member deflection, utilizing an effective moment of inertia calibrated based on test observations. This equation integrates the fibre aspect ratio (d_f/l_f), fibre length (l_f), fibre diameter (d_f), and volume fraction coefficients derived from regression analysis of test results (Alsayed, 1993). A later mechanistic approach incorporated the post-cracking tensile capacity of fibres to calculate the effective moment of inertia, eliminating the reliance on specific data sets (Bischoff, 2007).

Anticipating reinforcement strain in FRC is crucial for incorporating FRC contributions into crack width expressions, as crack width is significantly influenced by the bond between reinforcement and surrounding concrete. Numerous codes and standards, such as ACI-318-19 (2019), ACI 440.11 (2022), and CSA S806-12 (2012), include a bond-dependent coefficient, k_b, in their design equations, ranging from 0.9 to 1.4. Determining k_b, experimentally is recommended, particularly by CSA S806-12 (2012). The accuracy of crack width expressions heavily relies on k_b(Wang and Belarbi, 2011), posing challenges in modelling due to limited test data or the inclusion of k_b, in models.

2.7 Application

Applications for FRC are extensive and cover a wide range of sectors and construction needs, as presented in Table 2-1. The versatility of FRC makes it a preferred choice for various purposes and notable applications encompass.

Table 2-1: Applications and utilizations of FRC

Application	**Utilizations**
Structural Reinforcement	Used for providing minimum shear reinforcement in components such as beams, structural walls, and elevated slabs.
Residential	Employed in various residential applications, including driveways, sidewalks, basements, shotcrete pool construction, foundations, drainage, and coloured concrete.
Agricultural	Construction of farm and animal storage structures, including building walls, silos, and paved areas for feedlots.
Commercial	Utilization in interior and exterior flooring, encompassing polished concrete, slabs, parking areas, and roadways.
Elevated Decks	Composite steel deck construction and elevated formwork for commercial and industrial purposes, such as those found at airports and shopping centers.
Industrial	Application in constructing lock structures, dams, channel linings, ditches, storm-water structures, and 3D printing.
Waterways	Implementation in the construction of dams, lock structures, channel linings, ditches, and storm-water structures.
Precast Concrete and Products	Inclusion in architectural panels, tilt-up construction, building walls, septic tanks, bank vaults, grease traps, and sculptures.

2.8 Previous Experimental and Numerical Studies

This section presents details on prior research involving experimental and Finite Element Analysis (FEA) conducted on members of RC-FRC beams.

2.8.1 Experimental Studies

Studies (Aziz and Taha 2013; Vakili et al. 2019) investigated the effect of fibres (glass, polypropylene, carbon and steel) on reinforced concrete beams with GFRP and CFRP bars with and without stirrups. These beams had small dimensions, 1500×100×200 mm (Vakili et al. 2019) and 2250×100×150 mm (Aziz and Taha 2013). Results show that flexural strength increases by 16% relative to the plain concrete beams. First cracking load, crack spacing, ultimate load, and ductility index increased with the percentage of carbon fibres in high-strength concrete (Aziz and Taha 2013). Shear strength increased up to 183%, 98%, and 55% using steel, glass and polypropylene fibres, respectively (Vakili et al. 2019).

Wang and Belarbi (2011) studied the flexural performance of 178×229×2032 mm RC beams reinforced by GFRP and CFRP bars with polypropylene fibres. The crack width of FRP-FRC beams was smaller than the FRC-RC beam, especially at service loads and ultimate concrete strains measured in the FRP-FRC beams were 50% larger than the FRP-RC beams. Adding fibres was shown to be an effective way to enhance the ductility of the FRP-RC system. Based on the deformation-based approach, the ductility indices increased by more than 30% with the addition of polypropylene fibre.

Studies performed by Folino et al. (2020); Krassowska and Lapko (2013); Sahoo et al. (2015) considered the influence of steel, basalt, and hybrid (polypropylene/steel) fibres on conventional steel RC beams with different beam dimensions, such as 120×300×2400 mm (Folino et al. 2020), 150×200×2000 mm (Sahoo et al. 2015), and 80×160×2000 mm (Krassowska and Lapko 2013). The most obvious findings to emerge from those studies are that an improvement of shear and flexural capacity was observed compared to reference reinforced concrete beams without fibres (Folino et al. 2020; Krassowska and Lapko 2013). Sahoo et al. (2015) stated that the shear strength was reduced significantly by adding polypropylene fibres and a slight reduction by adding SF due to mix design issues (e.g. poor consolidation); conversely, shear strength and deformability were improved by adding hybrid fibres. The failure mode changed from brittle shear failure to ductile flexural failure by adding SF (Folino et al. 2020); however, the shear failure mode was not modified by adding steel and polypropylene fibres; multiple cracks of smaller crack width were noticed at the failure stage with hybrid fibres (Sahoo et al. 2015).

2.8.2 Numerical Studies Using Finite Element Analysis (FEA) Models

Multiple studies have evaluated FEA's capacity to accurately model the experimental behaviour of SR-RC, as evidenced by research conducted by Alshaarbaf et al., (2023); Harba et al., (2022); Smarzewski and Stolarski, (2017). Results consistently demonstrate that FEA effectively predicts test outcomes. Similarly, investigations have delved into simulating SR-RC beams using FRC and diverse fibre types, as explored by Ayub et al., (2018); Facconi et al., (2021); Khaleel Ibrahim et al., (2023); Shewalul, (2021); Sliseris, (2018). These inquiries also affirm agreement between FEA predictions and test results for SR-FRC. Moreover, these studies emphasize FEA's capability to capture the nuanced complexities associated with introducing various fibres into concrete.

Numerous numerical studies have investigated GFRP-RC beams (Ahmad et al., 2021; Gouda et al., 2023; Saleh et al., 2019; Tsivolas et al., 2022). These studies have explored the effects of increased concrete compressive strength on both strength and serviceability (Gouda et al., 2023), crack growth and intensity (Tsivolas et al., 2022), as well as moment redistribution due to flexural and shear loading in continuous GFRP-RC beams (Ahmad et al., 2021). In a study by (Saleh et al., 2019), FEA was conducted on GFRP-RC beams subjected to impact loads, demonstrating the effective representation of midspan deflections and dynamic GFRP bar strains.

1.2 Digital Image Correlation (DIC)

Various methods have been used to detect cracks and track crack propagation, including notches and the red dye penetrant technique. Digital Image Correlation (DIC) emerges as an alternative for assessing crack propagation and widths due to its high accuracy in measuring the complete field surface crack monitoring. This capability allows for the identification of small cracks that may go unnoticed when using red dye penetrant (McCormick and Lord, 2010). While sensors like extensometers, strain gauges, and linear variable differential transducers (LVDT) are commonly used in experiments, they fall short in displaying full-field displacements/strains and may lack early crack detection and local failure identification compared to DIC (Ibeawuchi et al., 2019). Figure **2-6** displays the Digital Image Correlation (DIC) image featuring crack visualization.

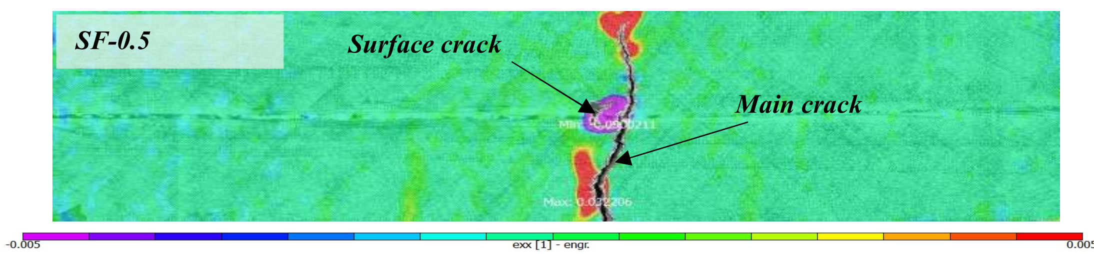

Figure 2-6: DIC analysis for FRC prism test (from the experimental program).

2.9 Research Gaps and Motivations

Though past studies have shown extensive efforts in characterizing various forms of FRC in multiple applications, gaps are observed in the literature. The identified gaps, presented below, warrant careful consideration for future academic and practical endeavours:

1. Performance of GF and hybrid fibres:
   - Limited studies evaluating the performance of GF and combinations of SF and GF on fresh and hardened concrete properties underscore a need for further research in this specific aspect.

2. Compressive response with diverse fibres:
   - While several studies have examined the impact of various fibres on compressive parameters, there is a scarcity of research evaluating the effects of GFs and combinations of steel and glass on compressive response. This research gap calls for focused investigations in this direction.
3. Flexural response with different fibres:
   - Limited research on the flexural impact of SF and GF in (NSC) prompts this study, which explores the combination's benefits. Exploring the integration of non-corrosive and deformable GF with higher-stiffness SF is essential, with the potential to reduce production and construction costs.
4. Application of Inverse Analysis in FRC Studies:
   - The study highlights the use of inverse analysis, a general approach gaining attention in various fields. However, the application of this approach, as seen in the latest Canadian bridge code and the American Concrete Institute's report, indicates a potential area for further exploration and refinement.
5. SLS Performance of FRP-FRC:
   - Comprehensive investigations into the SLS performance of FRP in combination with FRC remain relatively unexplored, highlighting a potential avenue for future research.
6. Shear Strength of Large-Scale FRP-FRC Members:
   - While some researchers have delved into the shear strength of FRP-FRC using small-scale specimens, there is a notable absence of studies focusing on larger-scale FRP-FRC members. This gap in research emphasizes the need for exploration in this specific domain.

7. The motivation for using numerical analysis, specifically FEA,
    - Literature gaps exist in studying large-scale SR and GFRP beams combined with FRC. Current research lacks comprehensive numerical models considering SF and/or GF, with limited exploration of SLS and ULS performance.
8. Design Provisions for RC-FRC Beams:
    - The gap in designing FRC beams is evident in the limited dataset, primarily reliant on regression analysis of steel FRC beam test data. This dataset lacks diversity, including fibre types like GF and their combinations with SF, variations in *a/d* (shear span to depth) ratios, and GFRP of primary reinforcement.
    - Existing models formulated and validated exclusively for SF with steel bars as primary reinforcement present limitations. Future investigations are needed to broaden these models, incorporating various fibres like GF and different primary reinforcements.
    - There's also a notable absence of studies providing design provisions for FRP-FRC beams, indicating a need for comprehensive research in this area.

As indicated in Chapter 1, many of these gaps will be addressed over the course of this thesis to enhance the knowledge of FRC in reinforced concrete structures.

CHAPTER 3

EXPERIMENTAL AND ANALYTICAL STUDY OF STEEL AND CHOPPED GLASS FIBRE REINFORCED CONCRETE UNDER COMPRESSION

3.1 Introduction

Fibre Reinforced Concrete (FRC) has been used in many applications, such as tunnel walls, railway slabs, concrete barriers, and ground slabs. Plain concrete is brittle with low tensile strength compared to its compressive strength. Fibres can improve concrete tensile behaviour as they act as bridges between cracks to prevent them from propagating, improving concrete strength and post-cracking behaviour. Normal Strength Concrete (NSC) is used in common practice, but NSC also suffers from plastic shrinkage cracking and drying shrinkage cracking. Steel fibres can control plastic shrinkage cracking and drying shrinkage cracking (Eren and Marar, 2010), while glass fibres lower concrete permeability and reduce water bleeding (Pannirselvam and Manivel, 2021).

Several recent studies have been conducted on FRC with different fibres, including metal, synthetic, and mineral fibres, each having different properties. Some studies (Altun et al., 2007; Mebarkia and Vipulanandan, 1992; Neves and Fernandes de Almeida, 2005; Sun et al., 2018) investigated the compressive response of steel, glass, and polyvinyl alcohol fibres and found that compressive strength increased with fibre dosage. However, others reported that steel fibres do not significantly affect compressive strength (Bencardino et al., 2008; Chasioti and Vecchio, 2017). Some researchers found a slight reduction of modulus of elasticity with the use of steel (Lee et al., 2015; Suksawang et al., 2018a) and glass fibres (Mebarkia and Vipulanandan, 1992); however, others found that there is almost no effect of adding steel fibre (Sun et al., 2018) on modulus of elasticity. Though several researchers have studied the impact of fibres on compressive parameters, limited studies evaluate glass fibres and a combination of steel and glass on compressive parameters. Additionally, many previous studies did not consider statistical tools to assess these parameters in their work.

Stress block parameters, commonly used to assess reinforced concrete performance in flexural design, have been developed for different kinds of concrete, such as flexural members reinforced with shape memory alloys (Elbahy et al., 2009), high-strength concrete (Ibrahim and MacGregor, 1997; Ozbakkaloglu and Saatcioglu, 2004), confined and unconfined concrete (Karthik and Mander, 2011) and under fire (El-Fitiany and Youssef, 2011). However, the effect of adding fibres on stress block parameters has not yet been investigated.

Glass fibre has a higher modulus of elasticity and tensile strength with lower water absorption than synthetic and natural fibres (Madhkhan and Katirai, 2019); these properties can improve the mechanical behaviour of NSC. In addition, glass fibres contribute more to the durability performance of different alkali concrete environments (D'Antino and Pisani, 2019). Glass fibres are non-corrosive and continue to perform their original function over extended periods (Holubová et al., 2017).

This paper evaluates the effect of material (steel and/or glass) and dosage (0.5, 1.0 and 1.5% by volume fraction) on concrete's compressive response. Statistical analyses, including one-way ANOVA, significance test, and clinical significance, were done to investigate the influence of type and dosages of fibres on these parameters. Results were used to propose a simplified design stress-strain model that considers the effect of fibres. The proposed analytical model can be used to consider the tested FRC concrete mixture's compressive response in engineering practice.

3.2 Experimental study

An investigation was carried out using 50 concrete cylinders. Tests included plain concrete as well as concrete with steel fibres, glass fibres, and combinations of the two. Tests were completed under uniaxial compression to study the influence of fibre type and dosage on compressive response.

3.2.1 Mixing, casting, and curing

Ten mixtures were designed using the American Concrete Institute (ACI) Absolute Volume method (ACI 211.1-91 1991), one control mix and nine FRC mixtures. These mixtures were developed after completing trial batches to obtain a 28-day concrete strength between 35 MPa and 55 MPa. A slump of 150 mm for the control mixture was targeted to provide adequate workability after adding fibres since fibres are expected to reduce workability (Han et al., 2019; Liao et al., 2020). The FRC mixtures were assigned a name with two identifiers. The first identifier was fibre type: steel fibres (SF), glass fibres (GF), and a combination of steel and glass referred to as a hybrid (H). The second identifier was fibre dosage: 0.5, 1.0, and 1.5% volume fraction. For the hybrid mixtures, a constant fibre volume fraction of 1.0% was used with three ratios of steel to glass fibres: H1: 0.75% steel + 0.25% glass, H2: 0.50% steel + 0.50% glass, and H3: 0.25% steel + 0.75% glass. The mixture proportions for each batch are shown in Table 3-1.

Table 3-1: Proportions for each concrete mixture per cubic metre

Mix ID	Fibre Type and Dosage	W/CM	Cement (kg)	Fly ash (kg)	Water* (kg)	CA (kg)	FA (kg)	Fibre (kg)	SP (kg)
Control	No fibres	0.35	280	120	166	1147	764	0.00	2.0
SF-0.5	0.5% SF		280	120	166	1138	759	37.5	2.0
SF-1.0	1.0% SF	0.35	280	120	166	1130	754	75.0	2.0
SF-1.5	1.5% SF		280	120	166	1122	748	113	2.0
GF-0.5	0.5% GF		280	120	166	1138	759	12.9	2.0
GF-1.0	1.0% GF	0.35	280	120	166	1130	754	25.8	2.0
GF-1.5	1.5% GF		280	120	166	1122	748	38.7	2.0
H1-1.0	1.0% (0.75%SF+0.25%GF)		280	120	166	1130	754	___	2.0
H2-1.0	1.0% (0.50%SF+0.50%GF)	0.35	280	120	166	1130	754	___	2.0
H3-1.0	1.0% (0.25%SF+0.75%GF)		280	120	166	1130	754		2.0

*SF: Steel fibre, GF: Glass Fibre, H: Hybrid, CM: Cementitious materials, CA: Coarse aggregate, FA: Fine aggregate, and SP: Superplasticizer. *Includes allowance for absorption by fibres and aggregates*

The optimum volumetric percentage of FRC dosages is expected to be between 0.5% and 1.5%. Dosages larger than 1.5% were not considered since there are physical difficulties in creating a homogenous mixture leading to a decrease in compressive strength compared to plain concrete (Altun et al., 2007). The addition of less than 0.5% fibres will not affect workability remarkably but this amount is not expected to have meaningful effects on the post-cracking behaviour of concrete (Branston et al., 2016), which is the primary goal of this study.

A portable electrical drum mixer with a 155-litre capacity was used for all mixtures. The drum mixer was rinsed with water and completely drained before each batch was mixed. First, coarse and fine aggregates were added and mixed for one minute. Then, the cementitious materials (cement and fly ash) were added and mixed for two more minutes. After that, water was added gradually for 2 to 3 minutes. Then fibres were added gradually for 3 to 4 minutes. Finally, a superplasticizer was added to the mixture. The total mixing time for each FRC batch was between 8 and 10 minutes. Mixed concrete was placed in cylinder moulds in two layers and compacted using a vibrating table with a frequency of 60 to 90 Hz. Specimens were demoulded 24 hours after casting and placed in a lab room (temperature 25±2°C and relative humidity 35±5%), and then these samples were placed in a controlled humidity room (temperature 20±2°C and relative humidity 70±5%) until testing (28-32 days).

3.2.2 Materials

3.2.2.1 Binders and water

The main binder used is type general use cement (70% by weight), and the supplementary binder was fly ash (30% by weight), a common ratio used for concrete in Alberta. This ratio improves concrete's long-term strength and durability (Johnston, 1996) while reducing cement content. The cement specifications are according to CSA A3000 (CAN/CSA-A3000-13, 2013) and ASTM C150 (ASTM C150, 2000). Type F fly ash originated from anthracite and bituminous coals and was used to increase strength without reducing the workability of cementitious paste. It is one of the industry's most used pozzolans. Type-F fly ash is classified based on ASTM C618 (ASTM-C 618-15, 2015). Tap water was used for all mixes.

3.2.2.2 *Admixtures*

A high-range water reducer-HRWR Sika ViscoCrete® 1000 was added to concrete mixtures to reduce water content and improve workability. Adding more water to increase the workability (or slump) resulted in weaker concrete, as observed in trial batches.

3.2.2.3 Aggregate

Coarse and fine aggregates were selected as typical aggregates used in normal strength-ready mix concrete in the Edmonton, Canada, region. Pea gravel with a maximum size of 20 mm was used as ,the coarse aggregate and natural river sand with a maximum particle size of 4.75 mm was used as the fine aggregate. The measured bulk-specific gravity and water absorption of coarse and fine aggregates are 2.6 and 2.8 and 1.32 and 1.43%, respectively.

3.2.2.4 *Fibres*

Two different fibres were used: double-hooked end steel fibres (SF) and Alkali Resistant- glass fibres (AR)-(GF), as shown in Figure 3-1. The GF has an irregular diameter, so the aspect ratio was reported from the manufacturer. Table 3-2 gives the properties of the fibres obtained from manufacturers. Double-hooked end steel fibres with 50 mm lengths were used in this study. The compressive strength of steel FRC mixtures generally increases with steel fibre length (Han et al., 2019), and these were used in this study as reference fibre since they are commonly used in engineering practice. This study uses an AR-GF with added zirconium oxide to help resist alkalinity attacks. AR is an essential element as concrete is a very alkaline environment. AR-GFs were used for extra durability compared to steel fibres, and their expected lower demand for water absorption and increased chemical resistance were compared to other fibres such as steel and natural fibres.

Table 3-2. Properties of chopped fibres provided by manufacturers

Properties	SF	GF
The name of the manufacturers	Optimet®	Owens Corning®
Material	Cold Drawn Wire Steel	Alkali Resistant Glass
Diameter (mm)	0.92	0.54
Length (mm)	50	36
Aspect ratio (length/diameter)	55	67
Tensile modulus of elasticity (GPa)	200	72
Tensile strength (MPa)	1200	1700
Specific gravity	7.75	2.68

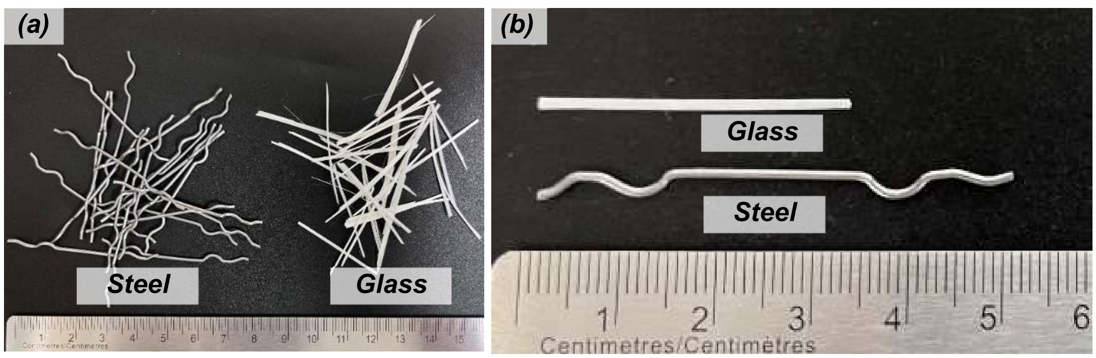

Figure 3-1: (a) Photo of fibres used in test program and (b) zoomed-in photo showing shapes and sizes of each fibre. Ruler shown for scale with dimensions in mm.

3.3 Test setup and procedure

3.3.1 Compression test

The compressive response was obtained by testing cylinders with 100 mm diameter and 200 mm length after a minimum of 28 days of curing (ASTM C39 / C39M-05a, 2005). Before testing, each end of each cylinder was ground using an automatic grinder to ensure that the test specimens had parallel and smooth surfaces. Lateral and axial strains in the concrete were measured using a compressometer (ASTM C469/C469M, 2014) using three linear variable differential transducers (LVDT) mounted on the compressometer, as shown in Figure 3-2. All samples were tested using a 1000 kN capacity MTS 311.31 machine at 1.0 mm/min, corresponding to a loading rate of 0.25 ± 0.05 MPa/s during the elastic range. LVDT data was continuously recorded, together with the load measured from a load cell attached to the MTS 311.31, using a QuantumX MX1601B (2.4 bit) data acquisition system.

Figure 3-2: A photo of the compression test setup showing compressometer and LVDTs.

Compressive strength, f_c', was obtained directly as the peak stress observed from the stress-strain curves. The chord modulus of elasticity E_c and Poisson ratio μ were calculated using Eq. (3-1) and (3-2), respectively (ASTM C469/C469M, 2014):

$$E_c = \frac{S_2 - S_1}{\varepsilon_2 - 0.00005} \tag{3-1}$$

$$\mu_c = \frac{\varepsilon_{t2} - \varepsilon_{t1}}{\varepsilon_2 - 0.00005} \tag{3-2}$$

where S_2 is the stress corresponding to the 40% of the peak stress, S_1 is the stress corresponding to a strain of 0.00005, ε_2 is the longitudinal strain corresponding to S_2, ε_{t2} is the transverse strain at mid-height of the specimen corresponding to S_2, and ε_{t1} is the transverse strain at midheight of the specimen corresponding to stress S_1.

3.3.2 Concrete ductility (Toughness Index)

Ductility of concrete is described as its ability to undergo inelastic deformation before failure and can be linked to toughness (a measure of the energy absorption capacity of the material) and used to characterize the material's ability to resist fracture. Several studies have proposed nondimensional relative toughness indices ($T.I._c$) for FRC; these indices, irrespective of concrete strength, depend on the extent of the stress-strain curves obtained. These indices provide a means of comparing the toughness of different FRC mixes or evaluating the effect of various parameters (such as fibre type and content). In contrast, compression's toughness specifically quantifies FRC's energy absorption capacity under compressive loading conditions. A typical strain value is usually selected. (Hsu and Hsu, 1994) described $T.I._c$ as the ratio of the area under the stress-strain curve of FRC up to a compressive strain of 0.012 to a corresponding plain concrete mixture up to the same strain. (Mansur et al., 1999) defined $T.I._c$ as the toughness based on a strain equal to three times the strain at peak stress to the strain at peak stress. This study calculated $T.I._c$. as the ratio of the area under the concrete stress-strain curve when axial stress reduced by 50% from the peak stress to the area under the concrete stress-strain curve up to peak stress. A similar approach was used by (Sun et al., 2018).

3.3.3 Statistical analysis

Statistical analysis was carried out using Analysis of Variance (ANOVA) to define the statistical significance level using (p-value) of control variables (Fibre type and dosage) and their interaction. The clinical significance level or effect size (a way to quantify the difference between two groups) of different variables in ANOVA models is evaluated using eta square (η^2) (Richardson, 2011), which can be calculated using Eq. (3-3). Cohen (1992) suggested that small, medium and large effects are reflected in values of η^2 0.0099, 0.0588, and 0.1379, respectively and the larger the effect size, the stronger the relationship between the two variables.

$$\eta^2 = \frac{SS_{groups}}{SS_{total}} \tag{3-3}$$

Where SS_{groups} is the sum of squares for the effect of the independent variable and SS_{total}, is the total sum of squares.

The observed power or sensitivity is also found, which indicates the percentage of the probability of detecting differences between groups. High power indicates a large chance of a test detecting a true effect, while low power means that the test only has a small chance of detecting a true effect or that the results are likely to be inaccurate or distorted by random and systematic error. The power is largely influenced by effect size, sample size, size, and significance level.

3.4 Results and Discussion

The key test results of the average of five nominally identical specimens are summarized in Table 3-3, including density at 28 days ρ, peak load, P_0, peak stress f_c', modulus of elasticity E_c, Poisson ratio μ, yield strain ε_{cy} corresponding to 85% of peak stress, peak strain ε_{c0} at peak stress , ultimate strain ε_{cu} at 80% of peak stress, and toughness index *T.I.*$_c$.

Table 3-3: Summary of Compression Test Results. Results presented are the mean of each parameter with $\pm$ indicating standard deviation.

Mixture ID	ρ, kg/m^3	P_0, kN	f'_c, MPa	E_c, GPa	μ	ε_{cy}, %	ε_{c0}, %	ε_{cu}, %	*T.I.*$_c$
C	2456±29	345±38	41.8±2.8	24.5±1.6	0.146±0.04	0.163±0.02	0.226±0.02	0.329±0.04	2.28±0.3
SF-0.5	2586±30	382±44	46.2±2.3	25.4±1.0	0.136±0.02	0.180±0.02	0.273±0.02	0.448±0.05	2.75±0.8
SF-1.0	2615±27	410±20	49.8±2.5	23.6±1.1	0.143±0.02	0.208±0.01	0.342±0.04	0.528±0.06	2.92±0.7
SF-1.5	2640±33	428±33	52.5±4.4	25.1±1.7	0.137±0.03	0.214±0.01	0.341±0.03	0.584±0.05	3.37±0.4
GF-0.5	2384±19	361±19	45.6±2.1	23.8±1.2	0.117±0.03	0.183±0.01	0.280±0.02	0.420±0.07	2.39±0.5
GF-1.0	2408±09	372±21	47.0±2.6	22.7±2.0	0.136±0.04	0.211±0.02	0.339±0.05	0.537±0.06	2.51±0.4
GF-1.5	2407±15	376±13	47.5±1.7	22.2±1.1	0.105±0.03	0.220±0.02	0.364±0.05	0.566±0.08	2.17±0.3
H1-1.0	2446±19	417±16	52.7±2.0	24.6±1.1	0.092±0.02	0.203±0.02	0.293±0.04	0.406±0.09	2.34±0.8
H2-1.0	2417±07	412±25	51.9±3.1	24.2±0.9	0.104±0.03	0.197±0.01	0.304±0.03	0.466±0.05	2.54±0.5
H3-1.0	2406±13	377±34	47.5±4.3	23.2±3.2	0.108±0.02	0.199±0.02	0.332±0.02	0.527±0.08	2.30±0.4

3.4.1 Compressive stress-strain response

The axial and lateral stress-strain curves of the average readings of five samples are plotted in Figure 3-3. The axial stress was assumed to be uniformly distributed across the section. Findings show that generally, there is no significant effect of adding fibres for both initial stiffness and modulus of elasticity since micro-cracks have not initiated at this stage and the fibre bridging process is inactive. The peak stress increased for FRC with steel fibres and continued increasing with dosage because fibres arrest the growth of microcracks at the micro-level, and confinement induced by transverse fibres leads to larger peak stress. The glass fibres slightly increase compressive strength due to their lower stiffness compared to steel fibres, with this increase noted most when dosages exceed 1.0%. This effect is further seen in hybrid mixtures, where larger ratios of glass fibres reduce compressive strength compared to mixtures with only steel fibres. For the post-peak response, the addition of steel fibres has more effect on the descending branches of the stress-strain diagram.

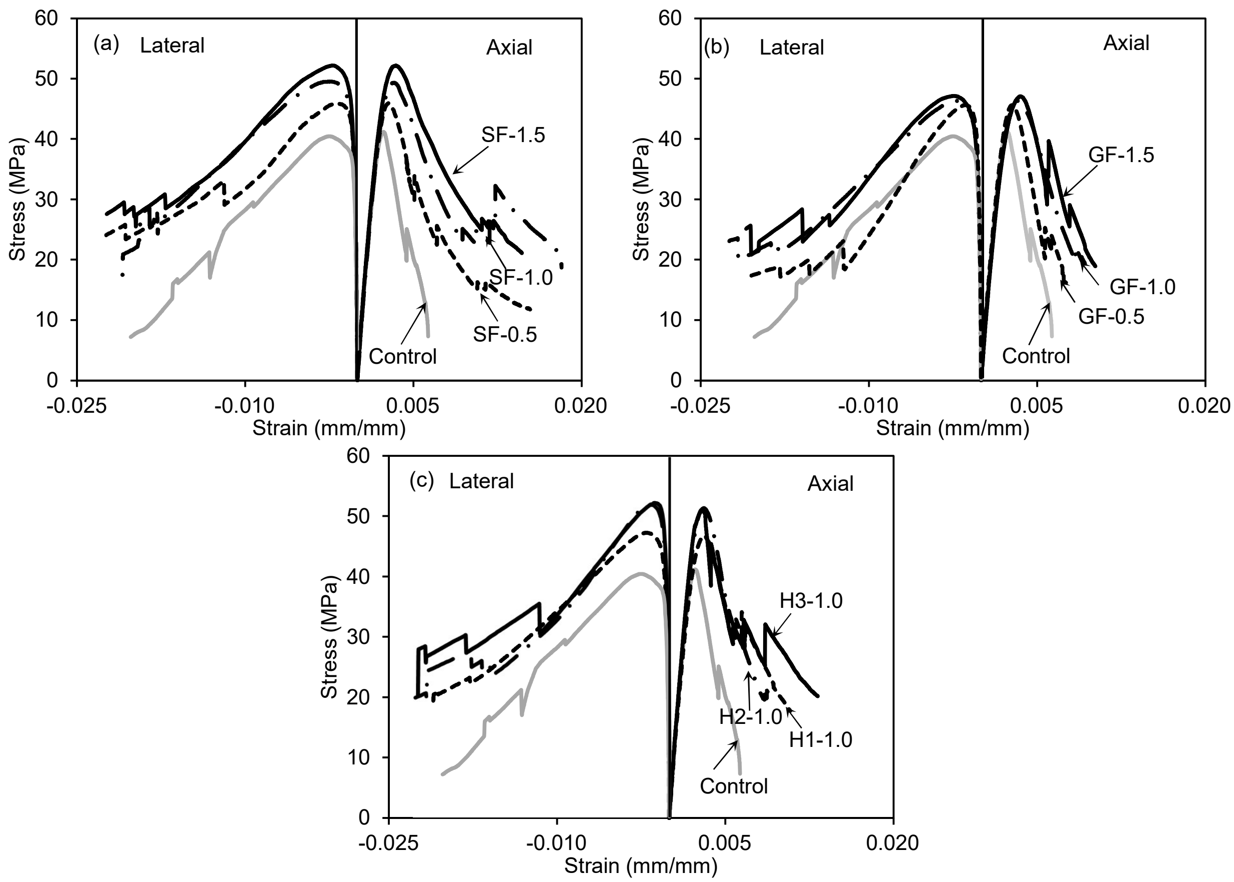

Figure 3-3: Stress-strain curves for chopped fibre-reinforced concrete. All plots are averages of five-cylinder tests for each mixture (a) effect of steel fibre dosage, (b) effect of glass fibre dosage, and (c) effect of hybrid dosages. Control curve for plain concrete is shown on each plot for comparison.

In particular, the increase in ultimate strain corresponding to the ultimate load, P_u This is because fibres bridge cracks and limit lateral expansion. This effect was less pronounced for glass fibres, with fibre contributions only noticeably affecting post-peak response at dosages exceeding 1.0%. In terms of the lateral response, both compressive strength and toughness increased when steel fibres were added because of the effect of the fibres in the plane of lateral tensile strain perpendicular to the applied compressive load. Glass fibres have almost no effect with 0.5% dosage on toughness.

3.4.2 Statistical analysis results

Data measured for each isolated factor ($\rho, f_c', E_c, \mu, \varepsilon_{cy}, \varepsilon_{c0}, \varepsilon_{cu},$ and TI_c) was analyzed using descriptive statistical parameters such as the mean, X, standard deviation, SD, and coefficient of variation CV. Data variation was defined in terms of CV. Slight variation is defined for CV values lower than 10%, moderate variation for CV values between 10% and 35%, and high variation for CV values higher than 35%. A similar approach was used by (Carrillo et al., 2019). The verbality of most parameters is considered to be slight with the exception of μ and TI_c which are moderate due to the randomness of fibre distribution and orientation. Evaluating the results of the one-way ANOVA are presented in Table 3-4. Adding fibres had a significant effect on all isolated factors with a calculated p-value less than the tabulated p-value at a confidence level of 95%, except for modulus of elasticity with p-value (0.0538), which indicates that adding fibres has an insignificant effect on modulus of elasticity. The effect size is also shown in Table 3-4. Adding fibres has a very large effect size on density, compressive strength, yield strain, strain at peak load, and ultimate strain. Elastic modulus, Poisson ratio, and toughness index have a large effect size. The observed power for adding chopped fibres on density, compressive strength, yield strain, peak strain and ultimate strain is larger than the elastic modulus, Poisson ratio, and toughness index. The effect of fibre type and dosage on compressive parameters (see Figure 3-3) indicates that adding steel and glass fibre and a blend of them significantly affects density, except for H1-1.0. Adding a small amount of steel fibre (0.5%) and dosages of 0.5 and 1.0% for glass fibre and H-3 did not significantly affect compressive strength. There are no significant effects of type and dosages on both modulus of elasticity and Poisson ratio, except H1-1.0 has a significant effect on Poisson ratio. The only mixture that significantly affected the toughness index was SF-1.5. The effect of this dosage on $T.I._c$ is statistically significant compared to other dosages. SF-0.5, GF-0.5, and H1-1.0 did not affect yield and peak load strains significantly compared to the plain concrete mixture. This small dosage of SFs and GFs did not fully activate the crack-bridging due to fewer micro-cracks at these stages (pre-peak and peak). Adding fibres with different dosages significantly affects ultimate strain except for SF-0.5, GF-0.5, H1-1.0, and H2-1.0 mixtures. That means that these smaller dosages affect the ultimate strain response. Still, compared with other fibres' material and dosages, it is insignificant due to the lower contribution in post-peak response's crack-bridging.

Table 3-4: ANOVA results for the density, compressive strength, elastic modulus, Poisson ratio, yield strain, strain at peak, ultimate strain, and toughness index

Factor	df	Tabulated P-Value (at 95% probability)	Calculated P-value	Significant?	Eta Squared	Size effect	Observed Power %
Density, ρ	9	0.0500	0.0000	Yes	0.947	Very large	100
Compressive strength, f_c'	9	0.0500	0.0002	Yes	0.526	Very large	99.7
Elastic modulus, E_c	9	0.0500	0.0539	No	0.320	Large	79.2
Poisson's ratio, μ	9	0.0500	0.0226	Yes	0.360	Large	87.2
Yield strain, ε_{cy}	9	0.0500	0.0001	Yes	0.546	Very large	99.8
Strain at peak stress, ε_{c0}	9	0.0500	0.0000	Yes	0.601	Very large	100
Ultimate strain, ε_{cu}	9	0.0500	0.0000	Yes	0.578	Very large	100
Toughness index, TI	9	0.0500	0.0442	Yes	0.329	Large	81.3

Table 3-5: Significance of fibre type and dosages affecting the density, compressive strength, elastic modulus, Poisson ratio, yield strain, strain at peak load and toughness index of control mix

Factor	ρ	f'_c	E_c	μ	ε_{cy}	ε_{c0}	ε_{cu}	$T.I._c$
SF-0.5	*YES*	*NO*	*NO*	*NO*	*NO*	*NO*	*NO*	*NO*
SF-1.0	*YES*	*YES*	*NO*	*NO*	*YES*	*YES*	*YES*	*NO*
SF-1.5	*YES*	*YES*	*NO*	*NO*	*YES*	*YES*	*YES*	*YES*
GF-0.5	*YES*	*NO*	*NO*	*NO*	*NO*	*NO*	*NO*	*NO*

GF-1.0	*YES*	*NO*	*NO*	*NO*	*YES*	*YES*	*YES*	*NO*
GF-1.5	*YES*	*YES*	*NO*	*NO*	*YES*	*YES*	*YES*	*NO*
H1-1.0	*NO*	*YES*	*NO*	*YES*	*YES*	*NO*	*NO*	*NO*
H2-1.0	*YES*	*YES*	*NO*	*NO*	*NO*	*YES*	*NO*	*NO*
H3-1.0	*YES*	*NO*	*NO*	*NO*	*YES*	*YES*	*YES*	*NO*

3.4.3 Compressive response parameter discussion

Trends in the compressive strength between parameters are shown in Figure 3-4, including error bars showing standard deviations. Compressive strength increased when adding fibres. For steel fibres, the compressive strength increased by 11, 19, and 29% for SF-0.5, SF-1.0, and SF-1.5, respectively. Adding glass fibres also increased compressive strength, though less effectively than with steel. These increases were 9, 12, and 14% for GF-0.5, GF-1.0, and GF-1.5, respectively. Figure 3-4 shows that strength increases almost linearly with steel fibre dosages over the investigated range. In contrast, glass fibres show a plateauing capacity between GF-1.0 and GF-1.5 due to conflicts between the crack bridging and increased porosity with increasing fibre dosage from the entanglement of some fibres, which induce pores that cause a decrease in the FRC strength. The second reason is a decrease in density due to a lower specific gravity (2.68), which is approximately one-third of the SF specific gravity (7.75) (Alguhi and Tomlinson, 2022).

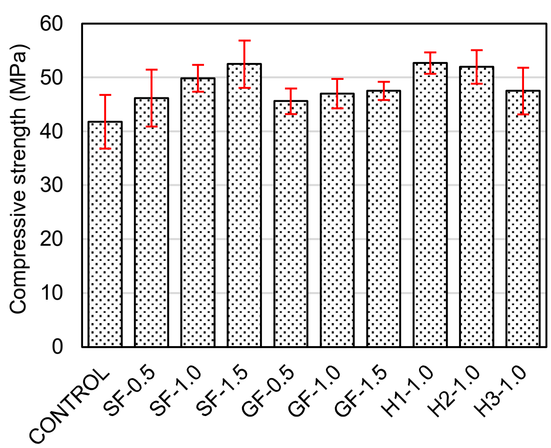

Figure 3-4: Average compressive strength for each parameter. Error bars denote one standard deviation from the mean.

Figure 3-4 shows the effect on the compressive strength of systems with both steel and glass fibres, so the replacement of 25% of the SFs with GFs, as in H1-1.0, increases compressive strength by 6% and 12% compared with SF-1 and GF-1.0, respectively. Replacement of 50% of the SFs with GFs (H2-1.0) increased compressive strength by 4% and 11% compared with SF-1.0 and GF-1.0, respectively. This result is attributed to the shorter (36 mm) deformable GFs better-controlling microcracks at earlier loading stages while the longer (50 mm) and stiffer SFs better control macrocracks. However, 75% replacement of SFs with GFs (H-3-1.0) decreases compressive strength by 5% compared to SF-1.0, and it has a very slight increase in compressive strength compared to GF-1.0 due to a reduction in density (see Table 3-3) with an increase in GFs dosages.

Figure 3-5 shows the effect of tested parameters on modulus of elasticity. There is essentially no change in modulus when adding steel fibres, with a similar trend found by Suksawang et al. (2018). Glass fibres decreased the average modulus of elasticity slightly, with similar results found by Mebarkia and Vipulanandan (1992). This is attributed to the entanglement of some glass fibres, which induce pores that cause a decrease in FRC stiffness. A similar trend was observed with hybrid mixtures where larger ratios of glass fibre led to a reduced modulus of elasticity.

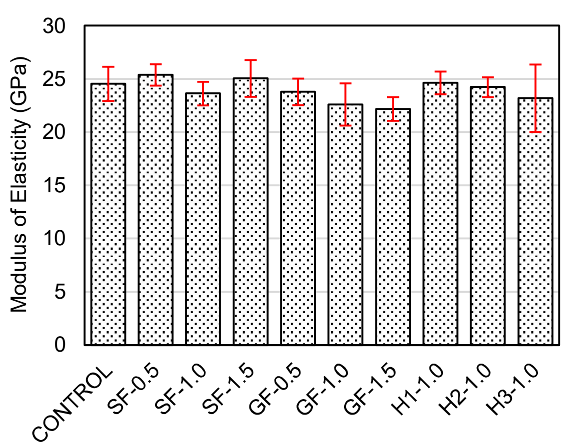

Figure 3-5: Average modulus of elasticity for each parameter. Error bars denote one standard deviation from the mean.

Figure 3-6 shows the effect of fibre type and dosage on Poisson's ratio. Poisson's ratio influences the speed of propagation and reflection of stress waves. Adding fibres reduces Poisson's ratio marginally compared to the control mix due to the lateral confining effect provided by fibres, which is noticed in statistical analysis (see Table 3-5); similar results were found by (Chu et al., 2018). There is no clear trend in increasing fibre dosages for both SFs and GFs, as shown in Figure 3-6. However, in hybrid mixes, increasing the glass amount has a diminutive increase in Poisson's and this is probably due to lower stiffness of GFs compared to SFs.

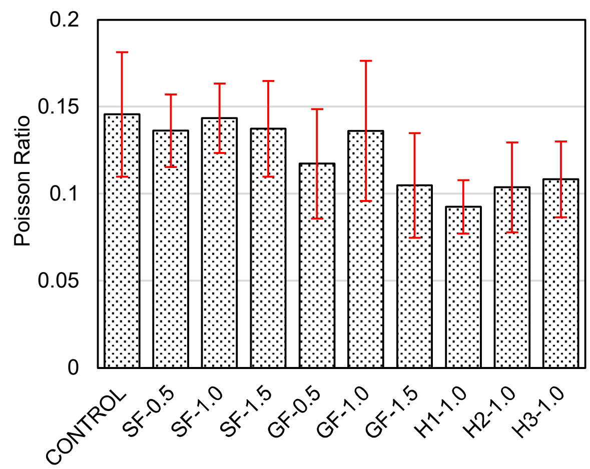

Figure 3-6: Average Poisson's ratio for each parameter. Error bars denote one standard deviation from the mean.

Figure 3-7 presents the effect of fibres on yield strain (strain corresponding to 85% of peak stress). Adding steel and glass fibres increases yield strain remarkably (10, 30, and 35% for 0.5, 1.0, and 1.5% dosage) for steel and glass fibres. Both steel and glass fibres had almost the same response regarding yield strain. This was also evident in hybrid mixtures, where there is no noticeable change in yield strain response by increasing or decreasing the steel and glass fibre dosage, as shown in Figure 3-7.

The strain corresponding to peak stress for each mixture is shown in Figure 3-8. Adding glass fibre increases this strain by 24, 50, and 60% for GF-0.5, GF-1.0, and GF-1.5, respectively. The steel fibres increased a similar amount for 0.5 and 1.0% dosages. However, the trend plateaued without any increase for SF-1.5 because after adding 1.0% SFs, the beneficial reduction in crack widths decreased, possibly due to fibre saturation, so SF-1.5 cylinders did not deform more at the point of peak stress. For hybrid mixtures, the larger the GF portion of the fibre dosage, the more the strain corresponds to peak stress compared with steel fibres due to the deformability of the GFs.

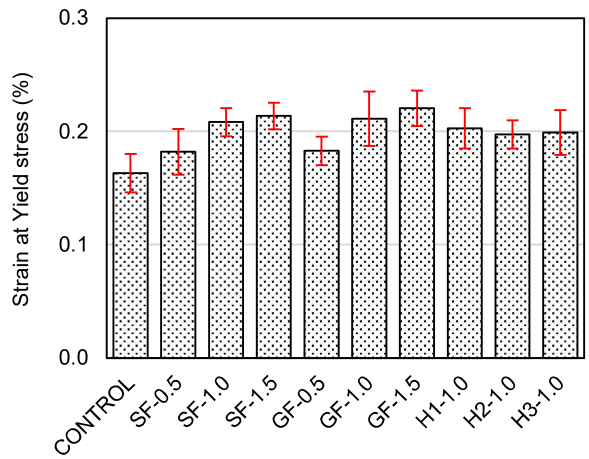

Figure 3-7: Average strain at yield stress for each parameter. Error bars denote one standard deviation from the mean.

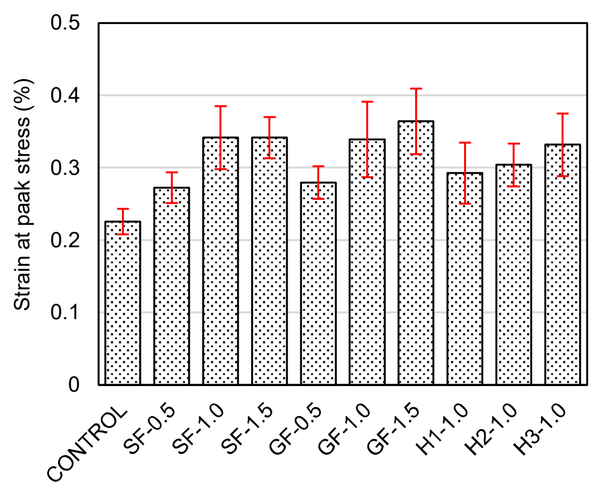

Figure 3-8: Average strain at peak stress for each parameter. Error bars denote one standard deviation from the mean.

Figure 3-9 shows the ultimate compressive strain, taken in this paper as strain corresponding to a stress of 80% of peak stress and used as an indication of concrete deformability. Adding fibres increases ultimate compressive strain remarkably, with averages of 35, 63, and 78% for 0.5, 1.0, and 1.5% dosages, respectively. It is worth mentioning that glass fibres increase ultimate strain more than steel fibres. Even with a lower failure load compared to steel fibre mixtures, glass fibre mixtures have almost the same strain. This is attributed to the deformable GFs bending more than the SFs; this effect can be noticed in hybrid mixes where the larger the ratio of fibres being glass, the larger the ultimate strain (see Figure 3-9).

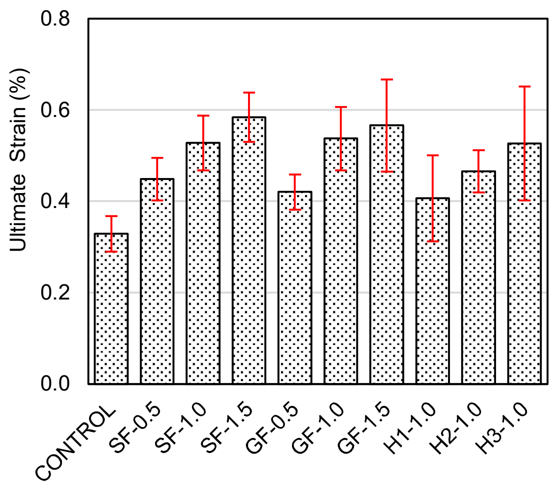

Figure 3-9: Average ultimate strain for each parameter. Error bars denote one standard deviation from the mean.

The toughness index (TI) shown in Figure 3-10 shows an increase of $T.I._c$. with increased steel fibre dosages of 20, 28, and 48% for SF-0.5, SF-1.0, and SF-1.5, respectively. GFs show a slight increase with increased fibre dosages of 5 and 11% for GF-0.5 and GF-1.0, though *T.I.c* decreased by 5% with a 1.5% dosage. This decrease may be because increasing GF dosages up to 1.0% decreases crack width and propagation due to the crack-arresting process; however, increasing GF dosage to 1.5% produces more voids due to the lower GF workability (Alguhi and Tomlinson,

2022) leading to this amount of $T.I._c$.'s decreasing. Various combinations of steel and glass fibre has no noticeable effect on $T.I._c$, as shown in Figure 3-10.

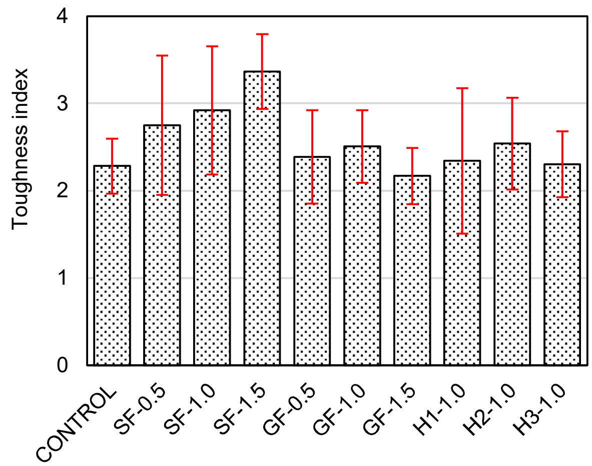

Figure 3-10: Average toughness index for each parameter. Error bars denote one standard deviation from the mean.

3.4.4 FRC design stress-strain relationship

A trilinear compressive stress-strain model is proposed for FRC in Figure 3-11. This model largely represents the FRC compressive stress-strain curves seen in the tests. The first stage (linear-elastic) represents the uncracked stage up to yield stress (σ_{cy}) taken as 85% of peak stress (σ_{c0}) per (ACI-544-16, 2016). The second stage is after the first crack is initiated from σ_{cy} to σ_{c0} at this stage the stiffness reduced as cracks propagate. The third stage (residual) describes the response from σ_{c0} to a residual stress ($\sigma_{c\ res}$) equal to 80% of σ_{c0} over the descending part of the stress-strain curve. The reason 80% was used is that this corresponds to the stress seen at an ultimate strain of 0.003 in the control mixtures. The model is shown using Eq. (3-4). Peak stress is significantly affected by fibre material and dosage, as demonstrated in statistical analysis (see Table 3-4), so Eq.(3-5) are proposed to predict the peak stress for steel, glass, and hybrid with mean and COV of experimental to predicted ratios (1.005 and 8%); (1.008 and 5%); and (1.06 and 7%) for steel, glass fibres, and hybrid mixtures with respectively, as seen in Figure 3-12. Note that these values are for the specific fibres and dosages studied in this paper and may not relate to all fibre types or with different dosages.

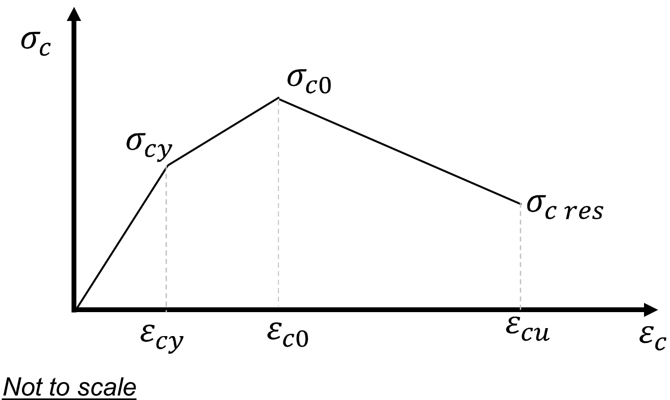

Figure 3-11: Proposed trilinear compressive stress-strain model for FRC.

$$\sigma_c = \begin{cases} \sigma_{cy}\left(\dfrac{\varepsilon_c}{\varepsilon_y}\right) & \text{for} \quad \varepsilon_c \leq \varepsilon_y \\ \sigma_{cy} + \left[\left(\dfrac{\sigma_{c0} - \sigma_{cy}}{\varepsilon_{c0} - \varepsilon_{cy}}\right)(\varepsilon_c - \varepsilon_y)\right] & \text{for} \quad \varepsilon_{cy} < \varepsilon_c \leq \varepsilon_{c0} \\ \sigma_{c0} + \left[\left(\dfrac{\sigma_{c0} - \sigma_{c\ res}}{\varepsilon_{c0} - \varepsilon_{cu}}\right)(\varepsilon_c - \varepsilon_{c0})\right] & \text{for} \quad \varepsilon_c > \varepsilon_{c0} \leq \varepsilon_{cu} \end{cases} \tag{3-4}$$

$$\begin{aligned} \sigma_{c0} &= f_c' + 750\ V_f && \text{for SFs} \\ \sigma_{c0} &= f_c' + 450\ V_f && \text{for GFs} \\ \sigma_{c0} &= \gamma\left[f_c' + \left(950V_f\right)\right] + (\gamma - 1)\left[f_c' + \left(750V_f\right)\right] && \text{for HFs} \end{aligned} \tag{3-5}$$

Where f_c' is the compressive strength of the control mix, γ is the hybrid mixture ratio ($\frac{SFs}{GFs}$), and ε_{cy}, ε_{c0} and ε_{cu}, are the yield, peak, and ultimate compressive strains. V_f, is the fibre volume fraction.

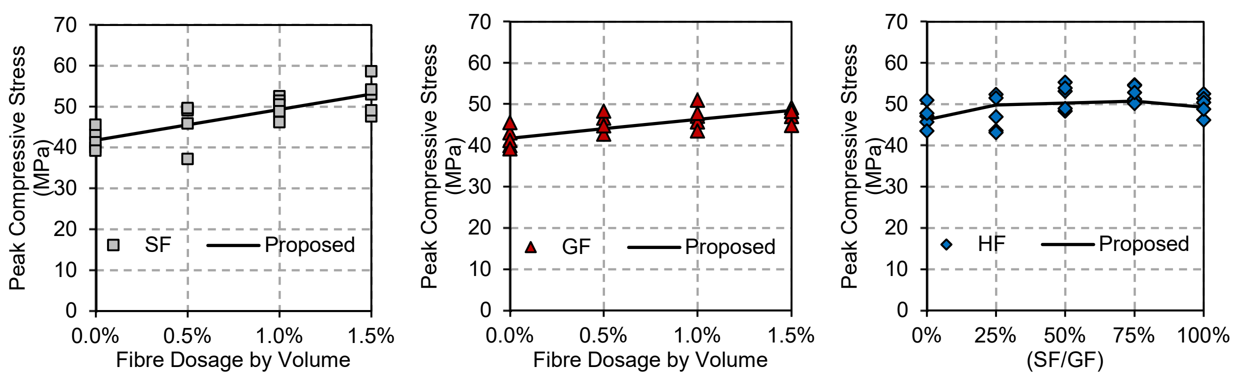

Figure 3-12:Measured and calculated of proposed peak compressive stress of (a) SF, (b) GF, and (c) HF.

3.4.5 Determining yield, peak, and ultimate strains

Conventional (i.e., without fibre) normal-strength concrete design peak and ultimate strain expressions do not accurately predict FRC's peak and ultimate strains because those expressions were developed for concretes without fibres. Proposed linear (slope-intercept) Eqs. ((3-6)-(3-8)) for yield, peak and ultimate strains are based on regression analysis of the control samples (no fibres) to get the y-intercept of each linear equation. Then, the fibre effect is added in terms of dosage as the equation's slope, which significantly affects design strains based on regression analysis. Similar observations were seen by Neves and Fernandes de Almeida (2005). The equations that predict the yield, peak, and ultimate strains of FRC are the same for SFs and GFs because these strains are affected by only V_f, with the effect of fibre material small enough to be neglected (see Figures 7, 8, and 9) which simplifies the proposal equations. These equations are suitable for FRC compared to the available design provision equations derived for conventional concretes, as seen in Figure 3-13. ACI-318-19 (2019) and CSA A23.3:19 (2019) ε_{c0} and ε_{cu} values are 0.002-0.003 and 0.002-0.0035, respectively.

Table 3-6 compares measured and calculated strains in terms of mean, coefficient of variation (COV), and Average Absolute Error (AEE). The prediction equation of ε_{cy}, for HFs is similar to SFs and GFs because the combination effect did not affect ε_{cy} (see Figure 3-7 (c)), but this influence is evident on ε_{c0} and ε_{cu}, as the more ratio of fibres that are GF, the larger the ε_{c0} and ε_{cu}, (see Figure 3-8 and Figure 3-9). The combination factor is added (γ) in prediction equations of ε_{c0} and ε_{cu} for HFs.

$$\varepsilon_{cy} = 0.0016 + 0.03(V_f) \qquad \text{for SF, GFs, and HFs} \tag{3-6}$$

$$\begin{aligned} \varepsilon_{c0} &= 0.002 + 0.1(V_f) && \text{for SFs and GFs} \\ \varepsilon_{c0} &= 0.002 + 0.15(V_f)(1-\gamma) && \text{for HFs} \end{aligned} \tag{3-7}$$

$$\begin{aligned} \varepsilon_{cu} &= 0.003 + 0.2(V_f) && \text{for SFs and GFs} \\ \varepsilon_{cu} &= 0.003 + 0.3(V_f)(1-\gamma) && \text{for HFs} \end{aligned} \tag{3-8}$$

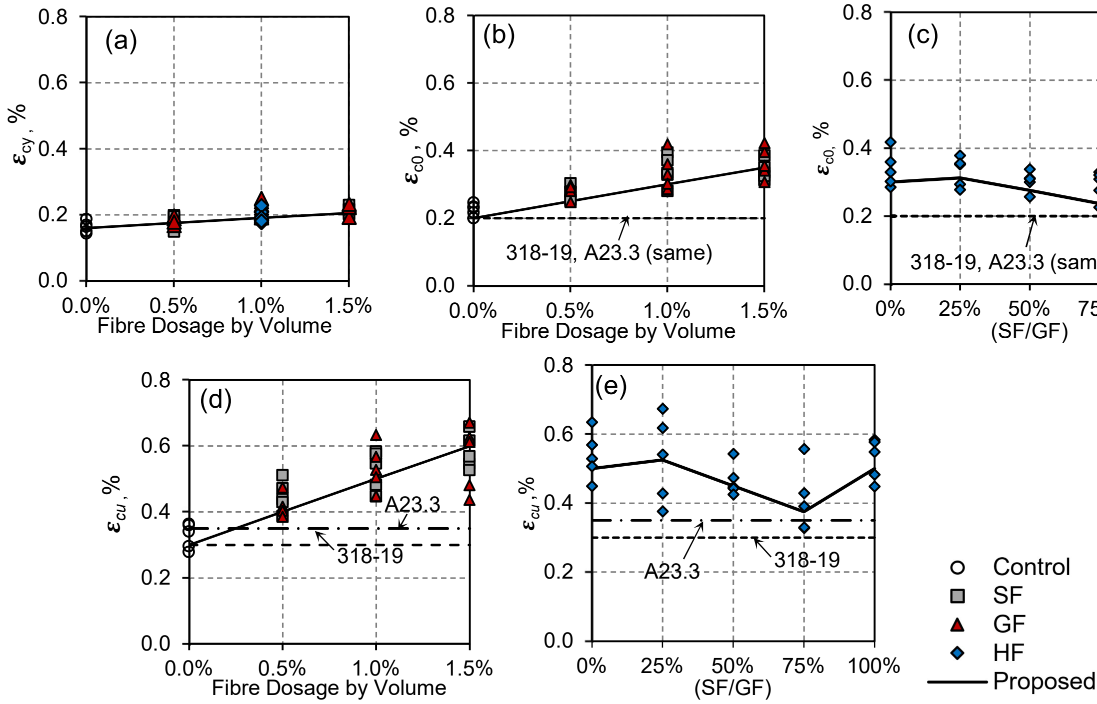

Figure 3-13: Measured and calculated of proposed and each considered code of (a) yield (all fibres), (b) peak (GF and SF only), (c) peak (hybrid), (d) ultimate (GF and SF only), (e) ultimate (hybrid) strains.

Table 3-6: Summary of performance measures of the ratio between experimental and predicted yield, peak, and ultimate strains for proposed and each considered provisions.

Mix	Factor	Proposed			ACI 318R-19			CSA A23.3:19		
		Mean	COV	AAE	Mean	COV	AAE	Mean	COV	AAE
Control	ε_y	**1.02**	**10%**	**8%**	-----	-----	-----	-----	-----	-----
	ε_{c0}	**1.13**	**8%**	**11%**	1.13	8%	11%	1.13	8%	11%
	ε_{cu}	**1.10**	**12%**	**11%**	1.10	12%	11%	0.94	12%	11%
SF.	ε_y	**1.06**	**8%**	**8%**	-----	-----	-----	-----	-----	-----
	ε_{c0}	**1.07**	**11%**	**9%**	1.59	14%	36%	1.59	14%	36%
	ε_{cu}	**1.05**	**11%**	**10%**	1.73	15%	41%	1.49	15%	31%
GF.	ε_y	**1.08**	**8%**	**8%**	-----	-----	-----	-----	-----	-----
	ε_{c0}	**1.09**	**11%**	**11%**	1.65	16%	38%	1.65	16%	38%
	ε_{cu}	**1.02**	**14%**	**11%**	1.71	18%	40%	1.47	18%	30%

	ε_y	**1.05**	**8%**	**7%**	-----	-----	-----	-----	-----	-----
HF.	ε_{c0}	**1.10**	**13%**	**14%**	1.55	13%	34%	1.55	13%	34%
	ε_{cu}	**1.04**	**15%**	**14%**	1.56	22%	33%	1.33	22%	23%

------ value does not exist in these provisions

3.4.6 Equivalent compressive stress block parameters

The trilinear model is further simplified to an equivalent tensile stress block for design. The analysis of conventional reinforced concrete flexural members at ultimate limit states is typically performed assuming a linear strain distribution and converting the concrete's nonlinear stress distribution into an equivalent stress block. This conversion is done using stress-block parameters α (ratio of maximum compressive stress to the concrete compressive strength) and β (ratio of the depth of rectangular compression block to depth to the neutral axis), which can be derived using Eqs. (3-9) and (3-10) for a range of strains, as shown in Figure 3-14, by taking the first and second moments of the area of the stress-strain relationships. The compressive concrete zone force C at crushing (ultimate) can be calculated as $\boldsymbol{\alpha_1\beta_1}\sigma_{c0}bc$ where c is the distance from the extreme compression fibre to the neutral axis and b is the section width (assuming a rectangular section).

$$\alpha\beta = \frac{\int_0^{\varepsilon_c} \sigma_c d\varepsilon_c}{\sigma_{c0}\varepsilon_c} \tag{3-9}$$

$$\beta = 2 - 2\,\frac{\int_0^{\varepsilon_c} \sigma_c d\varepsilon_c}{\varepsilon_c \int_0^{\varepsilon_c} \sigma_c d\varepsilon_c} \tag{3-10}$$

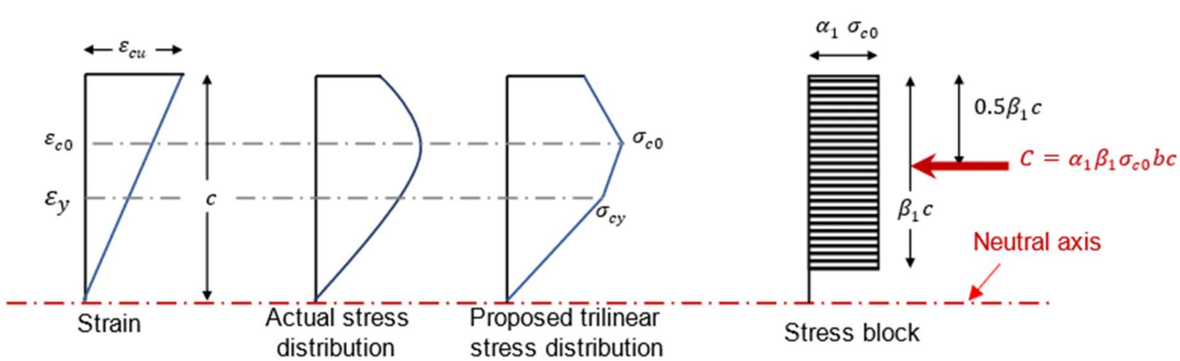

Figure 3-14: Rectangular compressive stress block at ultimate

Figure 3-15 shows the effect of fibres on stress block parameters α , β and their product $\alpha\beta$ over a range of normalized strains ($\frac{\varepsilon_c}{\varepsilon_{c0}}$). The first row of Figure 3-15 shows that increasing fibre dosage increases α due to the decreased slope of the descending branch due to increased fracture energy with increased fibre dosages (see Figure 3-3). For hybrid fibres, due to the compatibility between the larger stiffness of SFs and larger flexibility of GFs, H2-1.0 showed the largest peak α compared to H1-1.0 and H3-1.0. β increased with fibre dosage to normalized strain approximately (1.8) because adding fibres decreases the crack intensity, leading to increased ductility and an increase in β, and the response is flipped over. However, in hybrid fibres more GFs as a portion of the total dosage lead to slightly larger β because of the higher flexibility of GFs and larger peak and ultimate strain of GFs compared with SFs (see Figure 3-8 and Figure 3-9), as shown in the second row of Figure 3-15. Adding fibres increased the equivalent rectangular area, $\alpha\beta$, (third row of Figure 3-15) compared to the control mixture. Moreover, SFs increased stress-block parameters more than GFs. However, the hybrid mixtures revealed that the more GFs as a portion of the dosage, the larger the equivalent rectangular area because of the effect of increasing β with increased GFs.

Ultimate stress-block parameters in CSA A23.3:19 (plain concrete) are given by Eqs. (3-11) and (3-12):

$$\alpha_1 = 0.85 - 0.0015\, f_c' \tag{3-11}$$

$$\beta_1 = 0.97 - 0.0025\, f_c' \tag{3-12}$$

ACI-318-19 assumes α_1 equal 0.85 and β_1 is calculated as (in SI units):

$$\beta_1 = 0.85 - \frac{0.05(f_c' - 27.6)}{145000},\ 27.6 < f_c' < 55.2\ . \tag{3-13}$$

The proposed values of α_1 and β_1, can be calculated from Eqs. (3-14) and (3-15), and they are based on the conservative lower bound of α_1 and β_1 (0.75 and 0.8) found from the control cylinders in this program.

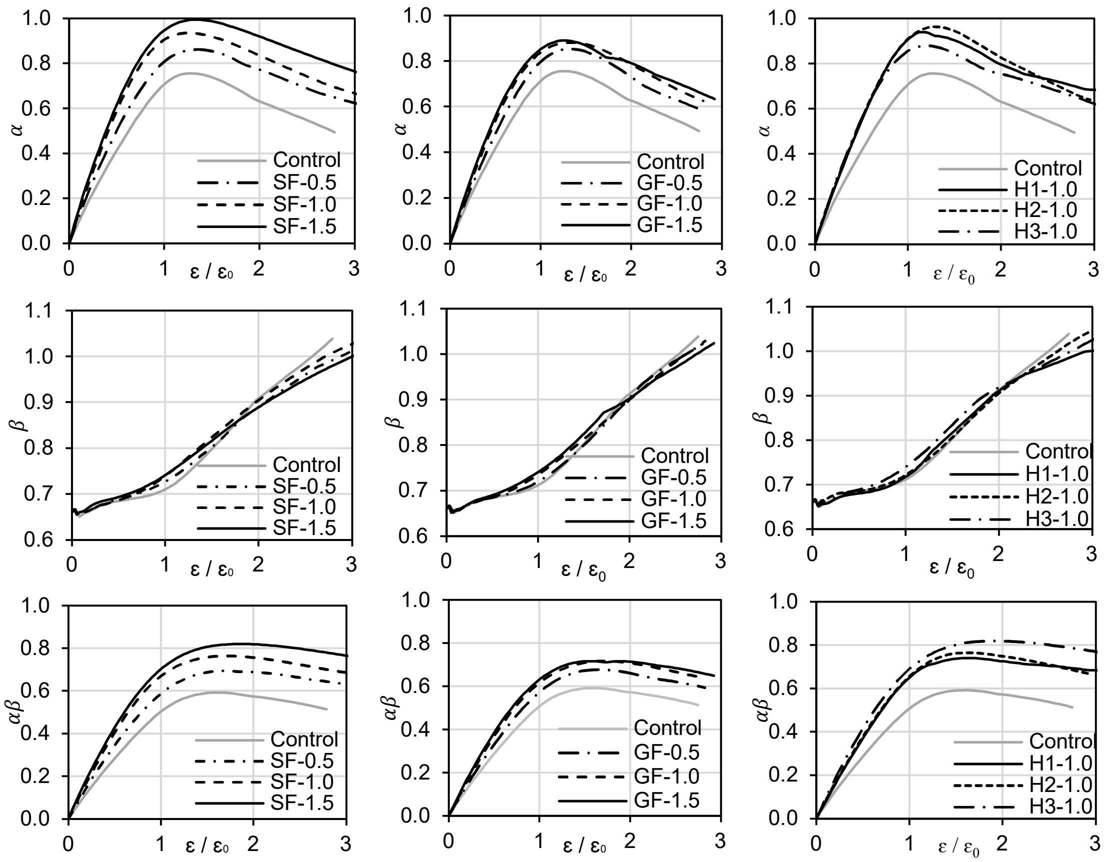

Figure 3-15: Stress-block parameters: α β and $\alpha\beta$ for control and FRC

$$\alpha_1 = 0.75 + (16V_f) \quad \text{for SF}$$

$$\alpha_1 = 0.75 + (7.5V_f) \quad \text{for GF} \tag{3-14}$$

$$\alpha_1 = 0.75 + \left[20\gamma V_f + 10(1-\gamma)V_f\right] \quad \text{for HF}$$

$$\beta_1 = 0.8 + 4V_f \quad \text{for SFs and GF}$$

$$\beta_1 = 0.8 + 4(1-\gamma)V_f \quad \text{for HFs} \tag{3-15}$$

Figure 3-16 shows the effect of fibres on stress block parameters at crushing ($\alpha_1$and β_1) corresponding to ε_{cu} from equation (8), and it can be seen that adding fibres increases $\alpha_1$and β_1 due to the effect of fibres increasing peak and residual stress. However, α_1 increased more when using SFs compared to GF. In hybrid fibres, α_1 decreases with increased portion of GFs due to their lower stiffness compared with SF, while β_1 increased with increased GFs portion due to higher flexibility of GFs and ε_{c0} and ε_{cu}. CSA A23.3-19 and ACI-319-19 expressions ((3-11)-

(3-13)) either overestimated (CSA A23.3-19) or underestimated (ACI-319-19) predictions of $\alpha_1$and β_1, since these codes are driven $\alpha_1$and β_1 for non-fibre conventional concrete, while the proposed equations (14 and 15) are more applicable in predicting FRC ($\alpha_1$and β_1), since they are based on regressing the actual data of FRC evaluated in this program.

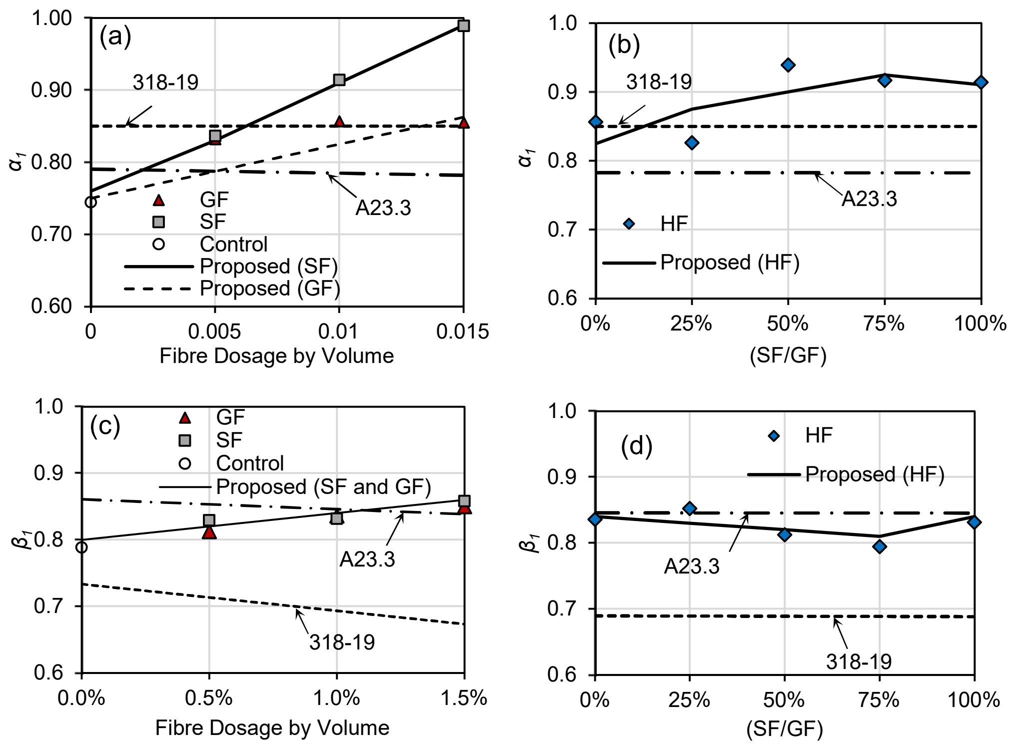

Figure 3-16: Measured (from experimental data) and calculated the proposed and each considered design code/standard for (a) α_1 (steel and glass fibre), (b) α_1 (hybrid fibres), (c) β_1 (steel and glass fibre), and (d) β_1 (hybrid fibres)

For a tension-controlled reinforced concrete beam with one layer of reinforcement, the ultimate moment strength, M_u, the neutral axis depth, c, and curvature, φ, can be obtained using equilibrium and compatibility (Eqs. (3-16)-(3-18)). Stress block parameters differ for FRC due to the effect of the fibre, leading to increased ultimate strength, decreased natural axis, and increased curvature at failure. Note that A_s, is the steel reinforcement area.

$$M_u = C\left[d - \frac{a}{2}\right] = \alpha_1\beta_1\sigma_{c0}bc\left[d - \frac{\beta_1 c}{2}\right] \tag{3-16}$$

$$c = \frac{f_y A_s}{\alpha_1\beta_1\sigma_{c0}b} \tag{3-17}$$

$$\varphi = \frac{\varepsilon_{cu}}{c} = \alpha_1\beta_1\left(\frac{\sigma_{c0}}{\sigma_{s0}}\right)\left(\frac{b}{A_s}\right)\varepsilon_{cu} \tag{3-18}$$

3.5 Conclusion and recommendations

The effect of steel and glass fibres and their combination on compressive response parameters in normal strength and density concrete mixtures was investigated. Parameters included compressive strength, elastic modulus, Poisson ratio, toughness index, strain at yield, peak, and ultimate strains. A simplified design model of the stress-strain relation for FRC was also proposed. The following was concluded:

1. Adding steel and glass fibres increases compressive strength strain at yield, peak, ultimate, and toughness index. The concrete elastic modulus was not affected significantly by adding fibres. Statistical results show that adding fibres significantly improves all compressive parameters except modulus of elasticity with a large effect (strong relation) between the groups.
2. The combinations of steel and glass (hybrid) at 1.0% dosage showed that increasing the proportion of steel fibres in the mixture increases compressive strength and toughness. However, Poisson's ratio and strain at peak and ultimate increases with increased GF percentage. This guides us to achieve better performance; for example, when stiff and deformable fibres are included, stiff fibres can increase strength and toughness, while deformable fibres can increase the deformation capacity. The proposed compressive design stress-strain relationship, both the trilinear approach and further simplified stress

block approaches, describes the behaviour of normal strength and density FRC. These relationships enable hand calculations to verify the computational results.

3. The ACI-318-19 and CSA-A23.3:19 expressions predicting design peak and ultimate strains are overestimated for FRC since they were derived for plain concrete. The proposed equations provide more accurate results in predicting the design strains in terms of mean, COV, and AAE for the tested concrete mixtures. The proposed stress block parameters at crushing account for the fibre effect and provide more accurate results than ACI-318-19 and CSA-A23.3-19, which were driven for conventional concrete and that is expected since this study is fitted the actual data.

The results of this study indicate that using more than one fibre (SFs and/or GFs) shows promise in FRC application compared to mono-fibre mixtures. Future work should investigate a different combination of fibres and how this will affect compressive response. The expressions here provide a tool to help engineers with the design of reinforced concrete structures when double-hooked SFs and GFs with V_f (0% to 1.5%) were added into the normal to medium strength concrete, f_c' (40 to 55 MPa). Future testing can improve these models with more fibre types, aspect ratios, and dosages beyond the ones used in this study to develop the proposed expressions.

CHAPTER 4

CRACK BEHAVIOUR AND FLEXURAL RESPONSE OF STEEL AND CHOPPED GLASS FIBRE-REINFORCED CONCRETE: EXPERIMENTAL AND ANALYTICAL STUDY

4.1 Introduction

Fibres have been utilized as reinforcement since prehistoric times when straw and mortar were used to produce mud bricks, and horse-hair was used for reinforcement. As technology developed, cement was reinforced by asbestos fibres (asbestos-cement) at the end of the 19th century. Asbestos cement was extensively used during World War II to make easily-built, sturdy and inexpensive structures for military purposes. Research in the mid-20th century on composite materials led to new materials like glass and synthetic fibres that replaced asbestos since asbestos exposure is directly related to life-threatening diseases (Campopiano et al. 2009).

Fibres can enhance concrete's brittle tensile behaviour because fibres arrest the cracks and act as bridges between cracks, leading to improved peak and post-cracking performance. Fibres are used in normal strength concrete (NSC) to control plastic shrinkage and drying shrinkage cracking (Eren and Marar 2010) while also lowering concrete permeability and reducing water bleeding (Pannirselvam and Manivel 2021).

Many recent studies have evaluated the flexural response of Fibre-Reinforced Concrete (FRC) with different fibres, including metal, synthetic, and mineral fibres. For instance, (Yoo, Yoon, and Banthia 2015; Simões et al. 2017; Branston et al. 2016; Shafiq, Ayub, and Khan 2016; Babaie, Abolfazli, and Fahimifar 2020; Jiang et al. 2014) investigated the use of steel, glass, basalt, polymer, and polyvinyl alcohol (PVA) fibres in concrete and found that flexural strength and post-cracking performance increased with fibre dosage. However, others reported that PVA did not significantly affect flexural strength; PVA and basalt fibres did not contribute to the post-cracking behaviour (Shafiq, Ayub, and Khan 2016). Adding fibres such as glass and basalt increases flexural strength and fracture energy (Kizilkanat et al. 2015; Arslan 2016). Glass fibres have attracted attention as they offer beneficial improvements to plain concrete such as crack control, impact resistance, fatigue resistance, and abrasion resistance (Madhkhan and Katirai 2019). Glass also contributes more to the durability performance of different alkali concrete environments (D'Antino and Pisani 2019; Holubová et al. 2017).

The effect of a hybrid combination of more than one fibre type on flexural and fracture properties has been examined. Many researchers identified mechanical and fracture properties enhancements with various fibre combinations (Almusallam et al. 2016; Babaie, Abolfazli, and Fahimifar 2020; Banthia and Sappakittipakorn 2007; Sivakumar 2011; Chasioti and Vecchio 2017; Pereira, Fischer, and Barros 2012). However, there are limited studies on the effect of using steel and glass fibres in NSC, especially with longer fibre lengths and larger dosages. Thus, this study investigated this combination to evaluate the benefits of non-corrosive and deformable glass fibre with higher stiffness steel fibres, potentially leading to reduced production and construction costs.

Several techniques have been proposed to model the tensile stress-strain relationship of FRC, with most of them developed for steel fibre-reinforced concrete (SFRC). (Lim, Paramasivam, and Lee 1987) Lim et al. (1987) developed relationships using the law of mixtures and steel fibre pullout tests. The limitation of the law of mixtures is that not all fibres are effective because of their random orientation in the concrete; only fibres aligned with the tensile stress are effective at controlling cracks. RILEM TC 162-TDF (RILEM TC 162-TDF 2000) and Barros and Figueiras (Barros and Figueiras 2001) suggested a relationship based on fracture energy that uses results from beam-bending tests to determine peak and post-cracking stresses. The main concern is the accuracy and objectivity of RILEM TC 162- TDF, which determines horizontal strains using vertical deflections (Kooiman and Walraven 2000).

The work presented in this study adopts inverse analysis, which is a general approach that is gaining researcher attention (Elsaigh, Robberts, and Kearsley 2012; Labib 2008; Tlemat, Pilakoutas, and Neocleous 2006; Alguhi and Elsaigh 2016). The inverse analysis is considered in the latest Canadian bridge code (CSA S6.1:19 2019). The American Concrete Institute adopted inverse analysis in ACI 544.4R-18 (2018) report based on the closed-form approach derived by Soranakom and Mobasher (2008, 2009). The advantage of inverse analysis is that the flexural response of FRC can be obtained with minimal complexities compared to procedures requiring results from direct tensile tests.

Different techniques, such as notches and the red dye penetrant method, have been used to locate cracks and direct crack propagation. Digital Image Correlation (DIC) is an alternative for measuring crack propagation and widths due to the high accuracy of measuring the full field surface crack mentoring that can identify small cracks that cannot be identified using a red dye penetrant (McCormick and Lord 2010). Sensors like extensometers, strain gauges, and linear variable differential transducers (LVDT) are used in many experiments but do not show full-field displacements/strains and may miss early crack detection and local failures in tests compared to DIC (Ibeawuchi, Moffatt, and Lloyd 2019).

Previous research has not extensively explored the use of steel and glass fibres in NSC, particularly with regard to longer fibre lengths and larger dosages. This study aims to fill this gap by examining the effect of material (steel and/or glass) and dosage (0.5, 1.0 and 1.5% volume fraction) to reap the advantages of combining non-corrosive, deformable glass fibres with higher stiffness steel fibres. The goal is to improve mechanical properties and reduce production and construction costs while still achieving the desired properties. To measure crack propagation and widths, this study explores the feasibility of using DIC instead of traditional sensors like extensometers, strain gauges, and LVDTs. DIC allows for full-field displacement and strain measurements, enabling early crack detection and local failure identification. Most available models for the tensile stress-strain relationship of FRC have been developed for SFRC. In contrast, this study uses a validated inverse analysis approach to generate a more general model for SFRC and GFRC as well as SFs and GFs in reinforced concrete, which can be simplified for practical engineering use.

4.2 Experimental Program

The flexural response and split tensile strength of FRC mixtures were investigated using 40 prisms and 100 cylinders. Steel and glass fibres were considered independently and blends between them.

4.2.1 Material proportions

General-use cement (70% by weight) and Type-F fly ash (30% by weight) were used as binders. This is a common ratio used for concrete in Alberta to improve concrete's long-term strength and durability (Johnston 1996) and reduce cement content. The cement specifications are according to CSA A3000 (CAN/CSA-A3000-13 2013) and ASTM C150 (ASTM C150 2000), while fly ash is classified based on ASTM C618 (ASTM-C 618-15 2015). The chemical composition and Physical properties of fly ash and cement are described in Table 4-1 and Table 4-2. Tap water was used for all mixes. A high-range water reducer, HRWR Sika® ViscoCrete® 1000, was added to concrete mixtures to reduce water content and improve workability.

Typical aggregates used in normal strength strength-ready mix concrete in the Edmonton, Canada region were also used in this study. Pea gravel with a maximum nominal size of 20 mm was used as ,the coarse aggregate while natural river sand with a nominal maximum particle size of 4.75 mm was used as fine aggregate. The measured bulk-specific gravity and water absorption of coarse and fine aggregates are 2.6 and 2.8 and 1.32 and 1.43%, respectively.

Table 4-1. Chemical composition for fly ash using X-ray diffraction and cement according to manufacturing mill test certificate report

Oxide composition (%)	FA
Al_2O^3	15.79
SiO^2	50.82
Fe_2O^3	7.81
Al_2O^3+ SiO^2+ Fe_2O^3	74.42
SO^3	1.21
K_2O	1.39
CaO	20.64
TiO^2	1.72
MnO	0.1
SrO	0.32
ZrO^2	0.2
Loss of ignition	1.04
Moisture content	0.10

Oxide composition (%)	Cement
CaO	62.85
SiO_2	19.50
Al_2O^3	4.84
Fe_2O^3	3.59
MnO	2.51
SO^3	2.72
Na_2O	0.49
K_2O	0.18
Loss of ignition (%)	2.70
Insoluble residue	0.40
Free calcium oxide	1.4
Potential Phase Compounds (%)	
C_3S	63
C_2S	9
C_3A	7
C_4AF	11
Equivalent Alkalis	0.5

Table 4-2. Chemical composites for fly ash and cement according to manufacturing test report

Propriety	Cement	FA
Type	General use (GU)	Type-F
Specific gravity	3.15	2.09
Blaine Fineness (m^2/kg)	426	--
Retained 45 µm (No.325) sieve (%)	4.7	26.1
Autoclave expansion (%)	0.5	-0.01

Double-hooked end steel fibres (SFs) and glass fibres (GFs), as shown in Figure 4-1, were used. Table 4-3 gives fibre properties obtained from manufacturers. SFs were used as a reference since they have been investigated more comprehensively. The fibre lengths play a major role in increasing splitting tensile strength and fracture energy (Han et al. 2019), so this study uses longer lengths of (SFs) and (GFs) This study uses Alkali Resistant (AR) GFs with added zirconium-oxide to help resist alkalinity-attack. This is essential since concrete is a very alkaline environment. AR-GFs provide extra deformability and durability as well as have expected lower water absorption and increased chemical resistance compared to other chopped fibres such as steel and natural fibres.

Table 4-3. Properties of chopped fibres

Properties	Steel Fibres (SF)	Glass Fibres (GF)
Material	Cold Drawn Wire Steel	Alkali Resistant Glass
Shape	Double-hook end	Plain
Diameter (mm)	0.92	0.54
Length (mm)	50	36
Aspect ratio (length/diameter)	55	67
Tensile modulus of elasticity (GPa)	200	72
Tensile strength (MPa)	1200	1700
Specific gravity	7.75	2.68

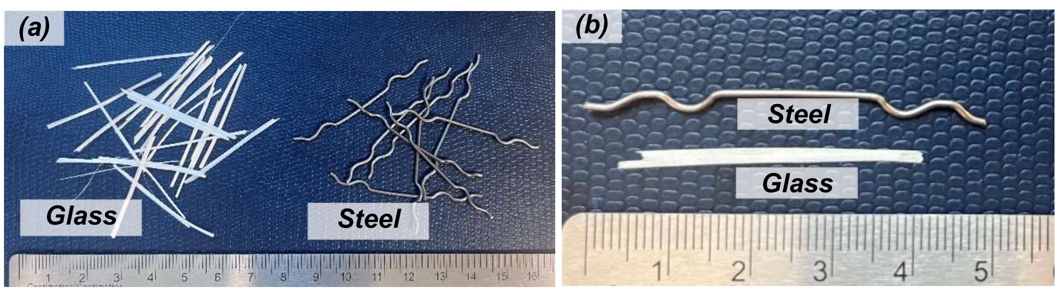

Figure 4-1: (a) Photo of fibres used in test program and (b) zoomed-in photo showing shapes and sizes of each fibre. Ruler shown for scale with dimensions in cm.

4.2.2 Concrete mix design, casting, and curing

The ACI Absolute Volume method (ACI 211.1-91 1991) was used to design ten mixtures: one control (no fibre) mixture and nine FRC mixtures. Mixtures were developed after completing trial batches that targeted a 28-day concrete compressive strength between 35 and 55 MPa with a minimum slump of 150 mm for the control. The FRC mixtures were divided into SFs, GFs, and a combination of steel and glass as a hybrid (H). Three fibre contents (0.5, 1.0, and 1.5% volume fraction) were studied for both SFs and GFs. For the hybrid mixtures, a fibre volume fraction of 1.0% was used with the three ratios of SFs to GFs: H1-1.0: 0.75% steel + 0.25% glass, H2-1.0: 0.50% steel + 0.50% glass, and H3-1.0: 0.25% steel + 0.75% glass, as shown in Table 4-4.

Table 4-4: Concrete mixture proportioning and designation. Quantities are given per cubic metre of concrete.

Mix ID	Fibre Type and Dosage	W/CM	Cement (kg)	Fly ash (kg)	Water* (kg)	CA (kg)	FA (kg)	Fibre (kg)	S.P (kg)
Control	No fibres	0.35	280	120	166	1147	764	0.00	2.0
SF-0.5	0.5% SF		280	120	166	1138	759	37.5	2.0
SF-1.0	1.0% SF	0.35	280	120	166	1130	754	75.0	2.0
SF-1.5	1.5% SF		280	120	166	1122	748	113	2.0
GF-0.5	0.5% GF		280	120	166	1138	759	12.9	2.0
GF-1.0	1.0% GF	0.35	280	120	166	1130	754	25.8	2.0
GF-1.5	1.5% GF		280	120	166	1122	748	38.7	2.0
H1-1.0	1.0% (0.75%SF+0.25%GF)		280	120	166	1130	754	---	2.0
H2-1.0	1.0% (0.50%SF+0.50%GF)	0.35	280	120	166	1130	754	---	2.0
H3-1.0	1.0% (0.25%SF+0.75%GF)		280	120	166	1130	754	---	2.0

SF: Steel fibre, GF: Glass Fibre, H: Hybrid, CM: Cementitious materials, CA: Coarse aggregate, FA: Fine aggregate, and SP: Superplasticizer. *Including allowance for absorption.

Dosages between 0.5% and 1.5% are expected to be optimal for FRC. Dosages less than 0.5% were not considered since they do not significantly affect post-cracking behaviour (Branston et al. 2016), which is the primary goal of this study. Dosages larger than 1.5% are expected to have physical difficulties in creating a homogenous FRC, leading to a decrease in performance compared to plain concrete (Altun, Haktanir, and Ari 2007).

FRC was mixed in a portable electrical drum mixer with a capacity of 155 litres. Coarse and fine aggregates were placed in the mixer first and mixed for one minute. Cementitious materials (cement and fly ash) were added and mixed for two more minutes; water was then added gradually for 2 to 3 minutes. Finally, fibres were added gradually with superplasticizer for 3 to 4 minutes to achieve more uniform fibre distribution. The total mixing time for each FRC batch was between 8 and 10 minutes. Mixed concrete was placed in cylinder and prism moulds in two layers and compacted using a vibrating table with a frequency of 60 to 90 Hz. Samples were demoulded 24 hours after casting and placed in a lab room (temperature 25±2°C and relative humidity 35±5%). After another 24 hours, these samples were placed in a controlled humidity room (temperature 20±2°C and relative humidity 70±5%) until testing (after 28-32 days).

4.3 Test protocols

4.3.1 Flexural test

Forty prisms (150 × 150 × 500 mm) were prepared in this study per ASTM C1609 (ASTM C1609/C1609M-10 2010). Prisms were tested using a 1000 kN capacity MTS 311.31 machine (Figure 4-2 (a) and (b)) at 1.0 mm/min, corresponding to a loading rate of 0.25±0.05 MPa/s in the elastic region. The deflection was measured using two LVDTs with a precision of ±0.002 mm. Data were continuously recorded at 5 Hz. Flexural strength, f_f, was obtained using Eq. (4-1) based on the peak load from the load-deflection (L-δ) curves.

$$f_f = \frac{PL}{bd^2} \tag{4-1}$$

Where, P, is the peak load (N), L, is the span length (mm), b, and d, are the width and depth of the specimen (mm).

The equivalent flexural strength ratio, $R_{T,150}^{D}$, can be obtained using Eq (4-3) .

$$R_{T,150}^{D} = \frac{150.T_{150}^{D}}{f_1.b.d^2}.100\% \tag{4-2}$$

Where, $R_{T,150}^{D}$, is the equivalent flexural strength ratio, T_{150}^{D} , is the area under load vs deflection (N.mm), f_1, flexural strength (MPa), and d, are the width and depth of the specimen (mm)

4.3.2 Splitting tensile strength test

Split tensile strength was measured by testing fifty 100 × 200 mm cylinders per ASTM C-496/496M (ASTM C469-11 2008) (Figure 4-2(c) and (d)). Tests were performed on a compression testing machine by applying a load at 1.0 MPa/min. Splitting tensile strength can be found using Eq. (4-3).

$$f_{s.t} = \frac{2P}{\pi l d} \tag{4-3}$$

Whare: $f_{s.t}$, is splitting tensile strength (MPa), P, is the maximum applied load indicated by the testing machine (N), l, is length, (mm), and d, is the diameter (mm).

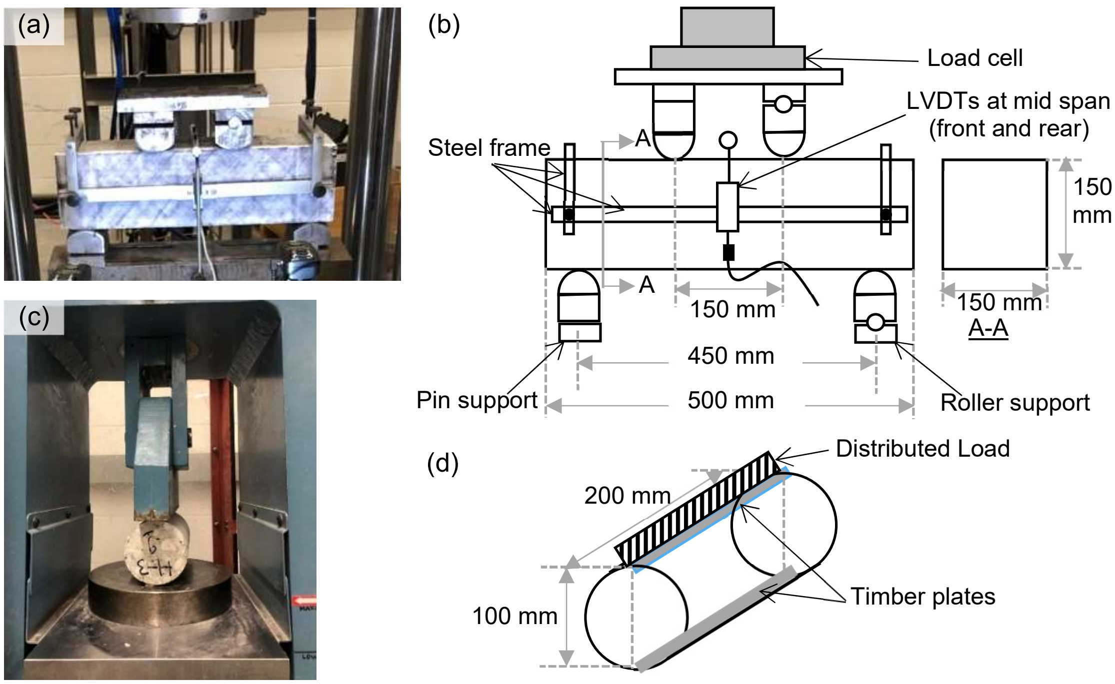

Figure 4-2: (a) a photo of a four-point loading (4PLB) test setup, (b) the dimensions of the loading system and the sensors used for the 4PLB test, (c) a photo of splitting tensile strength test setup, and (d) dimension of loading system used for the splitting tensile strength test

4.3.3 Digital image correlation (DIC) setup

Crack formation and growth along the gauge length are analyzed using DIC for four specimens for each mix. Three were assessed with the steel frame, while the fourth one was free of the steel frame to investigate the full-field displacements/strains. One face of each specimen was prepared with white paint and a random black speckle pattern (Figure 4-3 (a)) using stamp rollers with 0.33 mm dot size to obtain high contrast (Figure 4-3 (b)). This produces an area of interest with low noise that may be tracked with high certainty. As shown in Figure 4-3 (c), two Canon EOS Rebel-T6 cameras with a 5184 × 3456 resolution were positioned 200 mm apart on a tripod and 750 mm away from the specimen such that the specimen fills the field of view of both cameras. Images were taken every 10 seconds. A light source was used to illuminate the field of view. Necessary adjustments to focus, aperture and exposure time were made to ensure high image quality. Data were processed using Correlated Solutions Vic-2D software.

Crack Mouth Opening Displacement (CMOD) was measured using DIC, and virtual pairs of points were selected on either side of each crack at the extreme tension face of the member. These points measure the absolute horizontal displacement difference, which will be discussed later. The advantage of extracting CMOD with DIC is that results include all cracks in the tension zone, not just a single crack, as seen in the notched beam method. DIC can also track full-field cracks and gather more information about strains without needing particular load stages and specific strain gauges compared to the notched beam method, which provides discrete measurements of a single predefined location along the notch.

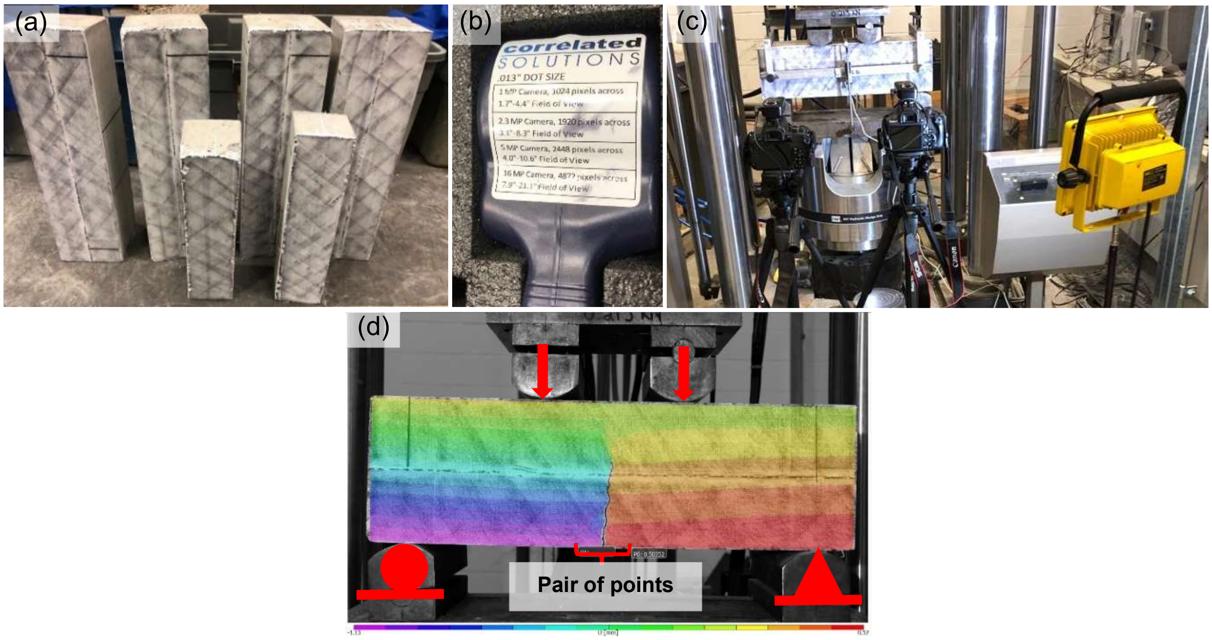

Figure 4-3: DIC: (a) speckle samples, (b) interchangeable stamp rollers, (c) set up, (d) CMOD measurements.

4.3.4 DIC Verification

DIC verification was done by comparing load-deflection curves for LVDT and DIC at mid-span for each prism, as shown in Figure 4-4. Agreement was observed between LVDT and DIC results for all prisms. This gives more confidence in DIC for tracking crack widths and fracture behaviour.

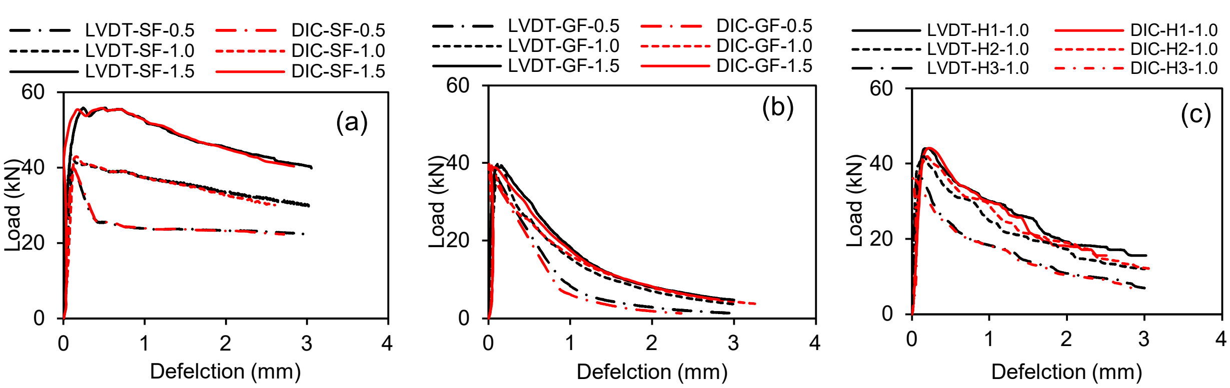

Figure 4-4: Measured (LVDT) and extracted (DIC) load-deflection responses of (a) SFs, (b) GFs, (c) hybrid

4.4 Test Results and Discussion.

The mechanical properties of the tested mixtures are summarized in Table 4-5. In particular, properties included density ρ, compressive strength f_c', modulus of elasticity E_c, flexural strength f_r, and split tensile strength $f_{s.t}$, respectively. The f_c', is measured using ASTM () standard (ASTM C39 / C39M-05a 2005) and E_c is calculated according to (ASTM C469/C469M 2014).

Table 4-5: Density, compressive strength, flexural strength, and splitting tensile strength.

Mix Type	ρ, kg/m^3	f_c', MPa	E_c, GPa	$f_{s.t}$, MPa
Control	2456±29	41.8±5	24.5±1.6	3.5±0.35
SF-0.5	2586±30	46.2±5	25.4±1.0	4.6±0.28
SF-1.0	2615±27	49.8±2	23.6±1.1	6.1±0.86
SF-1.5	2640±33	52.5±4	25.1±1.7	6.8±0.80
GF-0.5	2384±19	45.6±2	23.8±1.2	4.6±0.55
GF-1.0	2408±09	47.0±3	22.7±2.0	4.9±0.27
GF-1.5	2407±15	47.5±2	22.2±1.1	5.3±0.34
H1-1.0	2446±19	52.7±2	24.6±1.1	5.8±0.53
H2-1.0	2417±07	51.9±3	24.2±0.9	5.3±0.53
H3-1.0	2406±13	47.5±4	23.2±3.2	5.0±0.52

± is the standard deviation (SD)

Table 4-6 shows the average results from three flexural prism samples per ASTM C1609. Results reported include: P_p peak load, f_p peak strength, δ_p net deflection at peak load, P_{600}^D and f_{600}^D are the load and strength corresponding net deflection equal to L (prism's span)/600 (0.75 mm), P_{150}^D and f_{150}^D are load and strength corresponding net deflection equal to L/150 (3.0 mm), T_{150}^D is the area under the load-deflection curve between zero and L/150, and $R_{T,150}^D$, is the equivalent flexural strength ratio that refers to the remaining strength of concrete after the peak load at the deflection of L/150.

Table 4-6: Summary of Flexural test results.

Mix Type	P_p, kN	f_p, MPa	δ_p, mm	P_{600}^D, kN	f_{600}^D, MPa	P_{150}^D, kN	f_{150}^D, MPa	T_{150}^D, kNmm	$R_{T,150}^D$, %
Control	33.5±0.4	4.5±0.12	0.025±0.002	-----	-----	-----	-----	0.4±0.06	0.10±0.01
SF-0.5	37.3±3.2	5.0±0.43	0.079±0.005	19.0±1.7	2.5±0.2	15.7±1.2	2.1±0.16	57.1±5.34	50.8±4.43
SF-1.0	42.5±1.4	5.7±0.18	0.124±0.011	37.8±2.7	5.0±0.4	25.0±1.2	3.4±0.27	98.6±7.94	77.3±3.88
SF-1.5	53.5±5.7	7.1±0.77	0.152±0.009	51.3±3.6	6.8±0.5	35.9±4.0	4.8±0.53	133±10.7	83.4±5.19
GF-0.5	37.3±1.3	5.0±0.17	0.093±0.007	11.7±1.0	1.6±0.1	1.2±0.1	0.2±0.01	25.6±2.25	22.9±1.27
GF-1.0	41.6±2.3	5.5±0.32	0.121±0.007	17.4±1.9	2.3±0.3	2.6±0.3	0.3±0.03	36.7±4.01	29.6±3.78
GF-1.5	44.5±4.4	5.9±0.56	0.130±0.012	27.0±2.1	3.6±0.3	5.6±0.8	0.8±0.10	54.9±6.95	41.1±1.21
H1-1.0	43.0±1.3	5.7±0.17	0.142±0.016	32.3±0.7	4.3±0.1	14.7±1.8	2.0±0.23	73.8±4.59	57.2±1.92
H2-1.0	43.2±1.3	5.7±0.14	0.162±0.009	34.0±2.2	4.5±0.3	15.0±2.1	2.0±0.27	75.8±8.91	58.6±5.55
H3-1.0	39.3±1.7	5.2±0.27	0.105±0.004	23.4±1.2	3.1±0.2	7.8±0.75	1.0±0.14	52.6±6.28	45.0±5.46

---- No data available. term after ± is the standard deviation (SD).

4.4.1 Load-deflection response

The load-deflection response of the tested prisms is shown in Figure 4-5. In the pre-crack stage, adding fibres appears to decrease prism stiffness due to a decrease in the modulus of elasticity with adding fibres (parallel fibres act as voids that reduce stiffness (Suksawang, Wtaife, and Alsabbagh 2018)). Post-cracking response, including flexural strength, residual stress, and toughness, increased significantly with the addition of fibres since fibres activated crack bridging and enhanced post-cracking response. The GF prisms had lower flexural strength and toughness than SF prisms because of the weakness of the fibre in the transverse direction. The replacement of SFs with GFs by 50% (H2-1.0) had similar flexural strength and post-cracking as the replacement of 25% of SFs by GFs. Though GFs have lower stiffness than SFs, they control cracks at an early loading, and fracture is restrained at similar levels.

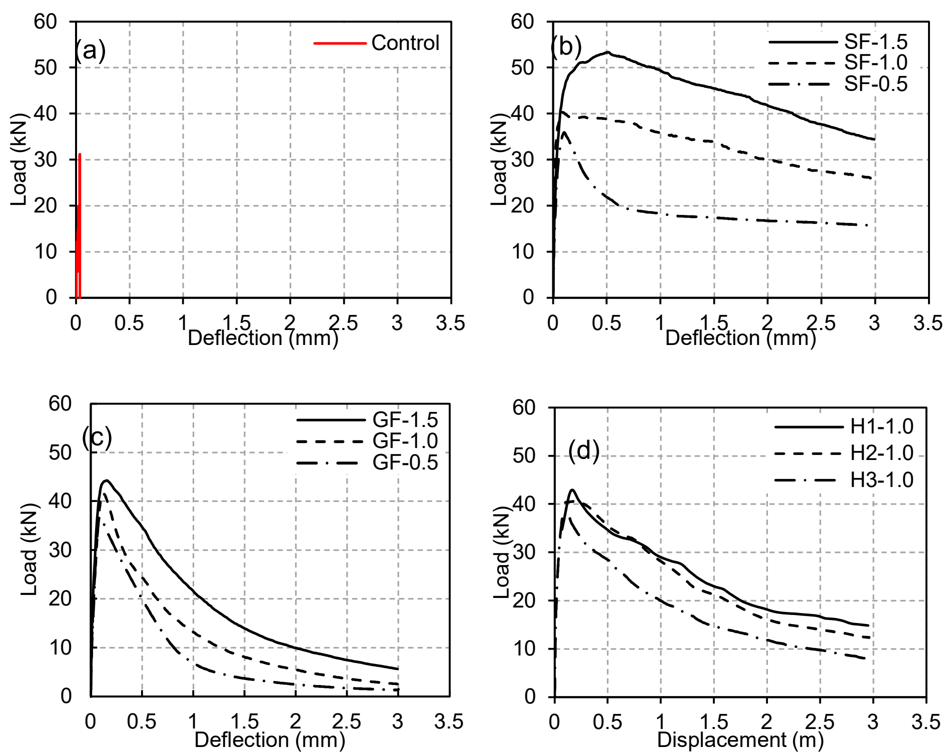

Figure 4-5: Load-deflection response of tested prisms (a) control, (b) SFs, (c) GFs, (d) hybrid.

4.4.2 Flexural response parameters

Flexural strength is shown in Figure 4-6(a). The flexural strength of SF prisms increased by 11, 27, and 58%, and GF prisms increased by 11, 22, and 31% for 0.5, 1.0, and 1.5% dosages respectively. This increase is attributed to crack bridging and delayed crack propagation. SFs increase flexural strength more than GFs because of GFs' anisotropic response, which is the weakness in the transversal direction controlled by resin. The SF profiles also have a double hook end that provides more anchorage than the unhooked GFs since GF hooks would be difficult to fabricate and have reduced capacity. There is almost no effect on flexural strength if GFs replace SFs up to 50% for H1-1.0 and H2-1.0. However, for 75% of GFs, the flexural strength decreased by 10% (H3-1.0) because this amount of GF replacement of SF leads to a decrease in the mix density.

The net deflection at peak load, δ_p, is presented in Figure 4-6 (b). δ_p increases with increased fibre dosage, so adding 0.5, 1.0, and 1.5% increased δ_p by 2.2, 4.0, and 5.1 times for SFs and 2.7, 3.8, and 4.2 times for GFs, respectively. SFs showed an almost linear increase with fibre dosage with a similar increase using GFs until 1.0%, but with lower peak load due to the GFs' flexibility (higher deformation), and further increasing GF dosages had little effect on δ_p. H2-1.0 had the largest δ_p which is attributed to interlocking between the two fibre types and the enhanced bond between fibres and concrete. However, increasing the GF percentage to 75% reduces the δ_p because of more tearing of GFs due to the weakness in the transverse direction.

Residual stress is investigated in terms of stresses corresponding to (0.75 and 3.0) mm deflection per ASTM C1609. As shown in Figure 4-6(c) and (d), residual strength increases with fibre dosage despite the fibre type. This is the main improvement of adding fibres that bridge cracks and limit crack propagation. Adding 0.5, 1.0, and 1.5% fibres increases the residual stress at 0.75 mm of SFs by 2.5, 5.0, and 6.8 times and by 1.6, 2.3, and 3.6 times for GFs, respectively. The residual stress corresponding to 3.0 mm improved by 2.1, 3.3, and 4.8 times and 0.20, 0.30, and 0.80 times for SFs and GFs, respectively. SFs exhibited a steep linear increase with an increase in fibre dosage for residual stresses at both 0.75 mm and 3.0 mm. GFs showed a more gradual linear increase in residual stresses at 0.75 mm with increased dosage. The residual stress at 3.0 mm slightly increased with increased GF dosage. Increasing the GF portion from 25% to 50% in hybrid mixtures did not change the residual stresses at 0.75 mm and 3.0 mm, but increasing the GF portion to 75% decreased residual stresses at both 0.75 mm and 3.0 mm. Adding GFs decreases workability and consolidation, which is expected to lead to reduced residual strengths.

What stands out in Figure 4-6(e) is the effectively linear increase in toughness with fibre dosage. When dosage increased from 0.5 to 1.0 and 1.5%, toughness increased by 73 and 130%, respectively, for SFs. For GFs, the increase was 43 and 110%, respectively. The reduced toughness increase with GFs may be due to damage to GFs' resin, which leads to tearing before fibres reach their capacity. Increasing the GF portion up to 50% in hybrid mixes has a limited effect on toughness, but increasing the GF portion to 75% reduces toughness by 40% compared with H1-1.0.

The equivalent flexural strength ratio R_T, is shown in Figure 4-6(f), determined from the energy absorption capacity and the strength measured from the tests. R_T is strongly dependent on fibre dosage. The increased fibre dosage from 0.5% to 1.0% and from 0.5% to 1.5% leads to an increase in R_T of 53 and 64% for SFs and 31 and 80% for GFs, respectively. The GF prisms had a gradual linear increase of R_T with dosage, whereas the SFs had a large increase of R_T with dosages up to 1.0% but reduced effectiveness with a 1.5% dosage. Increasing the GF portion to 50% in H2-1.0 has a trivial increase in R_T, but when this portion rises to 75%, R_T decreases by

23% attributed to the higher porosity associated with GF mixtures (Simões et al. 2017) compared with SF mixtures.

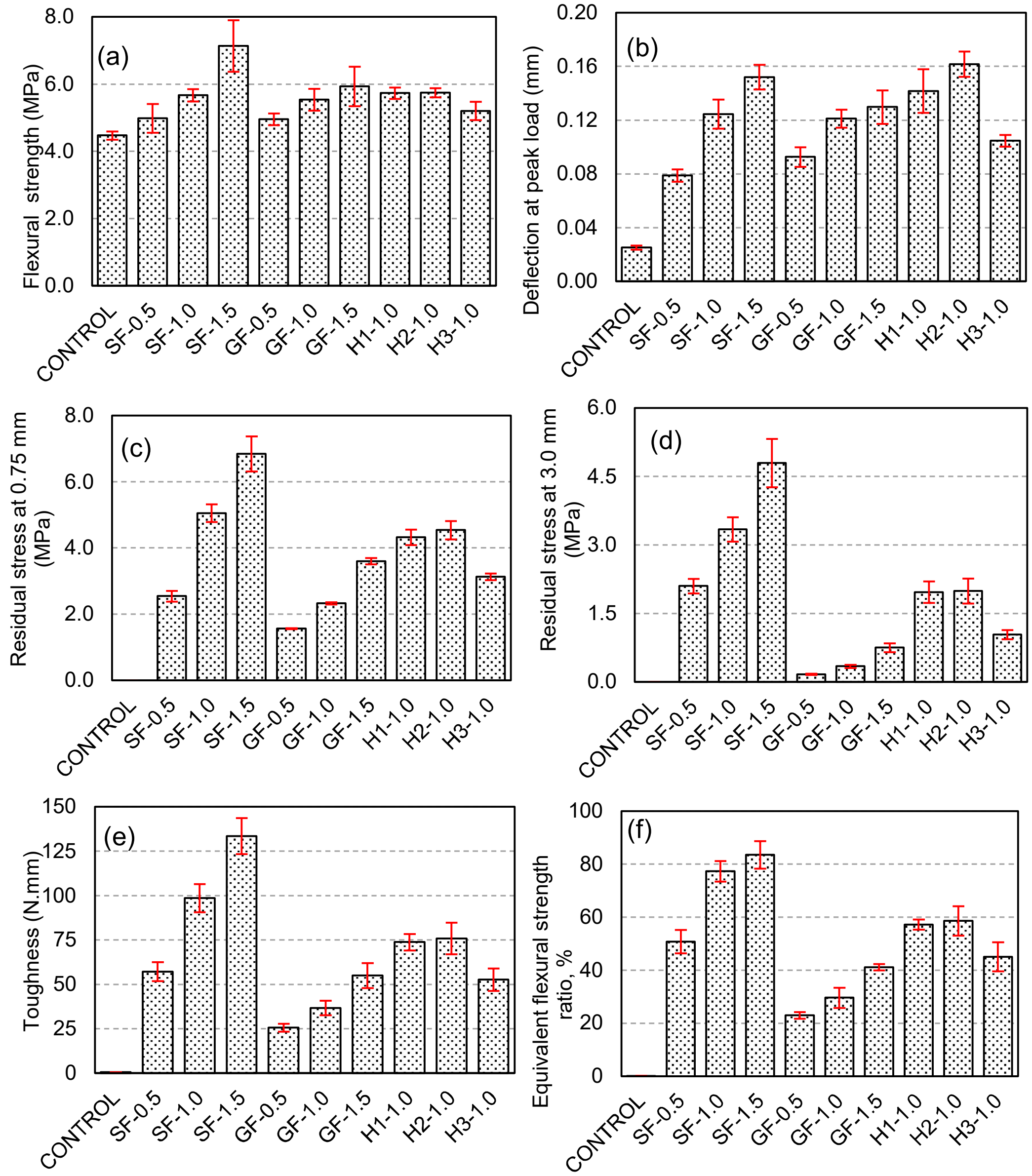

Figure 4-6: (a) Average flexural strength for each parameter, (b) Average net deflection at peak load for each parameter, (c) Average residual stress at 0.75 m and (d) 3.0 mm, (e) Average toughness, and (f) Average equivalent flexural strength ratio. Error bars denote one standard deviation from the mean.

4.4.3 Cracking response

The load-CMOD response is shown in Figure 4-7 for an average of three samples of each mixture. The average load-carrying capacity for control prisms was 20.3 kN with no descending branch, as failure occurs immediately after the prism cracks. All FRC samples showed strain softening after first cracking, except for SF-1.5, which showed strain hardening due to the higher content of SFs in the mixture. Peak load and flexural strength are remarkably improved, as discussed earlier. Adding fibres, as expected, decreased crack width due to fibre bridging. The beneficial reduction in crack widths decreased between 1.0 to 1.5% dosages, possibly due to fibre saturation.

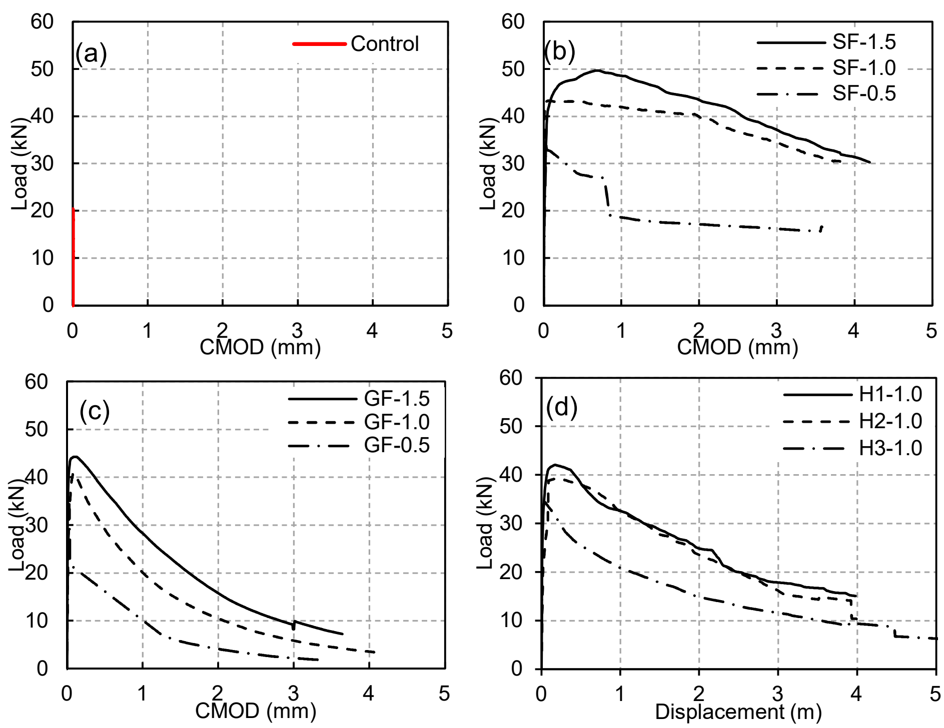

Figure 4-7: Flexural load and CMOD of FRC: (a) control, (b) SFs, (c) GFs, and (d) hybrid

Adding fibres increases residual strength and fracture energy. The GF prisms had lower peak load and fracture energy than SF prisms because of the weakness of the fibre in the transverse direction. Replacing up to 50% of SF by GF did not show any significant change in H1-1.0 and H2-1.0 prisms due to compatibility between SF's strength, GF's deformability, and the ability to restrain cracking at different scales of the cracking process. However, when the GF portion increased to 75% (H3-1.0), it negatively affected both peak load and fracture energy.

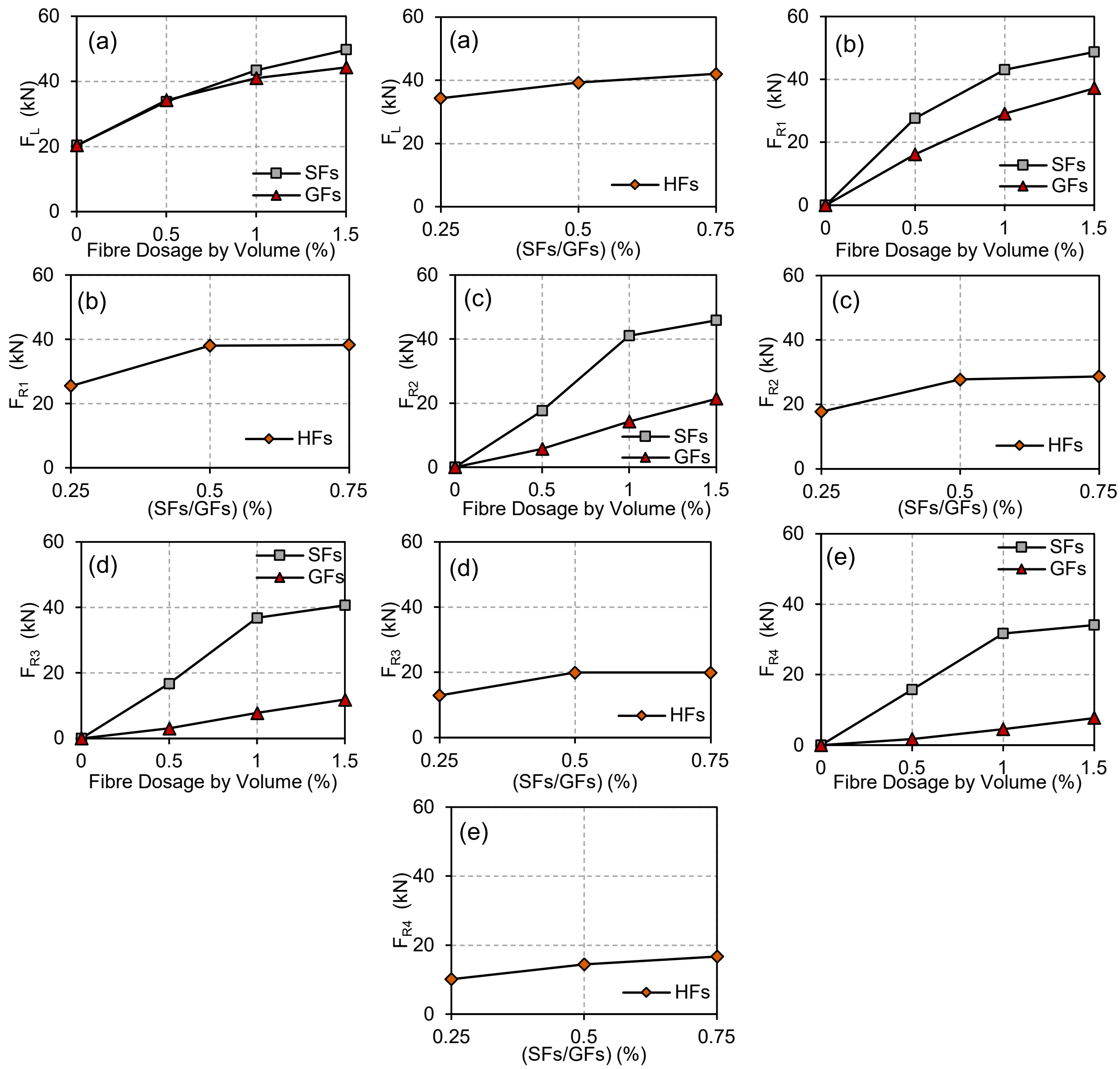

Figure 4-8: Average L-CMOD parameters: (a) peak load (F_L), (b) load corresponding COMD equal 0.5 mm (F_{R1}), (c) load corresponding COMD equal 1.5 mm (F_{R2}), (d) load corresponding COMD equal 2.5 mm (F_{R3}), (e) load corresponding COMD equal 3.5 mm (F_{R4})

Remarkably, the residual load corresponding to CMOD of 0.5 mm increased by 54% and 75% when the fibre dosage was increased from 0.5% to 1.0% and 1.5%, respectively, for SFs. For GFs, the increase was even more significant at 81% and 130% for 1.0% and 1.5% fibre dosages, respectively. The remaining residual parameters exhibit a similar trend of increasing with fibre dosages, with the exception of SFs, where it is worth noting that the benefits of increasing the residual loads diminished between 1.0% to 1.5% fibre dosages. This may be attributed to fibre oversaturation.

The performance of hybrid mixtures improved slightly with an increase in the proportion of SFs, as evidenced by the enhanced peak load capacity due to multi-level cracking bridging. Short fibres can arrest micro-cracks, while long fibres can arrest macro-cracks. However, further increasing the SFs portion beyond 50% did not show any considerable improvement in residual loads and this is due to the oversaturation of fibres.

4.4.4 Failure pattern

The failure patterns of the tested prisms are shown in Figure 4-9. All tests were stopped at 3 mm deflection except the control, which fractured well before 3.0 mm. The control prisms had sudden failures and split in two, as seen in Figure 4-9 (a). Fibre bridging holds the FRC prims from splitting apart, as shown in Figure 4-9 (b). Failure modes are shown in Figure 4-9 (c and d). The failure patterns of control prisms showed brittle failure, and the majority of cracks happened in the concrete paste with some of the debonding interface regions. This describes the sudden failures associated with control prims, as shown in Figure 4-9 (c). However, FRC failure is a combination of concrete paste cracks and either SFs debonding in SF prims or GFs tearing due to the weakness to transverse loading in GF prims, or a combination of SFs debonding and GFs tearing as in HF prims as shown in Figure 4-9 (d).

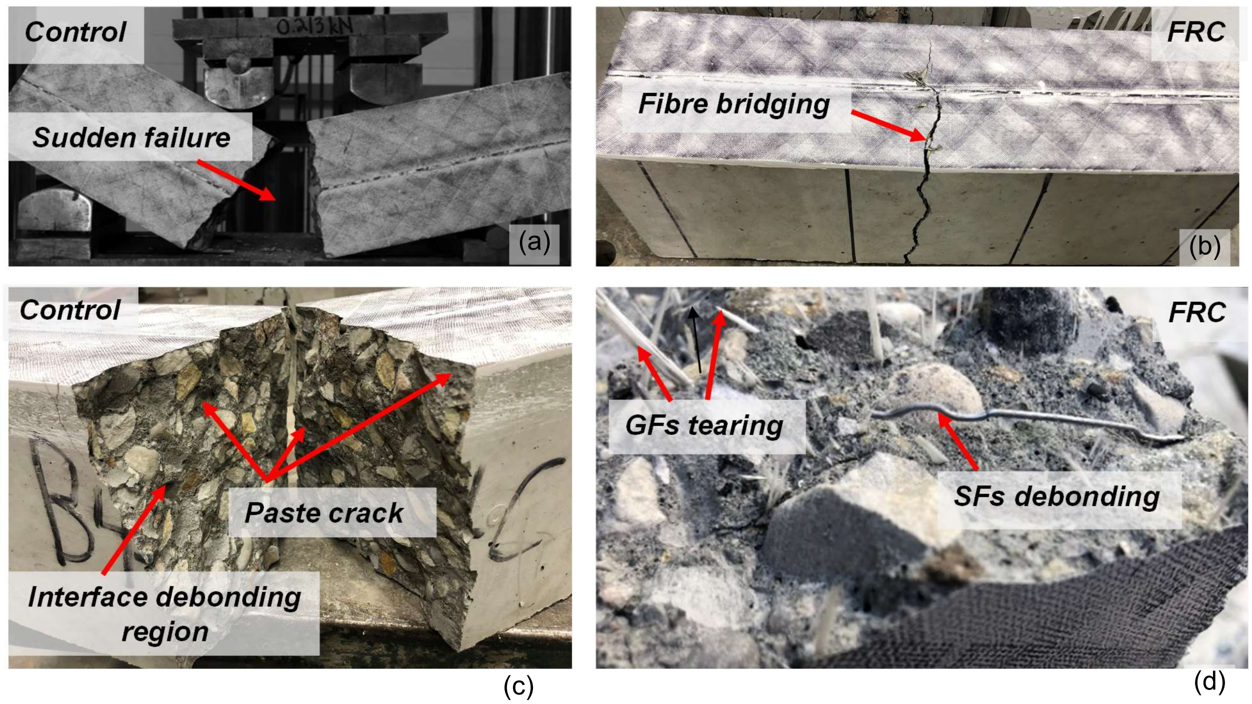

Figure 4-9: Failure mode: (a) control prism after sudden failure, (b) fibre-bridging of FRC prisms at deflection 3.0 mm, (c) control prims failure pattern, and (d) failure pattern of FRC.

4.4.5 Split tensile results.

The splitting tensile test is commonly used to determine the tensile strength of concrete as it is easier to conduct in more facilities than direct tensile tests and flexural tests. Often, concrete tensile strength is assumed to be proportional to the square root of its compressive strength (Choi and Yuan 2005), and there are good correlations between compressive strength and split tensile strength (Choi and Yuan 2005; Merve AÇIKGENÇ, ALYAMAÇ, and ULUCAN 2015). Tensile splitting strengths are shown in Figure 4-10 for each mixture (average of 5 samples). Adding fibres greatly increases split tensile strength relative to the control by 31, 72, and 93% for SF dosages of 0.5, 1.0, and 1.5%, respectively and 29, 40, and 51% for GF dosages of 0.5, 1.0, and 1.5% respectively for GFs due the activated bridging process, similar results were found by others (Merve AÇIKGENÇ, ALYAMAÇ, and ULUCAN 2015; Choi and Yuan 2005; Folino et al. 2020).

Adding 0.5% SF and GF has almost the same effect on split tensile strength. From 1.0 to 1.5% dosage, SF had a larger increase in split tensile strength compared with GF due to larger material stiffness and bonding of SFs' double-hook end profile. This reason is also why the hybrid mixtures show that the larger the SF portion of the dosage, the larger the split tensile strength.

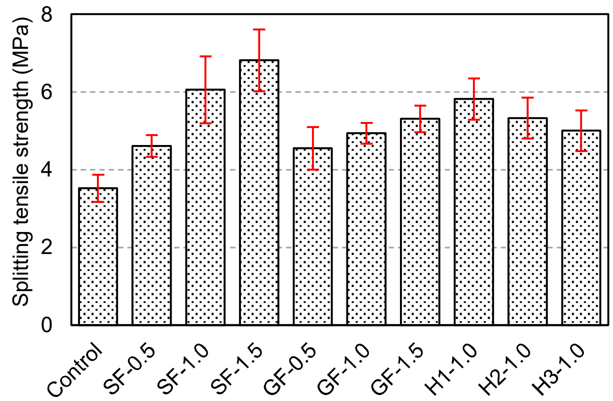

Figure 4-10: Average split tensile strength for each parameter. Error bars denote one standard deviation from the mean.

Figure 4-11 illustrates the failure patterns of cylinders subjected to the splitting tensile strength test. The fibres act as bridges across the cracks and prevent immediate specimen failure. This is because the fibres are capable of supporting load between initial cracking and the initiation of other cracks, resulting in increased splitting tensile strength, as depicted in Figure 4-11 (b). In contrast, the control specimens fail immediately after first cracking, as shown in Figure 4-11 (a). The fibre profile, specifically the double hooked end, enhances the crack bridging process due to increased debonding resistance and fibre stretching prior to debonding, as shown in Figure 4-11 (c). However, GFs tend to experience tearing as a common failure mode due to weaknesses in the traverse direction where fibre failure is controlled by resin, as depicted in Figure 4-11 (d)

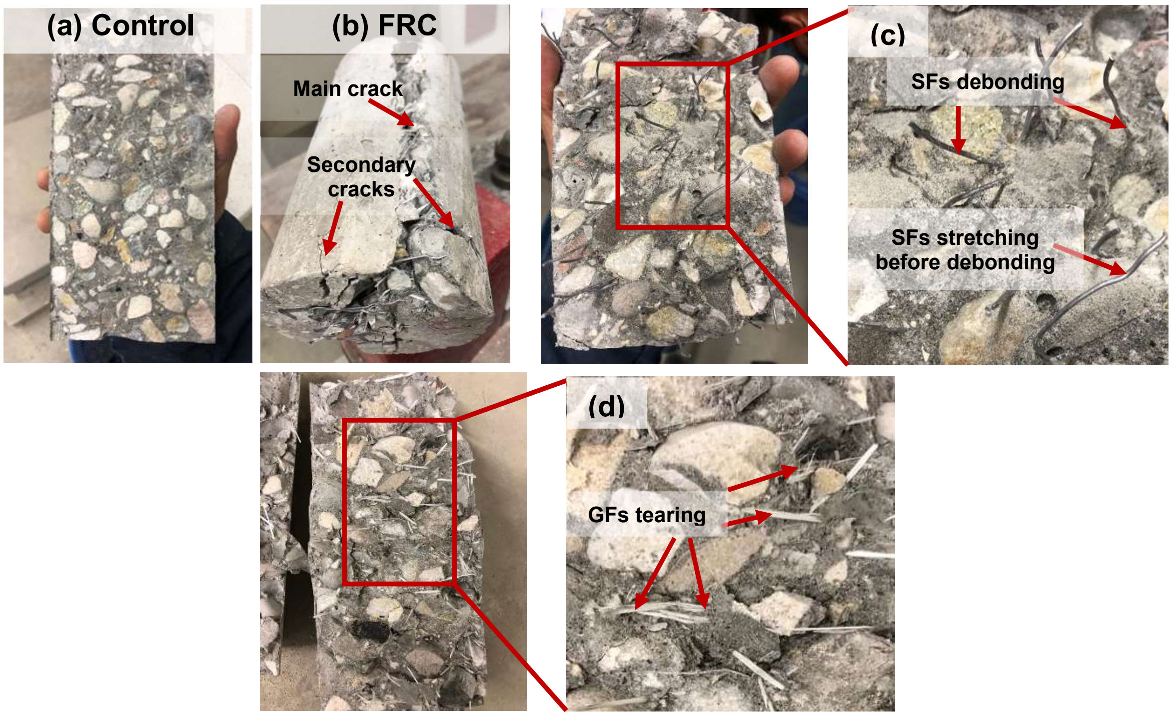

Figure 4-11: Fracture pattern: (a) control cylinder after sudden failure, (b) fibre bridging of FRC cylinder (c) zoom in photo showing SFs debonding (d) zoom in photo showing GFs tearing.

4.5 Analytical Tensile Model

There are several methods to orient fibres into the concrete mix, such as formwork constraint, roller pressing, mechanical orientation through special mesh passages, intensive vibration causing the fibre to align horizontally in one plane, and application of electromagnetic forces during moulding. However, these methods, tested in laboratory settings, prove to be challenging to implement in practice and often only partially achieve the desired directional orientation of fibres in larger structures(Mailyan, Shilov, and Shilov 2021). Therefore, the fibres are assumed to be distributed randomly into concrete, so detecting the orientation and location of each fibre is difficult and using a discrete modelling approach is complex. This study adopts the smeared approach to develop tensile stress-strain for SF, GF, and hybrid fibres, as described in Figure 4-12. The experimental load-deflection responses were first obtained from 4PLB tests (see Figure 4-12 (a)). A closed-form inverse analysis (IA), proposed by Soranakom and Mobasher (2008, 2009) and based on a trilinear model is used, as shown in Figure 4-12 (b). This approach is used to generate the tensile model for FRC from flexural tests which is a smeared approach that is mesh-size independent. The IA process is described in Figure 4-12 (c) and divided into two steps. First, changing input parameters for the initial tangent (E_t), peak stress (A), and cracking strain ($C@A$) and then comparing Stage 1 of the experimental and IA load-deflection responses. If they match (as described later in this section), then Stage 2 can be completed by changing a softening tangent (E_{st}), residual stress (B), strain at (B) ($D@B$), and ultimate strain ($E@B$) until experimental and IA load-deflection responses are matched. These stages are illustrated in Figure 4-13 for a closed-form IA and experimental load-deflection response after several iterations of changing input parameters.

Quantitative approaches are used to judge the match between the IA and test results. In particular, the Absolute Error (Eq. (4-4)) of the E_t, peak load and (T) (area under load-deflection curves), and ultimate deflection was not greater than 5%.

$$\text{Absolute Error} = \left\| \frac{IA - Test}{Test} \right\| \tag{4-4}$$

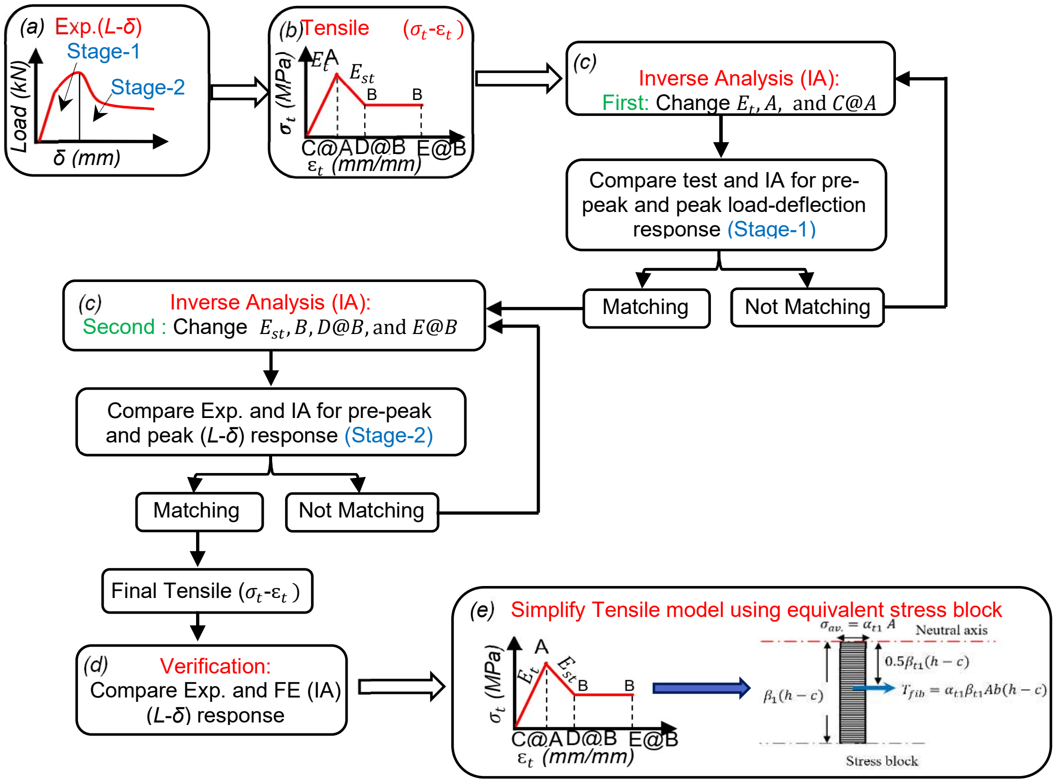

Figure 4-12: Analytical approach flow chart.

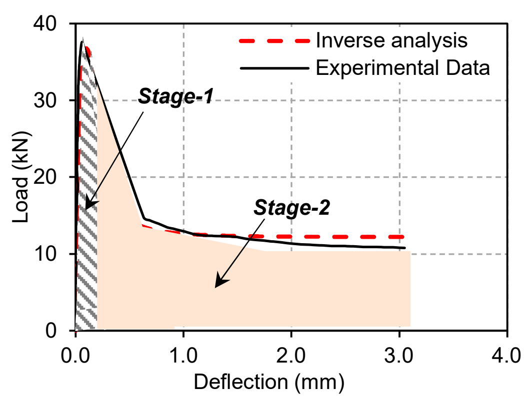

Figure 4-13: Experimental and calculated (closed-form inverse analysis) load-deflection response of SF-0.5.

4.5.1 Tensile response parameters generated from IA

After several iterations of changing input parameters until the IA and experimental results matched, the tension stress-strain output was generated, as shown in Table 4-7 and Figure 4-14 for the average of three prisms for SFs, GFs, and HFs mixtures.

Table 4-7: Tension stress-strain generated from IA for FRC.

Beam ID	Tension Model				
	Stress (MPa)		Strain (%)		
	A	*B*	*C@A*	*D@B*	*E@B*
SF-0.5	2.57±0.13	0.7±0.09	0.010±0.0003	0.17±0.010	3.1±0.18
SF-1.0	2.66±0.08	1.4±0.11	0.011±0.0015	0.48±0.086	2.9±0.08
SF-1.5	3.25±0.33	1.8±0.17	0.013±0.0013	0.74±0.091	2.9±0.05
GF-0.5	2.40±0.09	0.1±0.02	0.011±0.0009	0.35±0.003	3.1±0.04
GF-1.0	2.70±0.15	0.3±0.05	0.013±0.0008	0.40±0.023	3.1±0.04
GF-1.5	2.97±0.25	0.6±0.02	0.015±0.0013	0.48±0.066	3.0±0.05
H1-1.0	2.98±0.09	1.0±0.11	0.012±0.0004	0.24±0.003	3.0±0.04
H2-1.0	2.69±0.23	0.9±0.19	0.011±0.0009	0.25±0.023	2.9±0.30
H3-1.0	2.32±0.25	0.7±0.01	0.010±0.0010	0.28±0.066	3.1±0.02

± is the standard deviation (SD)

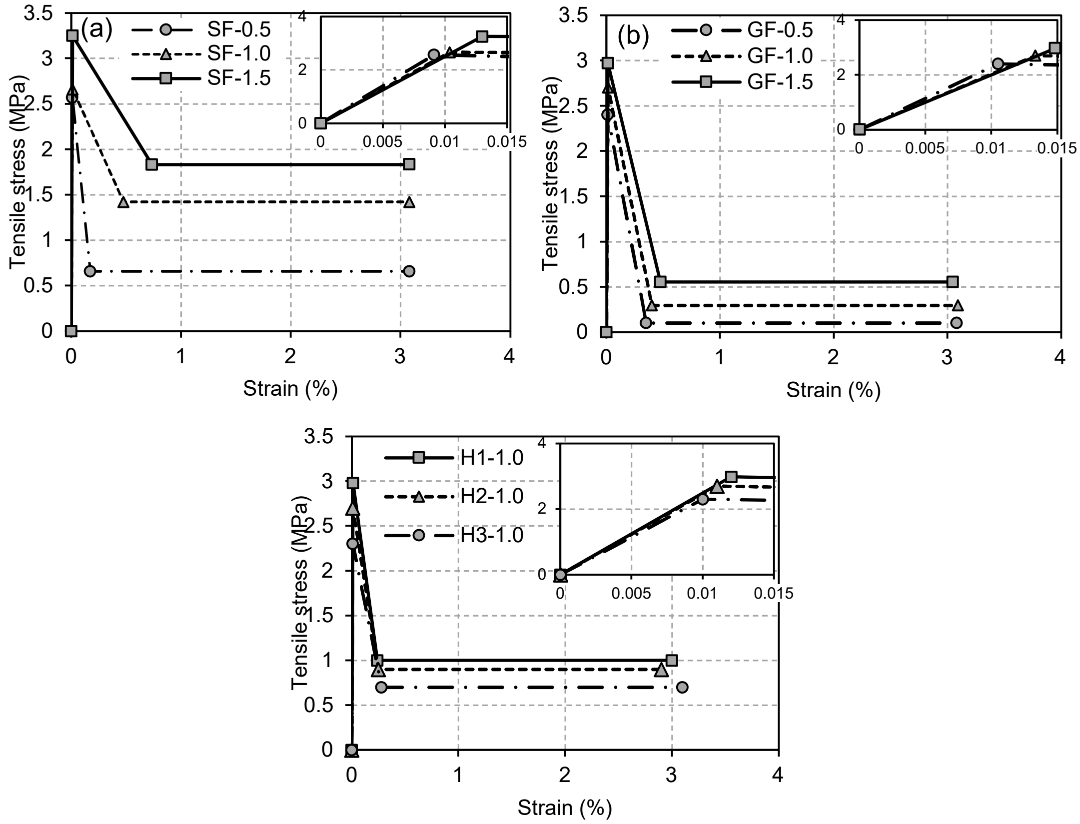

Figure 4-14: Tension stress-strain generated from IA for FRC (a)SF, (b)GF, and (c)HF. Subset plot in the corners shows the response under very small values of strain.

Increasing fibre dosage slightly influences peak stress, but residual tensile stress is more significantly affected by adding fibres. For instance, increasing SF dosage increases residual stress by 2 and 2.6 times for 1.0 and 1.5% dosage, respectively, compared to 0.5%, with even larger increases seen for GF (3 and 6 times for 1.0 and 1.5% dosage, respectively). The tensile strength is larger with SF compared to GF with the same dosage for the reasons explained in the experimental results section. The residual tensile strength increased almost linearly for SFs and GFs, and this is because the effect of fibres is more significant at the post-cracking stage due to the crack bridging process. The hybrid mixtures showed a marginal decrease in both tensile strength and residual tensile stress as the GF portion of the fibres increased, as also observed in the tests. It is clear that adding fibres increases cracking strain regardless of the material. The effect of adding SF on residual strain is remarkable and large compared to the GF. Ultimate strain was unaffected by adding fibres since tests were all stopped at the same displacement. For hybrid mixtures, the cracking tensile strain decreased as the GF portion increased, though residual strains showed a slight increase with the increase in the GF portion.

4.5.2 The verification of the tensile model using the Finite Element (FE) model

4.5.2.1 FE model

The tensile model generated from AI was inserted into the FE model (Figure 4-12(d)) using VecTor2 software (Wong, Vecchio, and Trommels 2014). 2D analysis was used to reduce computational time compared to 3D software. VecTor2 was selected as it was developed to assess reinforced concrete and contains constitutive models and optimized approaches to simulate reinforced concrete. The tensile model was inserted as a custom tension softening input (strain-based) by modifying the five points custom input-strain-based tension-softening model in VecTor2® to the three-point tension model (See Figure 4-14).

Mesh size sensitivity analysis was done to balance accuracy and computational time, as shown in Figure 4-15. Load capacity was compared for five different amounts of hybrid rectangular elements (5, 33, 120, 480, and 1920). With more than 120 elements, the capacity becomes essentially constant, so 120 elements with a mesh size of 25×25 mm were used in this model.

Other researchers adopted a similar mesh size (Tlemat, Pilakoutas, and Neocleous 2006; Labib 2008; Blazejowski 2012).

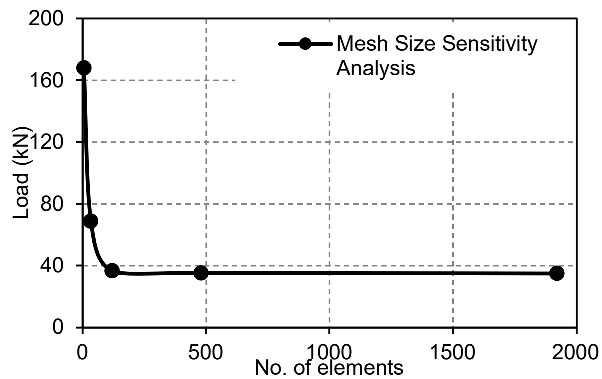

Figure 4-15: Mesh size sensitivity analysis.

Figure 4-16 shows the VecTor2® model details. The compression model is elastic-perfectly plastic since all prisms were governed by tension, and compression remained within the elastic range. The loading and boundary conditions are shown in Figure 4-16. Displacement-control loading is applied on both top edges of the prism's middle third. The left support is roller support, and the right support is pin support to simulate the prism tests.

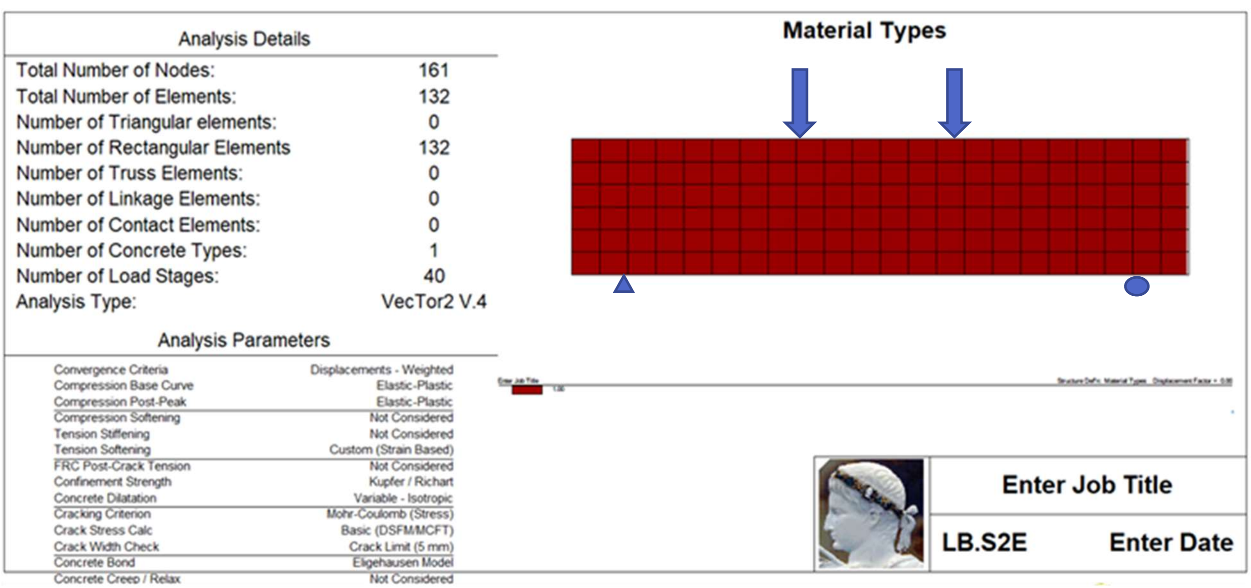

Figure 4-16: 2D VecTor2® model of FRC prisms mesh details, loading, and boundary conditions

4.5.2.2 Verification of IA results

Verification was done by comparing the test (three samples) with FE (based on IA) load-deflection responses of FRC prisms, as shown in Figure 4-17. The test and FE (IA) load-deflection responses show a good correlation with errors less than 10% for stiffness, peak load, and area under load-displacement curves for all FRC prisms. However, the FE results of GF showed a sharp drop after peak load, similar to IA results, but the area under load-deflection of FE (IA) and tests remain similar.

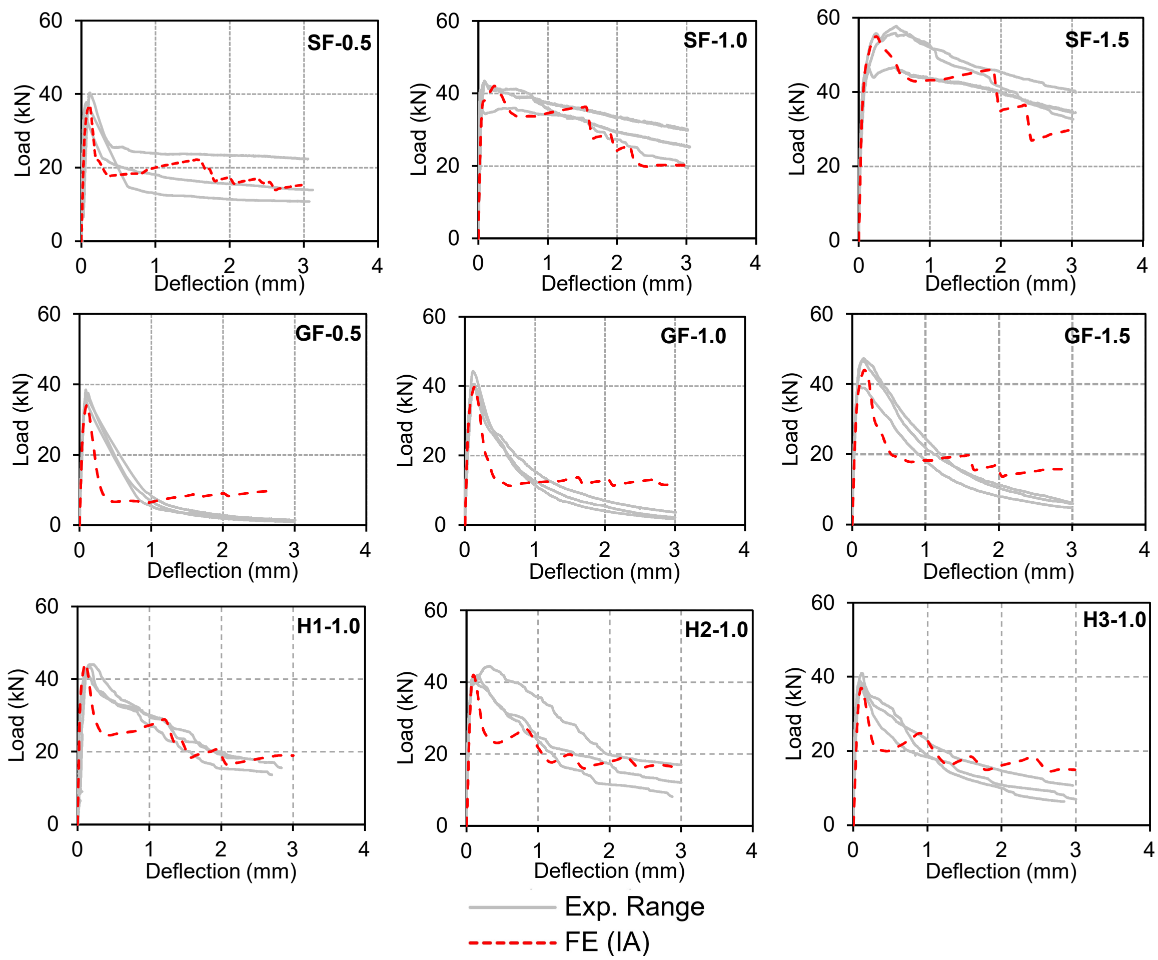

Figure 4-17: Comparison between FE (IA) and test load-displacement response.

4.5.3 Analytical tensile stress-strain model

The tensile stress-strain model generated from IA for FRC is simplified and expressed in Eqs. ((4-5)-(4-9)) for each mixture. The analytical tensile model of FRC is generated by investigating the effect of fibres on the tensile parameters (A, B, C@A, D@B, and E@B). The tensile strength can be obtained using equation (4-6). Based on the literature, the tensile peak stress depends mainly on V_f and its corresponding f_c' (Sujivorakul 2012). Therefore, Eq.(4-6) is based on regression analysis of f_c' and peak tensile stress, σ_{t0}, with a mean of 1.02 and COV of 11% for SFs, GFs, and HFs. Residual stress, $\sigma_{t,res.}$ depends mainly on V_f and aspect ratio $(\frac{L_f}{D_f})$ (Sujivorakul and Naaman 2003; Sujivorakul 2012). Thus, the factor, $\left(\frac{L_f}{D_f}\right)V_f$ is added to the regression analysis, and residual stress can be determined from Eq. (4-7) for SFs, GFs and HFs with a mean of 1.02 and COV of 16%.

$$\sigma_t = \begin{cases} \sigma_{t0}\left(\dfrac{\varepsilon_t}{\varepsilon_{t,cr.}}\right) & \text{for} \quad \varepsilon_t \le \varepsilon_{t,cr.} \\ \sigma_{t0} + \left[\left(\dfrac{\sigma_{t0} - \sigma_{t,res.}}{\varepsilon_{t,cr.} - \varepsilon_t}\right)(\varepsilon_t - \varepsilon_{t,cr.})\right] & \text{for} \quad \varepsilon_{t,cr.} < \varepsilon_t \le \varepsilon_{t,res.} \\ \sigma_{t\ res.} & \text{for} \quad \varepsilon_{t,res.} < \varepsilon_t \le \varepsilon_{tu} \end{cases} \tag{4-5}$$

$$\sigma_{t0} = 0.38\sqrt{f_c'} \qquad \text{for SFs, GFs, and HFs} \tag{4-6}$$

$$\begin{aligned} \sigma_{t,res.} &= 2.3\left(\frac{L_{Sf}}{D_{Sf}}\right)Vf && \text{for SFs} \\ \sigma_{t,res.} &= 0.75\left(\frac{L_{Gf}}{D_{Gf}}\right)Vf - 0.15 && \text{for GFs} \\ \sigma_{t,res.} &= = Vf\left[\gamma\left(2.3\left(\frac{L_{Sf}}{D_{Sf}}\right)\right) + (1-\gamma)\left(0.65\left(\frac{L_{Gf}}{D_{Gf}}\right)\right)\right] && \text{for HFs} \end{aligned} \tag{4-7}$$

Where: σ_{t0}, is the peak tensile stress, $\sigma_{t,res.}$, is the residual stress and, $\varepsilon_{t,cr.}$, $\varepsilon_{t\ res.}$, and ε_{tu} , are the cracking, residual, and ultimate tensile strains, respectively. V_f, is the fibre volume fraction; L_{Sf} and L_{Gf} are fibre length for SF and GF, respectively; D_{Sf} and D_{Sf}, is the fibre diameter for SF and GF, respectively; and γ, is the ratio of V_f of SFs to V_f of GFs.

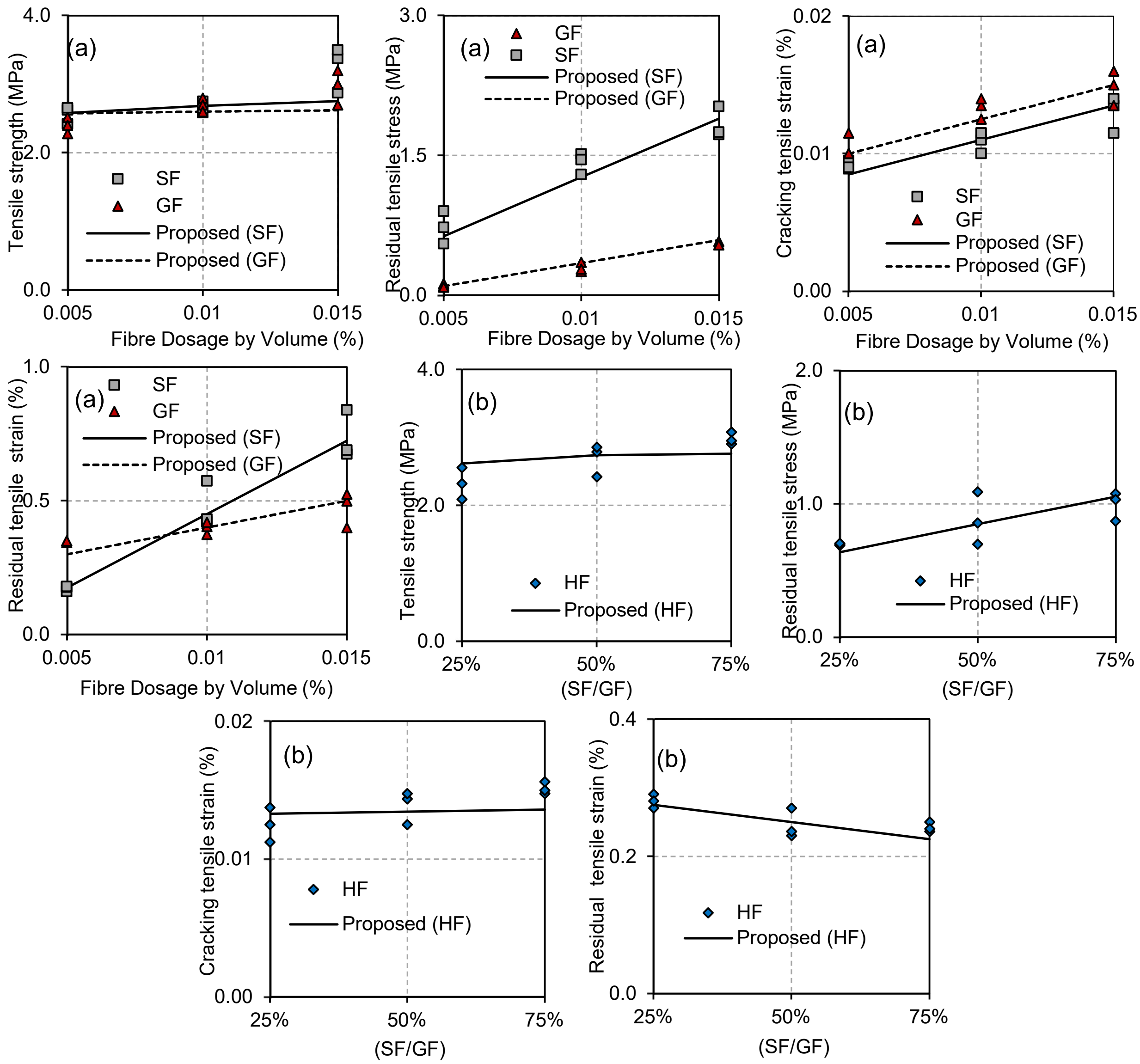

Figure 4-18: Calculated (from IA) and proposed tensile strength and residual tensile strength; and cracking and residual strains for (a) SFs and GFs; and (b)HFs

The proposed Eqs. (4-8) and (4-9) for tensile peak and residual stresses; and cracking and residual strains of FRC are based on regression. The comparison of the proposed and calculated (from IA) tensile strength and residual tensile stress; tensile cracking, and residual strains is shown in Figure 4-18. The means and COV of the IA over the proposed Eqs. (4-8) and (4-9) (7 and 8) are (1.01 and 1.04), (1.02 and 1.04); (9% and 8%) and (12% and 10%) for SFs, GFs, respectively. For HF the means and COV of the IA over the proposed equations (7 and 8) of are (1.03 and 1.03) and (15% and 7%), respectively.

$$\begin{aligned} &\varepsilon_{t,cr.}\% = 0.006 + 0.5(V_f) && \text{for SFs} \\ &\varepsilon_{t,cr.}\% = 0.0075 + 0.5(V_f) && \text{for GFs} \\ &\varepsilon_{t,cr.}\% = \gamma\left(0.001 + V_f\right) + (1-\gamma)(0.0005 + V_f) && \text{for HFs} \end{aligned} \tag{4-8}$$

$$\begin{aligned} &\varepsilon_{t,res.}\% = \left(55V_f\right) - 0.1 && \text{for SFs} \\ &\varepsilon_{t,res.}\% = 0.2 + (20V_f) && \text{for GFs} \\ &\varepsilon_{t,res.}\% = \gamma\left(40V_f - 0.2\right) + (1-\gamma)(30V_f) && \text{for HFs} \end{aligned} \tag{4-9}$$

4.5.4 Simplified tensile model using equivalent tensile stress block parameters (sectional analysis)

The trilinear model is further simplified using sectional analysis to an equivalent tensile stress block for design purposes. This approach is similar to the derivation of the compression stress blocks used in conventional reinforced concrete but accounts for the FRC in the tension zone for the reason that the assumption of ignoring concrete in the tension zone is not valid for FRC. The analysis and design of conventional reinforced concrete members are typically performed assuming a linear strain distribution and converting the nonlinear concrete stress distribution into an equivalent stress block using parameters α (the ratio of average stress to the peak stress; in this case, these will be in the tension zone as noted by α_t) and β (the ratio of the depth of the rectangular block to the depth of the difference between section height and the neutral axis, also focusing on the tension zone here as noted by β_t). These expressions can be derived using Eqs. (4-10) and (4-11) by taking the first and second moments of the area of the stress-strain curves. The tensile concrete zone force $T_{fib.}$ at can be calculated as $\alpha_{t1}\beta_{t1}\sigma_{t0}b(h-c)$ where c is the distance from the extreme compression fibre to the neutral axis and b is the section width (assuming rectangular).

$$\alpha_t\beta_t = \frac{\int_0^{\varepsilon_t} \sigma_t d\varepsilon_t}{\sigma_{t0}\varepsilon_t} \tag{4-10}$$

$$\beta_t = 2 - 2\,\frac{\int_0^{\varepsilon_t} \sigma_t d\varepsilon_t}{\varepsilon_t \int_0^{\varepsilon_t} \sigma_t d\varepsilon_t} \tag{4-11}$$

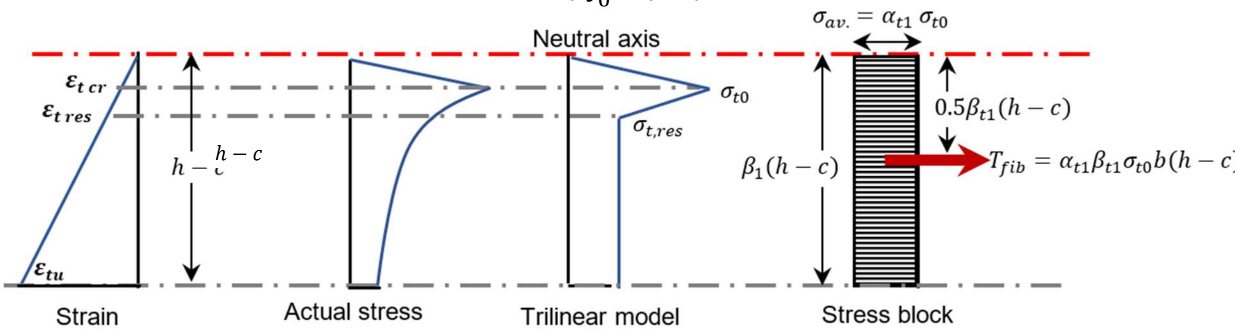

Figure 4-19: Rectangular tensile stress block at ultimate in the tension zone

The resulting average tensile stress-block parameters of three samples are shown in Figure 4-20. For α_t, adding fibres increased elastic strain up to cracking, corresponding to α_t= 0.75 (linear elastic stage). A similar trend is observed for β_t up to 0.667 (corresponding to the cracking strain) that adding fibres increased the elastic strain range since fibres marginally reduce the tension modulus of elasticity, which is generally less than the compressive modulus of elasticity (Martin and Jitka 2017) (Figure 4-14 and Table 4-5). The hybrid mixes show that the larger the portion of GF, the decrease of α_t and β_t did not affected before craking. However, after cracking, α_t increased with increasing fibre dosage due to increases in residual strength (Table 4-7) from the fibre bridging development. α_t, is almost constant after the residual tensile strain for SFs, GFs and HFs. The β_t, for SFs decreased with an increase in fibre dosage between cracking and residual tensile strains, and this is due to an increased softening tangent with a decrease in the fibre dosages, followed by a plateau response with almost β_t, equal to 1.05 up to ultimate strain, same as the tensile response, while GFs showed decreasing β_t with increased fibres dosages beween cracking and ultimate tensile strains. In hybrid mixes, β_t slightly increased with larger portions of GF in the mixture between cracking and residual tensile strains due to an increase in the residual strain with an increase in the GF portion, and then the trend plateaued with β_t equal to 1.05 up to the ultimate strain.

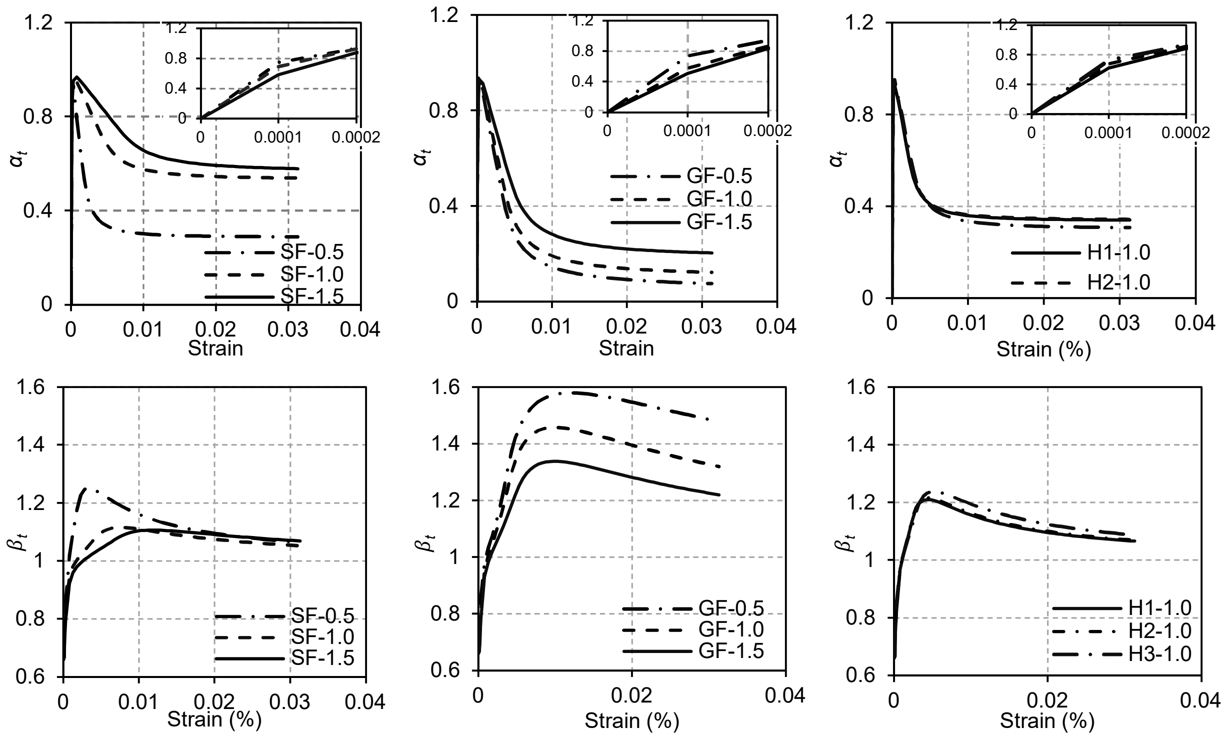

Figure 4-20: Average stress-block parameters: (a) α_t and (b) β_t

Stress-block parameters α_{t1} and β_{t1} are proposed to account for the tensile stress at ultimate (ε_{tu} = 3%). If this strain exceeds the maximum cross-section strain at ultimate (for instance, if a beam is reinforced and concrete crushes before ε_{tu} reaches 3%), α_t and β_t can be found in Figure 20 instead. Predicting average tensile stress, $\sigma_{av.}$, depends on α_{t1}, calculated in Eq. (4-12), which is affected by fibre type and dosage. Figure 4-21 shows the effect of fibres on α_{t1} and β_{t1} corresponding to ε_{tu}, generally α_{t1} increased with fibres dosages increasing for SFs, and GFs, moreover, it is increased with an increase in SFs portion for HFs mixtures, as shown in the first row of Figure 4-21. The β_{t1} expressed in Eq (4-13), which is close to 1.05 for SFs and HFs and for GFs it is decreased with increase GFs dosages as shown in the second row of Figure 4-21.

$$\alpha_{t1} = 0.20 + (0.25V_f)100 \quad \text{for SFs}$$
$$\alpha_{t1} = 0.03 + (0.10V_f)100 \quad \text{for GFs} \qquad (4\text{-}12)$$
$$\alpha_{t1} = \gamma[(0.10 + (30V_f)] + (1-\gamma)[(0.10 + (20V_f)] \quad \text{for HFs}$$
$$\beta_{t1} = 1.05 \quad \text{for SFs and HFs}$$
$$\beta_{t1} = 1.6 - (30V_f) \quad \text{for GFs} \qquad (4\text{-}13)$$

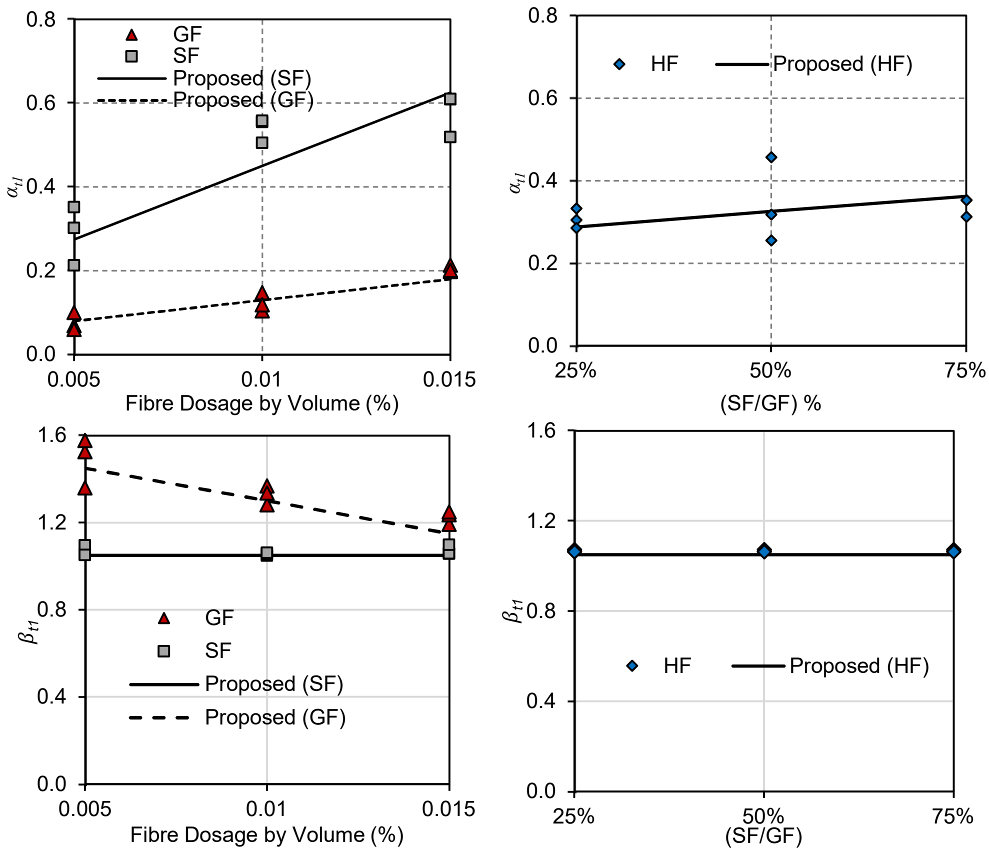

Figure 4-21: Calculated from IA tensile stress-strain and proposed (Eq. (4-12)and (4-13)) of α_{t1} and β_{t1}.

4.6 Conclusions and Recommendation

The effect of steel and glass fibres and their combination on crack and flexural response and split tensile strength in NSC mixtures was investigated. Parameters included flexural strength, peak strain, residual stress and strain, toughness, and equivalent flexural strength ratio. Inverse analysis was used to generate the tensile stress-strain for FRC. A simplified design analytical tensile model for FRC using stress block parameters was proposed. The following was concluded:

1. Adding SFs and GFs affects mechanical properties, such as flexural strength and splitting tensile strength. Flexural parameters, such as peak stress and strain, residual stresses, and toughness, increased with fibre dosages over the investigated range (zero to 1.5%). In hybrid mixtures, replacing half the SF with GF greatly increases peak strain and does not affect flexural strength. However, the larger the portion of GF in the mixture compared to SF, the lower the splitting tensile strength, residual stress, and toughness.
2. DIC and LVDT load-deflection responses matched well, and DIC was used to generate full-field measurements such as crack width (CMOD) with additional benefits of assessing crack propagation.
3. The addition of SF and GF increases FRC peak load, residual loads, and fracture energy. Hybrid mixtures show marginal increases in peak load compared with SF and GF mixtures and higher fracture energy compared to GF mixtures due to crack bridging.
4. The most common flexural and indirect tensile failure of SF mixtures is debonding, while GF mixtures are caused by fibre tearing. Increasing dosage leads to multiple narrow cracks instead of one dominant crack, which is attributed to fibre crack-bridging. In hybrid mixtures, the more the portion of GF in the mixture compared to SF, the lower the splitting tensile strength, peak strain, cracking load, residual stress, and toughness.
5. The tensile model generated using IA was implemented into FE models, and a good correlation between the test and FE results was observed. The proposed analytical tensile stress-strain model derived from IA for FRC is slightly conservative, with mean and COV of 1.04 and 12%, respectively. The tensile model can be further simplified using equivalent

tensile stress block parameters (α_{t1} and β_{t1}). This model may help structural engineers evaluate reinforced concrete members constructed with FRC similar to that used in these tests (hooked SFs and GFs with V_f, between 0% to 1.5% used in normal strength concrete).

This study used steel and glass fibres and combinations between them, so studying different kinds of combinations and the geometric properties of fibres, such as aspect ratio and fibre profile (e.g., straight, crimped) as well as other fibre types (e.g., basalt, polypropylene) on crack behaviour and flexural response should be investigated further. Replacing more than half the SF with GF did not greatly affect the mechanical properties of the concrete. However, other factors, including workability and construction cost, would need to be considered when developing an optimal mixture that incorporates the two fibre types. Therefore, more cost and fresh property analysis on these mixtures is needed in future. The analytical model generated in this research was based on this study's data, so more data is needed to increase model applicability for other situations.

CHAPTER 5

NUMERICAL ANALYSIS OF FULL-SCALE STEEL AND GFRP BEAM WITH STEEL AND CHOPPED GLASS FIBRE.

5.1 Introduction

Fibre-reinforced concrete (FRC) is widely used in different applications such as concrete pavements, ground slabs, tunnels, and water tanks because it offers improved properties compared to regular concrete. Adding fibres to concrete enhances its durability, toughness, and resistance to cracking. Fibres can mitigate the size effect by diminishing larger cracks typically associated with increased section sizes (Bažant, 1984). This results in better aggregate interlock and concrete tensile strength. The application of Finite Element Analysis (FEA) for modelling FRC provides valuable insights into the behaviour and performance of FRC structures. Inherent randomness in fibre distribution within FRC poses difficulties for conventional engineering methods in accurately predicting stress patterns and crack propagation. Consequently, FEA emerges as an effective tool for analyzing and optimizing FRC members, mainly through a smeared approach, which characterizes concrete combined with fibres into a single-modelled material effect (Bernardi et al., 2016).

Numerous studies have assessed the ability of FEA to accurately simulate the experimental response of steel reinforced bar (SR) with plain concrete (RC) beams (Alshaarbaf et al., 2023; Harba et al., 2022; Smarzewski and Stolarski, 2017) with findings showing that FEA can successfully predict test results. Similar investigations focused on the simulation of SR-RC beams using FRC with various fibre types (Ayub et al., 2018; Facconi et al., 2021; Khaleel Ibrahim et al., 2023; Liu et al., 2022; Shewalul, 2021; Sliseris, 2018) with findings also indicating that outcomes from FEA align with test results for SR-FRC. These studies also highlight that FEA can capture intricacies associated with introducing various fibres into concrete.

Glass fibre reinforced polymer (GFRP) bar is used in many applications, particularly those where steel corrosion is a concern. Multiple numerical studies have examined GFRP-RC beams (Ahmad et al., 2021; Gouda et al., 2023; Saleh et al., 2019; Tsivolas et al., 2022). Studies have evaluated the impact of increased concrete compressive strength on strength and serviceability (Gouda et al., 2023), crack growth and intensity (Tsivolas et al., 2022), and moment redistribution behaviour due to flexural and shear loading in continuous GFRP-RC beams (Ahmad et al., 2021). Saleh et al. (2019) conducted FEA on GFRP-RC beams subjected to impact loads and showed that FEA effectively represented midspan deflections and dynamic GFRP bar strains. However, there is a shortage of studies examining the combined impact of FRC on GFRP-RC members, leading to a gap in research, particularly in modelling GFRP with FRC.

Past studies have considered design considerations regarding adding steel fibres (SF) to SR-RC beams that include the possibility of substituting stirrups with SF (Ahmed et al., 2015; Facconi, Amin, et al., 2021; Facconi, Minelli, et al., 2021) whether fibres mitigate size effects (F. Minelli et al., 2014; Yoo et al., 2016), as well as altering failure modes from shear to flexure (Alguhi and Tomlinson, 2019; Folino et al., 2020). This study builds upon these considerations by considering various fibres, including glass fibres (GF) and GFRP longitudinal reinforcement. The FEA presented in this work is based on limitations, such as assuming a uniformly random orientation of fibres that can be simulated with constitutive relationships as developed and validated for experimental small-scale FRC beams by (Alguhi and Tomlinson, 2023). Additional fibre types and considerations like the effect of concrete flow are worthy of future research to develop a more comprehensive understanding of FRC in concrete.

The motivation for using numerical analysis, specifically FEA, in the study of large-scale SR-RC and GFRP-RC beams combined with FRC arises from gaps in the literature. A lack of comprehensive models integrating SR-RC and GFRP-RC, especially when incorporating SF and/or GF, exists with limited exploration of Serviceability Limit States (SLS) and Ultimate Limit State (ULS) performance. This study assesses the applicability of the generated FRC material model through FEA verification, which may be cost-effective compared to extensive test programs. Outcomes considered extend beyond load-displacement to include factors like crack width and strain within the reinforcement, which may form a basis for analytical works, including machine learning models, to predict RC-FRC beam performance. This research aims to contribute to understanding the structural benefits of using FRC in reinforced concrete. This study uses numerical analyses using the finite element program VecTor2 to construct 720 beam models that compare SR-RC and GFRP-RC beams with and without fibres. The goal is to investigate the impact of different fibre types and dosages, including steel fibres (SF) and/or glass fibres (GF), as well as the influence of various parameters such as shear span (*a*) to effective depth (*d*) ratio (*a/d*), size effect (*d*), flexural reinforcement ratio (ρ), and the effect of stirrups. Results compare ULS considerations such as strength and failure mode as well as SLS conditions such as crack width and deflection.

5.2 Methodology

The methodology used in this study is divided into two phases. The first phase involves creating a Finite Element (FE) model using VecTor2 software, which is based on the Modified Compression Field Theory (Wong et al., 2013) and the Distributed Stress Field Model (Vecchio, 2000) (Vecchio and Collins, 1986) that can be applied to FRC members (Foster et al., 2018). This software was used to generate the material model for FRC and study SR-RC and GFRP-RC beams, both with and without FRC. This phase consists of three distinct stages. The first stage focused on verifying the material model, as done in (chapter 3 and (Alguhi and Tomlinson, 2023)). In the second stage, verification is conducted on full-scale RC beams without fibres using steel and GFRP bars. The final stage includes the verification of FRC beams, considering both SF and GF. The second phase of the methodology involves a parametric study designed to evaluate the impact of FRC on SR-RC and GFRP-RC beams in terms of both SLS and ULS performance.

5.2.1 FEA

Half of each beam was modelled to optimize computational efficiency due to beam symmetry, as depicted in Figure 5-1. The hybrid plane stress rectangular element was used to model concrete with and without fibres because it is less excessively rigid than the constant strain triangle; it is preferred for modelling reinforced concrete regions (Wong et al., 2013). A truss element was used for primary reinforcement. A perfect bond between the concrete and the primary reinforcement was assigned to prevent the deformation of the bond element (Wong et al., 2013). The symmetrical constraints are implemented as pin supports along the y-direction, as demonstrated in Figure 5-1. The load was applied as displacement control to capture post-peak response.

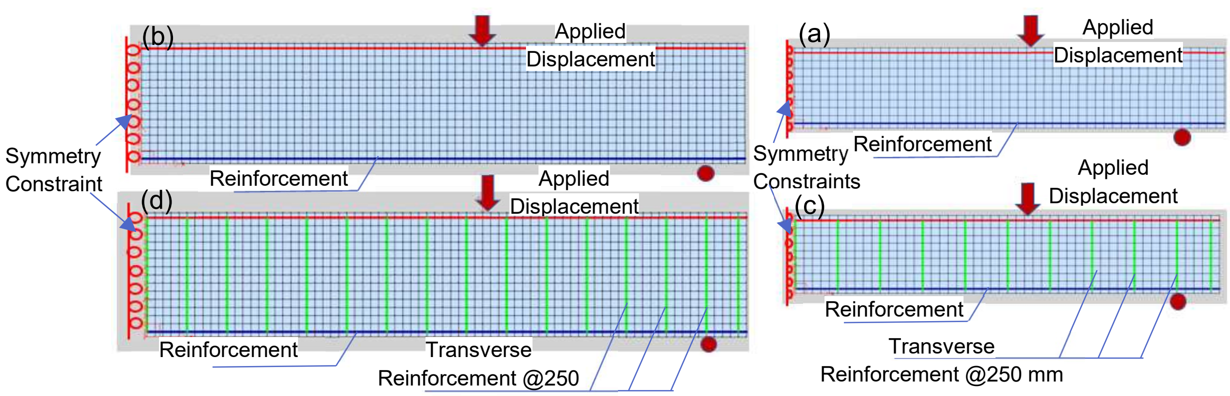

Figure 5-1: VecTor2 model of half beam for (a) beam with 500 mm height and no stirrups, (b) beam with 750 mm height and no stirrups, (c) beam with 500 mm height and stirrups, and (d) beam with height 750 mm height and stirrups.

5.2.2 Constitutive models

5.2.2.1 Concrete models

The compressive models are presented in Table 5-1. Plain concrete (*pc*) and FRC are modelled using the Hognestad parabola for pre-peak response because it is a simple response curve suitable for normal concrete strengths (Wong et al., 2013). The post-peak response was the Base Curve option (follows the Hognestad model as well) because it is a valid selection for the compression post-peak response if the Hognestad (Parabola) model is selected (Wong et al., 2013). The compressive softening Vecchio-Collins 1986 model was used because it was initially developed for the Hognestad Parabola compression stress-strain curve (Wong et al., 2013). The presence of fibres is incorporated by modifying parameters such as concrete compressive, f_c', and the associated strain as well as the modulus of elasticity, were extracted from (Alguhi and Tomlinson, 2023) and Chapter 3.

The concrete tension models are described in Table 5-1. The Collins-Mitchell 1987 tension stiffening model was used as it is appropriate for larger-scale elements and structures (Wong et al., 2013). The linear model was used for plain concrete since including a descending post-cracking stress-strain branch for plane concrete more accurately determines the load-deformation response and ductility of the member (Wong et al., 2013). FRC tension softening was defined as a custom tension softening input (strain-based) by modifying the five-point custom input-strain-based tension-softening model in VecTor2® to the trilinear three-point tension model derived by (Alguhi and Tomlinson, 2023a) as shown in Figure **5-2**.

Table 5-1: Concrete compressive and tension models used in FEA for plain concrete and FRC.

Compression for (FRC and *pc*)		Tension		
Concrete Stage	**Chosen model**	**Tension properties**	**Chosen model (FRC)**	**Chosen model (*pc*)**
Comp. pre-peak	Hognestad Parabola	Tension Stiffening	Collins-Mitchell 1987	Collins-Mitchell 1987
Comp. post-peak	Basic	Tension Softening	Custom input (Strain-based)	Linear
Comp. Softening	Vecchio-Collins 1986	FRC	Not consider	Not consider

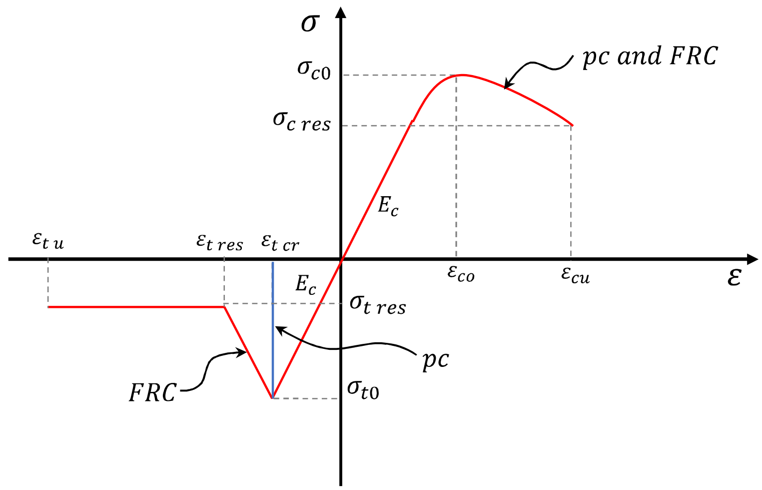

Figure 5-2: Compression and tension stress-strain adopted in VecTor2 (Wong et al., 2013)

5.2.2.2 Models for Reinforcement Materials

Steel reinforcement is defined as ‘ductile steel reinforcement’ in VecTor2 and based on a trilinear relationship: linear-elastic to yield, plastic yield plateau, and linear strain hardening, as shown in Figure 5-3 (a). The GFRP was modelled as ‘tension only’ reinforcement in VecTor2, which, when under tension, exhibits linear elasticity up to failure, as in Figure 5-3 (b). GFRP compression resistance is assumed to be negligible (Wong et al., 2013).

The dowel action model used for steel reinforcement is the default Tassios Crack Slip model. This option is used unless stability issues related to reinforcement shearing occur. For GFRP, dowel action is not considered as this contribution is small enough to be negligible (Nguyen-Minh and Rovňák, 2013).

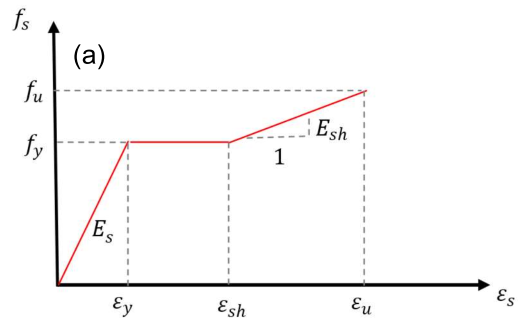

Figure 5-3: Stress-strain relationship for (a) steel reinforcement (tri-linear) (b) GFRP reinforcement (linear)

5.2.2.3 Mesh sensitivity analysis

Mesh sensitivity analysis was done to balance accuracy and computational time. Load capacity versus the number of hybrid rectangular elements (175, 272, 400, 1300, and 4400) is plotted in Figure 5-4 for a beam with *a/d* =2, ρ = 0.51, and height = 500 mm. The load changed with increased elements, but after 1300 elements, the response remained unchanged. Thus, 1300 elements with a mesh size of 50×50 mm were used. Similar outcomes were found from other beam parameters considered.

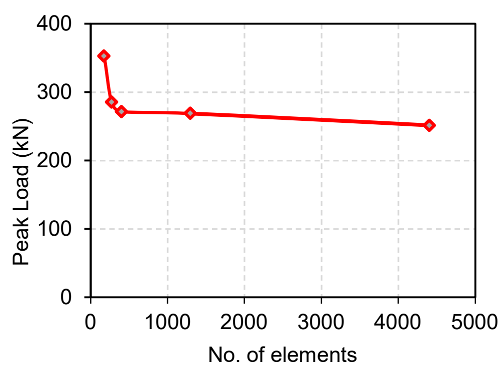

Figure 5-4: Mesh sensitivity analysis

5.2.3 Verification process of large-scale FEA model.

After a constitutive model was verified (see section 4.5.2 (Alguhi and Tomlinson, 2023)), this study delved into modelling a simply supported GFRP-RC and SR-RC beams with and without fibres with various dimensions. The verification procedure involved comparing load-deflection responses of both tests and FEA, as in Figure 5-5 (for more details, see Appendix C).

The first stage of the process, three large-scale tests on SR-RC and GFRP-RC beams without fibres and simple supports, as detailed by (Betschoga et al., 2021; El-sayed et al., 2007; F. Minelli et al., 2014) were modelled using VecTor2. The second verification included different main reinforcement bars (steel and GFRP) and secondary reinforcement fibres (SF and GF), as reported by (Issa et al., 2011; F. Minelli et al., 2014). Table 5-2 summarizes the verification results by calculating discrepancies between experimental and FEA outcomes regarding peak load and the area under the load-deflection curve. Results shown in Table 2 and Figure 5 indicate strong alignment between the FEA and test data, with average error falling below 10% and 15% of peak load and area under the load-deflection curve for all beams, regardless of whether they contain fibres.

Table 5-2: Summary of comparison between experimental and numerical results

Ref.	Beam ID	Beam dimensions (length×width× height), mm	Tension bars	Fibre	Peak load, kN			Area under curve, Nmm		
					Exp.	FEA	Error %	Exp.	FEA	Error %
Betschoga et al., 2021	ST 01	3900×170×450	GFRP	---	51	43	14.9	0.58	0.71	22.1
Issa et al., 2011	HG	1850×150×150	GFRP	GF	63	60	5.0	1.64	1.51	8.0
Minelli et al., 2014	H500 PC	2640×250×500	Steel	---	221	229	3.2	0.53	0.77	45.2
	H500 FRC50	2640×250×500	Steel	SF	460	473	2.6	9.07	9.89	9.1
	H500 FRC75	2640×250×500	Steel	SF	464	477	2.8	2.81	2.84	1.2
	H1000 FRC75	5640×250×1000	Steel	SF	671	750	11.8	7.54	6.84	9.3
El-Sayed et al., 2007	GN-3	3250×250×400	GFRP	---	156	146	5.8	1.88	1.98	5.6
					Average		**6.6**			**14.3**

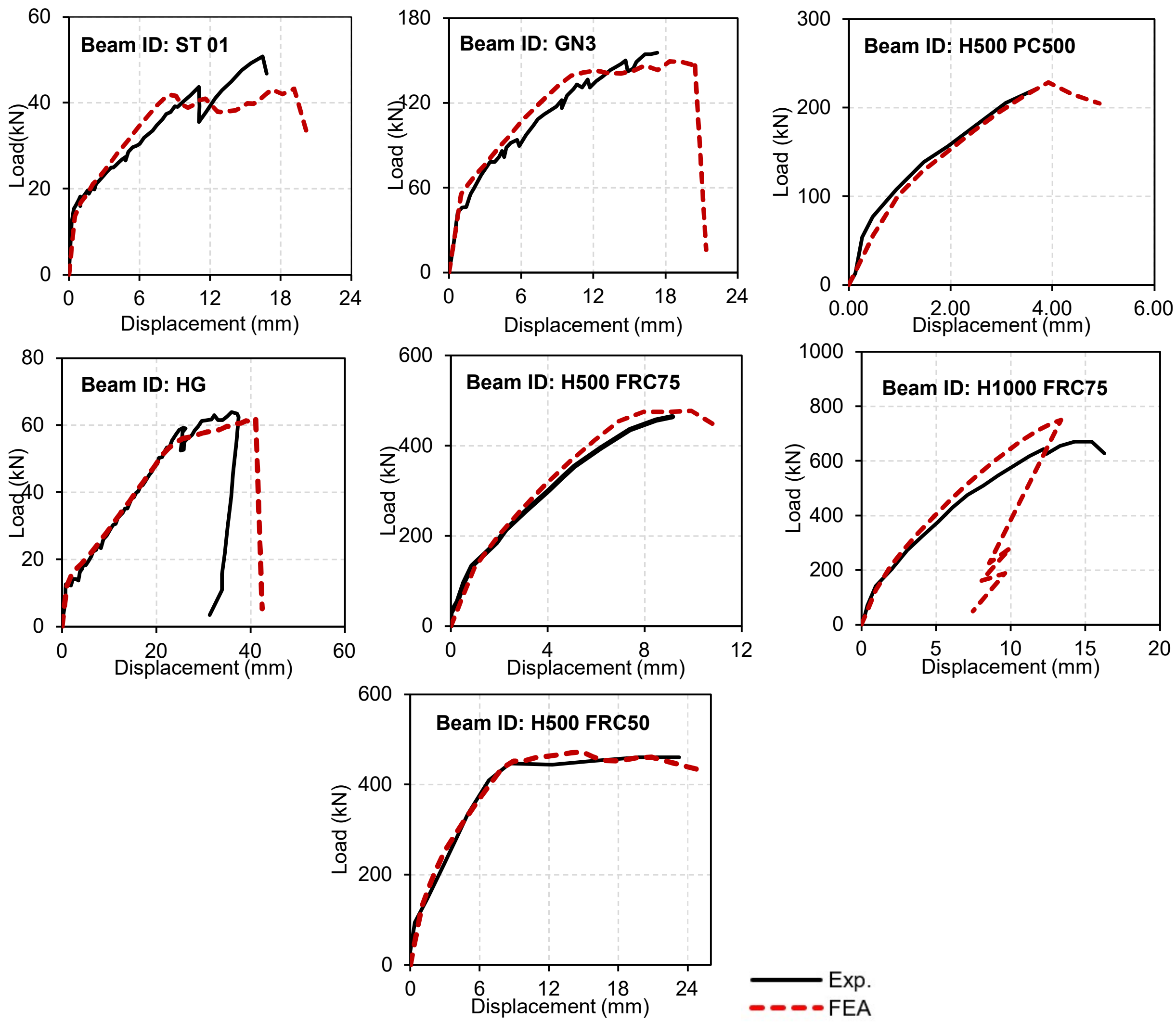

Figure 5-5: Summary of comparisons between experimental and FEA L-D results of SR GFRP with and without fibres. See Table 2 for references for each beam.

5.3 Parametric Study

A parametric study involved 720 modelled beams, exploring parameters including geometry (with beam heights of 500 mm and 750 mm), to study the size effect and 500 mm was selected to represent the common usage in residential buildings, load location (affecting *a/d* ratios with 2, 3, and 4 considered) to evaluate both shear and flexural failure, types of reinforcement bars (steel and GFRP), reinforcement ratios (ρ = 0.55%, 1.1%, and 2.2%, representing a range of reinforcement between the minimum (0.4%) and maximum (3.4%) according to (ACI-318-19, 2019), fibre materials (SF, GF, and HF), and fibre dosages (V_f = 0.5%, 1.0%, and 1.5%) with respect to both SLS and ULS. Figure **5-6** shows a flow chart illustrating the various parameters considered. The anticipated result is that more than 50% of beams will fail in shear, a phenomenon demanding further investigation due to its complexity. Practically, GFRP beams are known for their lower axial stiffness, with 30% of the data representing beams at *a/d* =2. These beams either lacked stirrups or had minimal stirrup reinforcement, emphasizing the occurrence of shear failure.

The identification code of the parametric study beams is described in Figure 5-7. The ρ values are associated with four and six bars with diameters of 14, 20, and 28 mm, which correspond to ρ values of 0.55%, 1.1%, and 2.2%, respectively.

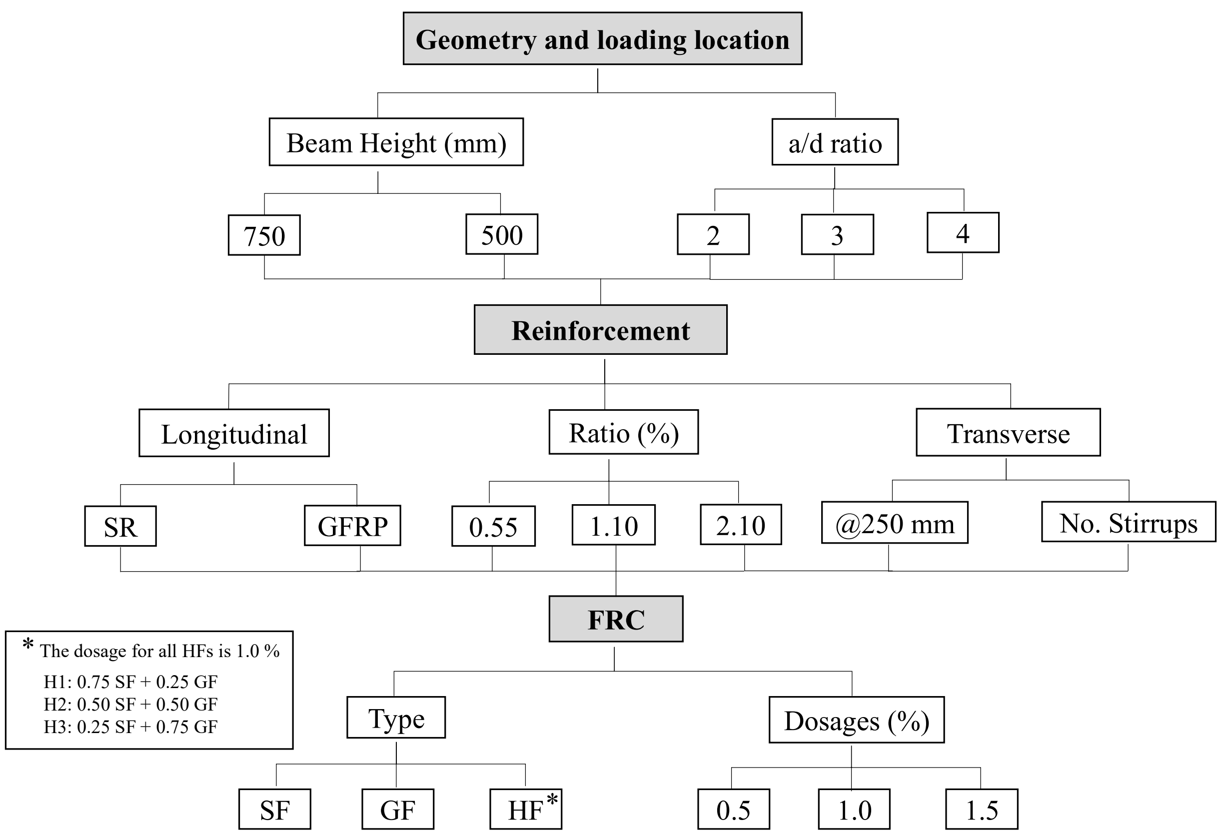

Figure 5-6: Parametric study flow chart.

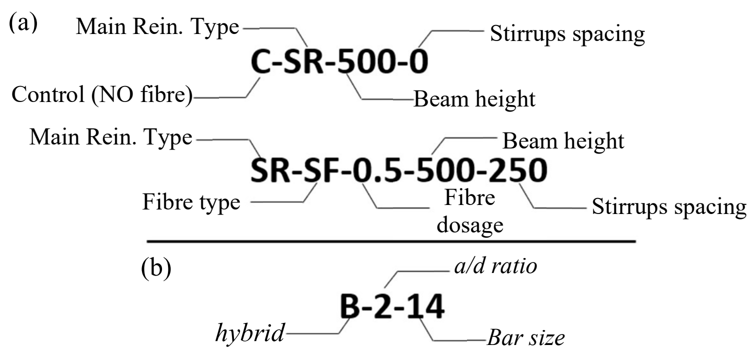

Figure 5-7: The parametric study code (a) first part (b) second part. All dimensions in mm.

Figure 5-8 illustrates the reference beams utilized in the parametric study. A cover of 30 mm was selected in accordance with (CSA A23.3:19, 2019). Two main reinforcement types were used for the parametric investigation: steel bars and GFRP bars, as described in Table 5-3. Furthermore, outlines the properties of the stirrups. The compressive strength of concrete without fibres was 40 MPa, and it had higher strengths (up to 55 MPa) for FRC, as noted from the tests in Chapter 3.

Table 5-3: Properties of main reinforcement chosen in FEA model

Propriety	SR	SR-Stirrups	GFRP	GFRP-Stirrups
Material	Steel	Steel	Glass Fibre	Glass Fibre
Yield strength,	400 MPa	400 MPa	-----	----
Ultimate strength	600 MPa	600 MPa	1100 MPa	450 MPa
Modulus of Elasticity	200 MPa	200 GPa	62.5 MPa	50 GPa

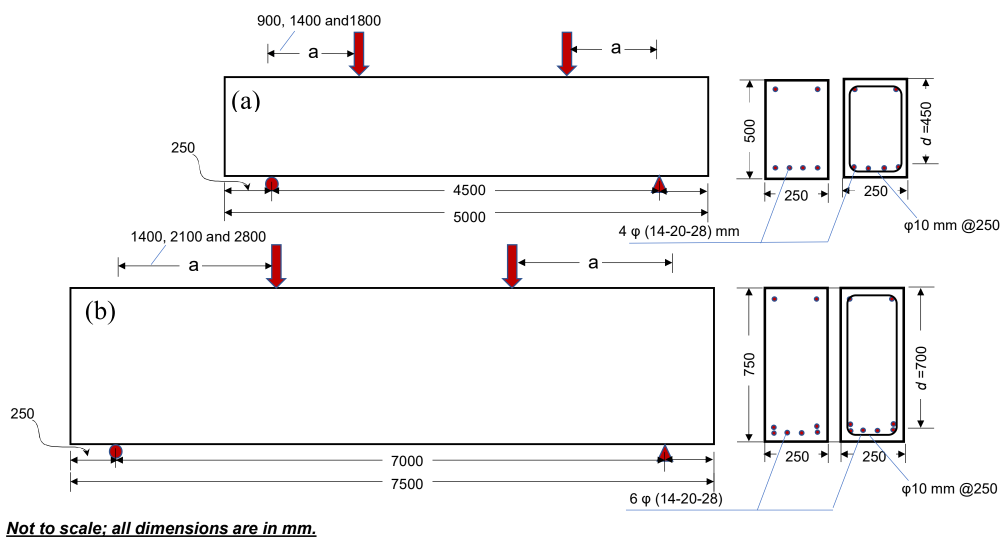

Figure 5-8: Details of specimen's geometry of beam (a) 500 mm height, and (b) 750 mm height

5.3.1 Control reinforced concrete beam without fibres (RC)

Parametric study results were compared to design codes and standards to check that peak loads were within reason. For shear failure, comparisons were made between CSA S6:19 for steel-RC and CSA-S806 2012 for GFRP-RC. For flexural failure, comparison was based on CSA A23.3:19. Results show a good correlation between FEA (P_{FEA}) and design codes and standards predicted (P_p) peak load. The mean and coefficients of variation (CoV) for SR-RC and GFRP-RC beams were 1.22 and 19%, 1.11 and 19%, respectively. GFRP-RC members were predominantly governed by shear failure; a similar variation was found by (Alguhi and Tomlinson, 2021) as they compared the test to predicted GFRP shear strength from the same codes and standards.

For SR-RC flexural members, the mean and COV of the FEA moment resistance over the predicted moment resistance were found to be 1.15 and 8.7%, respectively. These values were lower than the mean and COV of the FEA shear strength over the predicted shear strength, which were 1.34 and 22%, respectively, as shown in Figure 5-9 (a). GFRP-RC beams experienced shear failure, with a mean and COV between FEA and predicted from codes/standards equal to 1.11 and 19%, respectively. This discrepancy is expected because flexural behaviour is less complex compared to shear response, which is primarily influenced by shear stresses in the compressive zone, aggregate interlock, residual tensile stresses, dowel action(ASCE-ACI-426-73, 1973), and arch action in shorter beams (shear span to effective depth ratio less than 2.5). In such cases, strut-type action between loads and supports begins to dominate (MacGregor and Wight, 2006). Having checked that values were reasonable, further parameters were investigated with fibres.

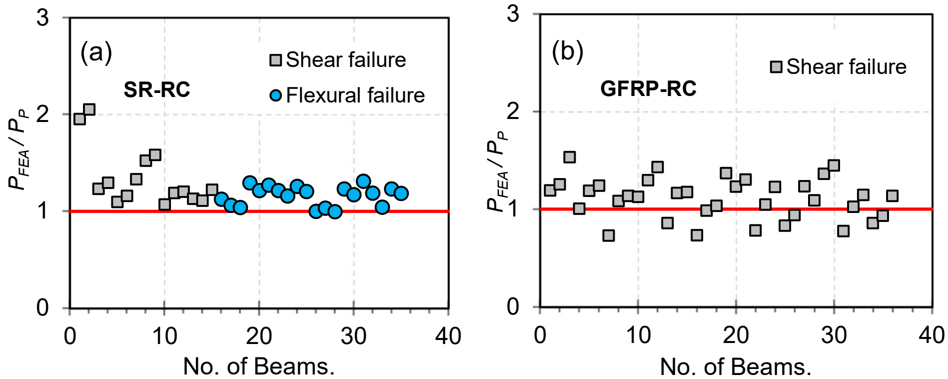

Figure 5-9: Numerical and predicted (theoretical) results: (a) SR-RC and (b) GFRP-RC.

5.4 Results and Discussion

5.4.1 General load-displacement and failure mode response

In this section, a qualitative analysis was conducted on a subset of numerical data (a/d = 3, h = 500, ρ = 1.1%, and V_f of SF = 1.0%) that represents common use cases in practice to examine load-displacement behaviour and failure mode, as illustrated in Figure 5-10.

During the pre-peak response, the addition of 1.0% SF resulted in an increase in the service load corresponding to the deflection limit (span over 360 considered). This enhancement can be attributed to the reduction in crack width, a consequence of the bridging process, which increases the cracked stiffness of FRC members with steel reinforcement, as shown in Figure 5-10(a). In contrast, GFRP showed smaller increases in service load, attributed to its lower modulus of elasticity compared to steel, as shown in Figure 5-10(b). The use of stirrups had no impact on the service deflections for both SR and GFRP, whether with or without fibres. Additionally, the deflection limit is inappropriate for SR control beams as it sometimes surpasses the deflection at yield. This situation leads us to choose the strength limit, where the peak load is divided by 1.5, per the live load factor specified in the National Building Code of Canada, rather than the deflection limit. Using fibres increases both the flexural strength of SR beams and the shear strength of GFRP. This improvement is more pronounced for members governed by shear compared to those governed by flexural failure. The fibres exhibit a similar effect to that of stirrups, improving the peak load, as in Figure 5-10.

Concerning failure mode and crack pattern, it is evident that incorporating 1.0% SF may shift failure mode from a brittle shear failure to a more ductile flexural failure, similar to stirrups, as illustrated in Figure 5-10(c). For GFRP-RC, despite still failing in shear, the addition of fibres greatly increased capacity and showed capacities and crack patterns similar to members with stirrups, as shown in Figure 5-10(b,d).

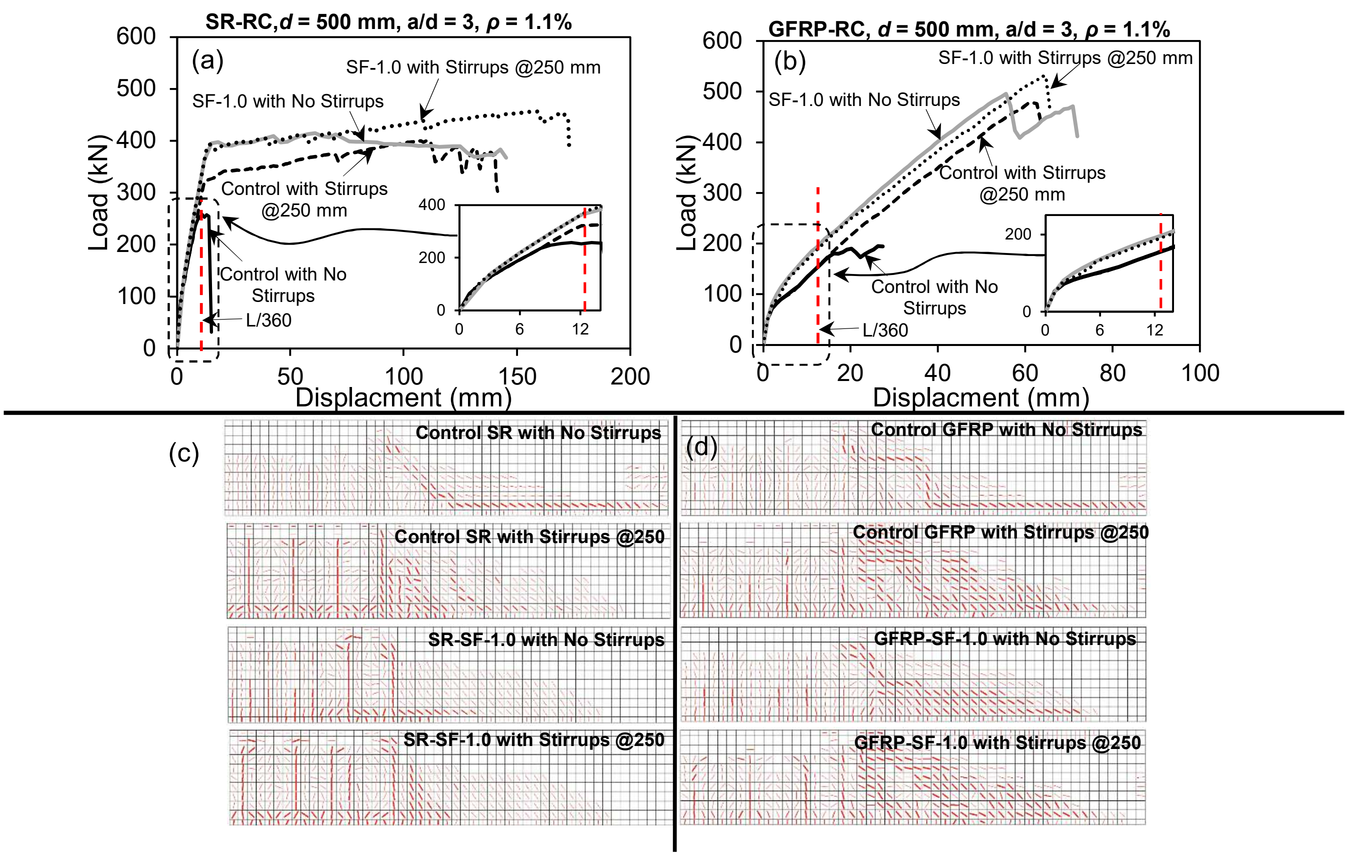

Figure 5-10: General load-displacement for (a)SR, (b)GFRP; and failure mode (c) SR, and (d) GFRP beams.

5.4.2 Effect of fibres on peak load.

The addition of FRC enhances concrete's tensile and compressive strength, which can also increase the peak load of RC. Figure 5-11 illustrates the impact of adding fibre on peak load.

Results show that adding fibre generally leads to a considerable increase in peak load as fibre dosage, whether SF or GF increase, for both SR-RC and GFRP-RC beams. However, these increases show diminishing returns for dosages of SF beyond 1.0%. For instance, for SR-B2-28 with $a/d = 2$ and $\rho = 2.1\%$, peak load compared to the plain concrete member increased 52%, 83%, and 97% for fibre dosages of 0.5%, 1.0%, and 1.5%, respectively. This suggests that the recommended optimum dosage for SF is around 1.0%, attributed to fibre saturation and a conflict between improved mechanical properties and workability (Alguhi and Tomlinson, 2022).

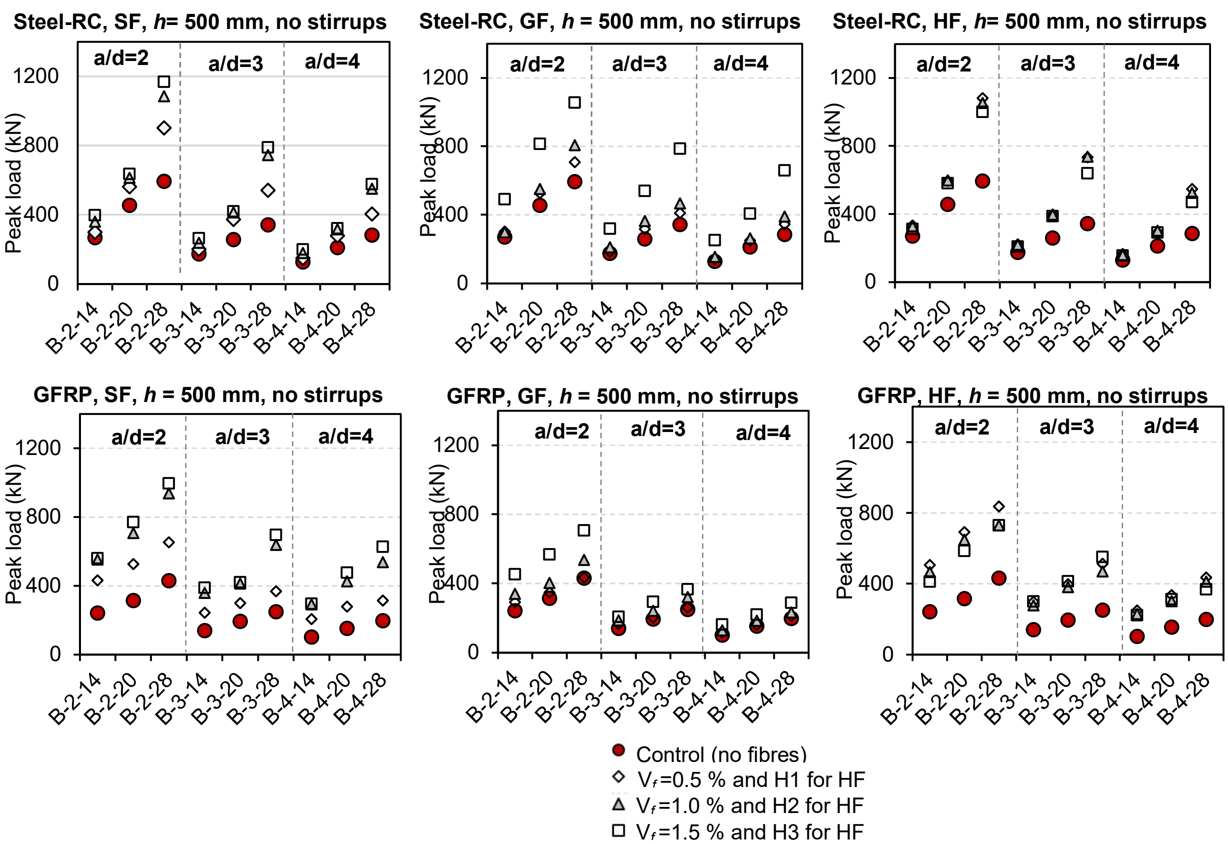

Figure 5-11: Effect of fibre on peak load for SR and GFRP beams

However, the trend of increasing peak load continues with increasing GF dosages over the investigated range. In the case of SR-B2-28 with $a/d = 2$ and $\rho = 2.1\%$, peak load increased by 19%, 35%, and 80% for dosages of 0.5%, 1.0%, and 1.5%, respectively. This indicates the need to investigate larger dosages of GF to determine the optimal dosage for improved member performance.

Replacing 50% of SF with GF, as in H2, provides almost the same peak load increase as H1 (0.75% SF and 0.25% GF). However, increasing the proportion of GF beyond 50% reduces peak load due to the lower stiffness of GF compared to SF.

5.4.3 Section utilization

Failure mode depends on factors such as beam size, material composition, and loading. In this section, the ratio between the numerical moment capacity, $M_{fib,FEA.}$, and the analytical moment capacity of the member $M_{fib,A}$, for each beam was calculated. The theoretical moment capacity was determined using a stress-block approach (Alguhi and Tomlinson, 2023). Larger ratios indicate a larger section utilization, with values exceeding 1.0 likely linked to flexural failure. Smaller ratios show less section utilization, which is generally linked to shear failure; a similar approach was used by (Kani, 1967; F. (Fausto) Minelli, 2005). Results revealed that ~64% of the modelled beams (461 beams) failed in shear; ~36% of the modelled beams (259 beams) failed in flexure.

Figure 5-12 illustrates the impacts of various parameters, such as *a/d* ratio, ρ, and stirrups, on section utilization. Results show that the *a/d* ratio has minimal effect on utilization for SR beams, particularly when steel stirrups are used and at lower reinforcement ratios. This is because adding stirrups increases shear capacity, promoting flexural failure and full section utilization. Reducing ρ leads to more likely flexural failure due to a decrease in moment resistance. This observation is consistent with the findings by (Ayub and Khan, 2022).

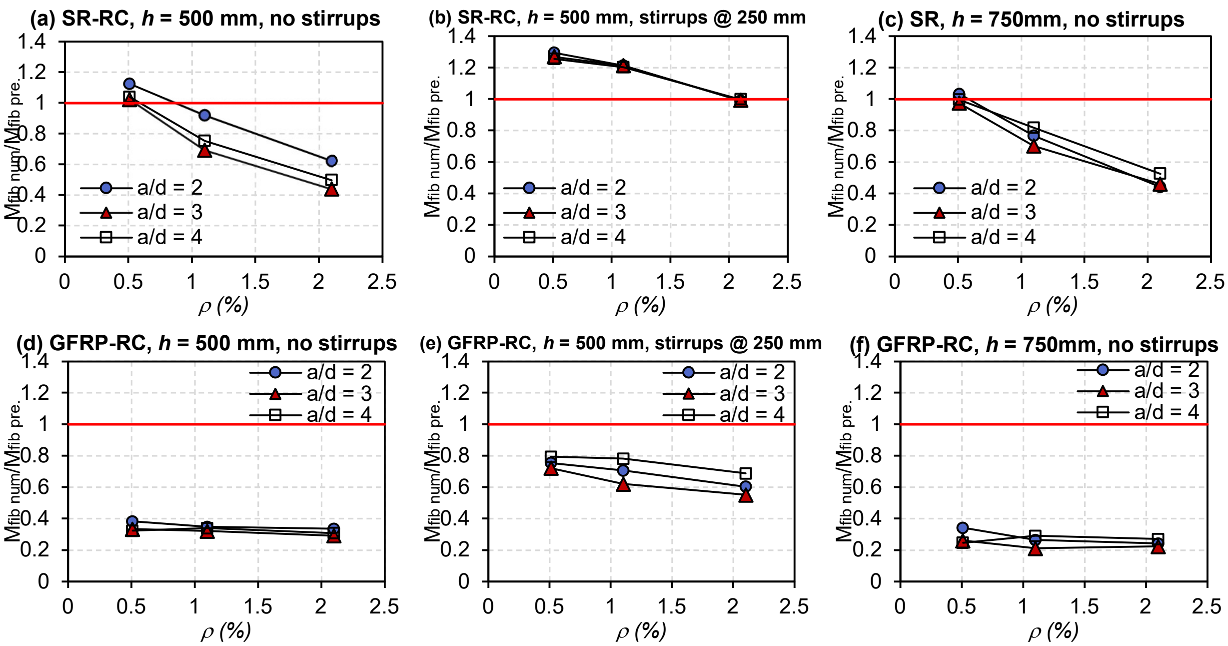

Figure 5-12: Effect of reinforcement ratio, ρ, beam size, and stirrups on failure mode of (a) SR-500, (b) SR-500 with stirrups @ 250 mm, (C) SR-750, (d) GFRP-500, (e) GFRP-500 with stirrups @ 250 mm and (f) GFRP-500 beams.

The effect of *a/d* is more apparent at larger reinforcement ratios for SR-RC beams. For all GFRP-RC beams, which were all shear controlled, the impact of *a/d* is evident; the utilization has lower values at *a/d* 3.0, with a reduction in capacity due to shear failure for SR-RC beams without stirrups and almost all GFRP-RC beams, similar finding was observed by (Kani, 1967). The smaller beams exhibited larger values of utilization compared to the larger beams, highlighting the presence of a size effect issue about a reduction in shear strength as beam size increases, attributed to wider cracks that lead to loss of aggregate interlock associated with the increasing the size of the beam, as seen in Figure 5-12 (c,f).

A central investigation of this analysis is determining whether fibres alter failure mode and how fibres' type and dosages impact utilization, as shown in Figure 5-13. Results show that the increase in fibre dosage makes flexural failure more likely and a corresponding increase in utilization. Specifically, for SR-RC beams without stirrups, addition of SF with dosages greater than 1.0% shifted failure mode from shear to flexure which is attributed to the fibres' capability to fill the role that stirrups play, shown in Figure 5-13(a) and these findings are aligned with failure mode, depicted in Figure 5-10 (c). However, for the investigated parameters, GF alone could not induce this change in failure mode. The addition of fibres enhances the capacity and utilization of beams. For example, beam capacity increased by 34% and 25% for 1.0% SF and GF in steel-reinforced beams compared to the control beam. In the case of GFRP-RC beams, the increase in beam capacity and utilization is more pronounced, with a 115% and 45% improvement when 1.0% of SF and GF is added. These outcomes are consistent with the findings illustrated in Figure 5-11. Remarkably, combining SF and GF showed similar utilization at each ratio considered due to the compatibility between SF's stiffness and GF's deformability, as shown in Figure 5-13 (c and f).

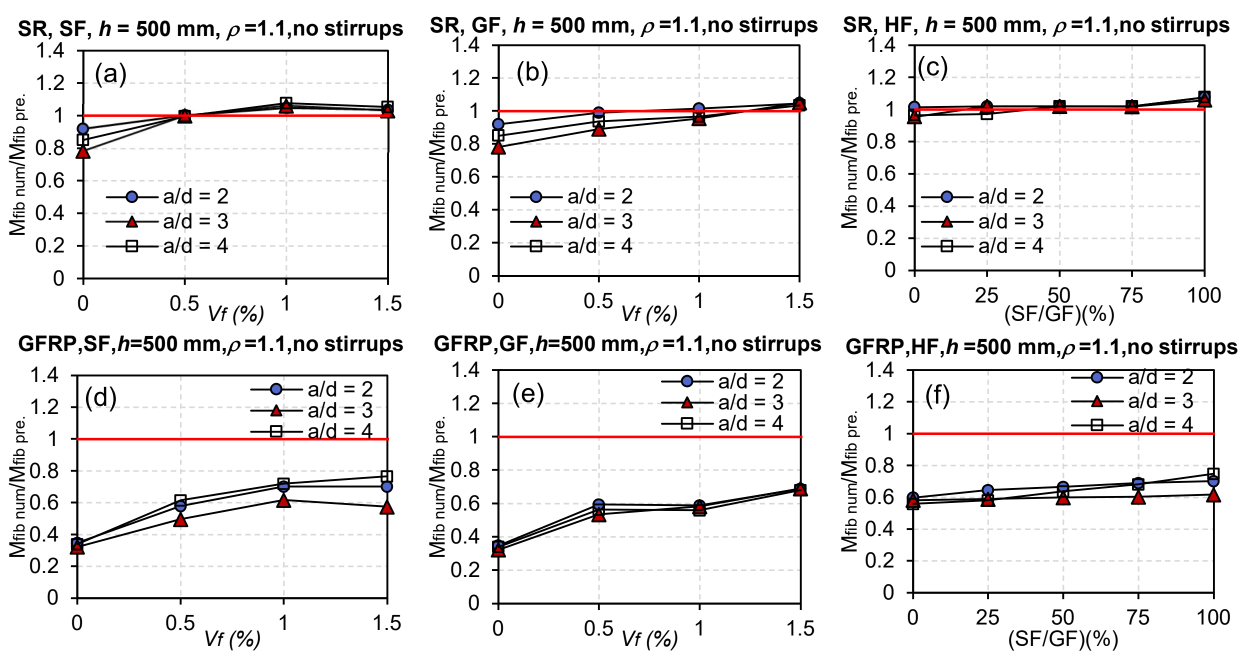

Figure 5-13: Effect of adding fibres on failure mode for beam 500H:(a) SR-SF, (b) SR-GF, (c) SR-HF, (d) GFRP-SF, (e) GFRP-GF, and (f) GFRP-HF.

5.4.4 Size effect

Two effective depths (450 and 700 mm) were considered in the study of the size effect. We also explored whether fibres could help minimize size effects by reducing larger cracks, leading to less degradation of aggregate interlock and tensile strength for members that fail in shear. CSA-S806-12 indicates that the size effect becomes evident when beam depth exceeds 300 mm, with similar values used in other codes and standards. An additional reason for selecting depths of 450 mm and 700 mm is that they fall within the range of beam depths used in the validation of the FEA in Section 5.2.3, which are 150 mm to 1000 mm. To ensure an accurate analysis of independent size effect parameters, a constant *l/d* ratio of 10 was recommended (Elakhras et al., 2022).

The shear strength was normalized relative to $\sqrt{f_c'}bd$ to investigate the size effect corresponding to different effective depths for beams without stirrups that failed in shear, as illustrated in Figure 5-14. For GFRP-RC beams with a/d = 3 and ρ = 1.1% (other parameters showing similar trends), the addition of fibres showed no distinct impact on the size effect for the considered effective depths. This aligns with experiments by (F. Minelli et al., 2014) for depths of 500 and 1000 mm, where the impact of fibres in mitigating the size effect was observed only for members 1000 mm deep.

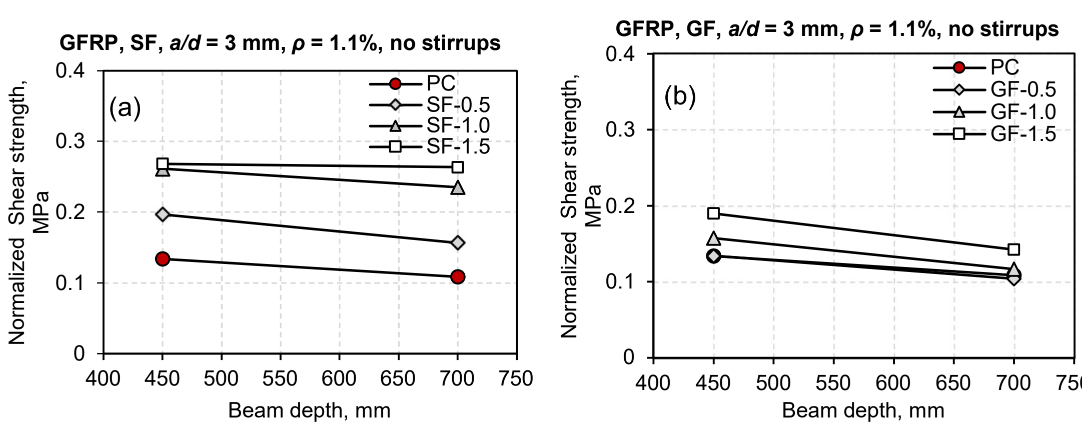

Figure 5-14: Trend in Shear Strength with variation in size for GFRP and FRC beams (ρ = 1.1%).

5.4.5 Effect of fibre on replacing minimum transverse shear reinforcement

This study compared the control beam with stirrups (without fibres) and equivalent beams without stirrups but with fibres, as shown in Figure 5-15. This section illustrates the influence of various types and quantities of fibres on the substitution of minimal shear reinforcement. Findings indicate that using SF at dosages greater than 0.5% effectively substitutes the need for minimum stirrups in both SR-RC and GFRP-RC beams of either 500 mm or 750 mm depth. GF at a dosage exceeding 1% can replace the minimum stirrups in 500 mm deep SR-RC beams considered in this study. However, in other cases, GF was unable to match the capacity achieved by stirrups due to GF's lower stiffness. For the same reason, combining SF and GF performs better than GF alone. In beams with at least 50% of GF replaced with SF, the fibres can replace the minimum stirrups for both SR-RC and GFRP-RC beams of different sizes, while an SF dosage of 50% or greater can replace the minimum stirrups in SR beams with a depth of 500 mm.

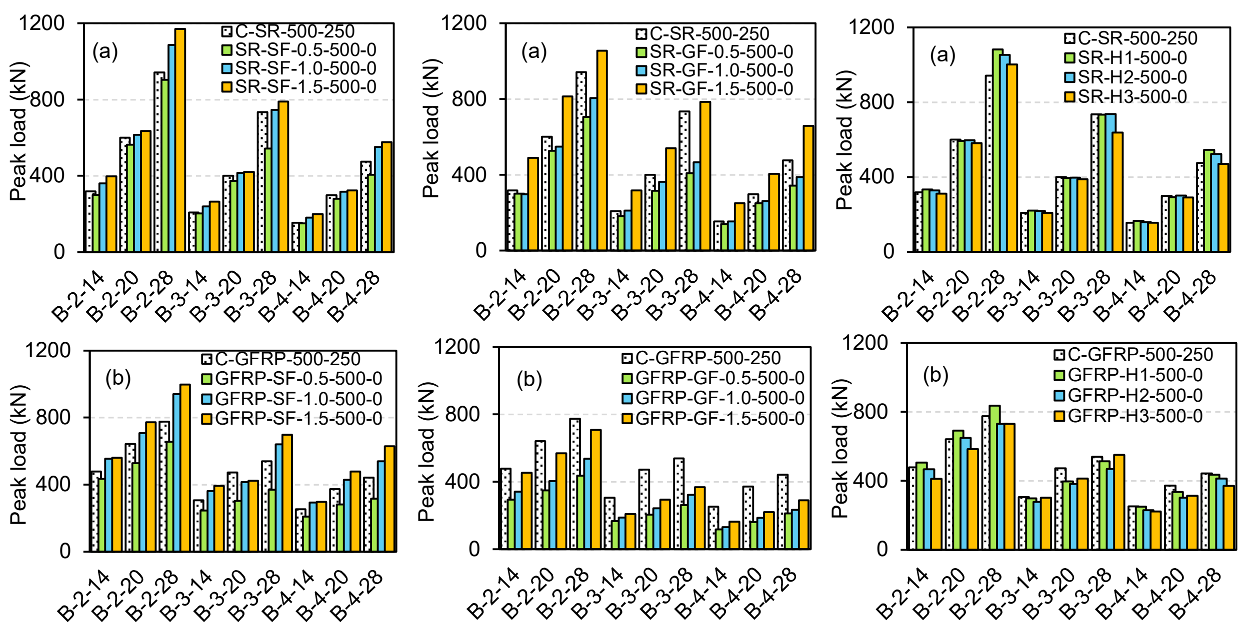

Figure 5-15: Effect of fibre type and dosages on replacing minimum transverse shear reinforcement of: (a) SR-500H, (b) GFRP-500H

5.5 Serviceability performance

The maximum service load of beams was determined to investigate how fibre type, dosages, and stirrups impact serviceability. The specific foci were crack width, deflection, and reinforcement strain. Service load was determined for each subset of beams (same reinforcement type, reinforcement ratio, *a/d* ratio, and depth) based on members without fibres and with stirrups. This identical load was then used to compare against all other members within the subset (with varying fibre types and dosages). Service load for steel-RC beams was chosen based on the minimum between strength (i.e., un-factoring failure load by dividing it by 1.5) and deflection limits following a similar approach to that used by Tomlinson and Fam (2015). The live-load deflection limit for beams was set at *l/360* and translates to 12.5 mm and 19.0 mm for beam depths of 500 mm and 750 mm, respectively, for both Steel-RC and GFRP-RC. This criterion is typically applied to elements where long-term deformations caused by factors like creep and shrinkage are not likely to damage connected elements or structure-function. Importantly, the deflection at yield for all Steel-RC beams was below the *l*/360, indicating that these members are ULS controlled, as detailed in Section 5.4.1. In contrast, GFRP-RC, with larger strength and lower stiffness than steel, requires a distinct approach for determining service load. The strength limit was set at 33% of the nominal capacity, $M_{fib,FEA}$, to ensure an acceptable limit of FRP bar strain and prevent creep rupture failure. This limit has been used in prior studies (Bischoff and Gross, 2011; Maher Elnemr et al., 2011). As an example, the service load for steel-RC beams belonging to the category of 500H beams with an *a/d* ratio of 3 and ρ = 1.1%, denoted as SR-500-250, was calculated by dividing the peak load (402 kN) by 1.5, the live load factor specified in the National Building Code of Canada, resulting in 268 kN.

Table 5-4 shows how SLS performance improves with added fibres, showing how, at an equivalent service load to a counterpart beam without fibres, fibres reduce maximum deflection, maximum crack width, and reinforcement strain. The overall observation is that the addition of fibres enhances all SLS checks. Each parameter will be discussed in detail in the subsequent sections.

Table 5-4: Percentage reduction in deflection, crack width, reinforcement strain at an equivalent service load between FRC beams and beams without fibres

SLS check	V_f (%)	SR-RC SF	SR-RC GF	GFRP-RC SF	GFRP-RC GF	V_f (1.0%)	Hybrid fibres* SR-RC	Hybrid fibres* GFRP-RC
Max deflection reduction	0.5	10	7	27	21	H1	19	31
	1.0	17	11	30	27	H2	15	28
	1.5	24	13	37	29	H3	10	14
Max crack width reduction	0.5	11	10	36	32	H1	27	56
	1.0	27	23	62	55	H2	25	52
	1.5	35	26	76	66	H3	14	39
Max reinforcement strain reduction	0.5	14	7	17	14	H1	32	64
	1.0	30	27	61	52	H2	29	58
	1.5	38	30	71	60	H3	18	27

* For hybrid fibres: H1 is (0.75+0.25GF), H2 is (0.50SF+0.5GF), and H3 is (0.25SF+0.75GF).

5.5.1 Maximum crack width

The maximum crack width was taken as the crack width at the extreme tension fibre in the largest flexural crack located near the mid-span (within the constant moment region) corresponding to the service load. The crack width under service load for various types and dosages of fibres is presented in Figure 5-16. Results indicate that, as anticipated, adding fibres decreases crack width. This reduction is attributed to the main attributes of fibres, such as crack bridging and the enhancement of the fracture propagation zone surrounding the cracks. Bridging restricts crack width, thereby limiting crack propagation.

As a caveat for interpreting the results, the bond between reinforcement and concrete significantly affects crack width. The precision of crack width expressions relies heavily on a bond-dependent coefficient, k_b (Wang and Belarbi, 2011), posing modelling challenges due to limited test data on k_b for the considered bars or incorporating into models. For this case, the specific crack widths may not represent what may be observed in a test, but the overall effect of fibre dosage is expected to be similar.

Crack widths reduced as fibre dosage increased. As dosage increased from 0.5% to 1.5%, crack width decreased by 11% to 35% for SF; for GF, reductions are 10% to 26% (Table 5-4) and Figure 5-16. The trend shows diminishing returns, which is attributed to fibre saturation. With dosages approaching 1.5%, the additional fibres do not contribute as much to reducing crack width because the concrete matrix becomes saturated with fibres.

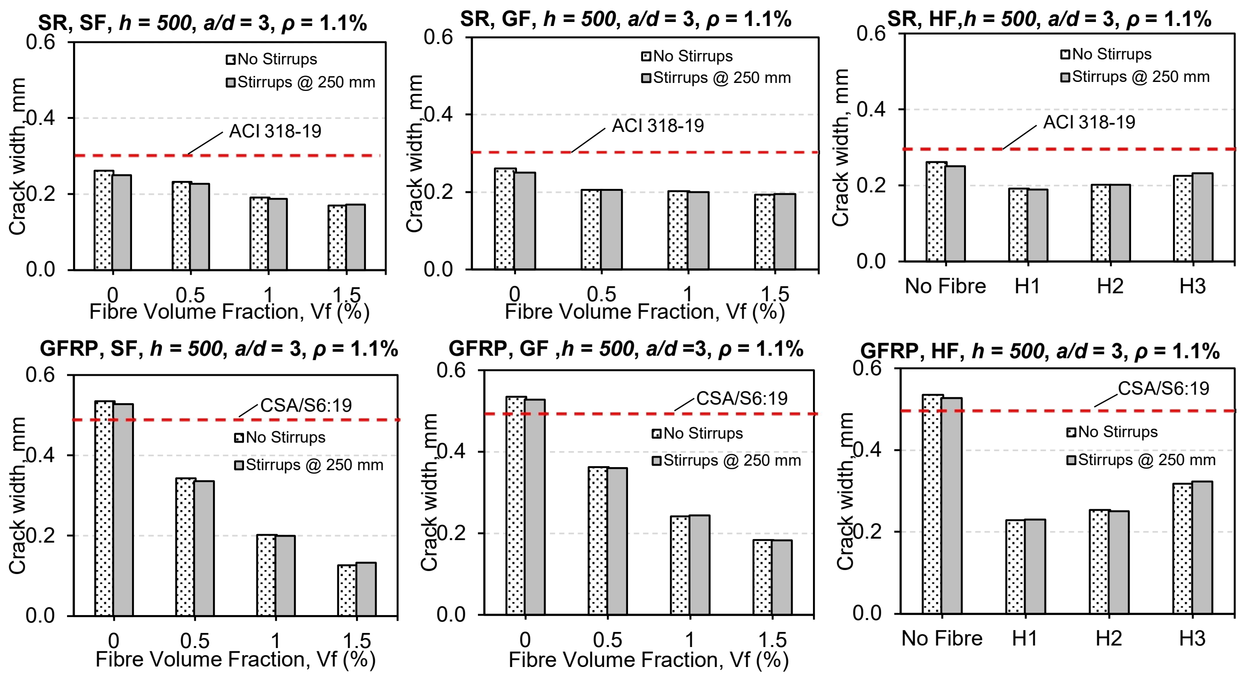

Figure 5-16: Effect of fibre type, dosages, and stirrups on crack width at service for beam for SR and GFRP

GFRP-RC beams show a remarkable reduction in crack width with fibre addition, with notable effects observed for both SF and GF. This trend is attributed to the lower stiffness of GFRP bars compared to steel, leading to fibres contributing more to section stiffness and reducing crack widths. Specifically, for SF, the crack width decreases with dosages of 0.5-1.5% by 33-76%, while for GF, the corresponding reductions are 32-66%, as illustrated in Table 5-4.

For beams with hybrid (combined steel and glass) fibres at a dosage of 1%, the crack widths observed show that replacing up to 50% of SF results in a comparable degree of enhancement as using SF alone and provides better performance than using GF alone or using only 25% SF in a hybrid mixture, for both SR-RC and GFRP-RC. Whether stirrups were added or not does not appear to affect crack width, which is expected as the region considered is under large moments and negligible shear force.

Regardless of fibre dosage, SR-RC beams are not governed by crack width at the considered loading as crack widths measure less than 0.30 mm, in compliance with (ACI-318-19, 2019). This is expected as these beams were previously found to be governed by ULS. GFRP-RC beams have larger crack widths, as expected, than SR-RC beams. GFRP-RC without fibres has crack widths exceeding 0.50 mm widths, which exceeds those permitted by (CSA S6.1:19, 2019) and stricter than the 0.70 mm width limits given in ACI 440.11, though GFRP-RC beams with fibres satisfied this limit.

5.5.2 Maximum mid-span service deflection

The assessment of fibre type and dosages on deflection at the service load, defined in Section 5.5.2, is illustrated in Figure 5-17. Like with crack widths, as fibre dosages increase, deflections under an equal service load decrease due to the increased flexural stiffness of FRC compared to plain concrete. The reduction in deflection is more prominent with SF compared to GF, primarily because of SF's larger stiffness. Specifically, fibre dosages from 0.5-1.5 results in deflection reductions relative to a beam without fibres of 10-24% for SF and 7-13% for GF, as shown in Figure 5-17 and Table 5-4. For GFRP-RC beams, 0.5-1.5% fibre dosages result in deflection reductions relative to a beam without fibres of 27-37% for SF and 21-29% for GF.

However, combining SF and GF with an SF/GF ratio of up to 50% has shown notably improved service deflection performance for SR-RC and GFRP-RC. The deflection of hybrid beams was reduced by 15% and 28%, compared to a control beam (without fibres), for SF/GF ratios of 0.5 for

SR and GFRP, respectively Figure 5-17 and Table 5-4. This favourable outcome is attributed to the compatibility between SF's higher stiffness and GF's greater deformability. The balanced interaction between the two fibre types enhances their effectiveness in minimizing service deflection.

Adding stirrups led to a marginal decrease in deflection (~3%). This slight reduction is attributed to stirrups limiting shear deformation in the beams. However, fibres also appear to reduce shear deformations, so the impact of adding stirrups on deflection is minimal for all FRC beams.

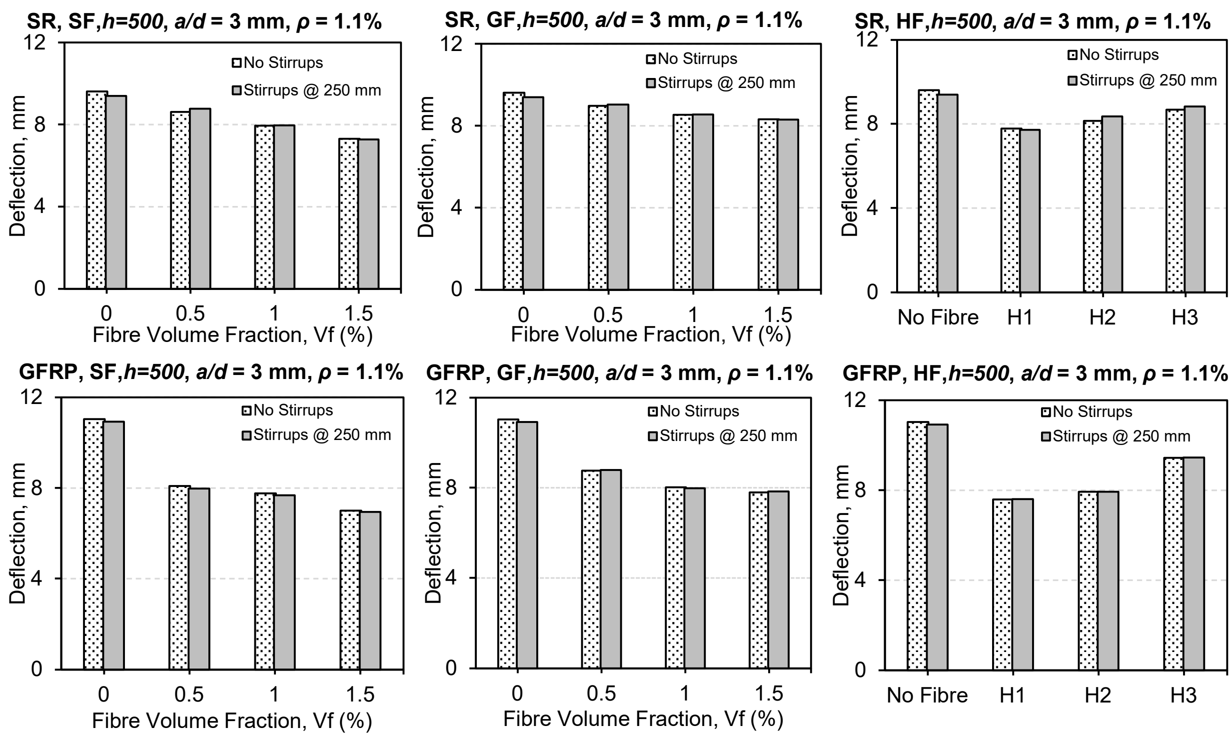

Figure 5-17: Effect of fibre type, dosages, and stirrups on deflection at service for SR-RC and GFRP-RC beams.

5.5.3 Maximum reinforcement strain at cracks

The reinforcement strain is a key parameter influencing the reinforcement stress, which is a primary factor in predicting crack width, as shown in Figure 5-18. Adding fibre decreases reinforcement strain at service as fibres act as micro-reinforcement and carry some tension that would otherwise transfer into the reinforcement bars.

In Figure 5-18 and Table 5-4, when fibre dosages of 0.5% to 1.5% were added, strain reductions for SF were 14-38%, while for GF, the reductions were 7-30%. GF has the best performance at 1.0% dosage, with larger dosages seeing minimal further benefits. This is attributed to the lower elastic modulus of GF, making their pre-peak contribution smaller after reaching 1.0% dosage.

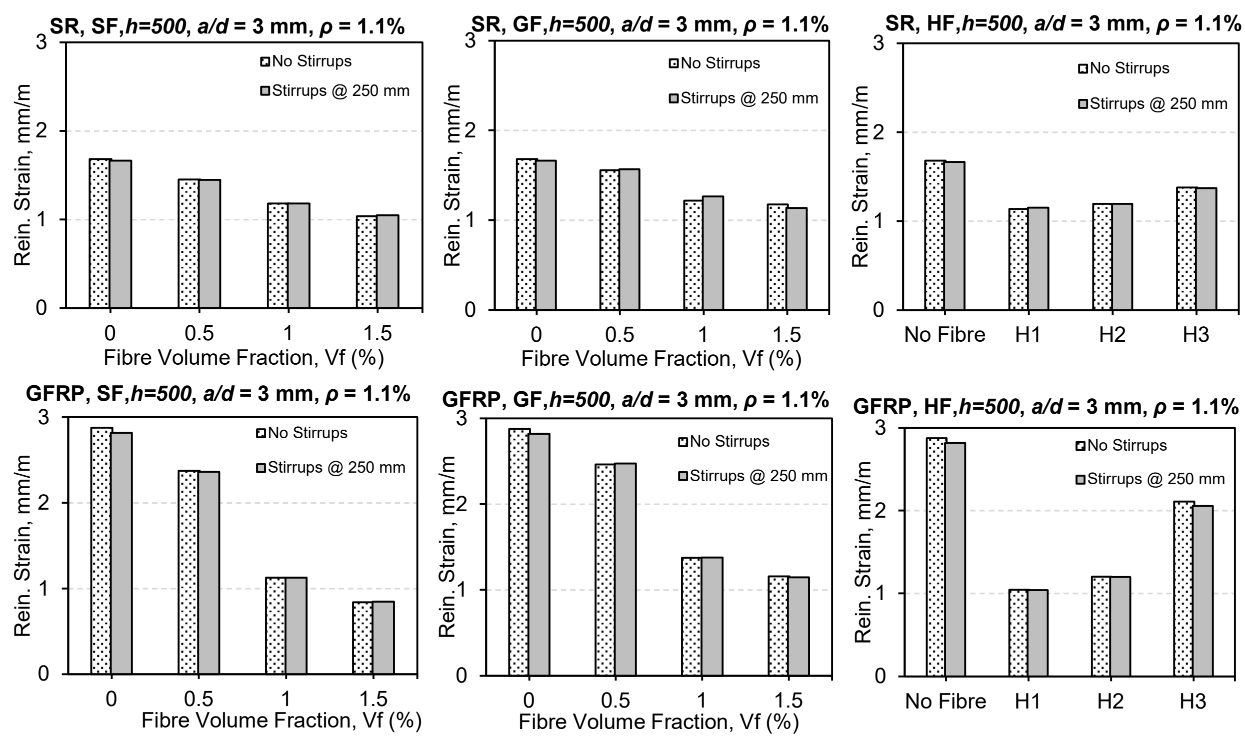

Figure 5-18: Effect of fibre type, dosages, and stirrups on reinforcement strain at service for SR and GFRP.

For beams with a hybrid fibre composition, a trend like that of crack width and deflection is observed for both SR-RC and GFRP-RC. Increasing the ratio of SF to GF results in a decrease in reinforcement strain, as seen in Figure 5-18 and Table 5-4. Like with crack widths and deflection, replacing up to 50% of SF with GF gives similar outcomes with less effectiveness at 75%

replacement of SF with GF. For both SR-RC and GFRP-RC, stirrups have negligible impact on reinforcement strain, irrespective of fibre type or dosage.

5.6 Design considerations and limitations

Using fibres in concrete can enhance the early-stage behaviour of structures by mitigating plastic and increasing the member stiffness. This, in turn, reduces tensile strain on reinforcing bars, resulting in diminished crack width and deflection. Consequently, there is an improvement in tension stiffening, which is particularly crucial for lower stiffness reinforcement (e.g., GFRP) and elements exposed to harsh environmental conditions. Adding fibres also enhances member capacity, which may allow designers to use smaller beams and/or reduce reinforcing bars needed to resist loading, which can mitigate bar congestion issues. Smaller beams may lead to cost savings (i.e., less material use as well as smaller dead load leading to smaller foundations and seismic forces) and an improvement in the performance of structures.

Adding fibres can potentially replace stirrups and contribute to shear resistance (Facconi, Amin, et al., 2021). Additionally, fibres can alter the failure mode from an abrupt shear failure to a flexural failure that provides more warning of failure through yielding (SR-RC) or excessive deformation (GFRP-RC).

The FRC is a complex material owing to the randomness of fibres, making it difficult to model exact fibre behaviour. This study adopted a smeared approach by simplifying the tension stress-strain relationship into a proposed trilinear model developed previously by the authors (Alguhi and Tomlinson, 2023). The utilization of inverse analysis in VecTor2 allowed the creation and verification of this model. The model was found to reasonably represent FRC within the scope of this study, which encompasses normal strength concrete and medium fibre dosages (0.5-1.5%). Increasing dosages by more than 1.5% leads to issues with workability (Alguhi and Tomlinson,

2022) and mechanical responses that may not be able to be modelled using the approaches used in this study. Findings from this study provide researchers and users with information that allows them to grasp and integrate intricacies of FRC behaviour into FEA and design considerations. FEA can successfully simulate different FRC members using various parameters. This success builds confidence regarding the validity of FEA results with FRC. This confidence is particularly valuable for the detailed design of potentially complex elements.

However, it is important to acknowledge that this study has limitations. One limitation is the assumption of full randomness in the arrangement of fibres. This assumption might not perfectly reflect real-world scenarios and should be considered when interpreting the results. Additionally, a notable gap exists in the literature review regarding the integration of GFRP bars with FRC. Understanding how these materials interact is crucial for FEA verification, yet available literature on GFRP-RC with FRC is limited. The model approach is also detailed, requiring considerable computational effort that may not be practical for conceptual and preliminary designs. This study also focused on short-term deflection, did not include any environmental loading, simply supported boundary conditions, and focused on a 4-point bending response.

5.7 Conclusions and recommendations

This paper used FEA to model 720 beams, both SR-RC and GFRP-RC, incorporating various parameters, such as beam depth, *a/d* ratio, reinforcement ratio, fibre type and dosage, combinations of fibres, and the inclusion of minimal stirrups. The aim was to assess SLS factors, including crack width, deflection, reinforcement strain, and ULS factors, specifically flexural and shear strength. The following are the conclusions drawn from the numerical results:

1. The models utilizing VecTor2 can predict responses consistent with test results for beams without fibres and FRC for beams reinforced with either steel or GFRP bars. The developed

constitutive model for FRC-RC effectively represents the SF and GF and is verified against test data, though data for some of the investigated parameters in the literature is sparse.

2. Using SF and GF enhances the strength of SR-RC and GFRP-RC beams; exceeding a 1.0% dosage of SF reduces this impact due to fibre saturation. However, GF consistently shows an increasing trend with higher fibre dosages, suggesting the need to explore higher GF percentages for optimization. The best performance was achieved with a 50% combination of both SF and GF, as this dosage capitalizes on the compatibility between the larger stiffness of SF and the superior deformability of GF.
3. The addition of fibres can shift failure from shear to flexural at dosages exceeding 1.0% over the investigated parameters. Notably, this shift did not occur with GF alone, and replacing 50% of SF with GF improves the outcome. SF at dosages over 0.5% effectively replaced minimum stirrups in both SR-RC and GFRP-RC beams. GF needs larger doses to achieve this replacement due to the lower fibre stiffness than steel. The combination of SF and GF outperforms using GF alone, especially with a 50% mix of both fibres.
4. Serviceability performance includes crack width, instantaneous deflection, and reinforcement strain. Each of these factors was affected by fibres in the same way. The use of fibres decreases crack width, deflections, and reinforcement strain in each beam considered. The largest improvements were seen in GFRP-RC beams, as fibres carry larger shares of the load compared to steel-RC members with stiffer reinforcement.

This study specifically examined two types of fibres, SF and GF, indicating the necessity to explore other fibre types. Steel fibres used to develop constitutive models for the current investigation use a double-hooked end fibre profile; other fibre profiles should be studied in future. Similarly, the model is based on normal strength and density concrete; different concrete types, such as high strength, should also be studied. Expanding the research to include other FRP materials, such as carbon and basalt fibres, is also suggested, as are further models where shear failure is prevented through additional stirrups. The authors also suggest the need for further experiments that report performance at both service and ultimate conditions, particularly for GFRP-RC using FRC.

CHAPTER 6

ONE-WAY SHEAR STRENGTH OF FRP REINFORCED CONCRETE MEMBERS WITHOUT STIRRUPS: DESIGN PROVISION REVIEW

6.1 Introduction

Recently, the American Concrete Institute (ACI) updated its one-way shear provisions for steel-reinforced concrete (RC) for the first time since the 1960s (ACI 2019). As part of this process, the ACI considered several different shear models for steel-RC, as shown in the September 2017 issue of Concrete International (Concrete International 2017). At the same time, the ACI is developing a design code for concrete reinforced with glass fibre-reinforced polymer (FRP).

The one-way shear strength of concrete members without dedicated shear reinforcement, V_c , is primarily influenced by five factors after the formation of diagonal cracks. Four of these factors are the shear stresses in uncracked concrete in the compression zone, aggregate interlock, residual tensile stresses transmitted directly across the cracks, and dowel action of the longitudinal reinforcing bars (ASCE-ACI 1973). The fifth factor, arch action, occurs in shorter beams (shear span to effective depth ratio less than 2.5), where strut-type action between loads and supports begins to dominate (MacGregor and Wight 2006).

The lower elastic modulus of FRP, particularly Glass FRP (GFRP), bars relative to steel leads to FRP-reinforced concrete (FRP-RC) members developing wider and deeper cracks than steel-RC members with the same reinforcement ratio under equivalent loading (Barris et al. 2017). Wider and deeper cracks in FRP-RC reduce the compression zone depth, reduce aggregate interlock, and reduce tensile stresses transferred across inclined cracks. To account for these reductions, some provisions modify steel-RC V_c equations by including a term reflecting the ratio between the FRP and steel moduli of elasticity (ISIS 2007, JSCE 1997 and BISE 1999). The considerably lower transverse strength of FRP bars relative to steel reduces the dowel action in FRP-RC members (Tottori and Wakui 1993), to the point where it can be neglected (Fico et al. 2008, ACI 440.1R-15 2015).

Several studies compare tested and predicted one-way shear strengths from FRP design guides and standards (Fico et al. 2008, El-Sayed and Soudki 2011, Razaqpur and Spadea 2015, Kotynia and Kaszubska 2016). Since then, additional models have been presented, and ACI 318 has updated its shear provisions. Subsequently, there is a need to evaluate one-way shear resistance predictions from recently presented models, and there are limited studies into which of these provisions (code, standard, guideline, or model) best predicts the shear capacity of FRP-RC.

Numerous models, codes, and guidelines have been developed to predict the one-way shear strength of FRP-reinforced concrete (FRP-RC) members. This study presents an experimental database of 147 test results for FRP-RC beams and one-way slabs without stirrups from the literature. This database was collected, arranged and compared to predictions from FRP-RC design guides, standards, and codes (JSCE 1997, BISE 1999, CSA S806-02 2002, CNR-DT 203/2006 2006, ISIS 2007, CSA S806-12 2012, ACI 440.1R-15 2015, and CSA S6:19 2019) as well as against models that were proposed for consideration by ACI 318 (Bentz and Collins 2017, Cladera et al. 2017, Frosch et al. 2017, Li et al. 2017, Park and Choi 2017, and Reineck 2017).

6.2 Experimental Database

To assess the shear strength of FRP-RC members and evaluate design codes, guidelines, and models, a database of 151 one-way shear-critical FRP-RC members without stirrups from sixteen studies was developed [Alkhrdaji et al. 2001, Yost et al. 2001, Tureyen and Frosch 2002, Gross et al. 2003, Tariq and Newhook 2003, El-Sayed et al. 2005, Ashour 2006, El-Sayed et al. 2006a, El-

Sayed et al. 2006b, Bentz et al. 2010, Alam and Hussein 2013, Matta et al. 2013, Ashour and Kara 2014, Tomlinson and Fam 2014, Issa et al. 2015, Kaszubska and Kotynia 2019]. Test summaries, including specimen names, geometries, material properties, and experimental shear strengths, are shown in Table 1. FRP was used as the flexural reinforcement in all specimens, with 111 specimens reinforced with glass FRP (GFRP) bars, 25 reinforced with carbon FRP (CFRP) bars, 9 reinforced with basalt FRP bars (BFRP), and two specimens reinforced with aramid FRP (AFRP) bars. Only test programs that reported measured FRP material properties (i.e. not nominal properties from manufacturer data) were included. FRP bars used in these members had modules of elasticity, E_f, between 32 and 144 GPa with longitudinal reinforcement ratios, ρ_f, between 0.12 and 2.63. The members were constructed with concrete cylinder compressive strengths, $f_c^{'}$, between 24 and 80 MPa. Shear spans ranged between 457 and 3050 mm. The member widths, b_w, were between 114 and 1000 mm. The tensile reinforcement effective depth, *d,* ranged between 146 and 937 mm. The tested FRP-RC members have shear span to effective depth (*a/d*) ratios between 2.4 and 7.0. The geometric and material properties of the test specimens is presented in Figure 6-1, using a four-bin frequency distribution, which is defined as the number of times the observation occurs in the data.

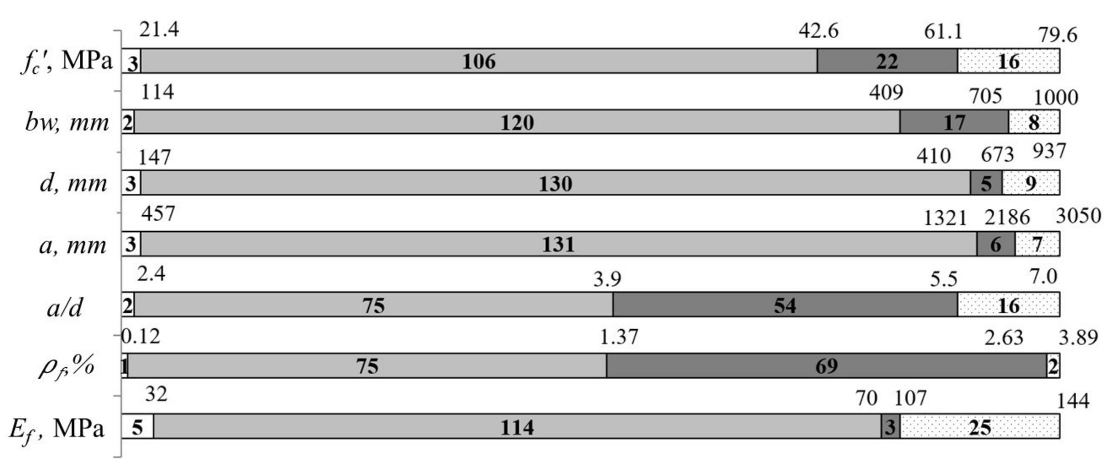

Figure 6-1: Data distribution of experimental parameters

This study focuses on shear-critical members without stirrups. Members with stirrups and members who failed in flexure are not included. Due to their small sample size, continuous, prestressed, or axially loaded members were not considered. The database was completed based on presented experimental data that often does not report factors including aggregate size, a_g, and measured concrete modulus of elasticity, E_c. Unless otherwise reported, a_g is taken as 19 mm, and E_c (in MPa) is calculated based on ACI 318-19 using $4700\sqrt{f_c'}$ (ACI 2019).

Table 6-1. Experimental Database of Shear-Controlled FRP-RC Specimens without Stirrups

No.	*Study*	*Beam ID*	*Fibre type*	*Concrete strength, f_c', MPa*	*Effective depth, d, mm*	*Width, b_w, mm*	*Shear span, a, mm*	*a/d*	*ρ_f %*	*E_f, GPa*	*ρ_f *(E_f / E_c)*	*V_{ult}, kN*
1	Kaszubska and Kotynia (2019)	G-512-30-15	GFRP	30.1	379	150	1099	2.9	0.99	52.0	0.02	34.3
2		G-316-30-15		31.1	377	150	1101	2.9	1.07	52.0	0.02	31.8
3		G-318-30-15		31.1	376	150	1102	2.9	1.35	52.0	0.03	38.6
4		G-416-30-15		30.5	377	150	1105	2.9	1.42	52.0	0.03	34.8
5		G-418-30-15		31.1	376	150	1102	2.9	1.80	52.0	0.04	38.1
6		G-512-30-35		31.1	359	150	1099	3.1	1.05	52.0	0.02	32.5
7		G-316-30-35		30.5	357	150	1100	3.1	1.13	52.0	0.02	31.0
8		G-318-30-35		30.5	356	150	1100	3.1	1.43	52.0	0.03	34.4
9		G-418-30-35		30.1	356	150	1100	3.1	1.91	52.0	0.04	39.4
10		G-316-35-15		37.1	377	150	1101	2.9	1.07	52.0	0.02	31.3
11		G-318-35-15		37.1	376	150	1102	2.9	1.35	52.0	0.03	33.8
12		G-416-35-15		36.0	377	150	1101	2.9	1.42	52.0	0.03	32.4
13		G-316-35-35		35.0	357	150	1100	3.1	1.13	52.0	0.02	29.9
14	Issa et al. (2015)	5-10N5	BFRP	35.9	170	300	961	5.7	0.80	53.0	0.02	29.3
15		5-13N5		35.9	170	300	961	5.7	1.33	51.0	0.03	38.7
16		5-16N5		35.9	170	300	961	5.7	2.06	51.0	0.04	45.2
17		6-16N7		35.9	170	300	1190	7.0	2.49	51.0	0.05	40.2
18		3-25N7		35.9	165	300	1155	7.0	3.09	48.0	0.06	48.4
19		4-25N7		35.9	175	300	1225	7.0	3.89	48.0	0.07	51.5
20	Ashour and Kara (2014)	B-400-2	CFRP	27.0	370	200	1000	2.7	0.12	141.4	0.01	32.9
21		B-400-4		27.0	370	200	1000	2.7	0.24	141.4	0.01	36.1
22		B-300-2		35.0	275	200	1000	3.6	0.16	141.4	0.01	32.9
23		B-300-4		35.0	275	200	1000	3.6	0.32	141.4	0.02	32.9
24		B-200-2		29.0	170	200	1000	5.9	0.26	141.4	0.02	17.6
25		B-200-4		29.0	170	200	1000	5.9	0.52	141.4	0.03	20.8
26	Tomlinson and Fam (2014)	NT	BFRP	60.0	270	150	1100	4.1	0.39	70.0	0.01	20.9
27		NB		59.9	270	150	1100	4.1	0.51	70.0	0.01	11.5
28		NC		56.5	245	150	1100	4.5	0.85	70.0	0.02	29.2
29	Matta et al. (2013)	S1-0.12-1A	GFRP	29.5	883	457	2743	3.1	0.12	41.0	0.00	154.1
30		S1-0.12-2B		29.6	883	457	2743	3.1	0.12	41.0	0.00	151.1
31		S1-0.12-SB		29.6	883	457	2743	3.1	0.12	41.0	0.00	253.8
32		S3-0.12-1A		32.1	292	114	914	3.1	0.13	43.2	0.00	19.2
33		S3-0.12-2A		32.1	292	114	914	3.1	0.13	43.2	0.00	17.9
34		S6-0.12-1A		59.7	146	229	457	3.1	0.13	43.2	0.00	28.6
35		S6-0.12-2A		32.1	146	229	457	3.1	0.13	43.2	0.00	36.9
36		S6-0.12-3A		32.1	146	229	457	3.1	0.13	43.2	0.00	26.3
37		S1-0.24-1A		29.5	880	457	2743	3.1	0.24	41.0	0.00	220.7
38		S1-0.24-2B		30.7	880	457	2743	3.1	0.24	41.0	0.00	212.7
39	Alam and Hussein (2013)	G-350	GFRP	39.8	305	300	763	2.5	0.86	46.3	0.01	61.0
40		C-350	CFRP	44.7	310	300	775	2.5	0.42	144.0	0.02	77.2
41		G-500	GFRP	37.4	440	300	1100	2.5	0.90	46.3	0.02	129.4
42		C-500	CFRP	34.5	460	300	1150	2.5	0.45	144.0	0.02	64.6
43		G-650	GFRP	37.0	584	300	1460	2.5	0.91	46.3	0.02	112.9

44		C-650	CFRP	42.4	594	300	1485	2.5	0.43	144.0	0.02	138.5
45[a]		G-800	GFRP	41.8	734	300	1762	2.4[a]	0.90	46.3	0.01	111.2
46[a]		C-800	CFRP	41.8	744	300	1786	2.4[a]	0.40	144.0	0.02	155.7
47		L05-0		46.0	937	450	3050	3.3	0.51	40.8	0.01	164.5
48		M05-0		35.0	438	450	1525	3.5	0.55	40.8	0.01	83.5
49	Bentz et	S05-0	GFRP	35.0	194	450	762	3.9	0.66	40.8	0.01	54.0
50	al. (2010)	L20-0		36.0	857	450	3050	3.6	2.23	40.8	0.03	217.5
51		M20-0		35.0	405	450	1525	3.8	2.36	40.8	0.04	136.0
52		S20-0		35.0	188	450	762	4.1	2.54	40.8	0.04	73.5
53		Beam 1		28.9	168	150	667	4.0	0.45	38.0	0.01	12.5
54		Beam 3		28.9	212	150	667	3.1	0.71	32.0	0.01	17.5
55	Ashour	Beam 5	GFRP	28.9	263	150	667	2.5	0.86	32.0	0.01	25.0
56	(2006)	Beam 7		50.2	163	150	667	4.1	1.39	32.0	0.01	17.5
57		Beam 9		50.2	213	150	667	3.1	1.06	32.0	0.01	27.5
58		Beam 11		50.2	262	150	667	2.5	1.15	32.0	0.01	30.0
59		CN-1.7	CFRP	43.6	326	250	1000	3.1	1.72	134.0	0.08	124.5
60		GN-1.7	GFRP	43.6	326	250	1000	3.1	1.71	42.0	0.02	77.5
61	Elsayed et	CH-1.7	CFRP	63.0	326	250	1000	3.1	1.71	135.0	0.06	130.0
62	al.(2006)a	GH-1.7	GFRP	63.0	326	250	1000	3.1	1.71	42.0	0.02	87.0
63		CH-2.2	CFRP	63.0	326	250	1000	3.1	2.20	135.0	0.08	174.0
64		GH-2.2	GFRP	63.0	326	250	1000	3.1	2.20	42.0	0.03	115.5
65		CN-1	CFRP	50.0	326	250	1000	3.1	0.87	128.0	0.03	77.5
66		GN-1	GFRP	50.0	326	250	1000	3.1	0.87	39.0	0.01	70.5
67	Elsayed et	CN-2	CFRP	44.6	326	250	1000	3.1	1.24	134.0	0.06	104.0
68	al.(2006)b	GN-2	GFRP	44.6	326	250	1000	3.1	1.22	42.0	0.02	60.0
69		CN-3	CFRP	43.6	326	250	1000	3.1	1.72	134.0	0.08	124.5
70		GN-3	GFRP	43.6	326	250	1000	3.1	1.71	42.0	0.02	77.5
71		S-C1		40.0	165	1000	1000	6.0	0.39	114.0	0.01	140.0
72		S-C2B	CFRP	40.0	165	1000	1000	6.0	0.78	114.0	0.03	167.0
73		S-C3B		40.0	161	1000	1000	6.2	1.18	114.0	0.04	190.0
74	Elsayed et	S-G1		40.0	162	1000	1000	6.2	0.86	40.0	0.01	113.0
75	al (2005)	S-G2		40.0	159	1000	1000	6.3	1.70	40.0	0.02	142.0
76		S-G2B	GFRP	40.0	162	1000	1000	6.2	1.71	40.0	0.02	163.0
77		S-G3		40.0	159	1000	1000	6.3	2.44	40.0	0.03	163.0
78		S-G3B		40.0	154	1000	1000	6.5	2.63	40.0	0.04	163.0
79		1a-26-NS		36.3	226	252	914	4.1	1.11	40.3	0.01	39.7
80		1b-26-NS		36.3	226	252	914	4.1	1.11	40.3	0.01	38.5
81		1c-26-NS		36.3	226	252	914	4.1	1.11	40.3	0.01	36.9
82		2a-26-NS		36.3	226	178	914	4.1	1.42	40.3	0.01	28.1
83		2b-26-NS		36.3	226	178	914	4.1	1.42	40.3	0.01	35.1
84		2c-26-NS		36.3	226	178	914	4.1	1.42	40.3	0.01	32.1
85		3a-36-NS		36.3	226	252	914	4.1	1.66	40.3	0.02	40.0
86		3b-36-NS		36.3	226	252	914	4.1	1.66	40.3	0.02	48.6
87		3c-36-NS		36.3	226	252	914	4.1	1.66	40.3	0.02	32.1
88		4a-46-NS		36.3	226	279	914	4.1	1.81	40.3	0.02	40.0
89		4b-46-NS		36.3	226	279	914	4.1	1.81	40.3	0.02	48.6
90		4c-46-NS		36.3	226	279	914	4.1	1.81	40.3	0.02	44.7
91		5a-37-NS		36.3	224	254	914	4.1	2.05	40.3	0.02	43.8
92		5b-37-NS		36.3	224	254	914	4.1	2.05	40.3	0.02	45.9
93	Gross et	5c-37-NS	GFRP	36.3	224	254	914	4.1	2.05	40.3	0.02	46.1
94	al. (2003)	6a-37-NS		36.3	224	252	914	4.1	2.27	40.3	0.02	37.7
95		6b-37-NS		36.3	224	252	914	4.1	2.27	40.3	0.02	51.1
96		6c-37-NS		36.3	224	252	914	4.1	2.27	40.3	0.02	46.7
97		1a-26-HS		79.6	226	203	914	4.1	1.25	40.3	0.01	43.5
98		1b-26-HS		79.6	226	203	914	4.1	1.25	40.3	0.01	41.8
99		1c-26-HS		79.6	226	203	914	4.1	1.25	40.3	0.01	41.3
100		2a-26-HS		79.6	226	152	914	4.1	1.66	40.3	0.01	41.6
101		2b-26-HS		79.6	226	152	914	4.1	1.66	40.3	0.01	30.4
102		2c-26-HS		79.6	226	152	914	4.1	1.66	40.3	0.01	42.1
103		3a-27-HS		79.6	224	165	914	4.1	2.10	40.3	0.02	31.0
104		3b-27-HS		79.6	224	165	914	4.1	2.10	40.3	0.02	33.0
105		3c-27-HS		79.6	224	165	914	4.1	2.10	40.3	0.02	33.5
106		4a-37-HS		79.6	224	203	914	4.1	2.56	40.3	0.02	38.4
107		4b-37-HS		79.6	224	203	914	4.1	2.56	40.3	0.02	32.2
108		4c-37-HS		79.6	224	203	914	4.1	2.56	40.3	0.02	36.7
109		G07N1		37.3	346	160	952	2.8	0.72	42.0	0.01	54.5
110	Tariq and	G07N2		43.2	346	160	952	2.8	0.72	42.0	0.01	63.7
111	Newhook	G10N1	GFRP	43.2	346	160	1149	3.3	1.10	42.0	0.02	42.7
112	(2003)	G10N2		34.1	346	160	1149	3.3	1.10	42.0	0.02	45.5
113		G15N1		34.1	325	160	1151	3.5	1.54	42.0	0.02	48.7

114		G15N2		37.3	325	160	1151	3.5	1.54	42.0	0.02	44.9
115		C07N1		37.3	310	130	949	3.1	0.72	120.0	0.03	49.2
116		C07N2		43.2	310	130	949	3.1	0.72	120.0	0.03	45.8
117		C10N1	CFRP	43.2	310	130	1150	3.7	1.10	120.0	0.04	47.6
118		C10N2		34.1	310	130	1150	3.7	1.10	120.0	0.05	52.7
119		C15N1		34.1	310	130	1150	3.7	1.54	120.0	0.07	55.9
120		C15N2		34.1	310	130	1150	3.7	1.54	120.0	0.07	58.3
121		V-G1-1	GFRP	39.7	360	457	1219	3.4	0.96	40.5	0.01	108.1
122	Tureyen	V-G2-1	GFRP	39.9	360	457	1219	3.4	0.96	37.6	0.01	94.8
123	and	V-A-1	AFRP	40.3	360	457	1219	3.4	0.96	47.1	0.02	114.8
124	Frosch	V-G1-2	GFRP	42.3	360	457	1219	3.4	0.36	40.5	0.00	137.0
125	(2002)	V-G2-2	GFRP	42.5	360	457	1219	3.4	1.92	37.6	0.02	152.6
126		V-A-2	AFRP	42.6	360	457	1219	3.4	1.92	47.1	0.03	168.2
127	Alkhrdaji	BM7		24.1	279	178	750	2.7	2.30	40.0	0.04	53.4
128	et	BM8	GFRP	24.1	287	178	750	2.6	0.77	40.0	0.01	36.1
129	al.(2001)	BM9		24.1	287	178	750	2.6	1.34	40.0	0.02	40.1
130		1FRPa		36.3	225	229	914	4.1	1.11	40.3	0.01	39.1
131		1FRPb		36.3	225	229	914	4.1	1.11	40.3	0.01	38.5
132		1FRPc		36.3	225	229	914	4.1	1.11	40.3	0.01	36.8
133		2FRPa		36.3	225	178	914	4.1	1.42	40.3	0.01	28.1
134		2FRPb		36.3	225	178	914	4.1	1.42	40.3	0.01	35.0
135		2FRPc		36.3	225	178	914	4.1	1.42	40.3	0.01	32.1
136		3FRPa		36.3	225	229	914	4.1	1.66	40.3	0.02	40.0
137		3FRPb		36.3	225	229	914	4.1	1.66	40.3	0.02	48.6
138	Yost et al.	3FRPc	GFRP	36.3	225	229	914	4.1	1.66	40.3	0.02	44.7
139	(2001)	4FRPa		36.3	225	279	914	4.1	1.81	40.3	0.02	43.8
140		4FRPb		36.3	225	279	914	4.1	1.81	40.3	0.02	45.9
141		4FRPc		36.3	225	279	914	4.1	1.81	40.3	0.02	46.1
142		5FRPa		36.3	224	254	914	4.1	2.01	40.3	0.02	37.7
143		5FRPb		36.3	224	254	914	4.1	2.01	40.3	0.02	51.0
144		5FRPc		36.3	224	254	914	4.1	2.01	40.3	0.02	46.6
145		6FRPa		36.3	224	229	914	4.1	2.27	40.3	0.02	43.5
146		6FRPb		36.3	224	229	914	4.1	2.27	40.3	0.02	41.8
147		6FRPc		36.3	224	229	914	4.1	2.27	40.3	0.02	41.3

[a] – members 44 and 45 had *a/d* ratios less than 2.5 (often considered to be the threshold for deep beam response). Members 44 and 45 were compared using the same expressions as the other beams and had similar outcomes as the other members from that study (Figure 6.8 and Figure 6-9).

6.3 Overview of One-Way Shear Design Provisions

Summaries of code, standard, and guideline predictions for the one-way shear resistance provided by concrete and flexural reinforcement, V_c , are presented in this section. To reduce confusion caused by excessive and potentially contradictory variable names between different provisions (e.g. b_v and b_w, may both mean the member effective shear width), some variable names have been changed from their original documents. Similarly, terms accounting for prestressing and axial loads are removed. Aside from these editorial changes, provisions remain as originally presented.

6.3.1 Summary of one-way shear predictions from design codes, standards, guidelines

Eight previous and current FRP-RC design codes, standards, and guidelines are discussed in this section. Some provisions are based on Modified Compression Field Theory (MCFT) (Vecchio and

Collins 1986), a general model for the load-deformation behaviour of RC elements developed by testing RC elements under pure shear using a membrane element tester. MCFT concrete models concrete consider stresses and strains in principal directions. Many other design provisions for FRP-RC shear strength are similar to those of steel-RC, with added factors accounting for the FRP ratio and steel's elasticity moduli. Different models based on Strut-and-Tie Models (STMs), Compression Zone Failure Mechanism (CZFM) and Compression Chord Capacity Model (CCCM) theories are discussed later.

6.3.1.1 Codes, standards, and guidelines

CSA S6:19

The Canadian Highway Bridge Design Code (CSA S6-14 2014) one-way shear strength provision for concrete without stirrups, V_c, is based on MCFT Eq. (6-1).

$$V_c = 2.5\beta\phi_c f_{cr} b_w d_v \tag{6-1}$$

where d_v is the effective shear depth (greater than $0.9d$ (effective depth to the centroid of the tensile reinforcement) and $0.72h$ (member depth)), b_w is the member's effective width, ϕ_c is the material reduction factor for concrete (taken as unity in this paper), f_{cr}, is the concrete cracking strength ($f_{cr}=0.4\sqrt{f_c'}$). In high-strength concrete, aggregates fail through the shear crack and no longer contribute significantly to crack roughness, so an upper limit of 3.2 MPa is imposed on ,f_{cr}, since experiments show that V_c does not significantly increase as f_c' increases beyond 64 MPa (Angelakos et al. 2001, Bentz and Collins 2017). β, is a factor accounting for the shear resistance of cracked concrete, which relates to the longitudinal strain at the mid-depth of the member, ε_x (Bentz et al. 2006) Eq. (6-2) and (6-3).

$$\beta = \left[\frac{0.4}{1+1500\varepsilon_x}\right]\left[\frac{1300}{1000+s_{ze}}\right] \tag{6-2}$$

$$\varepsilon_x = \frac{\frac{M_u}{d_v}+V_u}{2E_f A_f} \leq 0.003 \tag{6-3}$$

where V_u is the factored shear, M_u is the factored moment, E_f is the modulus of the FRP longitudinal reinforcement, and A_f, is the area of the FRP tension reinforcement. ε_x cannot exceed 0.003 to limit the redistribution of forces allowed (Bentz et al. 2006). s_{ze} is an effective crack spacing for members without stirrups found using Eq. (6-4).

$$s_{ze} = \frac{35\, s_z}{15+a_g} \leq 0.85 s_z \tag{6-4}$$

where s_z, is the smaller of d and the maximum spacing between longitudinal reinforcement layers, and a_g is the nominal maximum aggregate size.

CSA S806-02

The Canadian Standards Association S806-02 (2002) was one of the first standards that provided design requirements for building components reinforced with FRP. For sections having either minimum shear reinforcement or an effective depth not exceeding 300 mm, V_c can be calculated using Eq. (6-5).

$$V_c = 0.1\, \phi_c \sqrt{f'_c}\, b_w\, d \leq 0.035 \lambda \phi_c \left(f'_c\, \rho_f\, E_f \frac{V_u\, d}{M_u}\right)^{\frac{1}{3}} b_w\, d \leq 0.2\, \phi_c \sqrt{f'_c}\, b_w\, d \tag{6-5}$$

where ρ_f is the longitudinal reinforcement ratio calculated as $A_f/b_w d$, and λ is a concrete density factor equal to 1.0 for normal-density concrete. The value $\frac{V_u\, d}{M_u}$, shall not be taken as greater than 1.0. For sections with effective depths greater than 300 mm and with less than minimum stirrups, V_c is calculated using Eq. (6-6).

$$V_c = \left(\frac{130}{1000+d}\right) \lambda \phi_c \sqrt{f'_c}\, b_w\, d \geq 0.08 \lambda \phi_c \sqrt{f'_c}\, b_w\, d \tag{6-6}$$

CSA S806-12

The shear provisions from S806-02 were updated in the next version of the standard, S806-12 (CSA 2012). A size effect term, k_s, was added, and the shear strength limits were slightly increased. For sections having an effective depth not exceeding 300 mm and no axial load, V_c can be calculated using Eq. (6-7).

$$V_c=0.11\phi_c\sqrt{f'_c}b_w\, d_v \leq 0.05\lambda\phi_c k_m k_r \left(f'_c\right)^{\frac{1}{3}} b_w\, d_v \leq 0.22\phi_c\sqrt{f'_c}b_w\, d_v \tag{6-7}$$

where k_m is a moment-shear interaction value and k_r is a reinforcement stiffness value that is calculated as in Eqs.(6-8) and (6-9).

$$k_m=\sqrt{\frac{V_u\, d}{M_u}} \leq 1.0 \tag{6-8}$$

$$k_r=1+(E_f\, \rho_f)^{1/3} \tag{6-9}$$

If d exceeds 300 mm and if less than minimum shear reinforcement is provided (i.e. all beams in this study since they do not contain shear reinforcement), V_c from Eq. (6-7) is multiplied by a size effect factor, k_s given in Eq.(6-10).

$$k_s=\frac{750}{450+d} \leq 1.0 \tag{6-10}$$

ISIS-2007

The Intelligent Sensing for Innovative Structures' (now known as the Centre for Structural Innovation and Monitoring Technologies Inc. (SIMTReC)) guideline V_c equation is similar to others but uses the square root of E_f/E_s and does not consider ρ_f (ISIS 2007). The shear resistance of members with d not greater than 300 mm or members with minimum stirrups is determined using Eq. (6-11).

$$V_c=0.2\lambda\phi_c\sqrt{f'_c}b_w\, d\sqrt{\frac{E_f}{E_s}} \tag{6-11}$$

where $E_f/E_s<1.0$. For sections with d greater than 300 mm and not containing minimum shear reinforcement, V_c, is calculated using Eq.(6-12).

$$V_c = \left(\frac{260}{1000+d}\right) \lambda\, \phi_c \sqrt{f'_c} b_w\, d \sqrt{\frac{E_f}{E_s}} \tag{6-12}$$

ACI 440.1R-15

The provisions of ACI 440.1R are similar to those in ACI 318-14 but incorporate the axial stiffness of longitudinal reinforcement indirectly using the elastic neutral axis depth, *kd*. ACI 440.1R's provision for V_c is given in Eq. (6-13).

$$V_c = 0.4 \sqrt{f'_c} b_w\, d\, (kd) \tag{6-13}$$

Where k represents the ratio between the depth of the neutral axis of the cracked transformed section and the effective depth, d, of the member, and kd is a function of, ρ_f, and the modular ratio $n_f = E_f / E_c$. For rectangular cross sections used in all tests considered in this study, k can be calculated as per Eq.(6-14).

$$k = \sqrt{2\rho_f n_f + (\rho_f n_f)^2} - \rho_f n_f \tag{6-14}$$

BISE-1999

The British Institution of Structural Engineers (BISE 1999) interim guidance on the design of FRP-RC assumes that the shear strength is a function of the concrete strength and the area of effectively anchored longitudinal tension reinforcement. For FRP with a lower elastic modulus than steel, the area of the reinforcement is modified by multiplying it by E_f / E_s. This approach is recommended by (Nagasaka et al. 1993) and applied in BISE 1999 in Eq. (6-15).

$$V_c = 0.79 \left(100\rho_f \frac{E_f}{E_s}\right)^{\frac{1}{3}} \left(\frac{d}{400}\right)^{\frac{1}{4}} \left(\frac{f_{cu}}{25}\right)^{\frac{1}{3}} b_w d \tag{6-15}$$

where f_{cu} is the cube compressive strength of concrete and taken to be equal to $1.25 f'_c$.

JSCE-1997

The Japanese Society of Civil Engineering (JSCE 1997) recommendations for V_c are similar to those from BISE 1999. The shear strength of members without stirrups is found in Eq.(6-16).

$$V_c = \beta_d \beta_p f_{cr} b_w d/\gamma_b \tag{6-16}$$

where f_{cr} is the design concrete shear stress at failure, β_d is a size effect factor, and β_p, is a reinforcement axial stiffness factor. These parameters are calculated using Eqs.((6-17)-(6-19)). γ_b is a member safety factor that depends on the certainty of the member capacity prediction equation and the consequences of the corresponding failure mode, γ_b is generally taken as 1.3 (BISE 1999, Brigante 2014).

$$f_{cr} = 0.2(f'_c)^{\frac{1}{3}} \leq 0.72\ MPa \tag{6-17}$$

$$\beta_d = \left(\frac{1000}{d}\right)^{\frac{1}{4}} \leq 1.5 \tag{6-18}$$

$$\beta_p = \left(100\rho_f \frac{E_f}{E_s}\right)^{\frac{1}{3}} \leq 1.5 \tag{6-19}$$

CNR-DT 203/2006

The guide for the design and construction of FRP-RC (CNR-DT 203/2006 2006) evaluates the shear strength of FRP-RC members without stirrups using Eq.(6-20).

$$V_c = 1.3\left(\frac{E_f}{E_s}\right)^{\frac{1}{2}} \tau_{Rd} k_s (1.2 + 40\rho_f) b_w d \quad \text{provided} \quad 1.3\left(\frac{E_f}{E_s}\right)^{\frac{1}{2}} \leq 1 \tag{6-20}$$

where τ_{Rd} is the design shear stress defined as $0.25(0.33\sqrt{f'_c})$, k_s is taken as $(1600 - d) \geq 1$, and any ρ_f, larger than 0.02 is taken as 0.02.

6.3.1.2 Model design procedures

This section focuses on six proposed models from the September 2017 issue of Concrete International considered by the ACI for one-way shear in steel-RC (Concrete International 2017). These models were originally given in US units but were converted to metric to better compare with the previous section. Of these six models, three (Bentz and Collins (2017), Frosch (2017), and Clareda et al. (2017)) were mentioned to be directly applicable to FRP-RC members.

Bentz and Collins (2017)

The model proposed by Bentz and Collins (2017) is based on MCFT and similar to the shear provisions in CSA S6:19. The shear strength depends on s_{ze}, which relies on the effective member depth (i.e. size effect factor) and ε_x, which accounts for shear crack width and aggregate interlock. From this model, V_c can be found using Eq. (6-21).

$$V_c=0.166\sqrt{f_c}\left(\frac{2.25}{1+1500\varepsilon_x}\right)\left(\frac{1270}{965+S_x}\right)b_w d \tag{6-21}$$

where s_{ze}= 0.9d for members without stirrups with 19 mm aggregate size. ε_x can be calculated using Eq. (6-22).

$$\varepsilon_x=\left(\frac{M_u}{0.9d}+V_u\right)/(2A_f\,E_f) \tag{6-22}$$

Clareda et al. (2017)

The model proposed by Cladera et al. (2017) is based on the CCCM (Cladera et al. 2016), considering ACI 318-14 features. From this model, V_c can be obtained using Eq.(6-23).

$$V_c= 0.5\lambda\xi k\sqrt{f_c}\,b_w\,d > 0.332(1.25\xi k+\frac{1}{d})\sqrt{f_c}\,b_w\,d \tag{6-23}$$

Where k was previously defined in Eq. 14 but can be approximated as 0.75 $\left(n_f\rho_f\right)^{1/3}$ for rectangular cross sections and should not exceed 0.20. The combined size and slenderness factor, ξ, is found using Eq. (6-24).

$$\xi=\frac{2}{\sqrt{1+\frac{d}{203.2}}}\left(\frac{d}{a}\right)^{0.2} \tag{6-24}$$

Frosch et al. (2017)

(Frosch et al. 2017) proposed a modification to the ACI 318 one-way shear resistance expression that accounts for the reduction in shear resistance seen in deeper members (i.e. size effect). V_c is found from Equation 25, while γ_d is a size effect factor found in Eq. (6-25).

$$V_c=\left(0.415\lambda\sqrt{f_c}\,b_w\,kd\right)\gamma_d \tag{6-25}$$

$$\gamma_d=\frac{1.48}{\sqrt{1+\frac{d}{254}}} \tag{6-26}$$

Li et al. (2017)

The model proposed by (Li et al. 2017) modifies the provisions in ACI 318-14 to include contributions from arch action and size effect on V_c. The proposed V_c is found using Eq.(6-27).

$$V_c=1.41\lambda\left(\frac{V_u d}{M_u}\right)^{0.7}\sqrt{f_c}\,b_w kd\frac{1}{\sqrt{1+h/300}}\leq 0.83\lambda\sqrt{f_c'}b_w kd \tag{6-27}$$

Park and Choi (2017)

The model proposed by (Park and Choi 2017) is based on CZFM (Choi et al. 2016). Rankine's failure criterion defines the shear strength of the compression zone, which considers the effect of the normal stress caused by the moment. The proposed shear strength equation is given in Eq. (6-28).

$$V_c=k_s f_{cr}\,b_w c\cot\theta_c \tag{6-28}$$

where f_{cr} *is* $0.183\,\lambda\sqrt{f_c}$, θ_c is the inclined crack angle in the compression zone and the compression zone stress, $\bar{\sigma}_{ct}$, are given by Eqs. (6-29) and (6-30).

$$\cot\theta_c=\sqrt{1+\frac{\bar{\sigma}_{ct}}{f_{cr}}} \tag{6-29}$$

$$\bar{\sigma}_{ct}=\frac{M_u}{b_w kd\left(1-\frac{kd}{3}\right)} \tag{6-30}$$

The size effect factor, k_s, is given by Eq. (6-31).

$$k_s=\left(\frac{305}{d}\right)^{0.25}\leq 1.1 \tag{6-31}$$

Reineck (2017)

The model proposed by Reineck (2017) uses strut-and-tie models (STMs) derived with an inclined biaxial tension-compression field in the web (i.e. inclined concrete struts), and it explains the load transfer in the member from the location of the load to the member support. The model considers both section and load transfer analysis, and Eq. (6-32) can obtain the shear capacity.

$$V_c=7.5\lambda\left(\rho_f\frac{f_c}{d}\right)^{\frac{1}{3}}b_w\,d \tag{6-32}$$

6.4 Effect of Shear Strength Parameters

Table 6-2 describes parameters that affect shear strength and their effect on each provision. It is challenging to directly compare each parameter since methods account for these parameters using different approaches. For example, Bentz and Collins (2017) combine axial stiffness and shear/moment loading effects into one term while S806-12 calculates them independently. To facilitate comparisons showing the effect of different parameters on V_c, a simplysupported beam was considered with the following properties: f_c = 35MPa d = 270mm, b_w = 200mm, a/d = 2.6, a = 700 mm, E_f = 40 GPa and ρ_f=1.5%.

Table 6-2. Summary of design equation shear parameters.

	Design Provision	Concrete Strength Factor[a]	Size Effect Factor	Shear-Moment Interaction Factor	Reinforcement Stiffness Factor	Reinforcement Ratio Factor
Codes, standards. and guidelines	CSA S806-12	$(f_c')^{\frac{1}{3}}$	$\frac{750}{450+d} \leq 1.0$	$\sqrt{\frac{V_u d}{M_u}} \leq 1.0$	$(E_f)^{\frac{1}{3}}$	$(\rho_f)^{\frac{1}{3}}$
	CSA S806-02	$(f_c')^{\frac{1}{3}}$	$\frac{130}{1000+d}$	$\left(\frac{V_u d}{M_u}\right)^{\frac{1}{3}} \leq 1.0$	$(E_f)^{\frac{1}{3}}$	$(\rho_f)^{\frac{1}{3}}$
	CSA S6:19[b]	$\sqrt{f_c'}$	$\frac{1300}{1000+s_{ze}} \leq 1.$		$\varepsilon_x = \frac{M_u/d_v + V_u}{2E_f A_f} \leq 0.003$	
	ISIS 2007	$\sqrt{f_c'}$	$\left(\frac{260}{1000+d}\right)$	N/A	$\sqrt{\frac{E_f}{E_s}} \leq 1$	N/A
	ACI 440.1R-15	$\sqrt{f_c'}$	N/A	N/A	Indirect via kd[c]	
	CNR-DT 203/2006	$\sqrt{f_c'}$	$(1600 - d)/1000 \geq 1$	N/A	$\left(\frac{E_f}{E_s}\right)^{\frac{1}{2}}$	ρ_f
	BISE 1999	$(f_c')^{\frac{1}{3}}$	$\left(\frac{d}{400}\right)^{\frac{1}{4}}$	N/A	$\left(\frac{E_f}{E_s}\right)^{\frac{1}{3}}$	$(\rho_f)^{\frac{1}{3}}$
	JSCE 1997	$(f_c')^{\frac{1}{3}}$	$\left(\frac{1000}{d}\right)^{\frac{1}{4}} \leq 1.5$	N/A	$\left(\frac{E_f}{E_s}\right)^{\frac{1}{3}}$	$(\rho_f)^{\frac{1}{3}}$
Models	Bentz and Collins (2017)[b]	$\sqrt{f_c'}$	$\frac{1270}{965+S_x}$		$\varepsilon_x = \frac{M_u/0.9d + V_u}{2A_f E_f}$	
	Clareda et al. (2017)	$\sqrt{f_c'}$	$\frac{2}{\sqrt{1+\frac{d}{203.2}}}$	$\left(\frac{d}{a}\right)^{0.2}$	Indirect via kd[c]	
	Frosch et al. (2017)	$\sqrt{f_c'}$	$\frac{1.48}{\sqrt{1+\frac{d}{254}}}$	N/A	Indirect via kd[c]	
	Li et al. (2017)	$\sqrt{f_c'}$	$\frac{1}{\sqrt{1+h/11.8}}$	$\left(\frac{V_u d}{M_u}\right)^{0.7}$	Indirect via kd[c]	
	Park and Choi (2017)	$\sqrt{f_c'}$	$\left(\frac{305}{d}\right)^{0.25} \leq 1.1$	N/A	Indirect via kd[c]	
	Reineck (2017)	$(f_c')^{\frac{1}{3}}$	$\left(\frac{1}{d}\right)^{\frac{1}{3}}$	N/A	N/A	$(\rho_f)^{\frac{1}{3}}$

[a] – Concrete factor does not include coefficients (e.g. 0.4 for S6:19) since many provisions combine design concrete stress, f_{cr}, coefficient with other factors.[b] – Provisions combine shear-moment interaction, E_f and ρ_f in a single term (ε_x). Since ε_x is on the denominator of the shear effectiveness factor, β, larger ε_x means reduced V_c[c] – Accounts for E_f and ρ_f indirectly using elastic neutral axis depth, kd. See Eq. 6-14.

6.4.1 Effect of concrete compressive strength

A range of concrete strengths between 25 and 55 MPa, the limit for ordinary concrete (ACI 2010), was considered. The effect of changing f'_c on V_c for each provision is shown in Figure 6-2. When considering f'_c Table 2 indicates that CSA S806-12, CSA S806-02, JSCE 1997 and Reineck (2017) are less affected by f_c, since they use the cubic root of f'_c while other approaches use the square root of f_c. However, since E_c is related to f_c the modular ratio, and thus, compression zone depth will decrease as f_c' increases, reducing this parameter's effect on V_c for provisions (e.g. ACI 440.1R-15) that consider compression zone depth. Similar trends are seen with CSA S6:19 and the model proposed by Bentz and Collins's (2017), where increasing f_c leads to an increased ε_x due to the increase in both V_u and M_u on the cross-section at failure.

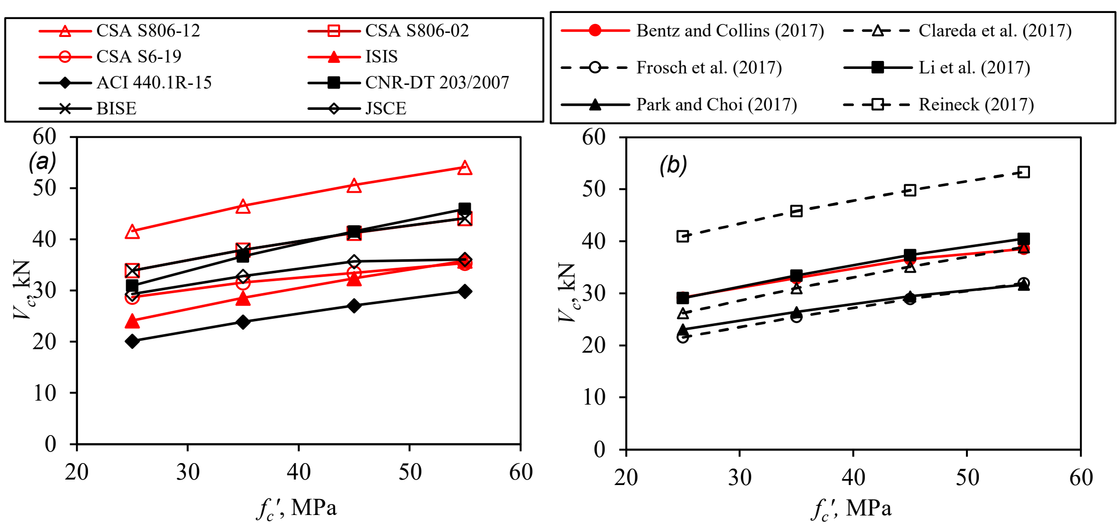

Figure 6-2: Effect of concrete compressive strength, f'_c, on shear strength, V_c: (a) design codes, standards, and guides and (b) models

6.4.2 Effect of cross-sectional size

The member dimensions (effective width and depth) were then varied between 175mm and 475 mm. The reinforcement ratio was kept constant as the dimensions changed. Most provisions show that shear strength increases linearly with b_w, because the shear stress at failure is often assumed to not change as member width changes, as shown in Figure 6-3. However, CSA S6:19 and the model from Bentz and Collins (2017) differ, showing a non-linear increase in V_c with an increase in b_w. For these approaches, increasing b_w increases the demand (i.e. V_u, M_u) at failure, increasing ε_x and thus reducing β (i.e. lowers shear stress) at failure.

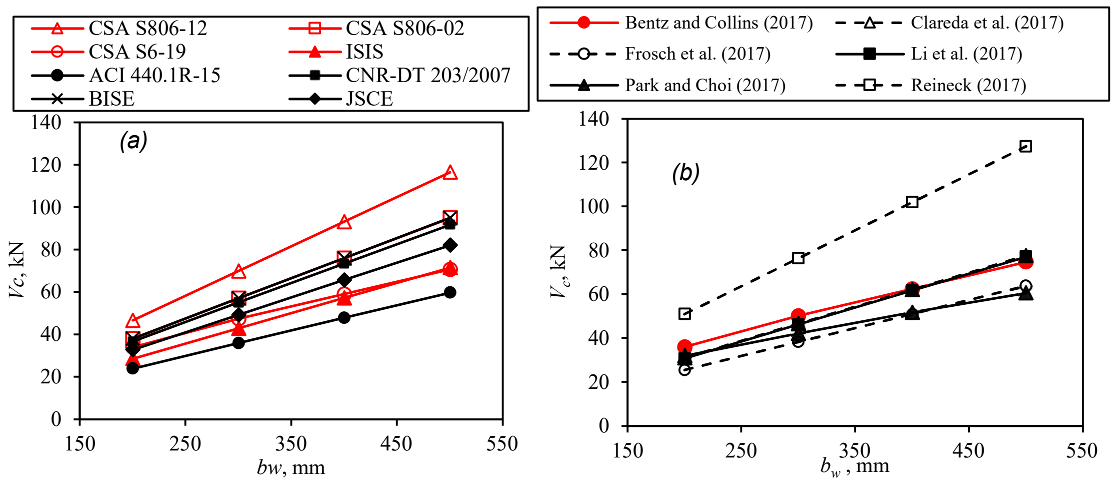

Figure 6-3: Effect of width, b_w, on shear strength, V_c: (a) design codes, standards, and guides and (b) models

As expected, increasing d increases V_c, for all provisions due to an increase in the concrete's elastic compression zone depth, kd (Figure 6-4). CSA S806-12 was initially most affected by d and gave the highest predicted shear strength results due to the k_m, factor for sections with $d \leq 300$ mm; however, when $d > 300$ mm, the size effect reduction factor (e.g. k_s) applies and reduces the predicted shear strength of CSA S806-12, CSA S806-02, and CSA S6:19. ACI 440.1R-15 is the only method that does not include size effect (Table 6-2). Other methods use similar size effect approaches but differ regarding the depth where size effect needs to be considered (typically ranging between 200 and 300 mm) and how shear strength decreases with depth ranging from a linear decrease in CNR-DT to a 0.25 exponent in JSCE and Park and Choi (2017).

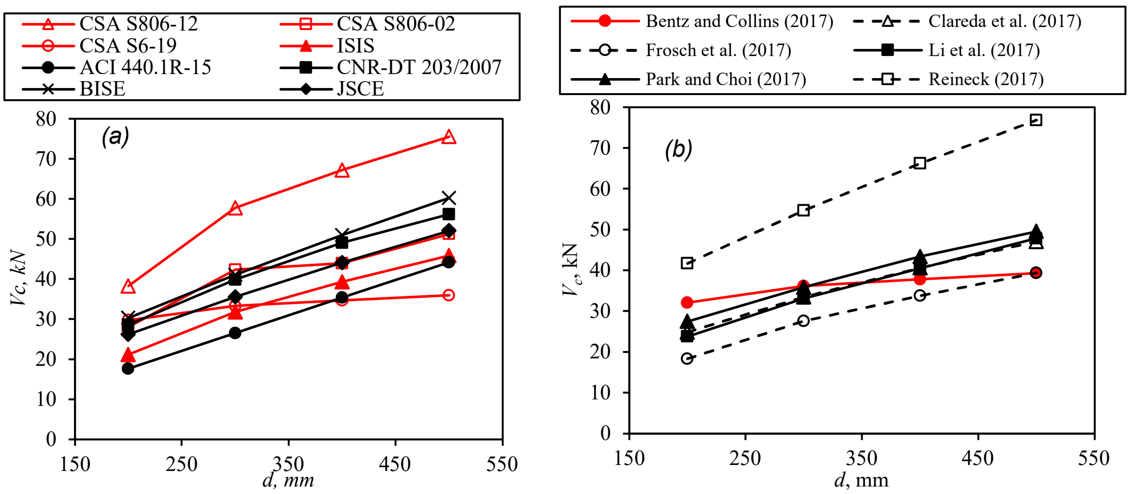

Figure 6-4: **Effect of effective depth, *d*, on shear strength, V_c: (a) design codes, standards, and guides and (b) models. For this parameter, shear span to depth ratio was kept constant as depth was varied.**

6.4.3 Effect of shear span-to-effective depth ratio

The shear span to effective depth ratio, which is the combined effect of shear and moment, was investigated by changing the shear span (Figure 6-5). About half of the considered provisions do not directly consider the *a/d* ratio. The exceptions are CSA S6:19, CSA S806-02, CSA S806-12, Bentz and Collins (2017), Clareda et al (2017), and Li et al (2017). Increasing the *a/d* ratio decreases V_c for two reasons. The first is that increasing moment on the member leads to wider cracks and lower aggregate interlock, while the second relates to the larger distance between support and loading, reducing arch action caused by a strut linking the load point and support. The probability of flexural failure becomes higher as *a/d* increases, while shear failure becomes more likely as *a/d* decreases. The lower limit of *a/d* is often taken as 1.0 since plane section analysis can no longer be used and is replaced by a different approach (e.g. strut-and-tie). The Li et al. (2017) model is more sensitive to *a/d* than other provisions since the shear-to-moment ratio term has an exponent of 0.7 rather than the 0.33 to 0.50 exponent used by other provisions that consider *a/d* ratio (Table 6-2). Moreover, the influence of the shear span of the model proposed by Clareda et al (2017) is small compared to the other models since the (*a/d*) term exponent is 0.2 (Figure 6-5). Interestingly, the model proposed by Park and Choi (2017) shows the opposite trend (i.e. V_c increases as *a/d* increases) since increasing, a, increases, M_u , or the same, V_u which increases the compressive normal stress, $\bar{\sigma}_{ct}$ caused by, M_u.

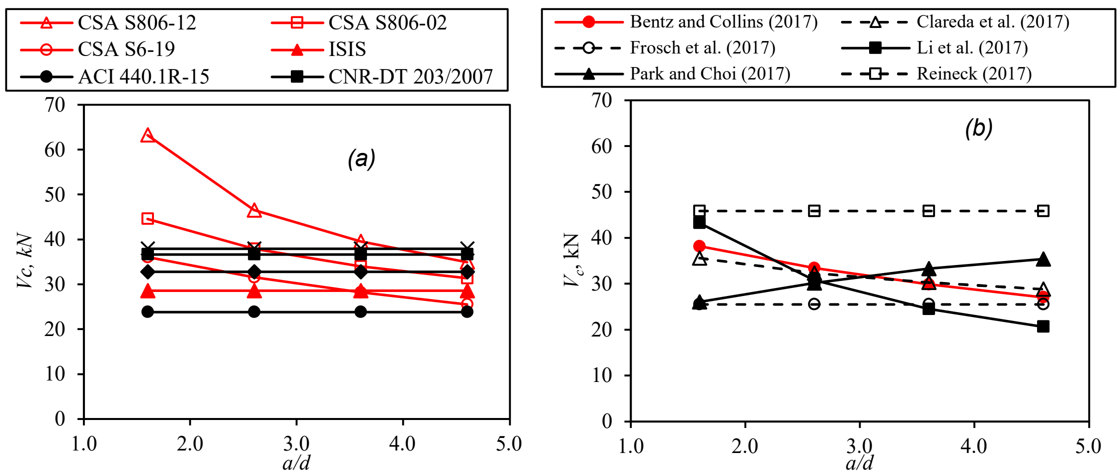

Figure 6-5: Effect of shear span to depth ratio, *a/d*, on shear strength, V_c:(a) design codes, standards, and guides and (b) models.

6.4.4 Effect of longitudinal FRP reinforcement ratio

Increasing ρ_f reduces crack widths and depths, leading to more effective aggregate interlock and larger uncracked regions that combine to increase V_c All provisions aside from ISIS 2007, which does not account for ρ_f show a non-linear increase in V_c as ρ_f increases (Figure 6-6), which agrees with researcher observations (Gross et al. 2004, El-Sayed et al. 2005, Zhao and Zhang 2007, Machial et al. 2012). As seen in Table 6-2, approaches either account for ρ_f directly (S806-02, S806-12, BISE 1999, JSCE 1997, CNR-DT 203/2006), incorporate ρ_f indirectly via *kd* (ACI 440.1R-15, Clareda et al. 2017, Frosch et al. 2017, Li et al 2017, Park and Choi 2017, and Reineck 2017), or incorporate ρ_f as an influence on ε_x (S6:19, Bentz and Collins 2017). CNR-DT 203/2006 shows that the shear strength increases with ρ_f up to 2%, which is the upper limit of ρ_f permitted by CNR-DT 203/2006. One consideration not directly included in this analysis or design provisions is that V_c is affected not only by reinforcement ratio but also by bar layout. For instance, Kaszubska et al. (2017) argue that two reinforcement layers more effectively enhance shear strength than a single layer with the same total bar area due to the higher tension stiffening provided by the reinforcement in the beams with two layers.

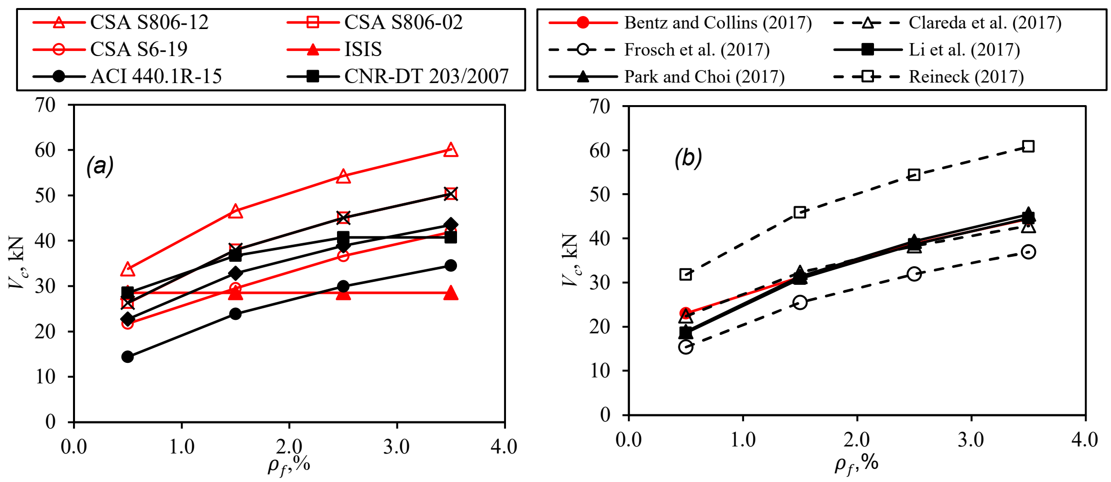

Figure 6-6: **Effect of reinforcement ratio, ρ_f, on shear strength, V_c: (a) design codes, standards, and guides and (b) models. Start**

6.4.5 Effect of FRP elastic modulus

Increasing E_f increases reinforcement axial rigidity, $E_f A_f$, which leads to smaller cracks and better aggregate interlock (i.e., the same reason why ρ_f affects V_c). Predictions show that shear strength generally increases with E_f along similar trends to those observed with ρ_f (Figure 6-7). As seen in Table 6-2, most provisions link E_f and ρ_f (or A_f) directly or as part of the *kd* calculation (i.e. n_f in Eq. 14). Many FRP-RC provisions adjust steel-RC provisions by adding in the ratio of E_f to the modulus of steel reinforcement (e.g. ACI 440.1R-15 modifies steel-RC provisions from ACI 318 to account for E_f by changing the coefficient from 0.18 in ACI 318 to 0.40kd). However, other methods (e.g. S6:19, Bentz and Collins 2017) use the same equations for both FRP-RC and steel-RC. One exception is the Reineck (2017) model, which is unaffected by changing E_f. The Reineck (2017) model presented for steel RC would need to account for the lower stiffness of FRP reinforcement relative to steel if it were to be used for FRP-RC members. The CSA S806-12 shear strength stops increasing once E_f exceeds ~100 GPa for the proposed member used in this study due to this standard having an upper limit for V_c (see Figure 6-7).

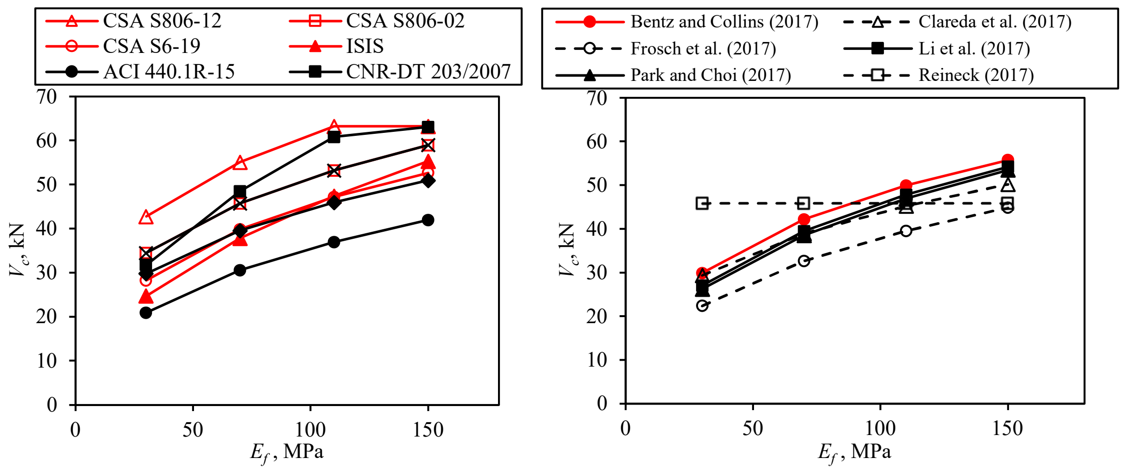

Figure 6-7: **Effect of FRP elastic modulus, E_f, on shear strength, V_c: (a) design codes, standards, and guides and (b) models.**

6.5 Shear Strength Predictions Compared to Test Data

The performance of the various methods at predicting the shear strength of FRP-RC members was evaluated using data from 147 different FRP-RC members without stirrups presented earlier (Table 1) using three evaluation measures: mean, Coefficient of Variation (COV), and Average Absolute Error (AAE) of the ratio between predicted ($V_{predicted}$) and experimental (V_{exp}) shear strength. The COV is a standardized measure of the dispersion of a probability distribution or frequency distribution. It is often expressed as a percentage and is defined as the ratio of the standard deviation to the mean. The AAE is a measure of how far 'off' a predicted value is from an experimental value or an indication of the uncertainty in the design equations related to the database. AAE is calculated using Eq. (6-33).

$$\text{AAE} = \frac{1}{n}\sum \frac{\left|V_{exp}\text{-}V_{predicted}\right|}{\mathrm{V_{exp}}} \text{ x } 100 \tag{6-33}$$

Where n is the number of samples (147 for the entire database). Figure **6-8** and Figure 6-9 compare the predicted and experimental shear strength for each provision. The existing design codes, guides, and standards were conservative, with highly scattered results. The design provisions from CSA S806-12, CSA S6:19 CNR-DT 203/2006, and BISE 1999 were the most accurate. CNR-DT 203/2006, ISIS 2007 and Bentz and Collins (2017) have the lowest COV. CSA S806-12, BISE1999, and CNR-DT 203/2006 had the lowest AAE. All other values obtained from the statistical analysis are given in Table 6-3.

Table 6-3. Summary of performance measures of the ratio between experimental and predicted shear strength for each considered provision. Bolded values have the closest mean value to 1.00 or lowest COV and AAE within the specific data set.

		Entire Dataset (n=147)			GFRP-RC only (n=111)			Members with d_v<300 mm (n=85)			Members with d_v ≥300 mm (n=62)		
	Design Provision	**Mean**	**COV, %**	**AAE, %**	**Mean**	**COV, %**	**AAE, %**	**Mean**	**COV, %**	**AAE, %**	**Mean**	**COV, %**	**AAE, %**
Codes, standards, and guidelines	CSA S806-12	**1.04**	30	**16.4**	**1.04**	33	**14.9**	1.03	27	17.5	**1.06**	34	**14.8**
	CSA S806-02	1.36	32	23.7	1.31	29	20.3	1.31	31	23.4	1.43	31	24.0
	CSA S6:19	1.72	27	38.2	1.69	26	35.6	1.66	**23**	39.3	1.80	31	36.7
	ISIS	1.31	26	28.1	1.38	**21**	24.2	1.32	26	30.6	1.29	27	24.7
	ACI 440.1R-15	1.89	45	39.4	1.96	49	39.2	1.89	51	41.4	1.89	35	36.7
	CNR-DT 203/2006	1.07	**25**	18.0	1.11	24	15.0	**1.02**	25	19.6	1.13	**24**	15.9
	BISE	1.15	33	17.8	1.16	35	16.2	1.06	33	**17.1**	1.27	30	18.7
	JSCE	1.36	33	22.8	1.38	35	22.0	1.27	34	20.1	1.48	30	26.4
Models	Bentz and Collins (2017)	1.59	**27**	35.6	1.56	**26**	33.1	1.54	**24**	35.6	1.66	31	35.6
	Clareda et al. (2017)	1.54	33	31.0	1.50	33	28.8	1.41	29	**27.4**	1.72	34	36.1
	Frosch et al. (2017)	1.91	49	41.6	1.98	53	42.2	1.82	51	39.3	2.03	45	44.7
	Li et al. (2017)	1.92	41	43.0	1.97	44	43.0	1.94	38	44.5	1.91	45	41.0
	Park and Choi (2017)	**0.99**	31	**23.1**	**1.02**	32	**21.9**	**0.87**	31	30.3	1.16	**24**	**13.2**
	Reineck (2017)	0.91	37	36.1	0.85	37	37.1	0.78	33	43.6	**1.10**	32	25.9

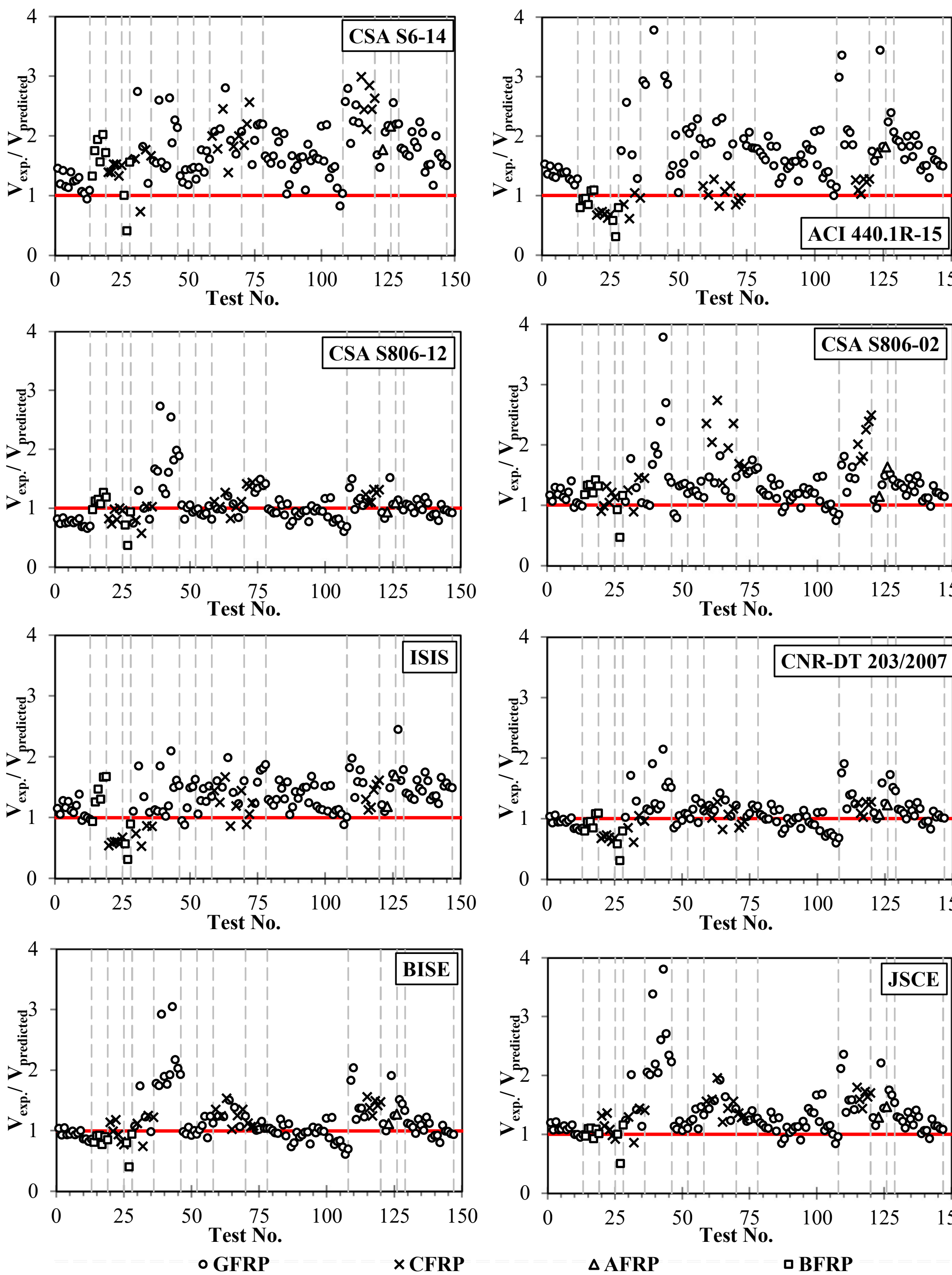

Figure 6-8: Ratio of code, standard, and guideline one-way shear strength predictions ($V_{predicted}$) to experimental one-way shear strength (V_{exp}) from tests reported in the literature. Values of $V_{exp}/V_{predicted}$ exceeding 1.0 are conservative. Vertical dashed lines used to differentiate studies (presented in Table 6-1) from each other.

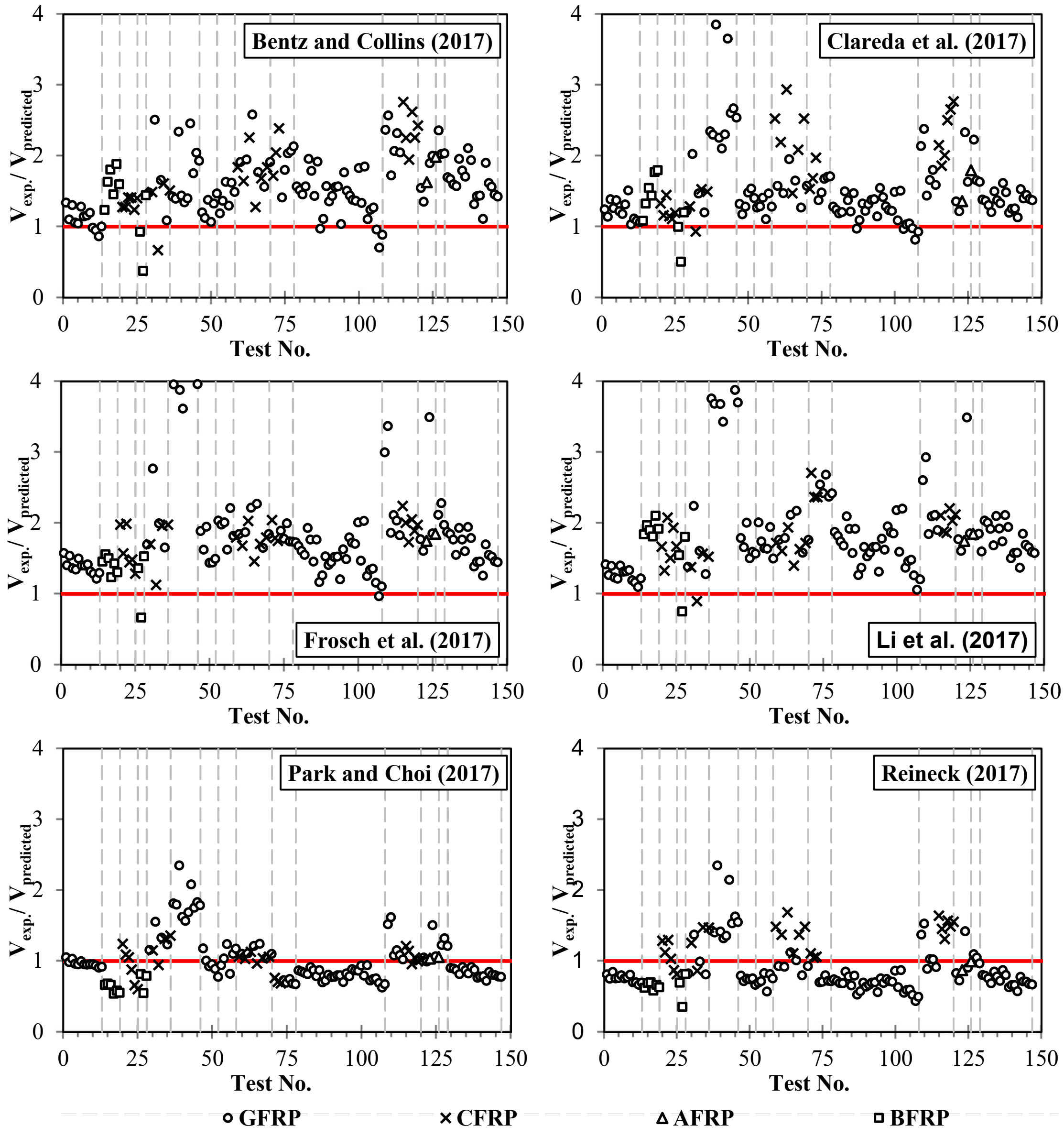

Figure 6-9: Ratio of model one-way shear strength predictions ($V_{predicted}$) to experimental one-way shear strength (V_{exp}) from tests reported in the literature. Values of $V_{exp}/V_{predicted}$ exceeding 1.0 are conservative. Vertical dashed lines used to differentiate studies (presented in Table 6-1) from each other.

Based on one-way Analysis of Variance (ANOVA) analysis of the entire data set, the mean comparison ratio of $V_{exp}/V_{predicted}$ was calculated, and the results were classified into four groups: unconservative, conservative, highly conservative and extremely conservative (Table 6-4). Park and Choi (2017) and Reineck (2017) are unconservative with a mean (0.91-0.99). CSA S806-12, CNR-DT 203/2006, and BISE are conservative with mean (1.04-1.15). The highly conservative provisions with a mean (1.31-1.59) are JSCE 1997, CSA S806-02, ISIS 2007, Clareda et al. (2017), and Bentz and Collins (2017). Lastly, CSA S6:19, ACI 440.1R-15, Frosch et al. (2017), and Li et al. (2017) were extremely conservative with a mean (1.72-1.92). Considering the different standards, the authors found that the BISE standard performed well, considering the relative ease with which it was calculated (i.e., it did not depend on results from structural analysis). For the models, Reineck (2017) was one of the easier models to use while still performing relatively well, albeit being unconservative.

Table 6-4. One-way ANOVA classification of design provisions

	Classification	Design Provision
Codes, standards, and guidelines	Conservative with mean (1.04-1.15)	CSA S806-12 CNR-DT 203/2006 BISE
	Highly conservative with mean (1.31-1.36)	ISIS JSCE CSA S806-02
	Extremely conservative with mean (1.72-1.89)	CSA S6-14 ACI 440.1R-15
Models	Unconservative with mean (0.91-0.99)	Park and Choi (2017) Reineck (2017)
	Conservative with mean (1.54-1.59)	Clareda et al.(2017) Bentz and Collins (2017)
	Extremely conservative with mean (1.91-1.92)	Li et al.(2017) Frosch et al.(2017)

Most of the members were reinforced with GFRP bars (111 out of 147), the most common type of FRP used as internal reinforcement in practice. Statistical comparisons were also completed for GFRP-RC members (Table 6-3). The design provisions for GFRP-RC members (111 members) had similar $V_{exp}/V_{predicted}$ results compared to the entire data set. The only exception was the CSA

S806-12 with the same mean (1.04), but with the lowest AAE (14.9) $V_{exp}/V_{predicted}$results compared to the entire data set. Reineck (2017), which was calibrated for steel-RC and did not include a term reflecting the lower elastic modulus of FRP reinforcement, had the largest drop-in $V_{exp}/V_{predicted}$ (~7%) when shifting from the overall dataset (mean of 0.91) to the GFRP-RC dataset (mean of 0.85). The Park and Choi model (2017) was the best-performing of the considered models (mean of 1.02) while also having the second lowest COV (32%) and the lowest AAE (21.9%) of the models.

Statistical comparisons were also completed to analyze the size effect parameter on shear predictions for different member sizes (Table 6-3). The results show that for the 85 members with effective depths less than 300 mm, both the CSA S806-12 standard and CNR-DT 203/2006 guideline provide the best $V_{exp}/V_{predicted}$ with a means of (1.03 and 1.02) while also having relatively low COV (27 and 25%) and AEE (17.5 and 19.6%) respectively. For the 62 members with effective depths greater than or equal to 300 mm, CSA S806-12 had the all-around best $V_{exp}/V_{predicted}$ with a mean of 1.06, COV of 34%, and AEE of 14.8%. However, for the nine members with the largest depth ($d > 600$ mm), the CNR-DT 203/2006 guideline had the all-around closest mean to one $V_{exp}/V_{predicted}$ performance with a mean (1.23), the second lowest COV 29%, and the lowest AEE 19.3%. Meanwhile, CSA S806-02 had the most consistent results (COV 22%), while the Frosch et al. (2017) model shows extremely conservative results with a mean 3.03 and the largest AEE 61.3%, which is linked to its more sensitive size effect factor as in (Eq. 26) than with other shear model design provisions.

6.6 Conclusion and Recommendations

Fourteen existing and proposed design provisions for calculating the one-way shear strength of FRP-RC members without stirrups were presented. The effect of changing design parameters (e.g.

concrete strength, reinforcement ratio) was assessed using a trial beam. These provisions were then compared to results from a database of 147 beams published in the literature. Based on the findings presented in this paper, the following conclusions were drawn:

1. Aside from the effect of combined shear and moment, the considered shear parameters had similar trends for each of the considered models and provisions. CSA S6:19 and Bentz and Collins (2017) model were less sensitive to increasing size effect and concrete compression strength, respectively, resulting in more conservative shear predictions than the other provisions.
2. The effect of combined shear and moment (often discussed using shear span-to-depth ratio) was only considered in about half of the design algorithms (CSA S6-19, CSA S806-12, CSA S806-02, Bentz and Collins (2017), Park and Choi (2017), Clareda et al.(2017), and Li et al. (2017)).
3. Based on the mean of $V_{exp}/V_{predicted}$ test, design provisions of codes, guidelines, and standards were categorized from conservative to extremely conservative groups, while models were categorized from un-conservative to extremely conservative groups.
4. The method proposed in the CSA S806-12 standard is the most consistent of the studied approaches at predicting the shear strength of the tested members with a mean of 1.04 and lowest AAE of 16.4%. The Park and Choi (2017) model is the most accurate, with a mean of 1.03, the second lowest COV of 31%, and the lowest AAE of 23.1%.

Most codes are conservative and all have a high scattered result, so research should be done on implementing new approaches such as genetic programming via Artificial Neural Networks (ANNs) for predicting the shear strength of FRP-RC elements. To improve shear predictions in future, experimental studies should report parameters (e.g. aggregate size, concrete modulus of elasticity, measured material properties for FRP reinforcement) that affect shear resistance but are often not reported. Additionally, researchers should investigate other factors such as reinforcement layout and support conditions (e.g. fixed-fixed rather than simply supported) as the sample size for these factors is small.

CHAPTER 7

PREDICTION OF ULTIMATE AND SERVICEABLY RESPONSE IN FRC BEAMS WITH LONGITUDINAL STEEL OR GFRP BARS

7.1 Introduction.

Fibres are ideally suited for concrete projects necessitating enhanced resistance against shrinkage, enhanced durability, extended service life, and reduced long-term construction expenses due to a lower maintenance cost and partial replacement of main reinforcement (Aidarov et al., 2022; Domingo et al., 2023; Hussain and Ali, 2018) and reduction of construction time (Aidarov et al., 2022; F. Minelli and Plizzari, 2010). Many applications for Fibre-Reinforced Concrete (FRC) include parking lots, runways, ground slabs, tunnels, barriers, railway tracks, site access road bridges and culverts. FRC can enhance the structure's resilience and flexibility (Pang et al., 2020). Unlike unreinforced concrete, which is prone to deterioration when it experiences fractures and cracks, FRC retains structural integrity by relying on fibres to carry tension after concrete.

Adding fibres into concrete reinforced with discrete reinforcement (e.g., rebar) (RC) enhances flexural and shear strength by increasing post-cracking tensile strength as observed in literature (Amin and Foster, 2016; Cuenca et al., 2018; Dinh et al., 2011; Issa et al., 2016; Marì Bernat et al., 2020; F. Minelli et al., 2014) and concluded in Chapter 5. Consequently, steel fibres (SFs) have the potential to reduce or eliminate the need for shear reinforcement, which mitigates reinforcement congestion, particularly in slender members, and reduces the cost of installation by lowering labour expenses (S. Foster, 2010; F. Minelli and Plizzari, 2010). Fibres can also improve service parameters such as deflection, crack width, and reinforcement strain due to reducing early-age cracking (shrinkage cracking). Previous work has shown that fibres can increase the possible limiting service moment by 60% (Barros et al., 2017).

Serviceability often controls design, particularly for reinforced concrete members of glass fibre reinforcement polymer (GFRP). When compared to steel reinforcement (SR), the reduced elastic modulus of GFRP results in GFRP-RC members developing wider and deeper cracks than SR-RC counterparts with the same reinforcement ratios under equivalent loading (Barris et al., 2017). Consequently, GFRP-RC members are often controlled by serviceability limits such as crack width and deflection. Therefore, it is crucial to develop and evaluate a design equation for FRC members under service conditions to enhance the efficiency and performance of structures.

Numerous models have been created to forecast the flexural strength of SF-reinforced concrete members (Carmona et al., 2022; Henager et al., 1975; Imam et al., 1995; Mobasher et al., 2015). These models are based on cross-sectional analysis, incorporating fibre effects as an additional tensile force which enhances moment resistance. Other models for flexural strength are based on fracture mechanics principles (Carmona et al., 2022). All of these models account for fibres' residual or post-cracking strength contribution. However, these models are formulated and validated exclusively for steel FRC with steel bars as the primary reinforcement, which limits the development of flexural strength models including other types of fibres (e.g., glass fibres (GFs)) and primary reinforcement (e.g., GFRP bars).

Several analytical models have been proposed for predicting the shear strength of FRC, primarily relying on the regression of test data (Ashour et al., 1992; Kwak et al., 2002; Mansur et al., 1986; RILEM TC 162-TDF, 2000; Sharma, 1986), while others are based on fracture mechanics (Gastebled and May, 2001; K. S. Kim et al., 2012; Nguyen-Minh and Rovňák, 2011). However, all of these models are tailored for SF and consider only a few parameters, such as fibre dosage and profile shape. There is a noticeable lack of models that evaluate shear strength across different shear spans to effective depth, a/d ratios, fibre types, combinations of fibres, and sizes.

SFs effectively manage the development of splitting cracks, resulting in substantial improvements in the tension stiffening of both normal and high-strength RC elements (Abrishami and Mitchell, 1997). Alsayed (1993) formulated an equation for estimating FRC member deflection using the effective moment of inertia calibrated based on test observations. This equation incorporates the fibre aspect ratio (d_f/l_f), fibre length, l_f, fibre diameter, d_f, and volume fraction, represented by coefficients generated through regression analysis of test results (Alsayed, 1993). A mechanistic approach was later utilized to calculate the effective moment of inertia incorporating the post-cracking tensile capacity of fibres, resulting in the advantage of not relying on specific data sets (Bischoff, 2007). This is the rationale behind this study's use of this approach, with the additional modification of incorporating effects from various types of fibres.

The research gap is highlighted by the fact that existing ultimate and serviceability design equations for FRC beams are often derived through a regression analysis of steel fibre RC beam test data, typically involving a limited range of fibre types and dosages. This constrained dataset needs more diversity concerning fibre types such as GFs and their combination with SFs, along with different a/d ratios and types of main reinforcement. A numerical database of 720 beams was used to investigate various parameters in response to this gap. The study examined different parameters, such as beam heights, a/d ratios, types of reinforcing bars (SR and GFRP), reinforcement ratios ρ, and various FRC (SFs, GFs, and hybrid of SFs and GFs (HFs)) with different reinforcement dosages, V_f. Using this database, models for predicting ultimate flexural and shear strength, as well as serviceability short term deflection and reinforcement strain, were developed. This study assumes randomly distributed fibres for normal-strength concrete (NSC) with SF and/or GF. These findings may have general limitations due to the specific nature of the fibre distribution and types considered.

7.2 Numerical Database.

Following a numerical model verification process (section 2.3 in Chapter 5), a dataset of numerical values was compiled from a parametric study involving 720 modelled beams, including 72 RC beams and 648 FRC beams. This study explored various parameters, including geometry (with beam heights (h) of 500 mm and 750 mm), load placement, and a/d ratios (2, 3, and 4), as shown in Figure 7-1. Two main reinforcement bar types (steel and GFRP) were used with tension reinforcement ratios ρ of 0.55%, 1.1%, and 2.2%; stirrups; fibre reinforcement materials SF, GF, and HFs; and fibre reinforcement dosages V_f of 0.5%, 1.0%, and 1.5% to study ultimate and serviceability performance.

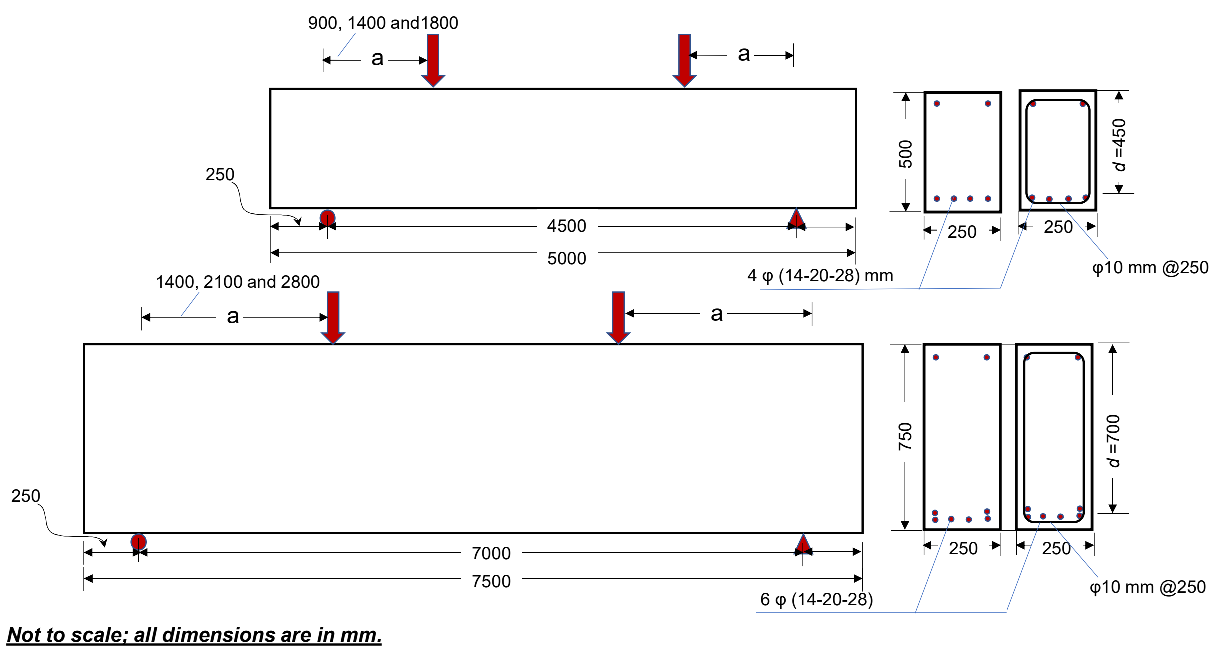

Figure 7-1: The geometry and layout of beams used in FE analyses.

Figure 7-2 depicts the 2D VecTor2 model based on Modified Compression Field Theory (MCFT) (Wong et al., 2013) Distributed Stress Field Model (Vecchio, 2000) that can be applied to FRC

(S. J. Foster et al., 2018). Half of the beam was modelled due to symmetry to reduce computational effort. Hybrid rectangular elements were used for concrete (plain and FRC), and truss elements were used for reinforcement bars. Mesh dimensions of 50 × 50 mm were selected based on mesh sensitivity analysis (Section 5.2.2.3). The loading protocol used monotonic displacement control to obtain the load-deflection behaviour of beams subject to 4-point bending, including post-peak response. Detailed descriptions of the compression and tension models used for concrete (including FRC) can be found in Sections 5.2.2.1 and 5.2.2.2. Fibres in FRC were modelled by considering the tension-softening tensile stress-strain input, while the pc does not exhibit post-cracking behaviour, as shown in Figure 7-2 (c). A custom strain-based approach was implemented by modifying the default five-point custom input-strain-based tension-softening model in VecTor2® to a three-point tension model (Alguhi and Tomlinson, 2023) (see section 5.2 for more details). The compression stress-strain response for both pc and FRC and incorporating fibres is achieved by adjusting parameters like peak compressive stress, σ_{c0} (equal to f_c', concrete compressive strength) and corresponding strain, ε_{c0} as well as σ_{res}, the residual compressive stresses, and ε_{cu} (ultimate compressive strain). σ_{t0} and $\sigma_{t\,res}$ are the peak and residual tensile stresses, respectively; $\varepsilon_{t\,cr}$, $\varepsilon_{t\,res}$, and ε_{tu} are cracking, peak, and ultimate tensile strain. The concrete elastic modulus, E_c is assumed the same for compression and tension.

In Figure 7-2 (d), reinforcement's characteristics are depicted. Steel shows a trilinear response with the initial elastic modulus (E_s), followed by a yield stress of f_{sy} which starts at yield strain ε_{sy}. Strain hardening was included and initiated at ε_{sh} with a strain hardening modulus of E_{sh}. Steel response was terminated at ultimate stress, f_{su} and corresponding ultimate strain ε_{su}. GFRP has a linear-elastic response until rupture, with elastic modulus E_f, ultimate stress f_{fu}, and corresponding ultimate strain ε_{fu}.

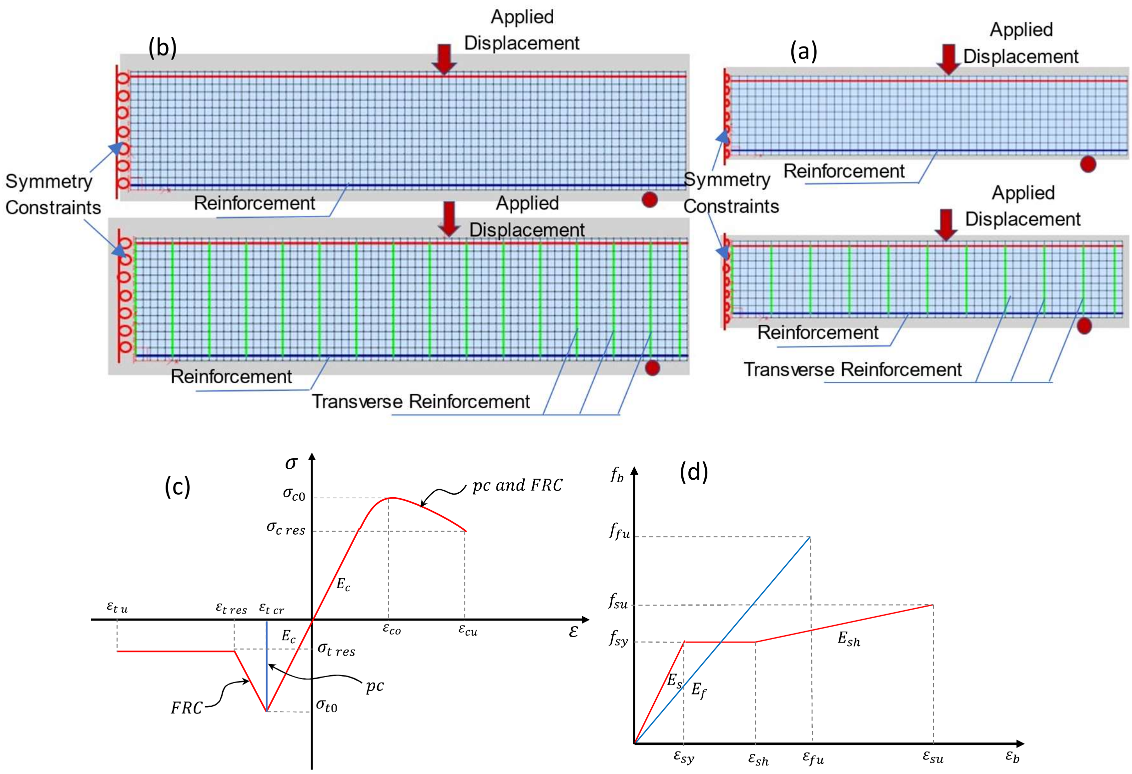

Figure 7-2: VecTor 2 model details and boundary condition depicting two-member depths considered ((a)750 mm and (b)500 mm). Stress-strain response for (c) compression and (d) tension employed within VecTor 2.

7.3 Ultimate Design Equations

Flexural and shear strength data from 720 modelled beams, encompassing SR-RC, GFRP-RC, SR-FRC, and GFRP-FRC, was collected. From this dataset, 259 beams were identified as flexural-critical, and 461 were deemed shear-critical.

7.3.1 Flexural strength

The effect of fibres on flexural strength was considered using a trilinear analytical model. This model was derived considering fibre effects on compression (Section 3.4.6) and tension (section 4.5.4,(Alguhi and Tomlinson, 2023)), as seen in Figure 7-3. This model is further simplified using stress block modification factors (α_1 and β_1 for compression, α_{1t} and β_{1t} for tension) derived in Chapter 3 and 4 and summarized in Table 6-1. Experimental Database of Shear-Controlled FRP-

RC Specimens without Stirrups for considered fibres and volume fractions. Expressions are intended for rectangular sections with a single layer of reinforcement. The tensile, σ_{t0} and compressive, σ_{c0} strengths σ_{t0} can be obtained from Eq (7-1) and (7-2) (see Chapter 3 and 4), respectively.

$$\sigma_{t0} = 0.38\sqrt{f_c'} \qquad \text{for SFs, GFs, and HFs} \qquad (7\text{-}1)$$

$$\sigma_{c0} = f_c' + (7.5V_f)100 \qquad \text{for SFs}$$
$$\sigma_{c0} = f_c' + (4.5V_f)100 \qquad \text{for GFs} \qquad (7\text{-}2)$$
$$\sigma_{c0} = \gamma[f_c' + (950V_f)] + (\gamma - 1)\,[f_c' + (950V_f)] \qquad \text{for HFs}$$

Where: σ_{cy}, is yield compressive stresses, ε_{c0}, is yield compressive strain, γ is the hybrid mixture ratio ($\frac{SFs}{GFs}$), and ultimate compressive strains. V_f, is the fibre volume fraction, which is the percentage of fibre volume in the entire volume of FRC composite ((the mass of fibres/density)/m^3), d is the effective depth, c_f is plastic neutral axis depth for FRC members, M_{fib} is the moment resistance for FRC flexural members, T_b is tension force of reinforcement bar, f_b is the reinforcement stress, A_b is the area of tension reinforcement, and C_c is the compression force.

Table 7-1: Stress block factors considered for FRC flexural analysis

Stress block factor	Fibre type		
	SF	GF	Hybrid (combined steel and glass fibre) (HF)
α_1	$0.75 + 16V_f$	$0.75 + 7.5V_f$	$0.75 + 20\gamma V_f + 10(1-\gamma)V_f$
β_1	$0.8 + 4V_f$	$0.8 + 4V_f$	$0.8 + 4(1-\gamma)V_f$
α_{1t}	$0.20 + 25V_f$	$0.03 + 10V_f$	$\gamma(0.10 + 30V_f) + (1-\gamma)(0.10 + 20V_f)$
β_{1t}	1.05	$1.6 - 30V_f$	1.05

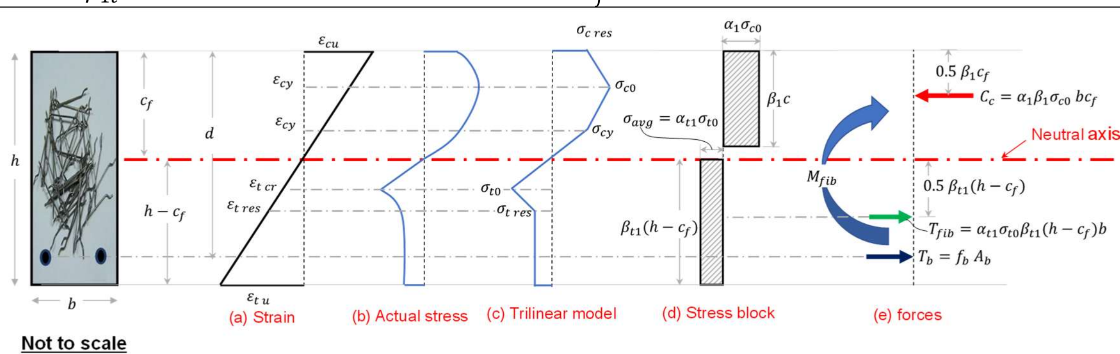

Figure 7-3: Simplified flexural model for FRC

7.3.1.1 *Analytical flexural strength model validation*

The flexural strength analytical model validation was completed using 259 flexural-critical beams from the FEA database of SR-RC, SR-SF, SR-GF, and SR-HF beams. These beams exhibit various *h*, *a/d* ratios, with and without minimum stirrups, and ρ. GFRP beams are not considered here since shear failure predominantly governed them. The outcomes demonstrate good performance, shown in Figure 7-4, mean and coefficient of variation (CoV) of numerical to analytical results equal to 1.10 and 8.6%, respectively, for all *a/d* with RC, SFs, GFs and HFs. There is no noticeable difference in the means or CoV for different *a/d* ratios, as shown in Table 7-2. The model's capability to predict flexural capacity is consistent with the FEA results. Observing the small variations among different fibre types or in the absence of fibres, as shown in Table 7-2, show similar means and variability for various *a/d* ratios and fibre types.

Table 7-2: Summary of performance indicators for flexural strength analytical model for different a/d ratios.

$\frac{M_{fib\,num.}}{M_{fib\,pre.}}$	*a/d*				Fibre type			
	All	**2**	**3**	**4**	**SR-RC**	**SR-SF**	**SR-GF**	**SR-HF**
Mean	1.10	1.11	1.11	1.09	1.13	1.06	1.12	1.10
SD	0.095	0.081	0.095	0.105	0.103	0.091	0.092	0.074
CV	8.6%	7.3%	8.6%	9.6%	8.9%	8.5%	8.0%	6.8%

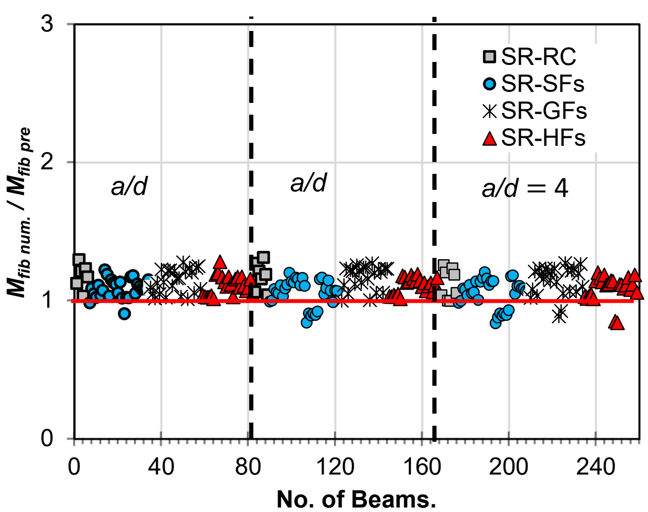

Figure 7-4: The ratio between the numerical and predicted moment resistance

7.3.2 Shear strength

The design provisions for RC-FRC shear strength are derived from equilibrium as shown in Figure 7-5. The total ultimate shear strength, V_u, is calculated as the sum of contributions from three components (Eq.(7-3)). This includes concrete contribution, V_c, fibre contribution, $V_{c.fib}$, and stirrup contribution, V_s.

$$V_u = V_c + V_{c.fib} + V_s \tag{7-3}$$

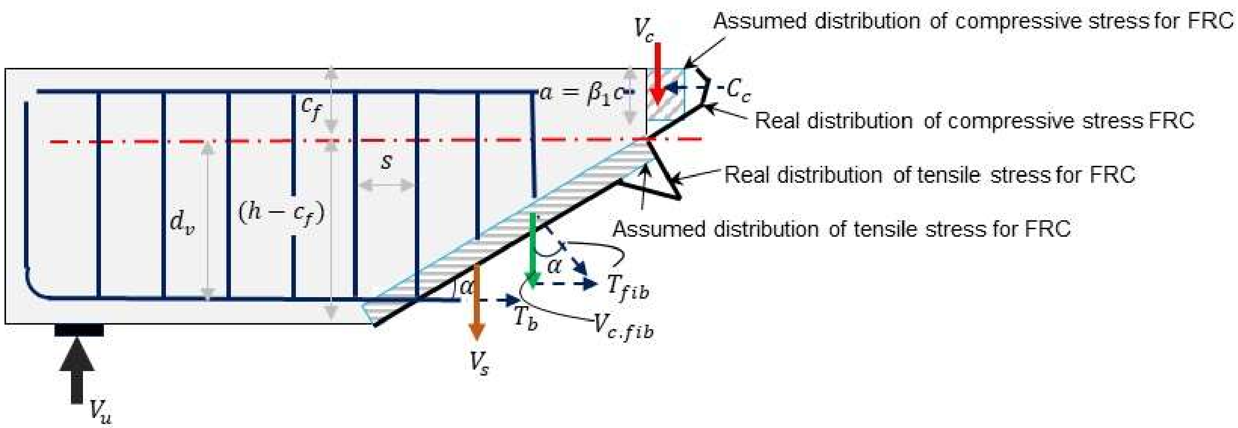

Figure 7-5: Free body diagram through shear crack showing the contribution of different components.

7.3.2.1 Concrete contribution, V_c

The concrete contribution, V_c includes contributions from the concrete compression zone, aggregate interlock, dowel action, and arch action. (Alguhi and Tomlinson, 2021) and section 6.4 delves into critical factors influencing shear strength, particularly in GFRP beams. These factors include compressive strength, section dimensions, reinforcement ratio, the elastic modulus of the tension reinforcement, the arch effect (pertains to shear-moment interaction), and the size effect (Bažant, 1984). These factors are essential in predicting the shear strength of GFRP-RC beams across various codes, guidelines, standards, and models. The results indicate that the most dependable provision is the (CSA S806-12, 2012) standard for GFRP-RC, demonstrated by (Alguhi and Tomlinson, 2021); for this reason, this study used the CSA S806-12 standard to predict

V_c for GFRP beams. The (CSA S6:19, 2019) expression is preferred for steel-RC beams due to its comprehensive consideration of factors affecting shear strength, especially arch effect and size effect, and axial stiffness (Alguhi and Tomlinson, 2021)

The (CSA S6.1:19, 2019) one-way shear strength provision for concrete without stirrups, V_c, given in Eq. (7-3) is based on an approximation of MCFT.

$$V_c = 2.5\beta\phi_c f_{cr} b_w d_v \tag{7-4}$$

Where d_v is the effective shear depth (greater of $0.9d$ and $0.72h$), b_w, is the member's effective width, ϕ_c is the material reduction factor for concrete (taken as unity in this paper), f_{cr} is the concrete cracking strength ($f_{cr}=0.4\sqrt{f_c'}$). β is a factor that accounts for the shear resistance of cracked concrete, which relates to the longitudinal strain at mid-depth of the member, ε_x (Bentz et al. 2006) Eqs. (7-5) and (7-6).

$$\beta = \left[\frac{0.4}{1+1500\varepsilon_x}\right]\left[\frac{1300}{1000+s_{ze}}\right] \tag{7-5}$$

$$\varepsilon_x = \frac{\frac{M_f}{d_v}+V_{fs}}{2E_s A_s} \leq 0.003 \tag{7-6}$$

where V_{fs} is the factored shear, M_f is the factored moment and A_s , is the area of the steel tension reinforcement. ε_x cannot exceed 0.003 as exceeding that strain limits how forces redistribute (Bentz et al. 2006). s_{ze} is an effective crack spacing for members without stirrups found using Eq. (7-7).

$$s_{ze} = \frac{35\, s_z}{15+a_g} \leq 0.85 s_z \tag{7-7}$$

where s_z, is the smaller of d and the maximum spacing between longitudinal reinforcement layers, and a_g is the nominal maximum aggregate size.

For GFRP-RC, S806-12 (CSA S806-12, 2012b) was used. For sections having an effective depth not exceeding 300 mm and no axial load, V_c can be calculated using Eq.(7-8).

$$V_c = 0.11\phi_c \sqrt{f_c'} b_w d_v \leq 0.05\lambda\phi_c k_m k_r (f_c')^{\frac{1}{3}} b_w d_v \leq 0.22\phi_c \sqrt{f_c'} b_w d_v \tag{7-8}$$

where k_m is a moment-shear interaction value and k_r is a reinforcement stiffness that is calculated in Eq. (7-9).

$$k_m = \sqrt{\frac{V_f d}{M_f}} \leq 1.0 \tag{7-9}$$

$$k_r = 1 + (E_f \rho_f)^{1/3} \tag{7-10}$$

If d exceeds 300 mm and if less than minimum shear reinforcement is provided, V_c from Eq. (7-3) is multiplied by a size effect factor, k_s given in Eq.(7-11).

$$k_s = \frac{750}{450+d} \leq 1.0 \tag{7-11}$$

7.3.2.2 Fibre contribution, $V_{c.fib}$

The fibre contribution is represented as $V_{c.fib}$, which relies on the tensile force transmitted through fibres across the diagonal shear crack, as illustrated in Figure 7-5. An equivalent uniform tensile stress is assumed constant along the length of the diagonal crack inclined at an angle α to the horizontal line. MCFT utilizes the inclination angle, α, to give conservative estimations of shear strength across a wide range of angles, as demonstrated by (Collins et al., 2007). This angle is influenced by longitudinal strain, ε_x, and increases with larger ε_x (Bentz and Collins, 2006). The assumed constant fibre stress has a magnitude of $\alpha_{t1}\beta_{t1}\,\sigma_{t0}$. $V_{c.fib}$, can be determined using Eq. (7-15). The influence of ρ and *a/d* is incorporated into k_f factor, as the degree of improvement in diagonal tension capacity, is contingent on the *a/d* ratio of a beam, as indicated by (F. (Fausto) Minelli, 2005).

$$V_{c.fib} = k_f\ T_{fib}\ \cos\alpha \tag{7-12}$$

$$30^{\circ} \leq \alpha = 29 + 7000\varepsilon_x \geq\ 60^{\circ} \tag{7-13}$$

$$T_{fib}\ =\ \alpha_{t1}\,\sigma_{t0}\,\beta_{t1}\ \frac{(h-c)}{\sin\alpha} b\cos\alpha \tag{7-14}$$

$$V_{c.fib} = k_f\,\alpha_{t1}\,\sigma_{t0}\,\beta_{t1}\ (h-c)\,b\ \cot\alpha \tag{7-15}$$

Where, $k_f = \rho\left(\frac{1}{(a/d)}\right)^{0.25}$

A review of the literature highlights that the increase ρ is attributed to reduced shear cracking in FRC. ρ and *a/d*, have the most significant impact on the shear capacity of FRC beams, as evidenced by findings from (Momani et al., 2022; Sharifi and Moghbeli, 2021).

7.3.2.3 Stirrup's contribution, V_s

The parallel chord truss model is widely acknowledged as the standard approach for assessing the influence of stirrups on shear capacity, V_s in slender RC beams. However, codes and standards offer different methods for determining α within this model. In this study, CSA S6:19 expressions are used to determine α, as in Eq.(7-13) and V_s can be calculated using Eq. (7-16).

$$V_s = \frac{A_{rv} f_{rv} d_v}{s} \cot\alpha \tag{7-16}$$

Where; A_{rv}, is the stirrup area, and f_{rv}, is the stirrup stress. For steel-RC, f_{rv} is the stirrup yield stress; for GFRP-RC, f_{rv} is the minimum of $0.4 f_{fu}$ and $0.005 E_f$ (CSA S806-12, 2012b).

7.3.2.4 Analytical Shear strength model validation

The developed model's performance was evaluated using an FEA database consisting of 461 shear-controlled beams. This dataset comprised 15 SR-RC, 86 SR-FRC, 36 GFRP-RC, and 324 GFRP-FRC beams, encompassing various characteristics described in Section 7.2.

The shear strength expression (Eq. (7-3)) is not valid in the *a/d* = 2 region, as the assumption that the plain section remains plane no longer holds (ACI-318-19, 2019). Using sectional approaches like Eq. (7-3) typically results in an overly conservative design prediction (Collins and Mitchell, 1997), with this obvious in Figure 7-6 for both SR beams. This is why other methods like strut-and-tie models (Schlaich and Schiifer, 1991) are often used for these situations (beyond the scope of this study). Beams with *a/d* ≥ 2.5, according to the guidelines outlined in (ACI-318-

19, 2019) provide better results than the full data set (*a/d* of 2, 3 and 4), as shown in Table 7-4, with the ratio of FEA to predicted having means between 0.95-1.13 and CoV less 20% for both Steel-RC and GFRP-RC beams, even when dealing with a large number of parameters. The analytical model exhibited reasonable performance, and similar results were observed when comparing the test data with common analytical models for FRP-RC (Alguhi and Tomlinson, 2021). The SR-FRC beams are overpredicted compared to GFRP beams, and this phenomenon is attributed to the fact that the predicted V_c contribution from CSA-S6:19 tends to overpredict strength for steel-RC beams for *a/d* = 2.5 (Collins and Mitchell, 1997). This overprediction is notably evident in control beams when compared to the predicted V_c contribution from CSA-S806-12, with mean values of 1.34 and 1.11 for Steel-RC and GFRP-RC beams, as discussed in section 5.3.1.

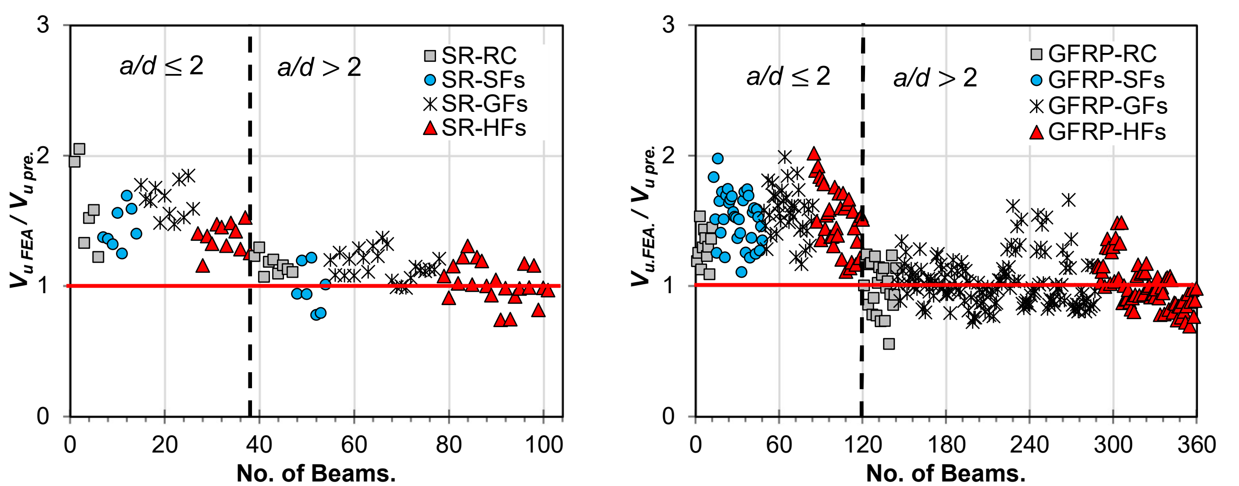

Figure 7-6: The ratio between the numerical and analytical shear strength for (a) SR-FRC and (b) GFRP-FRC.

Table 7-3: Summary of performance indicator for shear strength analytical model for all (*a/d*).

$\frac{V_{u\,num.}}{V_{u\,pre.}}$	SR-RC	SR-SF	SR-GF	SR-HF	GFRP-RC	GFRP-SF	GFRP-GFs	GFRP-HF
Mean	1.34	1.23	1.32	1.14	1.11	1.17	1.22	1.17
SD	0.306	0.286	0.264	0.223	0.209	0.259	0.277	0.267
CoV %	22.8%	23.3%	20.0%	19.5%	18.9%	22.1%	22.7%	22.8%

Table 7-4: Summary of performance indicator of shear strength analytical model for (*a/d*) > 2.0.

$\frac{V_{u\,num.}}{V_{u\,pre.}}$	SR-RC	SR-SF	SR-GF	SR-HF	GFRP-RC	GFRP-SF	GFRP-GF	GFRP-HF
Mean	1.13	0.98	1.15	0.95	1.01	1.00	1.05	1.00
SD	0.049	0.175	0.111	0.117	0.168	0.137	0.220	0.179
CoV %	4.3%	17.8%	9.7%	12.3%	16.6%	13.7%	20.9%	17.9%

7.4 Serviceability Design Equations

Incorporating fibres into concrete effectively reduces crack width and propagation through the bridging. Fibre bridging increases the element stiffness, decreasing deflection and reducing reinforcement strain for both SR and GFRP beams. This increases section stiffness, leading to increased maximum service load. FEA results substantially reduced crack width, deflection, and reinforcement strain. Data from 360 beams with stirrups was used to assess the serviceability of the analytical model. Beams with stirrups were used to reduce potential shear deformations (S. W. Kim et al., 2021), though there is no clear difference in deflection at service load for FRC beams with and without stirrups (see section 5.5).

Maximum service load is often assessed at approximately 65% of the nominal moment capacity for steel-reinforced concrete beams and is based on a back calculation of live load factors in the National Building Code of Canada (Tomlinson and Fam, 2015). This approach is adopted because short-term live load deflection limits for beams, often equal to $l/360$, exceed the yield deflection in most beams considered in this study. For GFRP beams, the service load level is around 30% of the nominal moment capacity, as reported by several researchers (Bischoff and Gross, 2011; Maher Elnemr et al., 2011), with this limit intended to limit creep-rupture or excessive deflections.

7.4.1 Midspan deflection, δ_{max}.

The influence of fibres at service was considered through an additional force, T_{fib}, illustrated in Figure 7-7(b) and the impact of fibres on the cracking moment, M_{cr}. All beams considered were cracked in service, so FRC contribution in tension was considered using the tensile stress block, as depicted in Figure 7-7(b), for simplicity. T_{fib} is generated based on this stress block, incorporating modification factors α_{1t} and β_{1t} for tension (refer to Table 7-1), similar approach was used by (Bischoff, 2007).

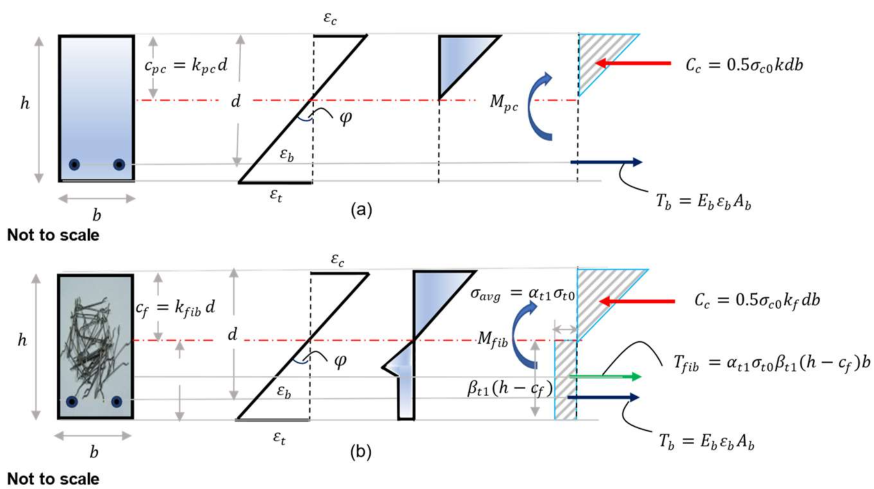

Figure 7-7: Stress-strain distribution of cracked-elastic section analysis for rectangular cross-section @ service, (a) RC-PC (b) RC-FRC.

The M_{cr}, shown in Eq. (7-17), is a major influence on an effective moment of inertia, and the accuracy of deflection predictions is highly dependent on the accuracy of M_{cr}. M_{cr} is influenced by reinforcement axial stiffness. Design codes and standards often conservatively ignore this contribution for ease of calculations. In this paper, M_{cr} is calculated using transformed section properties: I_t (transformed moment of inertia), and y_t (distance from transformed section centroid to extreme tension face) as shown in Eq. (7-17).

$$M_{cr} = \frac{f_r I_t}{y_t} \tag{7-17}$$

M_{cr} is also a function of the modulus of rupture, f_r. Current codes and standards do not account for the impacts of fibre type and dosage on f_r. The proposed Eq. (7-18) for f_r are derived from a regression analysis of data from 40 prisms of both fibre-reinforced and non-fibre-reinforced samples (Alguhi and Tomlinson, 2023b). These equations showed a high level of accuracy in predicting f_r for the concrete and fibres considered in that study, with mean and CoV values of 1.01 and 7% for SF, 1.02 and 5% for GF, and 0.99 and 5% for HF, respectively.

$$f_r = \begin{Bmatrix} 0.65\sqrt{f_c'} + 150V_f & \text{for SF} \\ 0.65\sqrt{f_c'} + 100V_f & \text{for GF, HF} \end{Bmatrix} \tag{7-18}$$

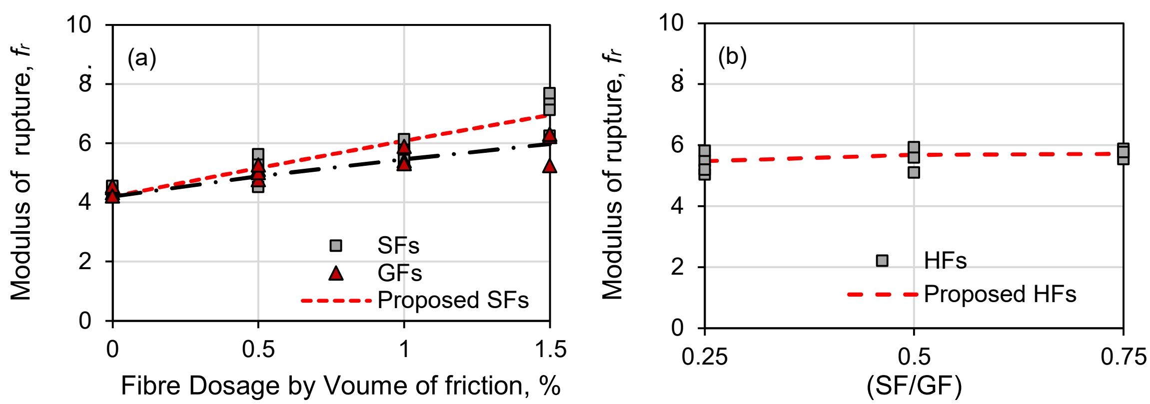

Figure 7-8: Effect of fibre type and dosages on the modulus of rupture of (a) SFs and GFs and (b) HFs, the data from (Chapter 4, (Alguhi and Tomlinson, 2023)**)**

The additional force carried by fibres and increased cracking moment are integrated into a method for evaluating member stiffness, incorporating the concept of effective moment of inertia for FRC members ($I_{e\,fib}$), as proposed by Bischoff (2007) in Eq. (18-21) and illustrated in Figure 7-9. This approach accounts for the tensile contribution of FRC, facilitating its integration into established design procedures. The fibres create an additional moment contribution, as shown in Figure 7-7(b), ΔM_{fib} in a cracked section which is equal to the difference between the moment carried by a cracked section with fibres, $M_{s\,fib}$ and the moment carried by a cracked section without fibres,

M_{pc}, as seen in Figure 7-9 and Eq.(7-22). ΔM_{fib} mitigates the increase in curvature, φ at initial cracking from the maximum (i.e., no fibres or tension stiffening) curvature increase at first cracking, $\Delta\varphi_{max}$ by a value of $\Delta\varphi_{fib}$, leading to $\Delta\varphi'_{max}$ which is the difference between $\Delta\varphi_{max}$ and $\Delta\varphi_{fib}$. Fibres thus increase the elastic, cracked neutral axis depth to effective depth ratio for FRC, k_{fib} and corresponding FRC cracked moment of inertia, $I_{cr\ fib}$ as shown in Eqs. (7-20) and (7-21), respectively.

$$I_{e\ fib} = \frac{I_{cr\ pc}}{1-\eta{\beta_{ts}}^2-\left(\frac{\Delta M_{fib}}{M_{s\ fib}}\right)(1-\beta_{ts})} \quad (7\text{-}19)$$

$$k_{fib} = \sqrt{\left[n\rho+\left(\frac{\alpha_{t1}\sigma_t\beta_{t1}I_{cr\ Pc}}{M_{pc}d}\right)\right]^2+2\left[n\rho+\left(\frac{\alpha_{t1}\sigma_t\beta_{t1}I_{cr\ pc}\,h}{M_{pc}d^2}\right)\right]}-\left[n\rho+\left(\frac{\alpha_{t1}\sigma_t\beta_{t1}I_{cr\ pc}}{M_{pc}d}\right)\right] \quad (7\text{-}20)$$

$$I_{cr\ fib} = \frac{b\left(k_{fib}d\right)^3}{3}+nA_s\left(d-k_{fib}d\right)^2 \quad (7\text{-}21)$$

$$\Delta M_{fib} = M_{s\ fib}-M_{pc} = M_{pc}\left[\frac{I_{c\ fib}}{I_{c\ pc}}-1\right]+\frac{\alpha_{t1}\sigma_t\beta_{t1}bd^2\left[1-k_{fib}\frac{d}{h}\right]^2}{2\left(\frac{d}{h}\right)^2} \quad (7\text{-}22)$$

Where: $\eta = 1-\frac{I_{cr}}{I_t}$, β_{ts} is a tension-stiffening factor equal to $\frac{M_{s\ fib}}{M_{cr\ pc}}$, and n is the modular ratio. Plain (i.e., ignoring fibres) reinforced concrete section properties can be found in Eqs. (22-24).

$$M_{cr\ pc} = \frac{f_r I_{cr\ pc}}{y_t} \quad (7\text{-}23)$$

$$k_{pc} = \sqrt{n\rho^2+2n\rho}-n\rho \quad (7\text{-}24)$$

$$I_{cr\ pc} = \frac{b(kd)^3}{3}+nA_s\left(d-k_{pc}d\right)^2 \quad (7\text{-}25)$$

Where: k_{pc} is the ratio of elastic, cracked neutral axis depth to effective depth for plain concrete and $I_{cr\ pc}$, is a cracked moment of inertia of plain concrete.

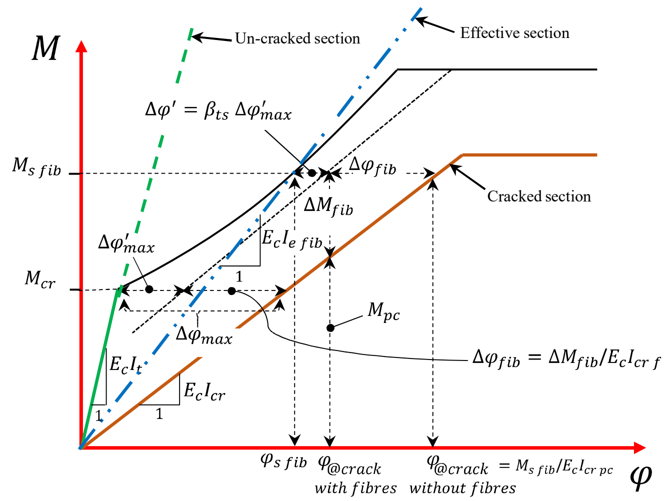

Figure 7-9: Moment-Curvature response for FRC at service adapted from (Bischoff, 2007)

The determination of $I_{e\,fib}$, depends on k_{fib}, ΔM_{fib}, $I_{cr\,fib}$, and M_{pc}, which makes an iterative process necessary (Bischoff, 2007). This study proposes a method of doing this iteration process, as outlined in Figure 7-10. The process begins with M_{pc} set equal to $M_{s\,fib}$, then calculating $k_{fib\,i}$, $I_{cr\,fib\,i}$, and $\Delta M_{fib\,i}$. Subsequent iterations are based on an updated $M_{pc\,i+1}$, and the process continues until $\Delta M_{s\,fib} - \Delta M_{fib\,i+1}$ becomes very close to zero.

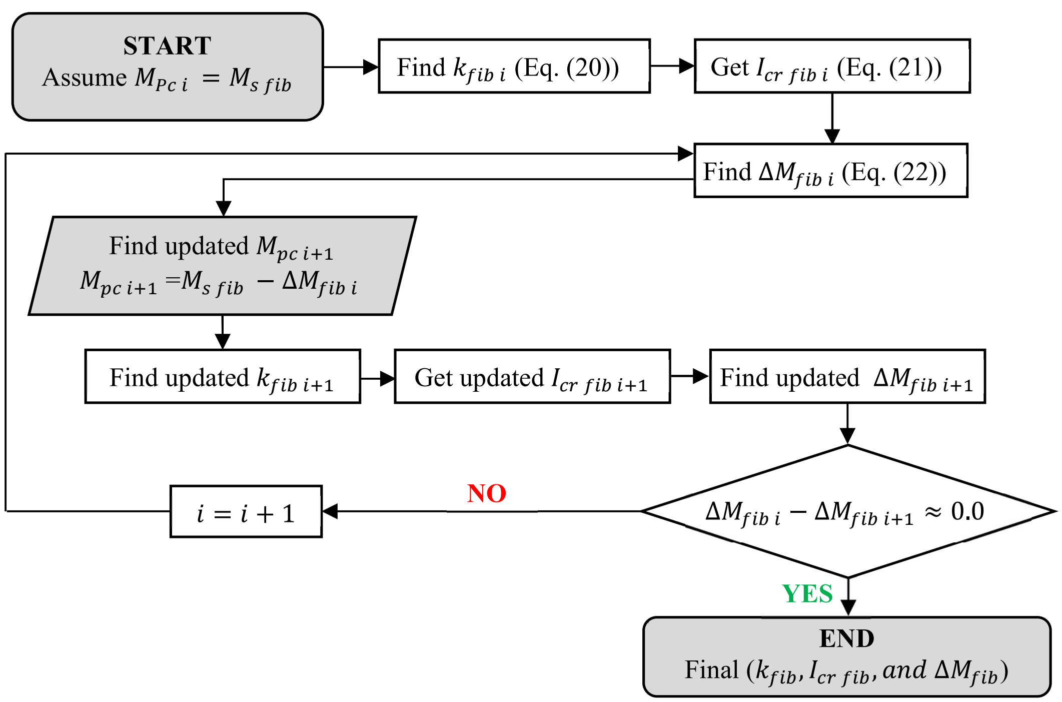

Figure 7-10: Flow chart for finding ΔM_{fib} and k_{fib}. i subscript is used to denote iterations.

The numerical maximum service deflection, $\delta_{max.\ FEA}$ under immediate loading was taken as the deflection at service load described in section 7.4 at mid-span for the 360 FEA models of RC and FRC beams with stirrups. Eq.(7-26), based on elastic deflection expressions for four-point loading, was used to calculate the analytical $\delta_{max.pre}$.

$$\delta_{max.pre} = \frac{P_s\, l_a}{48\, E_c\, I_{e\,fib}}(3l^2 - 4{l_a}^2) \tag{7-26}$$

$$E_c = 4700\sqrt{f_c'} \tag{7-27}$$

Here, l is the beam span, P_s is the total concentrated load at service, which is split into two concentrated loads (*P/2*), applied at a distance, l_a, from the nearest support. $I_{e\,fib}$ was obtained from Eq.(7-19). The concrete elastic modulus, E_c was found from (7-27)(ACI-318-19, 2019).

7.4.1.1 Analytical effective moment of inertia model validation

Figure 7-11 shows the ratio between FEA and analytical maximum deflection, denoted as, $\frac{\delta_{max.\ FEA.}}{\delta_{max.\ pre.}}$. Results indicate disparity between the FEA and analytical values. Part of the reason for this overestimation discrepancy can be attributed to the assumption of perfection in FEA, which operates under the assumption of ideal elastic conditions, including perfect material properties (such asf_c' and E_c)). Another factor contributing to this discrepancy is the assumption within FEA that the compression modulus of elasticity is equal to the tension modulus of elasticity (refer to Figure 5.2), whereas, according to (Martin and Jitka 2017), the tension modulus of elasticity should be lower than the compressive modulus of elasticity. The above are the suspected reasons why the average of $\frac{\delta_{max.\ FEA.}}{\delta_{max.\ pre.}}$ for the SR and GFRP data for all *a/d* ratios (2, 3, and 4) set are 0.71 and 0.66 respectively, an in Table 7-5.

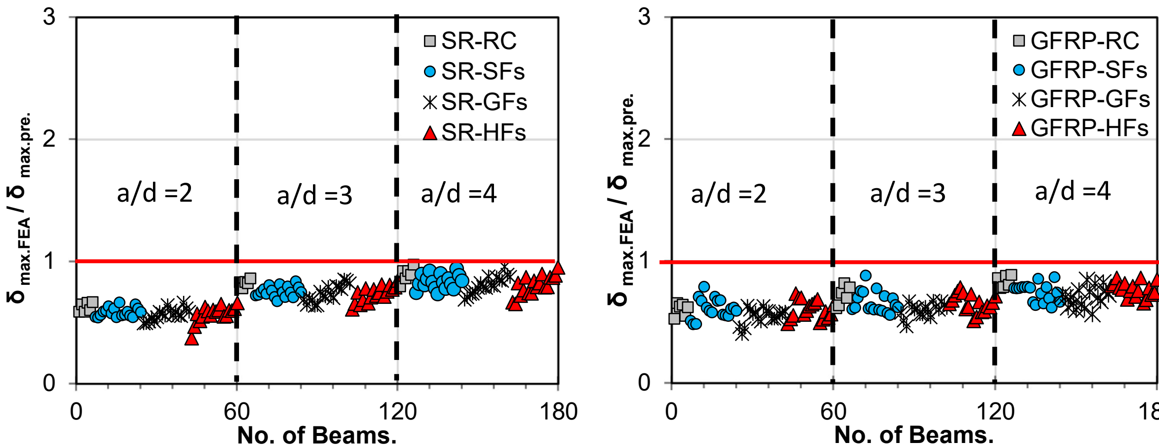

Figure 7-11: The ratio between the FEA and analytical maximum deflection at service

Table 7-5 : Summary of performance indicators for deflection model with different *a/d* ratio.

Main Tension Rein.	SR				GFRP			
$\frac{\delta_{max.\ FEA.}}{\delta_{max.\ pre.}}$	*a/d*				*a/d*			
	All	2	3	4	All	2	3	4
Mean	0.71	0.58	0.75	0.82	0.66	0.59	0.64	0.75
SD	0.12	0.05	0.06	0.07	0.10	0.08	0.08	0.08
CoV	17%	9%	8%	9%	16%	13%	12%	10%

Although the analytical results consistently predict larger deflections than FEA, , analytical results better align with FEA deflection results for a beam with a/d > 2.0, especially for a/d = 4 with mean and CoV equal to 0.82 and 9%; 0.75 and 10% for SR and GFRP, respectively; this may be due to the fact that for D-region when a/d < 2.5 assumptions for plane section remain plane are no longer valid (ACI-318-19, 2019) and the analytical model is not capable of including addition shear deformation.

7.4.2 Maximum reinforcement strain at crack

Reinforcement strain is proportional to crack width, as indicated by (Frosch, 1999). Considering reinforcement strain shows how fibres may reduce this strain (and reduce crack widths) through crack-bridging. Predicting reinforcement strain in FRC is a valuable tool for implementing it into crack width expressions. Crack width is considerably influenced by the bond between reinforcement and the surrounding concrete. That's why many codes, such as ACI-318-19 (2019) or ACI 440.11 (2022), and standards like CSA S806-12 (2012), incorporate a bond-dependent coefficient, k_b, into their design equations. k_b, varies between 0.9 and 1.4 depending on the type of reinforcement and concrete and should be determined experimentally, as CSA S806-12 (2012) recommends. The accuracy of crack width expressions is highly dependent on k_b, (Wang and Belarbi, 2011), which makes modelling challenging due to the limited availability of test data on k_b for the considered bars or including k_b in models. In this study, reinforcement strain is used as a proxy for assessing how fibres affect crack widths, given the complexities with k_b.

The FEA reinforcement strain, $\varepsilon_{b\,max.\ FEA.}$, at service load was taken as the maximum reinforcement strain in tension reinforcement across cracks within the mid-span region. A total of 360 beams, including RC and FRC beams with stirrups (Chapter 5), were used for comparison. The predicted reinforcement strain, $\varepsilon_{b\ pre.}$ can be found based on flexural elastic theory as in Eq.(7-29) using k_{fib} and $I_{e\ fib}$ from Eqs. (7-20) and (7-21)and, respectively.

$$f_b = n\frac{P_s a\,(d-k_{fib}d)}{I_{e\,fib}} \tag{7-28}$$

Since the analysis in the elastic stage, $E_{b.} = \frac{f_{b.}}{\varepsilon_{b\ pre.}}$, then:

$$\varepsilon_{b\,max.\ pre.} = n\frac{P_s a\,(d-k_{fib}d)}{I_{e\,fib}\,E_b} \tag{7-29}$$

7.4.2.1 Analytical maximum reinforcement strain at crack model validation

The ratio between the FEA reinforcement strain and the analytical reinforcement strain for both Steel-RC and GFRP-RC beams with and without fibre is evaluated in Figure 7-12. Both models give very similar results for reinforcement strain. Specifically, the mean $\frac{\varepsilon_{b\,max.\ FEA.}}{\varepsilon_{b\,max.\ pre.}}$, are 0.91 and 0.96 for Steel-RC and GFRP-RC beams, respectively, and CoV equals 10% for both cases. These results are consistent across all beam types, even when depths vary between 500 and 750 mm. Like the deflection model's performance, the analytical and FEA gave more similar results when *a/d* is 3 or 4, compared to *a/d* equal to 2. This effect is particularly notable for *a/d* = 4, where the mean values reach 0.98 and 1.0 for SR and GFRP beams, respectively, with a CoV of 7% for both SR and GFRP beams, as shown in Figure 7-12.

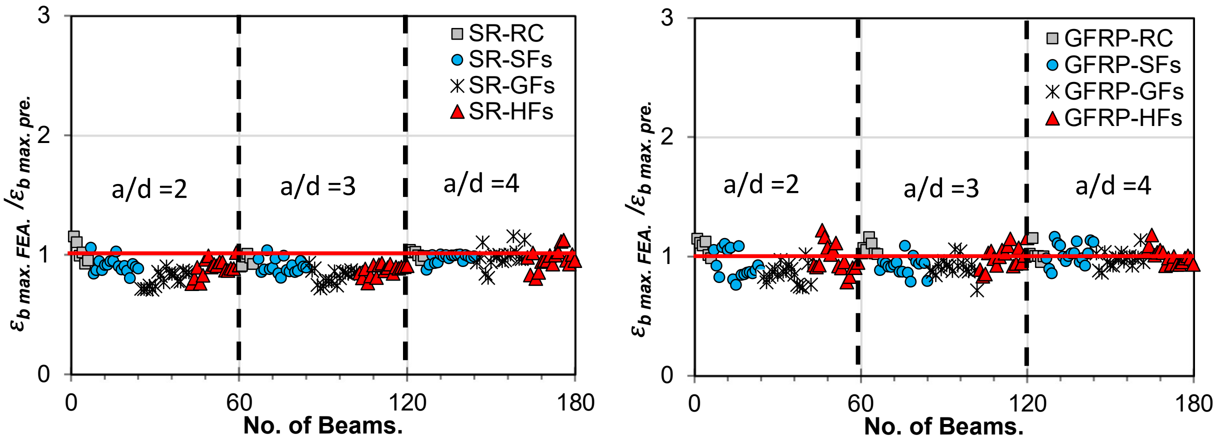

Figure 7-12: The ratio between the numerical and analytical reinforcement strain at service.

Table 7-6 : Summary of performance indicators for reinforcement's strain model for different *a/d* ratio.

Main Tension Rein.	SR				GFRP			
$\frac{\varepsilon_{b\ num.}}{\varepsilon_{b\ pre.}}$	*a/d*				*a/d*			
	All	**2**	**3**	**4**	**All**	**2**	**3**	**4**
Mean	0.91	0.88	0.88	0.98	0.96	0.94	0.95	1.00
SD	0.09	0.09	0.08	0.07	0.10	0.12	0.09	0.07
CoV	10%	11%	9%	7%	10%	13%	10%	7%

7.4.3 Experimental verification of analytical models

A literature review was completed with 73 tests related to shear- and flexure-critical FRC beams found to validate both shear and flexural analytical models. Test data that provided information on deflection, cracking moments, and reinforcement strain could not be found for beams reinforced with fibres, so serviceability models could not be experimentally validated. Future testing should report these values to allow better validation and model development in future.

7.4.4 Experimental flexural strength model validation

A dataset consisting of 25 critical flexural beams, comprising 23 Steel-RC beams with steel fibres and 3 GFRP-RC beams with fibres, was examined, as described in Table **7-7** and visualized in Figure 7-13 (a). Beams have variations in parameters, including f_c' (22-55 MPa), V_f (0.38-1.5%), ρ (0.2-2.5%), *a/d* (2.6-6.6), h (150-400 mm), and b (120-225 mm). The outcomes of the ratio $\frac{M_{fib\ exp.}}{M_{fib\ pre.}}$ show a mean of 1.06 and a CoV of 6%, which indicate that the flexural analytical expressions can predict response fairly accurately, though tests with GFRP-RC and fibres that are not steel were very limited.

Table 7-7: Experimental database validation of the analytical flexural strength model

Reference	*Beam ID*	**Main Rein.**	*Fibre*	V_f,%	*a/d*	f'_c, MPa	ρ, %	h, mm	b, mm	d, mm	M_{fib} exp (kNm)	M_{fib} pre. (kN\)	M_{fib} exp./ M_{fib} pre.
A. Meda et al, 2012	2 φ 16-B-30	SR	SF	0.38	4.6	45	0.8	300	200	260	54	58	1.07
	4 φ 16-B-30	SR	SF	0.38	4.6	45	1.5	300	200	260	100	105	1.05
	3 φ 16-B-30	SR	SF	0.75	4.6	45	0.8	300	200	260	56	58	1.03
Sahoo, et al, 2015	SFRC-1	SR	SF	0.5	3.8	37	1.4	200	150	160	30	32	1.07
	SFRC-2	SR	SF	1.0	3.8	37	1.4	200	150	160	30	33	1.09
Folino, et al.,2020	layout-1-FRC40	SR	SF	0.5	2.6	35	0.7	300	120	268	29	34	1.17
	layout-1-FRC60	SR	SF	0.76	2.6	32	0.7	300	120	268	30	36	1.20
	layout-2-FRC40	SR	SF	0.5	2.6	35	1.4	300	120	268	54	59	1.09
	layout-2-FRC60	SR	SF	0.76	2.6	32	1.4	300	120	268	54	59	1.08
Sahoo and Kumar, 2015	SFRC100	SR	SF	1.0	3.8	33	1.0	400	225	359	173	175	1.01
	SFRC125	SR	SF	1.25	3.8	34	1.0	400	225	359	176	180	1.03
	SFRC150	SR	SF	1.5	3.8	35	1.0	400	225	359	179	175	0.98
Mertol et al, 2015	SFRC0.2	SR	SF	1.0	6.7	35	0.2	250	180	210	13	13	1.05
	SFRC0.3	SR	SF	1.0	6.7	41	0.3	250	180	210	16	15	0.96
	SFRC0.4	SR	SF	1.0	6.7	31	0.4	250	180	210	19	19	1.02
	SFRC0.53	SR	SF	1.0	6.7	42	0.5	250	180	210	24	24	1.02
	SFRC0.81	SR	SF	1.0	6.7	30	0.8	250	180	210	32	33	1.02
	SFRC1.06	SR	SF	1.0	6.7	44	1.1	250	180	210	42	43	1.03
	SFRC1.6	SR	SF	1.0	6.7	32	1.6	250	180	210	58	58	1.00
	SFRC2.2	SR	SF	1.0	6.7	25	2.0	250	180	210	70	68	0.98
	SFRC2.13	SR	SF	1.0	6.7	32	2.1	250	180	210	74	70	0.94
	SFRC2.5	SR	SF	1.0	6.7	22	2.5	250	180	210	84	76	0.90
Issa et al, 2011	NG	GFRP	GF	0.5	4.2	33	1.8	150	150	125	14	15	1.04
	HG	GFRP	GF	0.5	4.2	55	1.8	150	150	125	15	17	1.07
	NS	GFRP	SF	0.5	4.2	28	1.8	150	150	125	15	16	1.09
												Mean	**1.04**
												CoV	**6%**

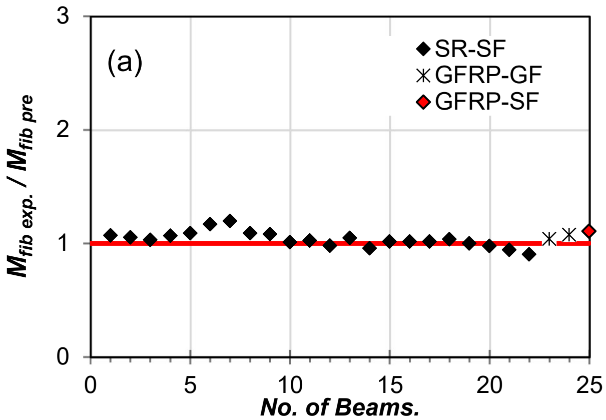

Figure 7-13: The ratio between the experimental and analytical (a) moment resistance and (b) shear strength

7.4.5 Experimental shear strength model validation

From the literature, 48 shear-critical Steel-RC beams with steel fibres were analyzed. Different boundary conditions, such as three and four-point loads, were used, and variations in parameters include f_c' (28.7-50.8), *a/d* (2.1-3.4), ρ (1.12-2.78), V_f (0.3-2.0)%, *h* (250-1500 mm), and *b* (150-300 mm), as in Table **7-8**. The available data on RC-FRC exhibits limitations, with a notable focus on GF and the utilization of FRP bars. The analytical shear model was validated using this dataset, and the findings indicate that the model offers a reasonably accurate prediction of shear strength for RC-FRC members, as shown in Figure 7-13(b). This conclusion is supported by the mean and CoV values of $\frac{Vu.exp.}{Vu.pre.}$, which are 1.07 and 19.7%, respectively. The findings are to those from FEA (mean values ranging from 0.95 to 1.13 and CoV below 20%) for both Steel-RC and GFRP-RC beams. The CoV being around 20% is comparable to the better shear analytical models studied for concrete without fibres by Alguhi and Tomlinson (2021).

Table 7-8: Experimental database validation of the analytical shear strength model

Ref.	Beam ID	Stirrups	a/d	ρ (%)	fc' (MPa)	Vf (%)	h (mm)	b (mm)	d (mm)	Vu exp. (kN)	Vu pre. (kN)	Vu exp. /Vu pre.
Minelli and Conforti, 2014	H500 FRC50	No	3.0	1.12	32.1	0.7	500	250	440	153	240	1.57
	H500 FRC75	No	3.0	1.12	33.1	1.0	500	250	440	169	235	1.39
	H1000 FRC50	No	3.0	1.07	32.1	0.7	1000	250	940	282	272	0.97

	H1000 FRC75	No	3.0	1.07	33.1	1.0	1000	250	940	314	351	1.12
	H1500 FRC50	No	3.0	1.01	32.1	0.7	1500	250	1440	389	484	1.25
	H1500 FRC75	No	3.0	1.01	33.1	1.0	1500	250	1440	437	554	1.27
Hameed and Al-Shaerrawi, 2018	B02-SF0.5SH	Yes	3.0	1.51	40.0	0.5	200	150	177	47	65	1.39
	B03-SF0.75SH	Yes	3.0	1.51	40.0	0.8	200	150	177	50	70	1.39
	B25-0-0-0	No	2.8	1.98	34.0	0.3	700	300	622	311	274	0.88
	B25-550-6-450	Yes	2.8	1.98	34.0	0.3	700	300	622	403	363	0.90
	B25-450-10-450	Yes	2.8	1.98	34.0	0.3	700	300	622	440	334	0.76
Amin and Foster, 2016	B25-400-6-300	Yes	2.8	1.98	46.0	0.3	700	300	622	467	322	0.69
	B25-300-10-300	Yes	2.8	1.98	46.0	0.3	700	300	622	479	357	0.75
	B50-0-0-0	No	2.8	1.98	36.0	0.6	700	300	622	362	344	0.95
	B25-550-6-450	Yes	2.8	1.98	36.0	0.6	700	300	622	453	462	1.02
	B25-450-10-450	Yes	2.8	1.98	36.0	0.6	700	300	622	479	535	1.12
	b18-1a	No	3.4	2.78	44.8	0.8	455	152	381	168	172	1.02
	b18-1b	No	3.4	2.78	44.8	0.8	455	152	381	168	162	0.96
	b18-2a	No	3.4	2.78	38.1	1.0	455	152	381	165	171	1.04
	b18-2b	No	3.5	2.78	38.1	1.0	455	152	381	164	174	1.06
	b18-3a	No	3.5	2.78	31.0	1.5	455	152	381	166	150	0.91
	b18-3b	No	3.5	2.78	31.0	1.5	455	152	381	166	198	1.19
	b18-3c	No	3.4	2.78	44.9	1.5	455	152	381	215	193	0.90
	b18-3d	No	3.4	2.78	44.9	1.5	455	152	381	215	191	0.89
	b18-5a	No	3.4	2.78	49.2	1.0	455	152	381	195	174	0.89
	b18-5b	No	3.4	2.78	49.2	1.0	455	152	381	195	220	1.13
Dinh et al, 2011	b18-7a	No	3.4	2.08	43.3	0.8	455	152	381	141	194	1.38
	b18-7b	No	3.4	2.08	43.3	0.8	455	152	381	141	191	1.35
	b27-1a	No	2.1	2.09	50.8	0.8	685	205	610	357	369	1.03
	b27-1b	No	2.1	2.09	50.8	0.8	685	205	610	357	341	0.96
	b27-2a	No	2.1	2.09	28.7	0.8	685	205	610	247	355	1.44
	b27-2b	No	2.1	2.09	28.7	0.8	685	205	610	247	348	1.41
	b27-3a	No	2.1	2.09	42.3	0.8	685	205	610	321	325	1.01
	b27-3b	No	2.1	1.61	42.3	0.8	685	205	610	276	351	1.27
	b27-4a	No	2.1	1.61	29.6	0.8	685	205	610	226	271	1.20
	b27-4b	No	2.1	1.61	29.6	0.8	685	205	610	226	228	1.01
	B27-5	No	2.1	2.09	44.4	1.5	685	205	610	420	438	1.04
	B27-6	No	2.1	2.09	42.8	1.5	685	205	610	412	424	1.03
	A10	No	2.8	1.91	40.9	1.0	250	150	219	89	110	1.24
	A20	No	2.8	1.91	43.2	2.0	250	150	219	116	118	1.02
	A11	Yes	2.8	1.91	40.8	1.0	250	150	219	128	114	0.89
	A12	Yes	2.8	1.91	40.8	1.0	250	150	219	205	132	0.64
Cucchiara et al, 2004	A21	Yes	2.8	1.91	43.9	2.0	250	150	219	150	140	0.93
	B10	No	2.1	1.91	40.9	1.0	250	150	219	99	131	1.33
	B20	No	2.1	1.91	43.2	2.0	250	150	219	130	132	1.02
	B11	Yes	2.1	1.91	40.8	1.0	250	150	219	141	138	0.98
	B12	Yes	2.1	1.91	40.8	1.0	250	150	219	217	179	0.82
	B21	Yes	2.1	1.91	43.9	2.0	250	150	219	167	198	1.18
											Mean	**1.07**
											CoV	**19.7%**

7.5 General Discussion

The provided findings revolve around the comparison of analytical expressions for flexural strength, shear strength, service deformations, and service reinforcement strains with FEA data across various conditions. In terms of flexural strength, the analytical model gives similar predictions to FEA across different *a/d* ratios. Conversely, for shear strength, the analytical model performance varies with *a/d* ratios, showing results comparable with FEA for *a/d* > 2.5. When *a/d* ≤ 2.5 and plane section assumptions no longer apply, models relying on sectional analysis like the presented analytical model tend to underestimate the precise solution (Collins and Mitchell, 1997). In future, exploration of other design approaches, such as strut-and-tie method, are encouraged to develop more effective design methods for beams with *a/d* ≤ 2.5.

Regarding deflection, the analytical model exhibits a tendency toward underprediction results may due to the FEA perfections, and it is advisable to take steps to minimize this overestimation. One of step is to use higher-order elements, which may reduce (though not eliminate). Another effective approach is the adoption of specialized elements that incorporate Timoshenko beam functions into displacement shape functions, which can greatly mitigate the higher stiffness results in FEA. However, the performance of deflection model leads to closer agreements between model estimations when *a/d* ratios exceed 2.5. Concerning reinforcement strain prediction, the analytical model reasonably matches with FEA results, showing slight improvements at larger *a/d* ratios.

As a whole, the simplified compression and tension model, which incorporates stress block parameters, successfully captures the influence of fibres in RC beams and may reduce the need for FEA for beams like those considered. The presented analytical models consider the additional stiffness and strength from fibres. Of particular benefit is that the model can seamlessly integrate into sectional analysis approaches typically used in design by introducing new force contributions from fibres. This approach provides an effective means to address challenges associated with evaluating the ultimate and serviceability responses of FRC members.

The developed constitutive model by (Alguhi and Tomlinson, 2023) for FRC-RC effectively represents both SF and GF, verified against test data, although literature data for some investigated parameters is sparse. The use of SF and GF enhances the strength of SR-RC and GFRP-RC beams

(Chapter 5). The optimal performance is achieved with a 50% combination of both SF and GF, capitalizing on the compatibility between the larger stiffness of SF and the superior deformability of GF (Alguhi and Tomlinson, 2023).

At SLS, fibres increase the post-cracking stiffness of RC members which may mitigate concerns such as excessive deflection and crack width. Fibres had a consistent impact on each of these factors. The inclusion of fibres led to a reduction in crack width, deflections, and reinforcement strain in all beams under consideration. The most significant improvements were observed in GFRP-RC beams, as fibres bear a larger proportion of the load compared to steel-RC members with stiffer reinforcement (see section 5.7).

This study has certain limitations as it focuses on the inclusion of fibres in normal to medium compressive strength concrete with a strain-softening response and does not consider high to ultra-high compressive strengths with a strain-hardening response. Additionally, the study assumes that the fibres are uniformly distributed and does not account for details such as flow direction which can affect performance (Mailyan et al., 2021). The considered beams have *a/d* ratios between 2 and 4, with insight into how analytical methods address *a/d* = 2, which creates a disturbed (plane sections not plane) region. Further research is needed to study the D-regions with *a/d* ratios of less than 2 and develop appropriate design methods for FRC in these conditions. Limited experimental data was available for validating the analytical model, particularly for GFRP-RC and members with fibre types beyond steel so tests on these types of members are recommended to confirm if analytical expressions presented here can apply in those cases.

7.6 Consultation and Recommendation

The research used a numerical database of 720 beams, covering SR-RC, GFRP-RC, SR-FRC, and GFRP-FRC beams with various parameters, to formulate design-oriented expressions for assessing strength (flexure and shear) and serviceability (deflections and reinforcement strain). Expressions consider FRC's compression and tensile contribution on member response based on first principles (equilibrium, strain compatibility) expressions. The following was concluded:

1. The flexural strength analytical model incorporated fibre influences using a stress block approach for both compression and tension. Results were compared to FEA on the same beams along with 25 tests from literature. The model demonstrated conservative and consistent results when compared with tests for all *a/d* ratios, indicating its capability to predict moment capacity.
2. The analytical shear model's evaluation, conducted on SR-FRC and GFRP-FRC beams, demonstrated reasonable match in predicting shear strength from FEA. Matching was particularly strong for SR-FRC and GFRP-FRC beams with a/d > 2.0. The model showcased its utility in predicting shear strength within this range. This model also showed somewhat conservative results, with a mean of 1.07 and CoV of 19.7% when compared to 48 shear critical tests.
3. The effective moment of inertia for FRC is derived using an iterative process involving. The study also addresses factors affecting the cracking moment, including fibre type, dosage, and section properties. Equations for predicting cracking moment are derived from experimental data and show good accuracy. Despite overprediction due to shear looking phenomenon, FEA and analytical models show similar estimates for deflection in beams with *a/d* > 2.0, especially for *a/d* = 4.
4. The analytical model predicts reinforcement strain with results similar to FEA. The predicted strain shows improved performance when *a/d* is set to 3 or 4 compared to *a/d*

equal to 2. The methodology presented here contributes to a better understanding of the behaviour of FRC structures and their design considerations for serviceability.

The scope of this study focused on beams subject to static point loads. Only instantaneous responses were considered (i.e., effects of creep/shrinkage not considered). The tension softening response associated with normal to medium strength concrete was considered (i.e., strain hardening responses were not considered).

Several recommendations can be made to enhance the understanding and application of FRC in structural engineering. Further exploration of different fibre types and dosages are recommended to better understand their effects on FRC mechanical properties, covering aspects like flexural and shear strength, deflection, and reinforcement strain. Future studies should report SLS test data including cracking moment, deflections at key points (e.g., span/360), as well as reinforcement strain, to assist with developing and validating SLS design provisions. There is also a need to develop analytical models' systems where fibres create a strain-hardening response.

CHAPTER 8

SUMMARY AND CONCLUSIONS

8.1 Summary

The comprehensive study involved ten mixtures exploring the influence of fiber type (SF, GF, and/or a combination), aspect ratios (55 for SF and 67 for GF) and dosage (0.5, 1.0, and 1.5% by a volume of friction), on fresh concrete properties, including workability and densities. This investigation extended to the compressive response parameters of FRC mixtures, proposing a simplified design model for the stress-strain relation in FRC. The effect of these fibres on crack, flexural response, and split tensile strength in NSC mixtures was examined, utilizing inverse analysis to generate tensile stress-strain data for FRC. FEA modeled 720 beams, covering different reinforcement types and dosage combinations, assessing SLS and ULS parameters. Additionally, fourteen design provisions for one-way shear strength of FRP-RC members without stirrups were presented and compared against a database of 147 beams from the literature. Leveraging a numerical database of 720 beams, the research formulated design-oriented expressions of FRC-RC considering compression and tensile contributions of FRC on member response, grounded in first principles of equilibrium and strain compatibility.

8.2 Conclusions

8.2.1 Experimental Phase

Conclusions drawn from the experimental phases of this study on serviceability and ultimate performance of SF chopped GF flexural members are as follows:

- The addition of fibres, especially GF, significantly diminishes workability, impacting slump values; hybrid mixtures further reveal a consistent trend of decreasing workability with escalating GF dosage.
- A strong correlation is established between slump and Ve-Be time, underscoring the suitability of the Ve-Be time test for assessing workability, especially in stiffer concretes like FRC.
- Concrete density in FRC is notably affected by the specific gravity and dosage of chopped fibres. While steel fibres increase density, glass fibres have a minor impact, allowing for conservative neglect in member self-weight considerations.
- Both SF and GF contribute to heightened compressive strength, strain characteristics, and toughness indices.
- Fibre addition positively influences mechanical properties, showcasing improved flexural and splitting tensile strengths.
- Hybrid mixtures exhibit superior compressive strength and toughness with an increasing proportion of steel fibres. These mixtures reveal nuanced effects, suggesting a balance between stiff and deformable fibres for optimal performance.
- Fibre addition enhances FRC peak load, residual loads, and fracture energy, with hybrid mixtures demonstrating unique characteristics. Distinct failure mechanisms emerge, with SF mixtures experiencing debonding and GF mixtures exhibiting fibre tearing.
- DIC and LVDT responses align effectively, facilitating comprehensive crack analysis.

8.2.2 Analytical phase

8.2.2.1 Numerical analysis

- The successful implementation of inverse analysis in VecTor2® establishes its efficacy in determining the tensile σ-ε relationship of FRC beams.
- Substantial increases in beam strength and ductility are observed with higher SF percentages, particularly in simply supported beams with varying concrete strengths.
- Models employing VecTor2 consistently predict responses of large-scale beams in alignment with test results, irrespective of the presence of fibres or reinforcement type. The developed constitutive model for FRC-RC effectively captures the behavior of both SF and GF, demonstrating strong through validation against available test data.
- Incorporating SF and GF in beams enhances strength, with the 50% combination of both fibres proving optimal. This combination leverages the compatibility between SF stiffness and GF deformability, showcasing superior performance beyond individual fibre use.
- Adding fibres, mainly SF, induces a shift in failure modes from shear to flexural, with SF effectively replacing minimum stirrups. The transformative shift from shear diagonal failure to flexural failure was coupled with a significant reduction in crack width.
- Serviceability parameters, including crack width, deflections, and reinforcement strain, exhibit consistent improvements with fibre inclusion. GFRP-RC beams, in particular, demonstrate significant enhancements, emphasizing the positive impact of fibres on serviceability.

8.2.2.2 *Design relationships and comparisons*

- The proposed compressive design stress-strain relationships provide a dependable framework essential for precise hand calculations in FRC designs.
- The analytical tensile stress-strain model derived from Inverse Analysis aligns effectively with FE results, presenting a practical tool for structural evaluation.
- The analytical flexural model, incorporating fibre influences, demonstrates conservative and consistent outcomes across various *a/d*. This underscores its reliability in predicting moment capacity.
- The analytical shear model exhibits reasonable accuracy in predicting shear strength for SR-FRC and GFRP-FRC beams, especially for *a/d* > 2.0, contributing valuable insights for shear strength prediction.
- The derivation of effective moment of inertia for FRC, considering factors like fibre type, dosage, and section properties, results in equations predicting cracking moment with good accuracy. Despite overprediction due to the FEA perfection, both FEA and analytical models provide similar estimates for deflection, particularly for *a/d* = 4.
- The analytical model successfully predicts reinforcement strain, showcasing improved performance for *a/d* set to 3 or 4 compared to *a/d* equal to 2. This methodology enhances our understanding of FRC structures, contributing essential insights for serviceability considerations in design.

8.3 Recommendations

- Investigate the influence of maximum aggregate size and shape on fresh concrete properties and densities of (SF and/or GF) RC beyond the 20 mm gravel used in this study.

- Further explore the impact of geometric properties of chopped fibres, including aspect ratio and fibre profile (e.g., straight, hooked), as well as the introduction of other fibre types (e.g., basalt, polypropylene) on concrete's fresh properties.
- Investigate different combinations of fibres beyond SF and GF to assess their influence on compressive response. Evaluate the effects on structures incorporating double-hooked SF and GF in normal to medium strength concrete.
- Study different combinations and geometric properties of fibres, such as aspect ratio and fibre profile, including straight and crimped varieties. Extend the analysis to include other fibre types like basalt and polypropylene to understand their impact on crack behavior and flexural response.
- Investigate the mechanical properties, workability, and construction cost implications of mixtures incorporating both SFs and GF. Assess the effects of replacing more than half of SF with GF, considering factors beyond mechanical properties.
- Explore other fibre types beyond SF and GF, examining various fibre profiles. Study different concrete types, including high-strength concrete, and include other FRP-FRC materials like carbon and basalt fibres in constitutive models.
- Research and implement new approaches, such as the Genetic Programming approach via Artificial Neural Networks (ANNs), for predicting the shear strength of FRP-RC elements. Consider parameters not commonly reported, such as aggregate size and concrete modulus of elasticity.
- Encourage experimental studies to report parameters that affect shear resistance but are often not reported, such as aggregate size, concrete modulus of elasticity, and material properties for FRP reinforcement.

- Explore the impact of reinforcement layout and support conditions (e.g., fixed-fixed rather than simply supported) on shear resistance, considering factors with limited available data.
- Develop analytical model systems where FRC creates a strain-hardening response, enhancing understanding and applicability in structural engineering.

REFERENCES

Abdallah, S., Fan, M., and Rees, D. W. A. (2016). Analysis and modelling of mechanical anchorage of 4D/5D hooked end steel fibres. Materials and Design, 112, 539–552. https://doi.org/10.1016/j.matdes.2016.09.107

Abdelrazik, A. T., and Khayat, K. H. (2020). Effect of fiber characteristics on fresh properties of fiber-reinforced concrete with adapted rheology. Construction and Building Materials, 230, 116852. https://doi.org/10.1016/j.conbuildmat.2019.116852

Abousnina, R., Premasiri, S., Anise, V., Lokuge, W., Vimonsatit, V., Ferdous, W., and Alajarmeh, O. (2021). Mechanical properties of macro polypropylene fibre-reinforced concrete. Polymers, 13(23), 1–25. https://doi.org/10.3390/polym13234112

Abrishami, H. H., and Mitchell, D. (1997). Influence of Steel Fibers on Tension Stiffening.

ACI (2010). "Report on High-Strength Concrete (ACI 363R-10)." American Concrete Institute. Farmington Hills, MI.

ACI 318-19 (2019) "Building Code Requirements for Structural Concrete (ACI 318-19): An ACI Standard: Commentary on Building Code Requirements for Structural Concrete (ACI 318R-19)." American Concrete Institute.

ACI 440.1 R-15 (2015) "Guide for the Design and Construction of structural concrete reinforced with Fiber Reinforced Polymer (FRP) bars" American Concrete Institute. Farmington Hills, MI.

ACI 544.4R-18. (2018). 544.4R-18: Guide to Design with Fiber-Reinforced Concrete. In Aci 544.4R-18.

ACI Committee 440., and Committee, A. (2015). Guide for the Design and Construction of Structural Concrete Reinforced with FRP Bars. In Aci 440.1R-15. American Concrete Institute. https://doi.org/10.1061/40753(171)158

ACI-318-19. (2019). Building Code Requirements Available for Public Review (ACI 318-19).

ACI-544-16. (2016). Report on Indirect Method to Obtain Stress-Strain Response of Fiber-Reinforced Concrete (FRC).

Ahmad, H., Elnemr, A., Ali, N., Hussain, Q., Chaiyasarn, K., and Joyklad, P. (2021). Finite element analysis of glass fiber-reinforced polymer-(Gfrp) reinforced continuous concrete beams. Polymers, 13(24). https://doi.org/10.3390/polym13244468

Aidarov, S., Nadaždi, A., Pugach, E., Tošić, N., and de la Fuente, A. (2022). Cost-oriented analysis of fibre reinforced concrete column-supported flat slabs construction. Journal of Building Engineering, 51. https://doi.org/10.1016/j.jobe.2022.104205

Alam, M., and Hussein, A. (2013). "Size effect on shear strength of FRP reinforced concrete beams without stirrups." Journal of Composites for Construction, 17(4), 507-516.

Alguhi, H. A., and Elsaigh, W. A. (2016). Development of tensile stress-strain relationship for high-strength steel fiber reinforced concrete. International Journal of Civil Engineering and Environmental Engineering, 10(2), 190–196.

Alguhi, H., and Tomlinson, D. (2019). Evaluation of steel fibre reinforced concrete beams under ultimate and serviceability limit states. Proceedings, Annual Conference - Canadian Society for Civil Engineering, 2019-June (Vandewalle 2000), 1–10.

Alguhi, H., and Tomlinson, D. (2021). One-Way Shear Strength of FRP–Reinforced Concrete Members Without Stirrups: Design Provision Review. Journal of Composites for Construction, 25(3), 04021016. https://doi.org/10.1061/(asce)cc.1943-5614.0001125

Alguhi, H., and Tomlinson, D. (2022). Chopped Fibre Dosage and Material Effects on the Fresh Properties of Normal Strength and Density Concrete. 1–9. https://www.researchgate.net/publication/360504694

Alguhi, H., and Tomlinson, D. (2023). Crack behaviour and flexural response of steel and chopped glass fibre-reinforced concrete: Experimental and analytical study. Journal of Building Engineering, 75. https://doi.org/10.1016/j.jobe.2023.106914

Alkhrdaji, T., Wideman, M., Belarbi, A., and Nanni, A. (2001). "Shear strength of GFRP RC beams and slabs." Proceedings of the international conference, composites in construction-CCC, 409-414.

Almusallam, T., Ibrahim, S. M., Al-Salloum, Y., Abadel, A., and Abbas, H. (2016). Analytical and experimental investigations on the fracture behavior of hybrid fiber reinforced concrete. Cement and Concrete Composites, 74, 201–217. https://doi.org/10.1016/j.cemconcomp.2016.10.002

Alsayed, S. H. (1993). Flexural Deflection of Reinforced Fibrous Concrete Beams.

Alshaarbaf, I. A. S., Mouwainea, E. M., and Said, A. M. I. (2023). Numerical analysis of reinforced concrete beams subjected to impact loads. Journal of the Mechanical Behavior of Materials, 32(1). https://doi.org/10.1515/jmbm-2022-0232

Altun, F., Haktanir, T. and Ari, K. (2007). Effects of steel fiber addition on mechanical properties of concrete and RC beams. Construction and Building Materials, 21(3), 654–661. https://doi.org/10.1016/J.CONBUILDMAT.2005.12.006

Altun, F., Haktanir, T., and Ari, K. (2007). Effects of steel fiber addition on mechanical properties of concrete and RC beams. Construction and Building Materials, 21(3), 654–661. https://doi.org/10.1016/J.CONBUILDMAT.2005.12.006

Amin, A., and Foster, S. J. (2016). Shear strength of steel fibre reinforced concrete beams with stirrups. Engineering Structures, 111, 323–332. https://doi.org/10.1016/j.engstruct.2015.12.026

Arslan, M. E. (2016). Effect of basalt fibers on fracture energy and mechanical properties of HSC. Computers and Concrete, 17(4), 553–566. https://doi.org/10.12989/cac.2016.17.4.553

ASCE–ACI Joint Task Committee 426 (1973) "The shear strength of reinforced concrete members." ASCE Proceedings, 1091-1187.

ASCE-ACI-426-73. (1973). ASCE-ACI Committee 426 on Shear and Diagonal Tension of the Committee on Masonry and Reinforced Concrete of the Structural Division.

Ashour, A. (2006). "Flexural and shear capacities of concrete beams reinforced with GFRP bars." Construction and Building Materials, 20(10), 1005-1015.

Ashour, A. F., and Kara, I. F. (2014). "Size effect on shear strength of FRP reinforced concrete beams." Composites Part B: Engineering, 60, 612-620.

Ashour, S. A., Hasanain, G. S., and Wafa, F. F. (1992). Shear behavior of high-strength fiber reinforced concrete beams. Structural Journal, 89(2), 176–184.

ASTM C150. (2000). Standard Specification for Ferrosilicon. Practice, 93(Reapproved), 2–6. https://doi.org/10.1520/C0150

ASTM C1609/C1609M-10. (2010). Standerd Test Method for Flexural Performance of Fiber-Reinforced Concrete (Using Beam With Third-Point Loading).

ASTM C39 / C39M-05a. (2005). Standard Test Method for Bulk Density ("Unit Weight") and Voids in Aggregate, ASTM International, West Conshohocken, PA,. Annual Book of ASTM Standards, C, 1–7.

ASTM C39/C39M − 17b. (2017). Standard Test Method for Compressive Strength of Cylindrical Concrete Specimens. i, 1–7. https://doi.org/10.1520/C0039

ASTM C469/C469M. (2014). Standard Test Method for Static Modulus of Elasticity and Poisson's Ratio of Concrete in Compression. ASTM Standard Book, 1–5. https://doi.org/10.1520/C0469

ASTM C469-11. (2008). Standard Test Method for Splitting Tensile Strength of Cylindrical Concrete Specimens. Manual on Hydrocarbon Analysis, 6th Edition, i, 545-545–3. https://doi.org/10.1520/C0496

ASTM-C 618-15. (2015). Standard Specification for Coal Fly Ash and Raw or Calcined Natural Pozzolan for Use as a Mineral Admixture in Concrete (ASTM C618-15). ASTM International, 1–4. https://doi.org/10.1520/C0618-15.2

ASTM-C 618-15. (2015). Standard Specification for Coal Fly Ash and Raw or Calcined Natural Pozzolan for Use as a Mineral Admixture in Concrete (ASTM C618-15). ASTM International, 1–4. https://doi.org/10.1520/C0618-15.2

Ayub, T., Khan, S. U., and Shafiq, N. (2018). Flexural modelling and finite element analysis of frc beams reinforced with PVA and basalt fibres and their validation. Advances in Civil Engineering, 2018. https://doi.org/10.1155/2018/8060852

Babaie, R., Abolfazli, M., and Fahimifar, A. (2020). Mechanical properties of steel and polymer fiber reinforced concrete. Journal of the Mechanical Behavior of Materials, 28(1), 119–134. https://doi.org/10.1515/jmbm-2019-0014

Banthia, N., and Sappakittipakorn, M. (2007). Toughness enhancement in steel fiber reinforced concrete through fiber hybridization. Cement and Concrete Research, 37(9), 1366–1372. https://doi.org/10.1016/j.cemconres.2007.05.005

Barris, C., Torres, L., Vilanova, I., Mias, C., and Llorens, M. (2017). "Experimental study on crack width and crack spacing for Glass-FRP reinforced concrete beams." Engineering Structures, 131, 231-242.

Barros, J. A. O., and Figueiras, J. A. (2001). Model for the analysis of steel fibre reinforced concrete slabs on grade. Computers and Structures, 79(1), 97–106.

Barros, J., Taheri, M., and Salehian, H. (2017). A Model to Predict the Crack Width of FRC Members Reinforced with Longitudinal Bars. ACI Symposium Publication, 319. https://doi.org/10.14359/51700851

Bažant, Z. P. (1984). Size Effect in Blunt Fracture: Concrete, Rock, Metal. Journal of Engineering Mechanics, 110(4), 518–535. https://doi.org/10.1061/(asce)0733-9399(1984)110:4(518)

Behbahani, H., Behbahani, H. P., Nematollahi, B., and Farasatpour, M. (2011). Steel Fiber Reinforced Concrete: A Review. https://www.researchgate.net/publication/266174465

Bencardino, F., Rizzuti, L., Spadea, G., and Swamy, R. N. (2008). Stress-Strain Behavior of Steel Fiber-Reinforced Concrete in Compression. Journal of Materials in Civil Engineering, 20(3), 255–263. https://doi.org/10.1061/(asce)0899-1561(2008)20:3(255)

Bentz, E. C., and Collins, M. P. (2006). Development of the 2004 Canadian Standards Association (CSA) A23.3 shear provisions for reinforced concrete. Canadian Journal of Civil Engineering, 33(5), 521–534. https://doi.org/10.1139/L06-005

Bentz, E. C., and Collins, M. P. (2017). "Updating the ACI shear design provisions." Concrete International, 39(9), 33-38.

Bentz, E. C., Massam, L., and Collins, M. P. (2010). "Shear strength of large concrete members with FRP reinforcement." Journal of Composites for Construction, 14(6), 637-646.

Bentz, E. C., Vecchio, F. J., and Collins, M. P. (2006). "Simplified modified compression field theory for calculating shear strength of reinforced concrete elements." ACI Materials Journal, 103(4), 614.

Bernardi, P., Michelini, E., Minelli, F., and Tiberti, G. (2016). Experimental and numerical study on cracking process in RC and R/FRC ties. Materials and Structures/Materiaux et Constructions, 49(1–2), 261–277. https://doi.org/10.1617/s11527-014-0494-1

Betschoga, C., Tung, N. D., and Tue, N. V. (2021). Investigations on the influence of boundary and loading conditions on the shear resistance of FRP concrete beams without shear reinforcement. Composite Structures, 262(October), 113335. https://doi.org/10.1016/j.compstruct.2020.113335

Bischoff, P. H. (2007). Deflection Calculation Using an Effective Moment Inertia for FRC.

Bischoff, P. H., and Gross, S. P. (2011). Equivalent Moment of Inertia Based on Integration of Curvature. Journal of Composites for Construction, 15(3), 263–273. https://doi.org/10.1061/(asce)cc.1943-5614.0000164

BISE (1999). "Interim guidance on the design of reinforced concrete structures using fiber composite reinforcement." IStructE, SETO London.

Blazejowski, M. (2012). Flexural Behaviour of Steel Fibre Reinforced Concrete Tunnel Linings. 167. https://ir.lib.uwo.ca/etd/768

Branston, J., Das, S., Kenno, S. Y. and Taylor, C. (2016). Mechanical behaviour of basalt fibre reinforced concrete. Construction and Building Materials, 124, 878–886. https://doi.org/10.1016/j.conbuildmat.2016.08.009

Brigante, D. (2014). New composite materials, Springer.

Campopiano, A., Ramires, D., Zakrzewska, A. M., Ferri, R., D'Annibale, A., and Pizzutelli, G. (2009). Risk assessment of the decay of asbestos cement roofs. Annals of Occupational Hygiene, 53(6), 627–638. https://doi.org/10.1093/annhyg/mep036

CAN/CSA-A3000-13. (2013). CAN/CSA-A3000-13 | Product | CSA Group.

Canadian Standards Association (2002). "CSA S806-02, Design and Construction of Building Components with Fibre-Reinforced Polymers." Mississauga, ON, Canada.

Canadian Standards Association (2012). "CSA S806-12, Design and construction of building structures with fibre-reinforced polymers." Mississauga, ON, Canada.

Canadian Standards Association (2019). "CSA S6:19, Canadian Highway Bridge Design Code." Mississauga, ON, Canada.

Carmona, J. R., Cortés-Buitrago, R., Rey-Rey, J., and Ruiz, G. (2022). Planar Crack Approach to Evaluate the Flexural Strength of Fiber-Reinforced Concrete Sections. Materials, 15(17). https://doi.org/10.3390/ma15175821

Carrillo, J., Ramirez, J. and Lizarazo-Marriaga, J. (2019). Modulus of elasticity and Poisson's ratio of fiber-reinforced concrete in Colombia from ultrasonic pulse velocities. Journal of Building Engineering, 23(December 2018), 18–26. https://doi.org/10.1016/j.jobe.2019.01.016

Carroll, J. C., and Helminger, N. (2016). Fresh and Hardened Properties of Fiber-Reinforced Rubber Concrete. Journal of Materials in Civil Engineering, 28(7), 04016027. https://doi.org/10.1061/(asce)mt.1943-5533.0001541

Chao, S.-H., Ranjan Sahoo, D., and Yazdani, N. (2016). FRC PERFORMANCE COMPARISON: UNIAXIAL DIRECT TENSILE TEST, THIRD-POINT BENDING TEST, AND ROUND

PANEL TEST. American Concrete Institute. https://www.researchgate.net/publication/260322458

Chasioti, S. G. and Vecchio, F. J. (2017). Effect of fiber hybridization on basic mechanical properties of concrete. ACI Structural Journal, 114(3), 375–384. https://doi.org/10.14359/51689479

Choi, K.-K., Kim, J.-C., and Park, H.-G. (2016). "Shear strength model of concrete beams based on compression zone failure mechanism." ACI Structural Journal, 113(5), 1095.

Choi, Y., and Yuan, R. L. (2005). Experimental relationship between splitting tensile strength and compressive strength of GFRC and PFRC. Cement and Concrete Research, 35(8), 1587–1591. https://doi.org/10.1016/j.cemconres.2004.09.010

Chu, S. H., Li, L. G., and Kwan, A. K. H. (2018). Fibre factors governing the fresh and hardened properties of steel FRC. Construction and Building Materials, 186, 1228–1238. https://doi.org/10.1016/j.conbuildmat.2018.08.047

Cladera, A., Marí, A., Bairán, J. M., Ribas, C., Oller, E., and Duarte, N. (2016). "The compression chord capacity model for the shear design and assessment of reinforced and prestressed concrete beams." Structural concrete, 17(6), 1017-1032.

Cladera, A., Marí, A., Bairán, J.-M., Oller, E., and Ribas, C. (2017). "One-way shear design method based on a multi-action model." Concrete International, 39(9), 40-46.

CNR-DT 203/2006 (2006). "Guide for the design and construction of concrete structures reinforced with fiber-reinforced polymer bars." CNR-DT 203/2006, Italian National Research Council.

Collins, M. P., and Mitchell, D. M. (1997). prestressed concrete structures.

Collins, M. P., Bentz, E. C., Sherwood, E. G., and Xie, L. (2007). University of Cambridge 23 rd.

Concrete International (2017). "Design and Management Technologies." Concrete International, Concrete International, Farmington Hills,USA

CSA A23.3:19. (2019). Design of concrete structures.

CSA S806-12. (2012). Design and Construction of Building structures with Fibre-Reinforced Polymer, CAN/CSA S806-12. In Canadian Standards Association (Issue reaffirmed 2017).

Cuenca, E., Conforti, A., Minelli, F., Plizzari, G. A., Navarro Gregori, J., and Serna, P. (2018). A material-performance-based database for FRC and RC elements under shear loading. Materials and Structures/Materiaux et Constructions, 51(1). https://doi.org/10.1617/s11527-017-1130-7

D'Antino, T. and Pisani, M. A. (2019). Durability of glass FRP reinforcing bars: A state of the art. IABSE Symposium, Guimaraes 2019: Towards a Resilient Built Environment Risk and Asset Management - Report, 611–618.

Dinh, H. H., Parra-Montesinos, G. J., and Wight, J. K. (2011). Shear Strength Model for Steel Fiber Reinforced Concrete Beams without Stirrup Reinforcement. Journal of Structural Engineering, 137(10), 1039–1051. https://doi.org/10.1061/(asce)st.1943-541x.0000362

Domingo, M., Ramos, G., and Aparicio, Á. C. (2023). Use of fiber reinforced concrete in bridges – Metrorrey Line 2 case study. Engineering Structures, 276. https://doi.org/10.1016/j.engstruct.2022.115373

Edvardsen, C. (2010). THE CONSULTANT'S VIEW ON SERVICE LIFE DESIGN. 2nd International Symposium on Service Life Design for Infrastructure .

Elakhras, A. A., Seleem, M. H., and Sallam, H. E. M. (2022). Real fracture toughness of FRC and FGC: size and boundary effects. Archives of Civil and Mechanical Engineering, 22(2). https://doi.org/10.1007/s43452-022-00424-6

Elbahy, Y. I., Youssef, M. A. and Nehdi, M. (2009). Stress block parameters for concrete flexural members reinforced with superelastic shape memory alloys. Materials and Structures/Materiaux et Constructions, 42(10), 1335–1351. https://doi.org/10.1617/s11527-008-9453-z

El-Fitiany, S. F. and Youssef, M. A. (2011). Stress-block parameters for reinforced concrete beams during fire events. American Concrete Institute, ACI Special Publication, 279 SP, 1–39. https://doi.org/10.14359/51682964

Elsaigh, W. A., Robberts, J. M., and Kearsley, E. P. (2012). Modeling the Behavior of Steel-Fiber Reinforced Concrete Ground Slabs. I: Development of Material Model. Journal of Transportation Engineering, 137(12), 882–888. https://doi.org/10.1061/(ASCE)TE.1943-5436.0000276

El-Sayed, A. K., and Soudki, K. (2011). "Evaluation of shear design equations of concrete beams with FRP reinforcement." Journal of Composites for Construction, 15(1), 9-20.

El-Sayed, A. K., El-Salakawy, E. F., and Benmokrane, B. (2006a). "Shear capacity of high-strength concrete beams reinforced with FRP bars." ACI Structural Journal, 103(3), 383.

El-Sayed, A. K., El-Salakawy, E. F., and Benmokrane, B. (2006b). "Shear strength of FRP-reinforced concrete beams without transverse reinforcement." ACI Structural Journal, 103(2), 235.

El-sayed, A. K., El-salakawy, E., and Benmokrane, B. (2007). Shear Capacity of High-Strength Concrete Beams Reinforced with FRP Bars. ACI Structural Journal, 103(103), 383–389.

El-Sayed, A., El-Salakawy, E., and Benmokrane, B. (2005). "Shear strength of concrete beams reinforced with FRP bars: design method." Proceedings of the 7th International

Symposium on Fiber Reinforced Polymer Reinforcement for Concrete Structures-FRPRCS-7, 955-974.

El-Sayed, A., El-Salakawy, E., and Benmokrane, B. (2005). "Shear strength of one-way concrete slabs reinforced with fiber-reinforced polymer composite bars." Journal of Composites for Construction, 9(2), 147-157.

Eren, Ö. and Marar, K. (2010). Effect of steel fibers on plastic shrinkage cracking of normal and high strength concretes. Materials Research, 13(2), 135–141. https://doi.org/10.1590/S1516-14392010000200004

Facconi, L., Amin, A., Minelli, F., and Plizzari, G. (2021). A unified approach for determining the strength of FRC beams subjected to torsion–Part II: Analytical modeling. Structural Concrete, 22(6), 3780–3797. https://doi.org/10.1002/suco.202100162

Fico, R., Prota, A., and Manfredi, G. (2008). "Assessment of Eurocode-like design equations for the shear capacity of FRP RC members." Composites Part B: Engineering, 39(5), 792-806.

Folino, P., Ripani, M., Xargay, H., and Rocca, N. (2020). Comprehensive analysis of Fiber Reinforced Concrete beams with conventional reinforcement. Engineering Structures, 202(November 2019), 109862. https://doi.org/10.1016/j.engstruct.2019.109862

Foster, S. (2010). Design of FRC beams for shear using the VEM and the draft Model Code approach. Shear and Punching Shear in RC and FRC Elements: Technical Report: Proceedings of a Workshop Held on 15-16 October 2010, in Salò, Lake Garda, Italy, 57, 195.

Foster, S. J., Agarwal, A., and Amin, A. (2018). Design of steel fiber reinforced concrete beams for shear using inverse analysis for determination of residual tensile strength. Structural Concrete, 19(1), 129–140. https://doi.org/10.1002/suco.201700100

Frosch, R. J. (1999). Another look at cracking and crack control in reinforced concrete. ACI Structural Journal.

Frosch, R. J., Yu, Q., Cusatis, G., and Bažant, Z. P. (2017). "A unified approach to shear design." Concrete International, 39(9), 47-52.

Gastebled, O. J., and May, I. M. (2001). Fracture mechanics model applied to shear failure of reinforced concrete beams without stirrups. Structural Journal, 98(2), 184–190.

Gouda, O., Hassanein, A., and Galal, K. (2023). Experimental and numerical study on the crack width and deflection performance of GFRP reinforced concrete beams. Engineering Structures, 283. https://doi.org/10.1016/j.engstruct.2023.115721

Gross, S. P., Yost, J. R., Dinehart, D. W., Svensen, E., and Liu, N. (2003). "Shear strength of normal and high strength concrete beams reinforced with GFRP bars." High performance materials in bridges, 426-437.

Gross, S., Dinehart, D., Yost, J., and Theisz, P. "Experimental tests of high-strength concrete beams reinforced with CFRP bars." Proc., Proceedings of the 4th International Conference on Advanced Composite Materials in Bridges and Structures (ACMBS-4), Calgary, Alberta, Canada (quoted from Razaqpur and Isgor, 2006).

Gültekin, A., Beycioğlu, A., Arslan, M. E., Serdar, A. H., Dobiszewska, M., and Ramyar, K. (2022). Fresh Properties and Fracture Energy of Basalt and Glass Fiber–Reinforced Self-Compacting Concrete. Journal of Materials in Civil Engineering, 34(1). https://doi.org/10.1061/(asce)mt.1943-5533.0004043

Han, J., Zhao, M., Chen, J. and Lan, X. (2019). Effects of steel fiber length and coarse aggregate maximum size on mechanical properties of steel fiber reinforced concrete. Construction and Building Materials, 209, 577–591. https://doi.org/10.1016/J.CONBUILDMAT.2019.03.086

Harba, I. S. I., Abdulridha, A. J., and Al-Shaar, A. A. M. (2022). Numerical analysis of high-strength reinforcing steel with conventional strength in reinforced concrete beams under monotonic loading. Open Engineering, 12(1), 817–833. https://doi.org/10.1515/eng-2022-0365

Henager, C. H., Asce, M., and Doherty, T. J. (1975). JOURNAL OF THE STRUCTURAL DIVISION ANALYSIS OF REINFORCED FIBROUS CONCRETE BEAMS.

Holubová, B., Hradecká, H., Netušilová, M., Gavenda, T. and Helebrant, A. (2017). Corrosion of glass fibres in ultra high performance concrete and normal strength concrete. Ceramics - Silikaty, 61(4), 319–326. https://doi.org/10.13168/cs.2017.0031

Hsu, L. S. and Hsu, C. T. T. (1994). Stress-strain behavior of steel-fiber high-strength concrete under compression. ACI Structural Journal, 91(4), 448–457. https://doi.org/10.14359/4152

Huber, T., Huber, P., and Kollegger, J. (2019). Influence of aggregate interlock on the shear resistance of reinforced concrete beams without stirrups. Engineering Structures, 186, 26–42. https://doi.org/10.1016/j.engstruct.2019.01.074

Hussain, T., and Ali, M. (2018). UTILIZATION OF FRC TENSION ZONE FOR REINFORCEMENT REDUCTION IN SLABS-A SIMPLIFIED APPROACH. The Canadian Society for Civil Engineering.

Ibeawuchi, J., Moffatt, E., and Lloyd, A. (2019). Evaluation of flexural behaviour of low density fibre reinforced concrete using digital image correlation. 7th International Materials Specialty Conference 2018, Held as Part of the Canadian Society for Civil Engineering Annual Conference 2018, 194–204.

Ibrahim, H. H. H. and MacGregor, J. G. (1997). Modification of the ACI rectangular stress block for high-strength concrete. ACI Structural Journal, 94(1), 40–48. https://doi.org/10.14359/459

Imam, M., Vandewalle, L., and Mortelmans, F. (1995). Shear-moment analysis of reinforced high strength concrete beams containing steel fibres.

Intelligent Sensing for Innovative Structures (2007). “Reinforced Concrete Structures with Fibre-Reinforced Polymers, Design Manual No.3” Canadian Network of Centres of Excellence, Winnipeg, MB, Canada.

Issa, M. A., Ovitigala, T., and Ibrahim, M. (2016). Shear Behavior of Basalt Fiber Reinforced Concrete Beams with and without Basalt FRP Stirrups. Journal of Composites for Construction, 20(4), 04015083. https://doi.org/10.1061/(asce)cc.1943-5614.0000638

Issa, M. A., Ovitigala, T., and Ibrahim, M. (2015). "Shear behavior of basalt fiber reinforced concrete beams with and without basalt FRP stirrups." Journal of Composites for Construction, 20(4), 04015083.

Issa, M. S., Metwally, I. M., and Elzeiny, S. M. (2011). Influence of fibers on flexural behavior and ductility of concrete beams reinforced with GFRP rebars. Engineering Structures, 33(5), 1754–1763. https://doi.org/10.1016/j.engstruct.2011.02.014

Japanese Society of Civil Engineering (1997). "Recommendation for design and construction of concrete structures using continuous fiber reinforcing materials."

Jiang, C., Fan, K., Wu, F., and Chen, D. (2014). Experimental study on the mechanical properties and microstructure of chopped basalt fibre reinforced concrete. JOURNAL OF MATERIALSandDESIGN, 58, 187–193. https://doi.org/10.1016/j.matdes.2014.01.056

Johnston, C. D. (1996). Fly Ash Utilization Bridge Works .

Kani, G. N. J. (1967). How Safe Are Our Large Reinforced Concrete Beams?

Karthik, M. M. and Mander, J. B. (2011). Stress-Block Parameters for Unconfined and Confined Concrete Based on a Unified Stress-Strain Model. Journal of Structural Engineering, 137(2), 270–273. https://doi.org/10.1061/(asce)st.1943-541x.0000294

Kaszubska, M., and Kotynia, R. (2019) "Influence of concrete cover thickness and bar diameter on shear strength of glass fiber reinforced polymer concrete beams without stirrups." Proc., Conference: fib symposium “concrete – innovations in materials, design, and structures, CEB-FIB.

Kaszubska, M., Kotynia, R., and Barros, J. A. (2017). "Influence of longitudinal GFRP reinforcement ratio on shear capacity of concrete beams without stirrups." Procedia engineering, 193, 361-368.

Khaleel Ibrahim, S., Abbas Hadi, N., and Movahedi Rad, M. (2023). Experimental and Numerical Analysis of Steel-Polypropylene Hybrid Fibre Reinforced Concrete Deep Beams. Polymers, 15(10). https://doi.org/10.3390/polym15102340

Khaleel Ibrahim, S., Abbas Hadi, N., and Movahedi Rad, M. (2023). Experimental and Numerical Analysis of Steel-Polypropylene Hybrid Fibre Reinforced Concrete Deep Beams. Polymers, 15(10). https://doi.org/10.3390/polym15102340

Kim, K. S., Lee, D. H., Hwang, J. H., and Kuchma, D. A. (2012). Shear behavior model for steel fiber-reinforced concrete members without transverse reinforcements. Composites Part B: Engineering, 43(5), 2324–2334. https://doi.org/10.1016/j.compositesb.2011.11.064

Kim, S. W., Han, D. S., and Kim, K. H. (2021). Evaluation of shear effect on deflection of rc beams. Applied Sciences (Switzerland), 11(16). https://doi.org/10.3390/app11167690

Kizilkanat, A. B., Kabay, N., Akyüncü, V., Chowdhury, S., and Akça, A. H. (2015). Mechanical properties and fracture behavior of basalt and glass fiber reinforced concrete: An experimental study. Construction and Building Materials, 100, 218–224. https://doi.org/10.1016/j.conbuildmat.2015.10.006

Kooiman, A. G., and Walraven, C. (2000). Modelling the post-cracking behaviour of steel fibre reinforced concrete for structural design purposes. HERON, Vol. 45 (4), 2000.

Kotynia, R., and Kaszubska, M. (2016) "Analysis of concrete contribution in the shear strength of beams reinforced with FRP/steel bars without stirrups." Proc., fib Symposium 2016 proceedings.

Kwak, Y.-K., Eberhard, M. O., Kim, W.-S., and Kim, J. (2002). Shear strength of steel fiber-reinforced concrete beams without stirrups. ACI Structural Journal, 99(4), 530–538.

Labib, W. (2008). An Experimental Study and Finite Element Analysis of Punching Shear Failure in Steel Fibre-Reinforced Concrete Ground-Suspended Floor Slabs. August, 1–280.

Lee, S. C., Oh, J. H., and Cho, J. Y. (2015). Compressive behavior of fiber-reinforced concrete with end-hooked steel fibers. Materials, 8(4), 1442–1458. https://doi.org/10.3390/ma8041442

Li, Y.-A., Hsu, T. T., and Hwang, S.-J. (2017). "Shear strength of prestressed and nonprestressed concrete beams." Concrete International, 39(9), 53-57.

Liao, L., Zhao, J., Zhang, F., Li, S. and Wang, Z. (2020). Experimental study on compressive properties of SFRC under high strain rate with different fiber content and aspect ratio. Construction and Building Materials, 261, 119906. https://doi.org/10.1016/j.conbuildmat.2020.119906

Lim, T. Y., Paramasivam, P., and Lee, S. L. (1987). Analytical Model for Tensile Behavior of Steel-Fiber Concrete. ACI Materials Journal, 84(4), 286–298. https://doi.org/10.14359/1454

MacGregor, J. G., and Wight, J. K. (2006). Reinforced concrete: mechanics and design, Prentice Hall. Upper Saddle River, NJ.

Machial, R., Alam, M. S., and Rteil, A. (2012). "Revisiting the shear design equations for concrete beams reinforced with FRP rebar and stirrup." Materials and structures, 45(11), 1593-1612.

Madhkhan, M. and Katirai, R. (2019). Effect of pozzolanic materials on mechanical properties and aging of glass fiber reinforced concrete. Construction and Building Materials, 225, 146–158. https://doi.org/10.1016/j.conbuildmat.2019.07.128

Madhkhan, M., and Katirai, R. (2019). Effect of pozzolanic materials on mechanical properties and aging of glass fiber reinforced concrete. Construction and Building Materials, 225, 146–158. https://doi.org/10.1016/j.conbuildmat.2019.07.128

Maher Elnemr, A., Ahmed, E. A., El-Nemr, A., Ahmed, E., and Benmokrane, B. (2011). Instantaneous Deflection of Slender Concrete Beams Reinforced with GFRP Bars Second-order analysis for slender columns entirely reinforced with FRP bars and spirals View project Shear Behaviour of One-Way Slabs Reinforced with FRP bars View project . https://www.researchgate.net/publication/273142579

Mailyan, L. R., Shilov, P. A., and Shilov, A. A. (2021). Technologies for creating directional orientation of fiber reinforcement in concrete. IOP Conference Series: Materials Science and Engineering, 1083(1), 012039. https://doi.org/10.1088/1757-899x/1083/1/012039

Mansur, M. ., Chin, M. . and Wee, T. . (1999). STRESS-STRAIN RELATIONSHIP OF HIGH-STRENGTH FIBER CONCRETE IN COMPRESSION. Test, 11(February), 21–29.

Mansur, M. A., Ong, K. C. G., and Paramasivam, P. (1986). Shear Strength of Fibrous Concrete Beams Without Stirrups. Journal of Structural Engineering, 112(9), 2066–2079. https://doi.org/10.1061/(asce)0733-9445(1986)112:9(2066)

Marì Bernat, A., Spinella, N., Recupero, A., and Cladera, A. (2020). Mechanical model for the shear strength of steel fiber reinforced concrete (SFRC) beams without stirrups. Materials and Structures/Materiaux et Constructions, 53(2). https://doi.org/10.1617/s11527-020-01461-4

Martin, T., and Jitka, V. (2017). Modulus of Elasticity in Tension for Concrete and Fibre Reinforced Concrete. 259, 35–40. https://doi.org/10.4028/www.scientific.net/SSP.259.35

Matta, F., El-Sayed, A. K., Nanni, A., and Benmokrane, B. (2013). "Size Effect on Concrete Shear Strength in Beams Reinforced with Fiber-Reinforced Polymer Bars." ACI Structural Journal, 110(4).

McCormick, N. J., and Lord, J. D. (2010). Practical in-situ applications of DIC for large structures. Applied Mechanics and Materials, 24–25, 161–166. https://doi.org/10.4028/www.scientific.net/AMM.24-25.161

Mebarkia, S., and Vipulanandan, C. (1992). Compressive Behavior of Glass-Fiber Reinforced Polymer Concrete.pdf. ASCE J. Mater. Civ. Eng.

Merve AÇIKGENÇ, ALYAMAÇ, K. E., and ULUCAN, Z. Ç. (2015). Relation between Splitting Tensile and Flexural Strengths of Steel Fiber-Reinforced Concrete Relation between Splitting Tensile and Flexural Strengths. August 2016.

Minelli, F. (Fausto). (2005). Plain and fiber reinforced concrete beams under shear loading : structural behavior and design aspects. Starrylink Editrice.

Minelli, F., and Plizzari, G. A. (2010). Shear strength of FRC members with little or no shear reinforcement: a new analytical model. Fib Bulletin, 57, 211–225.

Minelli, F., and Plizzari, G. A. (2010). Shear strength of FRC members with little or no shear reinforcement: a new analytical model. Fib Bulletin, 57, 211–225.

Minelli, F., Conforti, A., Cuenca, E., and Plizzari, G. (2014). Are steel fibres able to mitigate or eliminate size effect in shear? Materials and Structures/Materiaux et Constructions, 47(3), 459–473. https://doi.org/10.1617/s11527-013-0072-y

Mobasher, B., Yao, Y., and Soranakom, C. (2015). Analytical solutions for flexural design of hybrid steel fiber reinforced concrete beams. Engineering Structures, 100, 164–177. https://doi.org/10.1016/j.engstruct.2015.06.006

Mohamed, O. A., and Khattab, R. (2017). Numerical analysis of concrete beam reinforced with glass fiber reinforced polymer bars. Proceedings of International Structural Engineering and Construction, 4(1). https://doi.org/10.14455/ISEC.res.2017.141

Momani, Y., Tarawneh, A., Alawadi, R., and Momani, Z. (2022). Shear strength prediction of steel fiber-reinforced concrete beams without stirrups. Innovative Infrastructure Solutions, 7(1). https://doi.org/10.1007/s41062-021-00703-w

Nagasaka, T., Fukuyama, H., and Tanigaki, M. (1993). "Shear performance of concrete beams reinforced with FRP stirrups." Special Publication, 138, 789-812.

Neves, R. D., and Fernandes de Almeida, J. C. O. (2005). Compressive behaviour of steel fibre reinforced concrete. Structural Concrete, 6(1), 1–8. https://doi.org/10.1680/stco.2005.6.1.1

Nguyen-Minh, L., and Rovňák, M. (2013). Punching Shear Resistance of Interior GFRP Reinforced Slab-Column Connections. Journal of Composites for Construction, 17(1), 2–13. https://doi.org/10.1061/(asce)cc.1943-5614.0000324

Ozbakkaloglu, T. and Saatcioglu, M. (2004). Rectangular stress block for high-strength concrete. ACI Structural Journal, 101(4), 475–483. https://doi.org/10.14359/13333

Pang, Y., Wei, K., and Yuan, W. (2020). Life-cycle seismic resilience assessment of highway bridges with fiber-reinforced concrete piers in the corrosive environment. Engineering Structures, 222. https://doi.org/10.1016/j.engstruct.2020.111120

Pannirselvam, N. and Manivel, S. (2021). Influence of Addition of Glass Fibre on Concrete. IOP Conference Series: Materials Science and Engineering, 1026(1), 012008. https://doi.org/10.1088/1757-899x/1026/1/012008

Park, H.-G., and Choi, K.-K. (2017). "Unified shear design method of concrete beams based on compression zone failure mechanism." Concrete International, 39(9), 59-63.

Paul, S. C., van Zijl, G. P. A. G., and Šavija, B. (2020). Effect of fibers on durability of concrete: A practical review. In Materials (Vol. 13, Issue 20, pp. 1–26). MDPI AG. https://doi.org/10.3390/ma13204562

Pereira, E. B., Fischer, G., and Barros, J. A. O. (2012). Effect of hybrid fiber reinforcement on the cracking process in fiber reinforced cementitious composites. Cement and Concrete Composites, 34(10), 1114–1123. https://doi.org/10.1016/j.cemconcomp.2012.08.004

Razaqpur, A. G., and Spadea, S. (2015). "Shear strength of FRP reinforced concrete members with stirrups." Journal of Composites for Construction, 19(1), 04014025.

Reineck, K.-H. (2017). "Proposal for ACI 318 Shear Design." Concrete International, 39(9), 65-70.

Richardson, J. T. E. (2011). Eta squared and partial eta squared as measures of effect size in educational research. Educational Research Review, 6(2), 135–147. https://doi.org/10.1016/j.edurev.2010.12.001

RILEM TC 162-TDF. (2000). Rilem TC 162-TDF: Test and design methods for steel fibre reinforced concrete: Uni-axial tension test for steel fibre reinforced concrete. Materials and Structures/Materiaux et Constructions, 33(235), 75–81. https://doi.org/10.1617/13628

RILEM TC 162-TDF. (2002). RILEM TC 162-TDF-TEST AND DESIGN METHODS FOR STEEL FIBRE-BENDING TEST. Materials and Structures, 35, 579–582.

Saleh, Z., Neaz Sheikh, M., Remennikov, A. M., and Basu, A. (2019). Numerical analysis of behavior of glass fiber-reinforced polymer bar-reinforced concrete beams under impact loads. Faculty of Engineering and Information Sciences - Papers: Part B. https://ro.uow.edu.au/eispapers1/3316

Schlaich, J., and Schiifer, K. (1991). Design and detailing of structural concrete using strut-and-tie models. The Structural Engineer, 69, 113–125.

Shafiq, N., Ayub, T., and Khan, S. U. (2016b). Investigating the performance of PVA and basalt fibre reinforced beams subjected to flexural action. Composite Structures, 153, 30–41. https://doi.org/10.1016/j.compstruct.2016.06.008

Sharifi, Y., and Moghbeli, A. (2021). Shear capacity assessment of steel fiber reinforced concrete beams using artificial neural network. Innovative Infrastructure Solutions, 6(2). https://doi.org/10.1007/s41062-021-00457-5

Sharma, A. K. (1986). Shear strength of steel fiber reinforced concrete beams. Journal Proceedings, 83(4), 624–628.

Shewalul, Y. W. (2021). Numerical and FEA investigation of sectional capacity and moment redistribution behavior of steel fiber reinforced concrete (SFRC) beam. Heliyon, 7(6). https://doi.org/10.1016/j.heliyon.2021.e07354

Simões, T., Costa, H., Dias-da-Costa, D., and Júlio, E. (2017). Influence of fibres on the mechanical behaviour of fibre reinforced concrete matrixes. Construction and Building Materials, 137, 548–556. https://doi.org/10.1016/j.conbuildmat.2017.01.104

Sivakumar, A. (2011). Influence of hybrid fibres on the post crack performance of high strength concrete: Part I experimental investigations. Journal of Civil Engineering and Construction Technology, 2(7), 147–159.

Sliseris, J. (2018). Numerical analysis of reinforced concrete structures with oriented steel fibers and re-bars. Engineering Fracture Mechanics, 194, 337–349. https://doi.org/10.1016/j.engfracmech.2018.03.017

Smarzewski, P., and Stolarski, A. (2017). Numerical Analysis on the High-Strength Concrete Beams Ultimate Behaviour. IOP Conference Series: Materials Science and Engineering, 245(3). https://doi.org/10.1088/1757-899X/245/3/032013

Soranakom, C., and Mobasher, B. (2008). Correlation of tensile and flexural responses of strain softening and strain hardening cement composites. Cement and Concrete Composites, 30(6), 465–477.

Soranakom, C., and Mobasher, B. (2009). Flexural design of fiber-reinforced concrete. ACI Materials Journal, 106(5), 461–469. https://doi.org/10.14359/51663147

Sujivorakul, C. (2012). Model of hooked steel fibers reinforced concrete under tension. RILEM Bookseries, 2(January 2012), 19–26. https://doi.org/10.1007/978-94-007-2436-5_3

Sujivorakul, C., and Naaman, A. E. (2003). Tensile Response of HPFRC Composites Using Twisted Polygonal Steel Fibers. Special Publication, 216, 161–180. https://doi.org/10.14359/12898

Suksawang, N., Wtaife, S., and Alsabbagh, A. (2018). Evaluation of elastic modulus of fiber-reinforced concrete. ACI Materials Journal, 115(2), 239–249. https://doi.org/10.14359/51701920

Sun, L., Hao, Q., Zhao, J., Wu, D., and Yang, F. (2018). Stress strain behavior of hybrid steel-PVA fiber reinforced cementitious composites under uniaxial compression. Construction and Building Materials, 188, 349–360. https://doi.org/10.1016/j.conbuildmat.2018.08.128

Tariq, M., and Newhook, J. (2003). "Shear testing of FRP reinforced concrete without transverse reinforcement." Proceedings, Annual Conference of the Canadian Society for Civil Engineering, 1330-1339.

Tlemat, H., Pilakoutas, K., and Neocleous, K. (2006). Modelling of SFRC using inverse finite element analysis. Materials and Structures/Materiaux et Constructions, 39(2), 221–233. https://doi.org/10.1617/s11527-005-9010-y

Tomlinson, D., and Fam, A. (2015). Flexural behavior of precast concrete sandwich wall panels with basalt FRP and steel reinforcement. PCI Journal, 60(6), 51–71. https://doi.org/10.15554/pcij.11012015.51.71

Tomlinson, D., and Fam, A. (2014). "Performance of concrete beams reinforced with basalt FRP for flexure and shear." Journal of Composites for Construction, 19(2), 04014036.

Tottori, S., and Wakui, H. (1993). "Shear capacity of RC and PC beams using FRP reinforcement." Special Publication, 138, 615-632.

Tsivolas, E., Gergidis, L. N., and Paipetis, A. S. (2022). Crack Growth and Delamination Analysis in GFRP Composite Materials. Applied Sciences (Switzerland), 12(4). https://doi.org/10.3390/app12041945

Tureyen, A. K., and Frosch, R. J. (2002). "Shear tests of FRP-reinforced concrete beams without stirrups." Structural Journal, 99(4), 427-434.

Vecchio, F. J. (2000). DISTURBED STRESS FIELD MODEL FOR REINFORCED CONCRETE: FORMULATION. In / JOURNAL OF STRUCTURAL ENGINEERING.

Vecchio, F. J., and Collins, M. P. (1986). The Modified Compression-Field Theory for Reinforced. ACI Structural Journal, 83(2), 219–231.

Wang, H., and Belarbi, A. (2011). Ductility characteristics of fiber-reinforced-concrete beams reinforced with FRP rebars. Construction and Building Materials, 25(5), 2391–2401. https://doi.org/10.1016/j.conbuildmat.2010.11.040

Wong, P. S., Vecchio, F. J., and Trommels, H. (2013). Vector2 and Formworks User's Manual Second Edition. In Dairy Science and Technology, CRC Taylor and Francis Group (Issue June).

Yoo, D. Y., Banthia, N., Yang, J. M., and Yoon, Y. S. (2016). Size effect in normal- and high-strength amorphous metallic and steel fiber reinforced concrete beams. Construction and Building Materials, 121, 676–685. https://doi.org/10.1016/j.conbuildmat.2016.06.040

Yoo, D. Y., Yoon, Y. S., and Banthia, N. (2015). Flexural response of steel-fiber-reinforced concrete beams: Effects of strength, fiber content, and strain-rate. Cement and Concrete Composites, 64, 84–92. https://doi.org/10.1016/j.cemconcomp.2015.10.001

Yost, J. R., Gross, S. P., and Dinehart, D. W. (2001). "Shear strength of normal strength concrete beams reinforced with deformed GFRP bars." Journal of Composites for Construction, 5(4), 268-275.

Zhao, X.-L., and Zhang, L. (2007). "State-of-the-art review on FRP strengthened steel structures." Engineering Structures, 29(8), 1808-1823.

APPENDICES

A EVALUATION OF PROPOSED STEEL FIBRE REINFORCED CONCRETE BEAMS UNDER ULTIMATE AND SERVICEABILITY LIMIT STATE

A.1 Introduction

Concrete has a low tensile strength compared to its compressive strength. It also has a low deformation capacity, resulting in a brittle material. This is a particular disadvantage when the material is used for members with lower flexural stiffness such as lightly or glass fibre reinforced polymer (GFRP) reinforced beams that develop wide cracks and low ultimate shear strength relative to than members with high flexural stiffness.

It is generally accepted that ductility of concrete mixtures can be improved by adding steel fibres into the concrete matrix. This results in Steel Fibre Reinforced Concrete (SFRC). Several techniques have been proposed to determine the tensile stress-strain (σ-ε) relationship of Steel Fibre Reinforced Concrete (SFRC). Lim et al. developed a tensile σ-ε relationship using laws of mixture and results from steel fibre pullout tests (Lim et al. 1987). A similar method was proposed by Lok and Pie with some modifications, (Lok and Pei 1998). RILEM TC 162-TDF (Vandewalle 2000) and Barros et al. (Barros and Figueiras 2001) proposed a tensile σ-ε relationship that uses results from a deformation-controlled beam-bending test to determine the peak and post-cracking stresses. The work presented in this study will focus on an inverse analysis which is a more general approach and so is becoming more attractive and gaining the attention of researchers in the past few years e.g., (Elsaigh et al. 2004; Hemmy 2002; Kohoutkova et al. 2004; Labib 2008; Tlemat et al. 2006).

VecTor2® is a 2D finite element software developed at the University of Toronto that is based on Modified Compression Field Theory (MCFT) (Wong et al. 2013). MCFT analysis, demonstrates that SFRC has smaller crack widths and so enhanced aggregate interlock compared to non-fibre reinforced concrete that leads to improved shear strength. Previous research has been conducted on the shear performance of SFRC beams (Abbas et al. 2014; Cucchiara et al. 2004; Ding et al. 2011; Dinh 2009; Lim and Oh 1999; Minelli et al. 2014). However, there are limited studies on of the effect of SFRC on crack width and its effect on shear performance. Therefore, the research presented in this paper considers the crack width under service loads.

A.2 Description of Experimental Program

The experimental program was conducted at King Saud University to study the effect of fibre content on the flexural behaviour of SFRC for ground slab applications. The load-deflection results of SFRC prisms from that program are used to verify the upcoming inverse analysis. Beam specimens measuring 150 x 150 x 600 mm under four-point loading were tested under displacement control at a rate of 0.2 mm/min. The two-point loads were applied symmetrically 150 mm apart. The prism supports were bolted to the machine body and set 450 mm apart. Mid-span deflection was measured by using the average of two LVDTs located at mid-span on both sides of the prism. Two concrete strengths were considered (30 MPa and 50 MPa) and three different fibre reinforcement percentages were considered (0.5%, 0.76%, and 1.0% by volume), making for six overall mixtures.

A.3 Numerical Analysis

The Finite Element Analysis (FEA) program VecTor2® version (4.2) was used (Wong 2013) for numerical analysis in this program. The FEA was divided into two phases: in Phase 1 the constitutive model of SFRC was developed, in Phase 2 the material model was used in a full-scale model to evaluate parameters such as fibre volume, concrete strength, and shear reinforcement. The phases are summarized in Figure A-1.

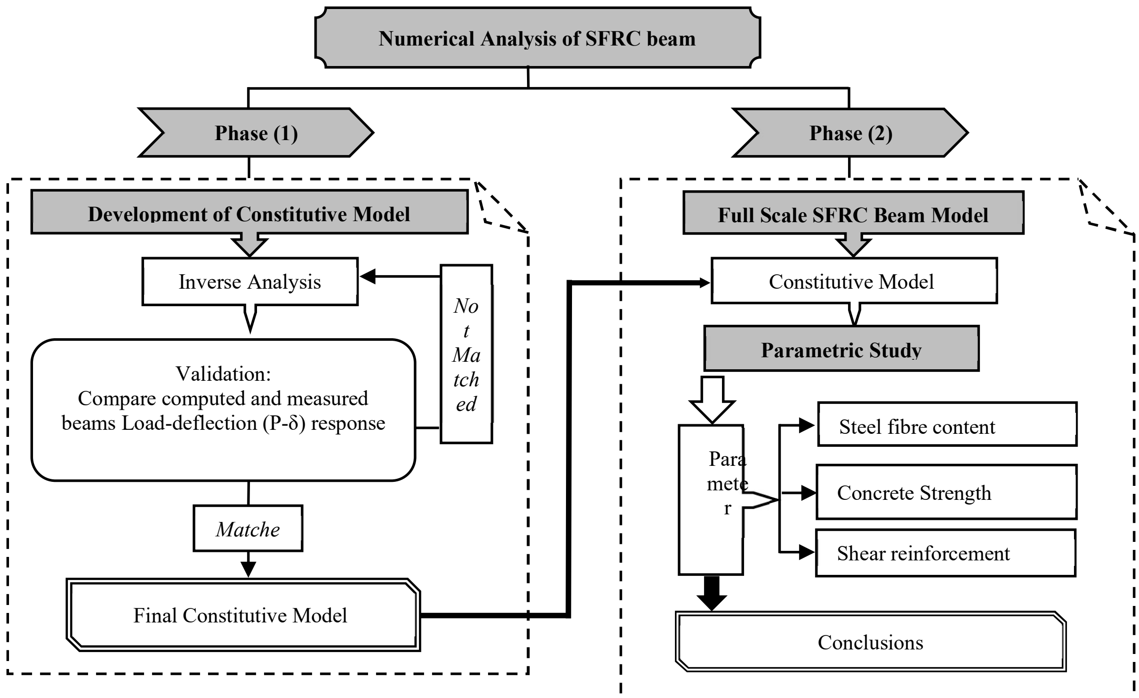

Figure A-1: Numerical analysis of SFRC beam flow chart

A.3.1 Phase 1: Constitutive Model

A.3.1.1 Finite element model of prism tests

The prisms were divided into 144 hybrid rectangular elements with a 25 x 25 mm mesh size as shown in Figure A-2. The same mesh dimensions was used and recommended for similar analyses conducted by other researchers (Blazejowski 2012; Labib 2008; Thomas and Ramaswamy 2007). Displacement control was used in this analysis and the boundary conditions of the model replicated those in the experimental setup.

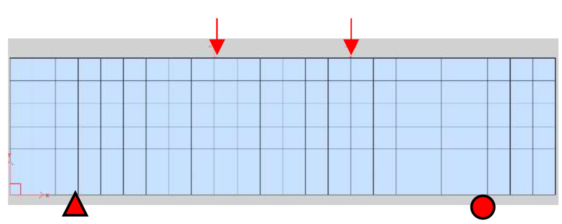

Figure A-2: Mesh, loading and boundary condition

A.3.1.2 Inverse analysis

In an inverse analysis, an iterative procedure is used to derive the tensile behaviour of SFRC for each of the six mixtures. The tensile behaviour of SFRC is assumed to follow a tri-linear response (Figure A-3).

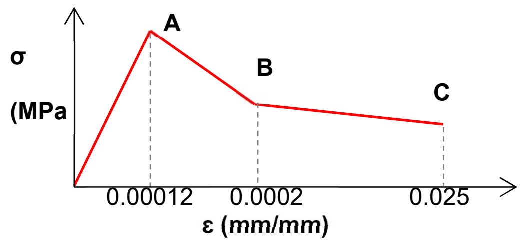

Figure A-3: General form of the tri-linear stress-strain relationship for SFRC

The development of the tensile σ-ε relationship for a specific SFRC material (concrete strength, fibre type) includes four steps and is illustrated in Figure A-4.

1. Obtain the load-deflection (*P-δ)* behaviour from a four-point bending prism test for the SFRC mix design under consideration. This was done by using information from (Aldossari 2014)
2. Choose a tensile model (tri-linear) shape (see Figure 3) to serve as the constitutive model for the tensile stress-strain behaviour of the concrete in the FEA.
3. Simulate the prism test using FEA using the constitutive model.
4. Use the results of Step 3 to adjust the tensile σ-ε relationship parameters in Step 2 (A, B, and C in Figure 3). Keep iterating until the experimental and numerically-determined load-deflection behaviour reach a reasonable match. Figure 4 shows the inverse analysis process.

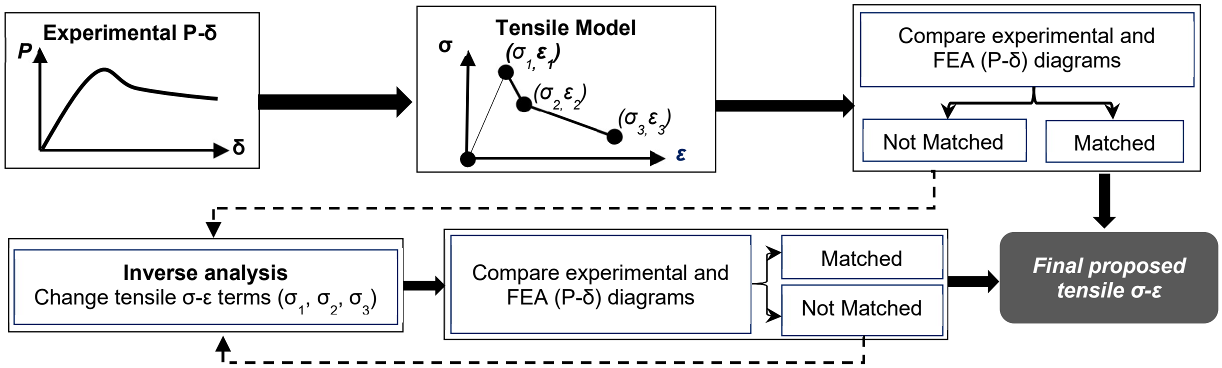

Figure A-4: Inverse analysis process flow chart

A.3.2 Phase 2: Full Scale Model

Three full-scale beam designs with two concrete strengths and three reinforcement ratios were considered. These beams are termed: SFB-C (control beam without stirrups), SFB-5S (beam with 10M stirrups @ 250mm), and SFB-11S (beam with 10M stirrups @ 100mm). The full-scale beam dimensions are 2800 x 300 x 150 mm, the longitudinal reinforcement ratio is 1.33%, yield strength of steel is 475 MPa, and the stirrups were located in the shear zone at distance 100 mm from the point load to end of the beam as shown in Figure A-5. Hybrid rectangular elements were selected to model the concrete. The concrete's tensile stress-strain response was the same as that developed in Phase 1. The beam was divided into 1456 elements with mesh size 25 x 25 mm (the same mesh dimensions were used in Phase 1). Truss elements were used to model longitudinal reinforcement; stirrups were modeled using smeared reinforcement properties.

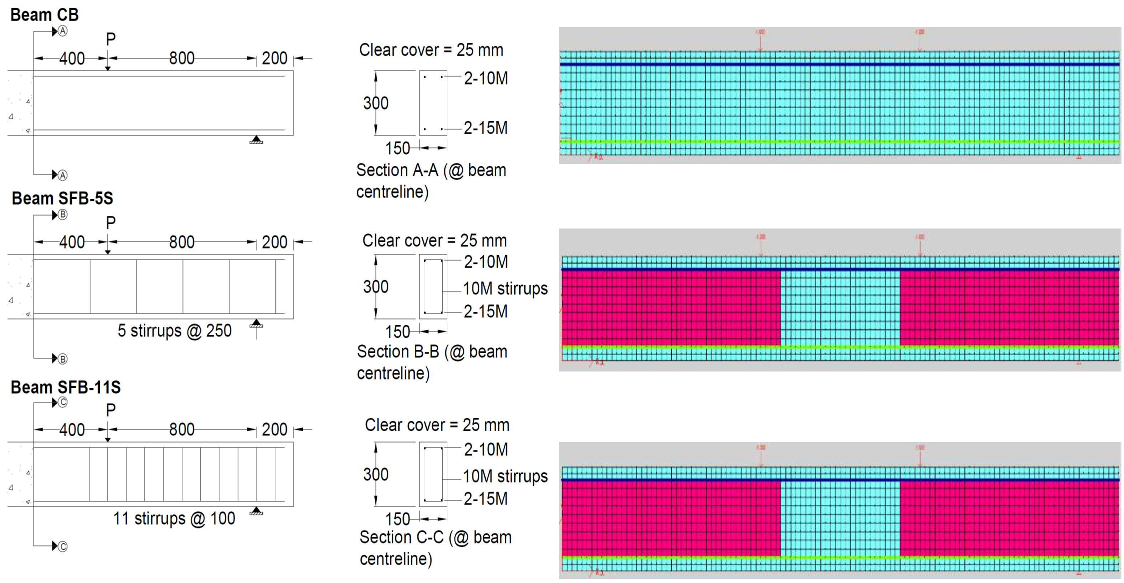

Figure A-5: Proposed and modelled SFRC full scale beams

Parametric studies were conducted on the full-scale model to investigate the effect of concrete strength (30 and 50 MPa), fibre content (0%, 0.5%, 0.76%, and 1.0%), and shear reinforcement spacing on the beam response. Based on the FEA information, a deeper understanding of the performance of beams can be obtained for ultimate limit state in terms of shear strength, stiffness, and ductility and serviceability limit state in terms of crack width and deflection.

A.4 Results and Discussion

The parameters of the initial tensile σ-ε relationship, σ_1,σ_2,σ_3, ε_1,ε_2, and ε_3 (see Figure 4) were adjusted in the model until the calculated and measured load-deflection (P-δ) behaviours matched. The experience gained from these iterations indicates that σ_1, σ_2, and σ_3 are interrelated. In other words, their influence is not confined to a single part of the P-δ response. Changing σ_1 has considerable influence on the cracking load but little effect on the post-cracking plateau of the P-δ response. σ_2 and σ_3 remarkably affect the post-cracking relationship with minimal influence on the cracking load. The latter σ_3 is more noticeable at higher deflection values on the P-δ response.

The pre-cracking part of the P-δ response is influenced by the concretes's elastic modulus as discussed earlier. Keeping in mind the narrow range of strain values, the change in $\varepsilon_1, \varepsilon_2$, and ε_3 were found to have an insignificant influence on the P-δ behaviour. Therefore, these strain values were kept unchanged at 0.00012, 0.002, and 0.025 during iterations (Figure A-3).

After several iterations, σ_1, σ_2, and σ_3, the calculated P-δ behaviour from the FEA reasonably matched the experimental results (Figure A-6). The slope of the pre-cracking part of falls within the range of data but in the border of the steeper slope. The cracking loads, and the post-cracking P-δ response fit well. The proposed tensile σ-ε relationships for each volume fraction and concrete strength are given in Table A-1.

Table A-1: Proposed tensile stress-strain points for each concrete mixture

Concrete Strength, f_c' *(MPa)*	*Fibre Volume Fraction, V_F, (%)*	*A (MPa), ε = 0.00012*	*B (MPa), ε = 0.0002*	*C (MPa), ε = 0.025*
	0.5	1.8	1.5	1.0
30	0.76	2.2	2.0	2.0
	1.0	2.6	2.4	2.4
	0.5	3	2.8	2.0
50	0.76	3.8	3.4	2.8
	1.0	4.2	4.0	2.6

Figure A-7 shows the load deflection of beams with different concrete compressive strengths (30 MPa, 50 MPa) steel fibre content (0%, 0.5%, 0.76%, and 1.0%) and stirrup spacing (no stirrups, 100 mm, 250 mm). The ultimate strength increased significantly and at pre-yielding load stage the section gains some stiffness due to the increased reinforcement ratio added by the steel fibres. The post-cracking response improved as well in terms of ductility. For example, adding 0.5% V_f to 30 MPa-CB increased the peak load by 48% from 79 kN to 117 kN and for 50 MPa-CB the peak load goes up by 50% from 90 kN to 135 kN. In addition, the ductility of 0.5% V_f of 30 MPa-CB increased 7 times compared to beams without steel fibres. Adding stirrups increases both ultimate shear strength and ductility.

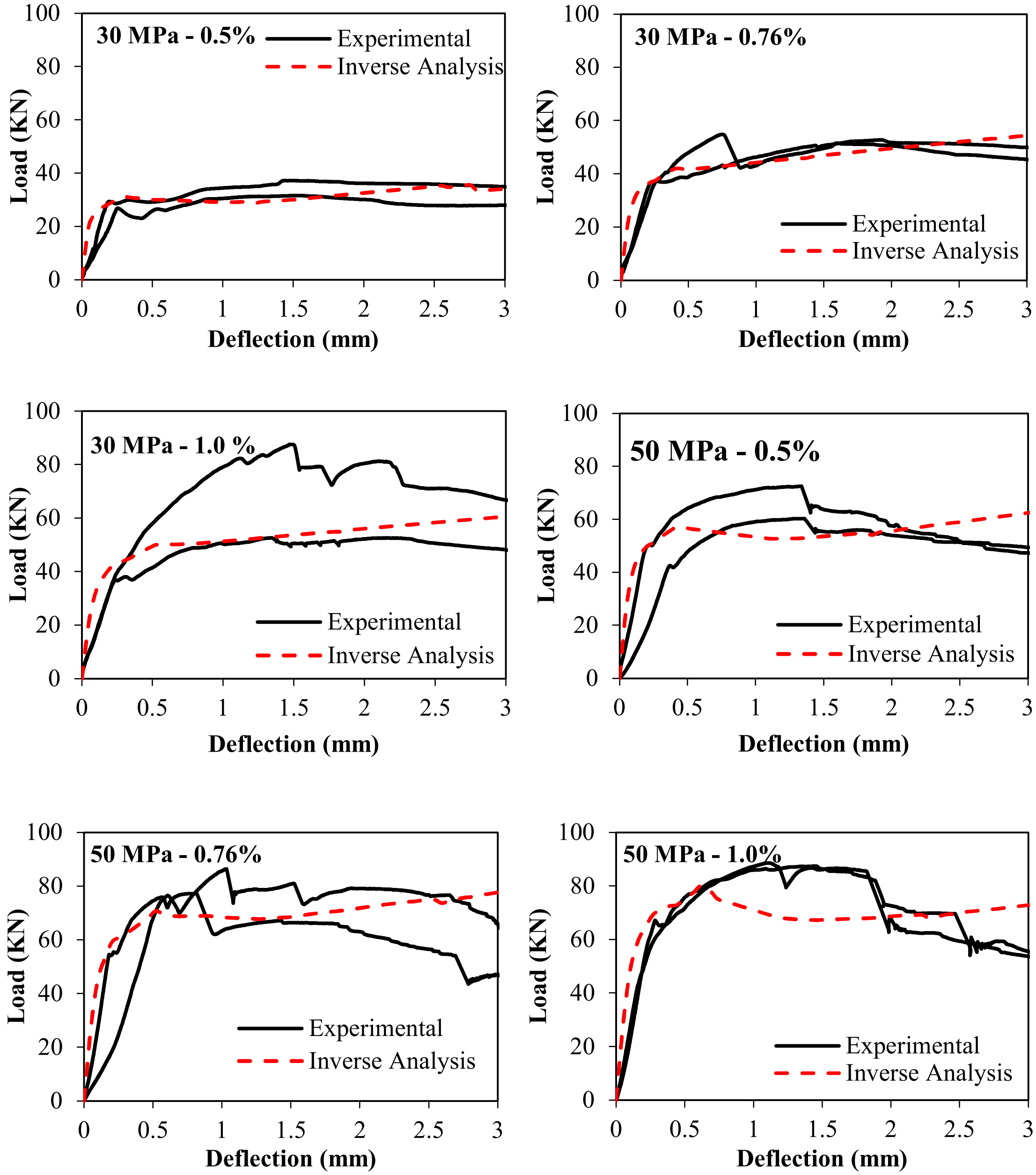

Figure A-6: Computed and modelled load deflection responses for the six different mixtures

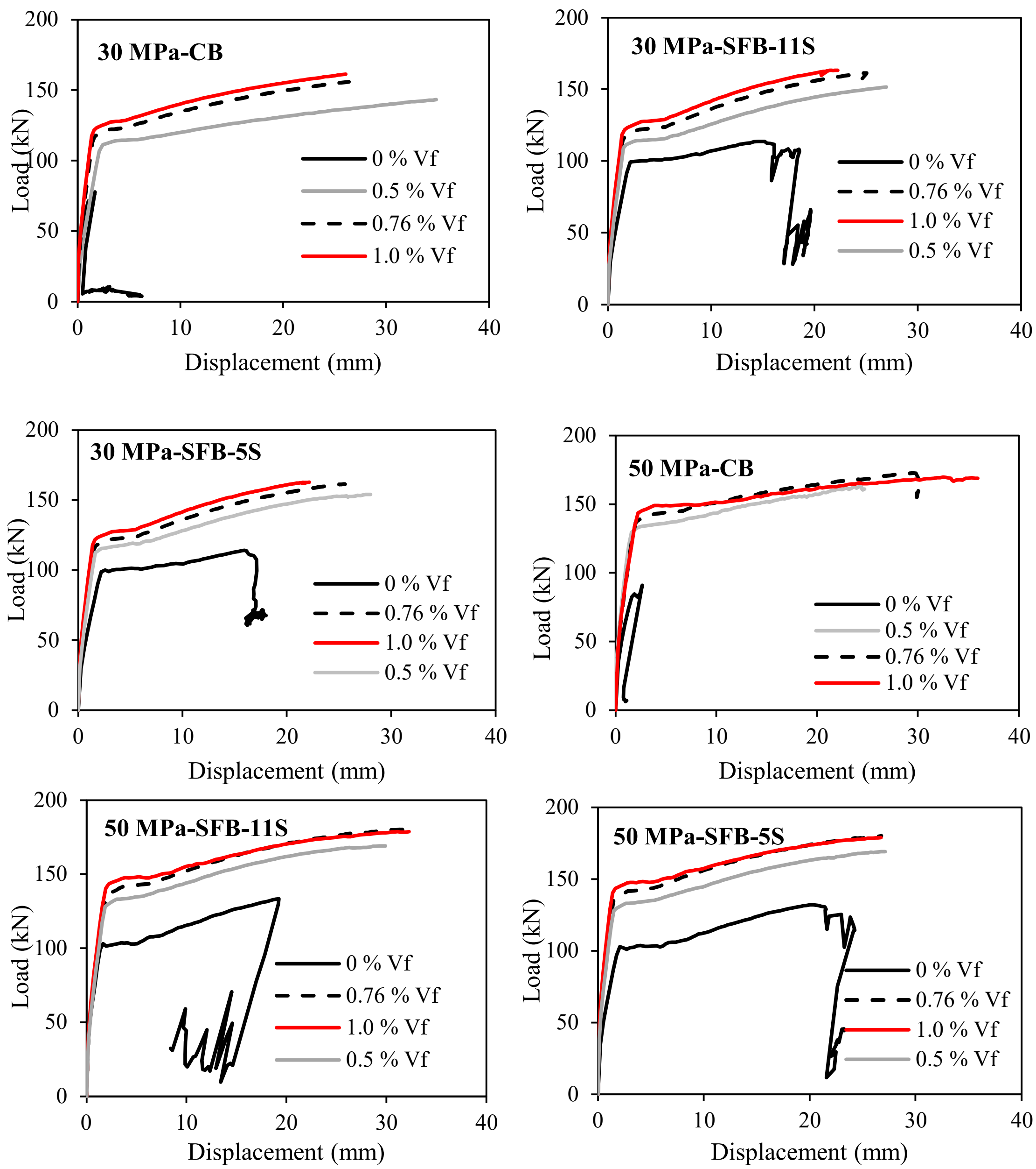

Figure A-7: Load deflection responses of full-scale beam models

Crack widths were extracted at a serviceability load equal to 65 kN for each beam. This load was determined based on dividing the yield load of the beam most representative of a typical beam, 30 MPa-SFB-11S-V_f-0%, by 1.5 (the load factor for live load in the National Building Code of Canada). Back calculations of factored loads were used to estimate service loads as these beams were not deflection-controlled (i.e. the typical deflection limit for beams, $L/360$, is 6.7 mm, higher than the yield deflection of all beams). The crack width reducing significantly by increasing the steel fibre content for each type of beam. The higher the concrete strength the lower the crack width because of the bond between the steel fibre content and concrete matrix goes up by increasing the compression strength as shown in Figure A-8.

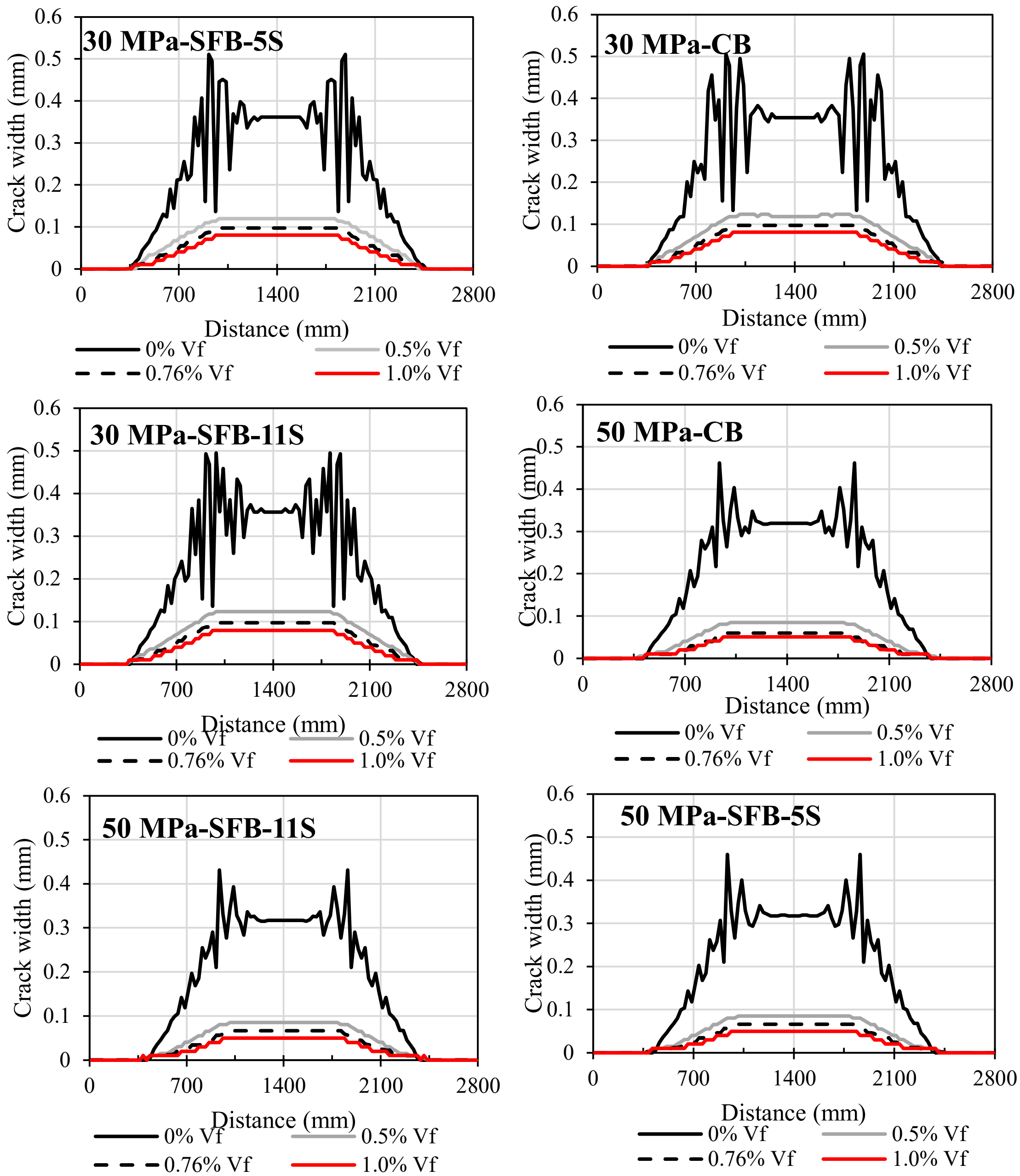

Figure A-8: Crack widths along each beam under a service load of 65 kN.

Figure A-9 compares the maximum crack width extracted at the extreme tension fibre of the 30 MPa and 50 MPa beams. For example, adding 0.5% V_f to 30 MPa-CB leads to decrease the maximum crack width by 60% from 0.52 mm to 0.12 mm and for 50 MPa-CB the crack width reduced by 62% from 0.46mm to 0.08mm. The shear reinforcement has a negligible effect on the crack width at service loads at the extreme tension fibre.

The failure mode changed in beams without stirrups when steel fibres were added. The failure mode shifted from diagonal tension shear failure (brittle failure) to flexural tension (ductile failure) by adding steel fibre as shown in Figure A-10. Table A-2 demonstrates the results summary of all beams.

Table A-2: Results Summary

Beam	Deflection at service*, mm	Maximum Crack width at Service, mm	Yield Load, kN	Peak Load, kN	Deflection at Peak, mm	Ductility Index	Energy Dissipated at Peak Load, kNmm	Failure Mode**
30-CB-0	1.20	0.505	65	78	2.26	1.87	125	D.T.S
30-CB-0.5	1.01	0.124	105	143	33.56	16.73	4182	F.T
30-CB-0.76	0.85	0.097	116	156	31.92	16.97	4323	F.T
30-CB-1.0	0.76	0.081	121	161	31.73	14.36	4457	F.T
30-SFB-5S-0.0	1.15	0.500	100	114	15.96	4.92	1550	F.T
30-SFB-5S-0.5	0.70	0.122	111	150	14.69	9.12	3716	F.T
30-SFB-5S-0.76	0.59	0.097	117	160	25.57	15.59	3531	F.T
30-SFB-5S-1.0	0.50	0.080	123	163	22.14	12.10	3101	F.T
30-SFB-11S-0.0	1.10	0.495	100	114	19.66	5.27	1453	F.T
30-SFB-11S-0.5	0.70	0.121	112	152	26.95	13.82	3486	F.T
30-SFB-11S-0.76	0.58	0.097	118	160	25.04	13.98	3389	F.T
30-SFB-11S-1.0	0.50	0.079	125	163	22.26	9.23	3127	F.T
50-CB-0	1.00	0.462	86	91	2.6	1.10	175	D.T.S
50-CB-0.5	0.43	0.085	129	163	23.68	15.80	4023	F.T
50-CB-0.76	0.51	0.060	137	173	29.80	14.90	4578	F.T
50-CB-1.0	0.50	0.051	143	170	32.78	14.90	5047	F.T
50-SFB-5S-0.0	0.89	0.459	102	132	20.34	10.01	2251	F.T
50-SFB-5S-0.5	0.43	0.085	127	169	27.14	18.21	4026	F.T
50-SFB-5S-0.76	0.33	0.066	130	180	26.76	19.82	4237	F.T
50-SFB-5S-1.0	0.27	0.050	144	179	26.72	15.72	4275	F.T
50-SFB-11S-0.0	0.64	0.431	102	133	19.25	8.02	2166	F.T
50-SFB-11S-0.5	0.60	0.085	128	169	29.90	16.00	4442	F.T
50-SFB-11S-0.76	0.27	0.066	140	179	26.61	19.00	4257	F.T
50-SFB-11S-1.0	0.45	0.049	145	179	30.60	17.52	4883	F.T

* Service load is defined as 65 kN,** D.T.S is diagonal tension shear failure and F.T is flexural tension failure.

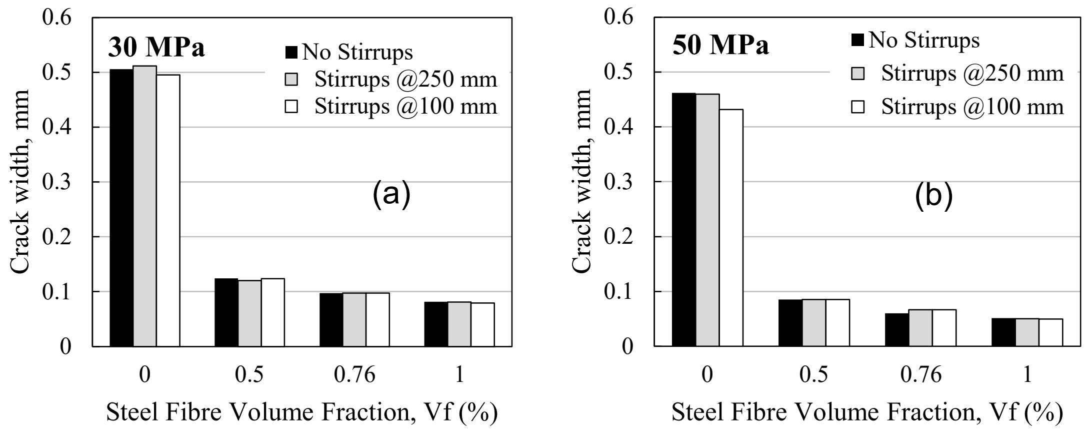

Figure A-9: Crack width comparison for different beam cases for (a) 30 MPa concrete strength, (b) 50 MPa concrete strength

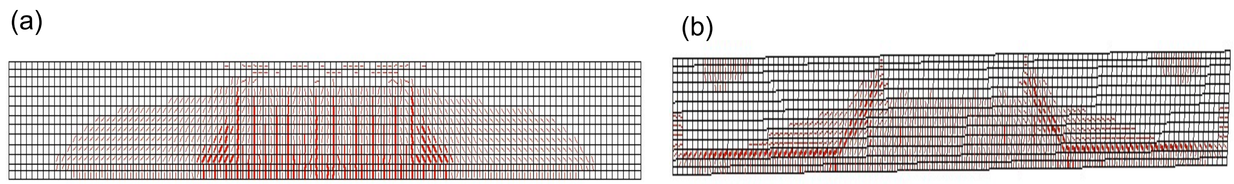

Figure A-10: Failure mode at peak load for beams with 30 MPa concrete without stirrups (a) V_f = 0.5%, (b) V_f = 0%.

A.5 Conclusions and Recommendations

A SFRC constitutive model was generated using the inverse analysis for two different concrete strengths and three different steel fibre contents. The constitutive model was used to model full-scale beams with different shear reinforcement configurations to study the effect of steel fibre content, concrete strength and stirrups on the beam's strength, ductility, deflection, and crack width. Based on the results presented in this paper, the following conclusions can be drawn:

- The inverse analysis can be successfully implemented in VecTor2® to appropriately determine the tensile σ-ε relationship of SFRC beams.

- The developed tensile σ-ε relationship is element-size dependent. For FEA analysis incorporating SFRC beams, the element size can be decided upon beforehand and the tensile σ-ε relationship can be generated accordingly.
- Beam strength and ductility significantly increased with an increase in the steel fibre percentage for typical simply supported beams with 30 MPa and 50 MPa.
- The failure mode changed from shear diagonal failure to flexural failure and crack width decreased significantly by adding steel fibres. Additionally, the higher the concrete strength the lower the crack width. In addition, the stirrups did not influence on the crack width in service loading and the stirrups can be partially replaced by steel fibres.

Based on the results, there is promise in using different chopped fibre with low modulus of elasticity materials such as GFRP to improve their shear resistance and crack width. These results should then be used to give predictions of experimental full scale FRP beams that are planned to evaluate the shear performance of reinforced beams with chopped fibers.

References

Abbas, A. A., Syed Mohsin, S. M., Cotsovos, D. M., and Ruiz-Teran, A. M. 2014. Shear Behaviouro Steel-Fibre-Reinforced Concrete Simply Supported Beams. *Proceedings of the Institution of Civil Engineers-Structures and Buildings*, **167**(9), 544-558.

Aldossari, K.M. 2014. Behavior of High Strength Steel Fibers Reinforced Concrete Ground Slabs. Master, King Saud University, Saudi Arabia.

Barros, J. A., and Figueiras, J. A. 2001. Model For The Analysis of Steel Fibre Reinforced Concrete Slabs on Grade.*Computers & Structures*, **79**(1), 97-106.

Blazejowski, M. 2012. Flexural Behaviour Of Steel Fibre Reinforced Concrete Tunnel Linings.

Cucchiara, C., La Mendola, L., and Papia, M. 2004. Effectiveness Of Stirrups And Steel Fibres As Shear Reinforcement. *Cement and concrete composites*, **26(**7), 777-786.

Ding, Y., You, Z., and Jalali, S. 2011. The Composite Effect of Steel Fibres And Stirrups on The Shear Behaviour of Beams Using Self-Consolidating Concrete." *Engineering structures*, **33**(1), 107-117.

Dinh, H. H. (2009). "Shear Behavior of Steel Fiber Reinforced Concrete Beams without Stirrup Reinforcement."

Elsaigh, W., Robberts, J., and Kearsley, E. 2004. Modelling Non-Linear Behaviour of Steel Fibre Reinforced Concrete." *6th International RILEM Symposium on Fibre Reinforced Concretes*, 837-846.

Hemmy, O. 2002. Recommendations for finite element analysis of FRC–report of subtask 3.5.*Brite-Euram project BRPR-CT98-0813: Test and Design Methods for Steel Fibre Reinforced Concrete, Project funded by the European Community under the Industrial and Materials Technologies Programme (Brite-Euram II)*.

Kohoutkova, A., Kristek, V., and Broukalova, I. 2004. Material Model of FRC-Inverse Analysis. *Proc., Fibre-reinforced Concretes: Proceedings of the Sixth International RILEM Symposium*, RILEM Publications, 857-864.

Labib, W. A. 2008. An experimental study and finite analysis of punching Shear Failure In Steel Fibre-Reinforced Concrete Ground-Suspended Floor Slabs. Liverpool John Moores University.

Lim, D., and Oh, B. 1999. Experimental And Theoretical Investigation on The Shear of Steel Fibre Reinforced Concrete Beams." *Engineering structures*, **21(**10), 937-944.

Lim, T., Paramasivam, P., and Lee, S. 1987. "Analytical Model for Tensile Behavior of Steel-Fiber Concrete." *ACI Materials Journal*, **84**(4).

Lok, T.-S., and Pei, J.-S. 1998. Flexural Behavior of Steel Fiber Reinforced Concrete. *Journal of Materials in Civil engineering*, **10**(2), 86-97.

Minelli, F., Conforti, A., Cuenca, E., and Plizzari, G. 2014. Are Steel Fibres Able to Mitigate or Eliminate Size Effect in Shear?" *Materials and structures*, **47**(3), 459-473.

Thomas, J., and Ramaswamy, A. 2007. Mechanical Properties of Steel Fiber-Reinforced Concrete. *Journal of materials in civil engineering*, **19(5),** 385-392.

Tlemat, H., Pilakoutas, K., and Neocleous, K. 2006. Modelling of SFRC Using Inverse Finite Element Analysis. Materials and Structures, **39(2),** 221-233.

Vandewalle, L. (2000). Recommendations of RILEM TC 162-TDF: Test and design methods for steel fibre reinforced concrete." Materials and Structures/Materiaux et Constructions, 33(225), 3-5

Wong, P., Vecchio, F., and Trommels, H. 2013. Vector2 & Formworks User's Manual Second Edition.Toronto,Canada

B CHOPPED FIBRE DOSAGE AND MATERIAL EFFECTS ON THE FRESH PROPERTIES OF NORMAL STRENGTH AND DENSITY CONCRETE

B.1 Introduction.

Chopped fibre reinforced concrete (CFRC) acts as a structural reinforcement for concrete and is most often used in shotcrete tunnel walls, bridge decks, road pavements, and concrete slabs. Plain concrete has a low tensile strength compared to its compressive strength. The service life and post-cracking behaviour of concrete mixtures can be improved by adding chopped fibres. One of the main reasons for this growing use of chopped fibres is the possibility of replacing shear reinforcement with chopped fibres in structural applications (Alguhi and Tomlinson 2019; Ding et al. 2011). These chopped fibres can also improve ductility (Abbas et al. 2014; Alguhi and Tomlinson 2019), mitigate the size effect for shear (Minelli et al. 2014), and can change failure modes from brittle shear failure to a more ductile flexural failure (Abbas et al. 2014; Alguhi and Tomlinson 2019; Cucchiara et al. 2004). Even though there are various improvements in the mechanical properties of hardened concrete when using chopped fibres, the use of fibres reduces the flowability of fresh concrete (Abdelrazik and Khayat 2020; Abousnina et al. 2021; Carroll and Helminger 2016; Gültekin et al. 2022), which causes negative impact on concrete's workability. In particular, these effects may cause challenges with fresh concrete mixing, handling, pouring, compaction, and finishing.

Several researchers have studied the effect of chopped fibre on fresh concrete properties (Abdelrazik and Khayat 2020; Abousnina et al. 2021; Carroll and Helminger 2016; Gültekin et al. 2022). However, there are limited studies that evaluate the performance of glass fibres and a combination of steel and -glass fibres on fresh concrete properties. Glass fibre has a higher modulus of elasticity, tensile strength, weight and lower water absorption compared to synthetic, and natural fibres (Madhkhan and Katirai 2019); these properties improve the mechanical behaviour of normal strength concrete (NSC). Glass fibres contribute more to the durability performance of high alkalinity concretes. Thus, this study evaluates the effect of dosage and materials of steel and glass fibres and a combination of these two chopped fibres on workability and densities for normal concrete strength (NSC).

B.2 Experimental Program

For conventional concrete, workability is the main factor that determines the optimum upper limits of chopped fibre dosage. Fibre dosages that are too large are result in issues with the mechanical properties (such as workability) of fresh concrete mixtures. However, fibre dosages that lead to acceptable workability or consistency (excessive fluidity can cause concrete ingredient segregation), can enhance the mechanical properties of concrete mixtures. Sufficient density is required to sustain a particular loading and provide durable concrete. Larger density concretes are often stronger and more durable than lower density concretes since there are minimum voids and water absorption capacity.

B.1.1 Materials

The main binder used is Type GU cement (70%), and the supplementary binder was fly ash (30%), which is a common ratio for concretes in Alberta. This ratio was selected to improve the concrete's long term strength and durability (Johnston 1996); the cement specifications are according to CSA A3000 and ASTM C150. Fly ash type F was used to increase strength without reducing the workability of cementitious paste. Fly ash is one of the construction industry's most used pozzolans. Class F-fly ash is classified based on ASTM C618 and originates from anthracite and bituminous coals. A high range water reducer-HRWR Sika® ViscoCrete® 1000 was added into concrete mixtures to reduce water content and improve workability since adding more water to increase the workability (or slump) resulted in a weaker concrete.

Coarse and fine aggregates were selected to be typical aggregates used in normal strength-ready mix concrete in the Edmonton, Canada region. Pea gravel with a maximum size of 20 mm was used as the coarse aggregate in this study, and natural river sand with a maximum particle size of 4.75 mm was used as fine aggregate. The bulk specific gravity and water absorption of coarse and fine aggregates are (2.6 and 2.8) and (1.32 and 1.43) %, respectively. Two different chopped fibres were used: hooked end steel fibres (SF) and AR-glass fibres (GF) as shown in Figure B-1; Table B-1 gives the properties of the fibres obtained from their manufacturers. The hooked end steel fibres with high fibres lengths were used in this study, given that the slump of fresh SFRC mixture presents an increasing trend with steel fibre length increasing (Han et al. 2019). AR-glass fibres were used in this study for extra durability as well as their expected lower demand for water absorption and increased chemical resistance compared to other chopped fibres as steel, and natural fibres.

Table B-1: Properties of steel and glass fibres

Properties	SF	GF
Diameter (mm)	0.92	0.54
Length (mm)	50	36
Aspect ratio (length/diameter)	54	67
Tensile modulus of elasticity (GPa)	200	72
Tensile strength (MPa)	1100-1500	1200-1800
Specific gravity	7.75	2.68

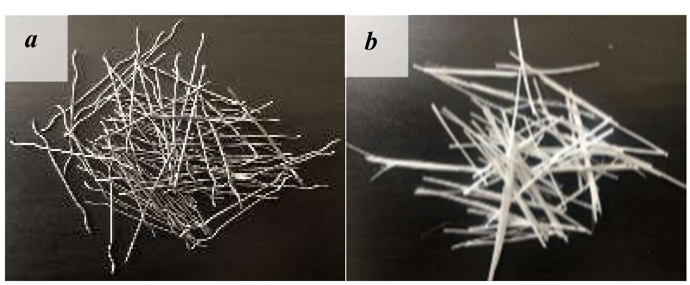

Figure B-1: Chopped fibres: (a) steel and (b) glass.

B.1.2 Preparation

The ACI Absolute Volume method (ACI 211.1-91 1991) was used to design trial concrete mixtures. This method is widely used in North America; it is generally accepted and convenient for normal concrete (ACI 211.1-91 1991). Ten mixtures were designed with a total volume of 0.08 m^3 per batch, one control mix and nine CFRC mixtures. These mixtures were developed after completing trial batches that are further described in Section 2.2.1. The CFRC mixtures were divided into those that used steel fibres (SF), those that used glass fibres (GF), and those that used a combination of steel and glass as a hybrid (H). Three different fibre contents (0.5, 1.0, and 1.5% volume fraction) were studied for both steel and glass fibres. For the hybrid mixtures, a constant fibre volume fraction of 1.0% was used with the three ratios of steel to glass fibres: 0.75% steel + 0.25% glass, 0.50% steel + 0.50% glass, and 0.25% steel + 0.75% glass, as shown in Table B-2. The optimum volumetric percentage of CFRC dosages should be in the range of between 0.5% to 1.5%. Dosages larger than 1.5% were not consider since there are physical difficulties in providing a homogenous CFRC leading to a decrease in compressive strength compared with plain concrete (Altun et al. 2007). The addition of chopped fibres less than 0.5% will not affect concrete workability remarkably; however, this amount will not have a meaningful effect on the post-cracking behaviour of concrete (Branston et al. 2016) which is the main goal of this overall research program.

A portable electrical drum mixer with a capacity of 155 litres was used for CFRC mixing. The drum mixer was rinsed with water and completely drained before each batch was mixed. First, fine, and coarse aggregates were added and mixed for one minute. Then, the cementitious material (cement+ fly ash) was added and mixed for 2 more minutes. After that, water was added gradually for 2-3 minutes. Then the chopped fibres were added gradually for 3-4 minutes. Finally, the superplasticizer was added to the mixture. The total mixing time for each CFRC batch was about 8~10 minutes. The concrete was placed in the molds in 2 layers and compacted by using a vibrating table with a frequency of 60 to 90 Hz. The specimens were demoulded 24 hours after casting and placed in a lab room (temperature 25±2ºC and relative humidity 35± 5%) and then these samples were placed in a controlled humidity room (temperature 20±2ºC and relative humidity 70±5%).

Table B-2: Mixture components and material quantities

TASK	Mix #	Mix ID	Fibre Type and Dosage	Batch vol.= 0.08 m^3								
				W/CM	Binder per m^3	Cement (kg)	Fly ash (kg)	Water* (kg)	CA (kg)	FA (kg)	Fibre (kg)	S.P (kg)
I	1	Control	No fibres	0.35	400	22.40	9.60	13.30	91.72	61.15	0.00	0.16
II	2	SF-0.5	0.5% SF	0.35	400	22.40	9.60	13.29	91.08	60.72	3.00	0.16
	3	SF-1.0	1.0% SF			22.40	9.60	13.27	90.44	60.29	6.00	0.16
	4	SF-1.5	1.5% SF			22.40	9.60	13.26	89.79	59.86	9.00	0.16
III	5	GF-0.5	0.5% GF	0.35	400	22.40	9.60	13.29	91.08	60.72	1.03	0.16
	6	GF-1.0	1.0% GF			22.40	9.60	13.27	90.44	60.29	2.06	0.16
	7	GF-1.5	1.5% GF			22.40	9.60	13.26	89.79	59.86	3.10	0.16
IV	8	H-1	1.0% (0.75%SF+0.25%GF)	0.35	400	22.40	9.60	13.27	91.08	60.29	___	0.16
	9	H-2	1.0% (0.50%SF+0.50%GF)			22.40	9.60	13.27	90.44	60.29	___	0.16
	10	H-3	1.0% (0.25%SF+0.75%GF)			22.40	9.60	13.27	89.79	60.29	___	0.16

SF: Steel fibre, GF: Glass Fibre, H: Hybrid, CM: Cementitious materials, CA: Coarse aggregate, FA: Fine aggregate, and SP: Superplasticizer.*Including absorption

B.1.3 Trial mixtures

Prior to batching the main mixtures, eleven trial mixtures were produced (Table 3) to optimize the mixture for CFRC. The target was compressive strengths between 35 and 55 MPa, which is within the range of compressive strength (25-55) MPa for NSC (Voort et al. 2009), and minimum slump of 150 mm for mixtures without fibres. Supplementary cementitious material (fly ash) was added to all trial mixes as 30% of the binder. Trial mixes T1 to T6 were prepared by hand to investigate concrete bleeding (a phenomenon in which free water in the mixture rises up to the surface) and mixture volume. The remaining mixtures (T7 to T11) were done using mini portable electrical drum mixer with a capacity of 50 litres to simulate the large electrical drum mixer with a capacity of 155 litres, which was used to mix large batches. The trial mixes T1 and T2 had the water to cementitious materials ratio w/cm of 0.45, and this results in both of them having concrete bleeding, as seen in Figure B-2(a) based on optical observations. The w/cm for T3 decreased to 0.35; this ratio leads to a decrease in the concrete bleeding and provides optimum volume (actual and measured cylinder volume are similar), as shown in Figure B-2(b) and obtained the estimated 28-day compressive strength of 44.9 MPa (see Table B-3).

Table B-3: Trial mixes for the NSC

Hand mixing						
Trial Mixes	**T1**	**T2**	**T3**	**T4**	**T5**	**T6**
Target Strength (MPa)	35-55	35-55	35-55	35-55	35-55	35-55
Max. Agg. Size (mm)	20	20	20	20	20	20
Material proportions per 1 m^3						
Cement-General Use type (kg)	280	280	280	315	280	280
Fly Ash-type F (kg)	120	120	120	135	120	120
w/cm ratio	0.45	0.45	0.35	0.35	0.35	0.35
Fine Agg. - River Sand (kg)	651	721	764	729	754	754
Coarse Agg. - Pea Gravel (kg)	977	1082	1147	1093	1130	1130
Steel Fibers (kg)	----	----	----	----	75	----
Glass Fibers (kg)	----	----	----	----	----	25.8
7-days water tank density (kg/m^3)	*	*	2440	2454	2477	2421
7-days water tank curing strength (MPa)	*	*	29.4	32.5	26.2	25.6
Estimated 28 days strength ** (MPa)	*	*	44.9	48.6	40.9	40.2

Electric drum mixer					
Trial Mixes	**T7**	**T8**	**T9**	**T10**	**T11**
Target Strength (MPa)	35-55	35-55	35-55	35-55	35-55
Max. Agg. Size (mm)	20	20	20	20	20
Material proportions per 1 m^3					
Cement-General Use type (kg)	280	315	280	315	280
Fly Ash-type F (kg)	120	135	120	135	120
w/cm ratio	0.35	0.35	0.35	0.35	0.35
Fine Agg. -River Sand (kg)	764	729	748	712	748
Coarse Agg. -Pea Gravel (kg)	1147	1193	1122	1069	1122
Steel Fibers (kg)	----	----	112.5	112.5	----
Glass Fibers (kg)	----	----	----	----	38.7
7-days water tank density (kg/m^3)	2484	2656	2490	2608	2462
7-days water tank curing strength (MPa)	38.6	40.8	33.7	37.6	29.1
Estimated 28 days strength** (MPa)	55.8	58.3	50.0	54.6	44.5

*Concrete bleeding occurs due to a high w/cm ratio.
**Strength at 28 days estimated based on $f'_{c,28} = 3(f'_{c,7})^{0.8}$ (Kabir et al. 2012)

The cement and fly ash proportions for trial mixes T1, T2, and T3 were identical, but for T4, the cement quantity was larger compared to T1, T2, and T3. Trial mixes T5 and T6 were CFRC mixes with 1% of steel, and glass fibres, respectively. Trial mixes T9, T10 and T11 were CFRC mixes with 1.5% of fibre volume, and T9 and T10 were SFRC mixes, but for T10, the cement quantity was larger compared to T10.

To have reasonable workability of CFRC mixes, the slump of control mixes should not be less than 150 mm, to provide adequate workability after the addition of steel fibres (>50 mm) (Bindiganavile et al. 2012); therefore, three trials of adding superplasticizer (0.4%, 0.5% and 0.6%) by weight of the binder were performed, and from the trial mixes, it was observed that the best amount was 0.5% by weight of the binder to get the target slump test for the control mix.

From the trial mixes described in this section, one mix was selected to evaluate the mechanical properties of CFRC. The selected mixes included a maximum aggregate size of 20 mm and achieved the target strength and workability was T3.

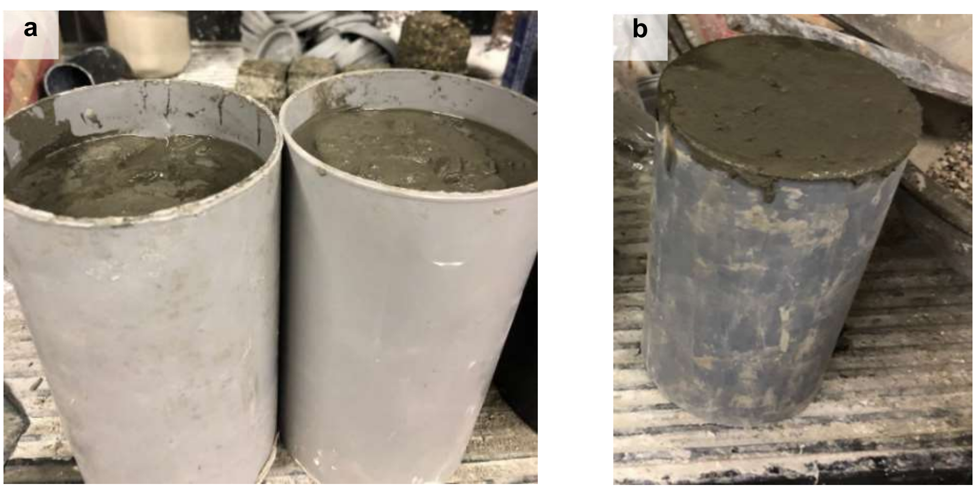

Figure B-2: (a) Concrete bleeding and (b) optimum volume.

B.1.4 Fresh concrete and densities measurements

Workability was measured using slump tests according to ASTM C143/C143M-15 and Ve-Be time tests according to ASTM C1170/C1170M-14 of all mixtures (Figure B-3). Since adding chopped fibres to the concrete reduces workability (Han et al. 2019; Liao et al. 2020), a minimum slump of 150 mm for plain concrete was targeted to provide adequate workability after the addition of chopped fibres. Fresh, one-day dry at lab room and 28-day humidity room densities were obtained as per ASTM C138/C138M-17a.

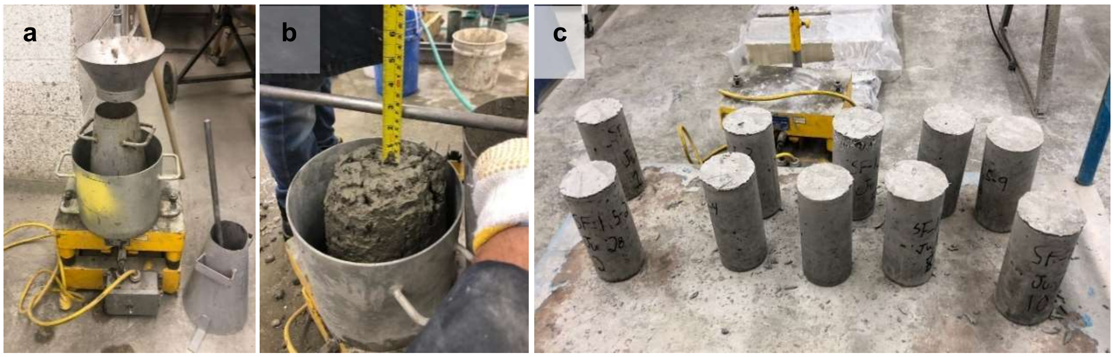

Figure B-3: Fresh concrete and densities measurements: (a) Ve-Be time test, (b) Slump test and (c) cylinders after one-day lab room temperature curing

B.3 Results and Discussion

The results from these tests are summarized in Table B-4. As expected, and shown in Figure B-4(a), there were meaningful reductions for all slump values with increased fibre content. The glass fibre mixtures had less workability than steel fibre mixtures. This is not only because glass fibres obstruct the mobility of the mixture's ingredients, but also these multifilament strands of glass fibre that are not intended to separate tend to do so and render the mixture unworkable because of their greatly increased surface area (Johnston 2014), which was also observed in the hybrid mixtures. For hybrid mixtures, the slump decreased as glass fibre content increased. The Ve-Be time results show a similar trend in terms of reducing the workability by adding chopped fibres, and the Ve-Be time increased as the fibre dosage increased. Glass fibre mixtures also had less workability compared to steel fibre mixtures; this is reflected in higher Ve-Be time results for glass fibre, and this is noticed in hybrid mixtures as the more the glass fibres, the higher the Ve-Be time results, as shown in Figure B-4(b).

Table B-4: Summary of test results

Mix ID	Ve-Be Time (seconds)	Slump (mm)	Density (kg/m^3)		
			Fresh	One-day dry at lab room	28-day at humidity room
Control	5.71	155	2523±51	2500±56	2456±29
SF-0.5	8.94	70	2651±50	2623±33	2586±30
SF-1.0	12.92	65	2668±35	2643±33	2615±27
SF-1.5	16.70	45	2707±41	2686±36	2640±33
GF-0.5	9.36	65	2419±18	2404±11	2384±19
GF-1.0	14.82	50	2448±13	2438±11	2408±09
GF-1.5	17.69	35	2438±20	2422±18	2407±15
H-1	13.15	60	2481±15	2454±17	2446±19
H-2	13.95	55	2454±16	2429±14	2417±07
H-3	14.53	50	2441±22	2417±16	2406±13

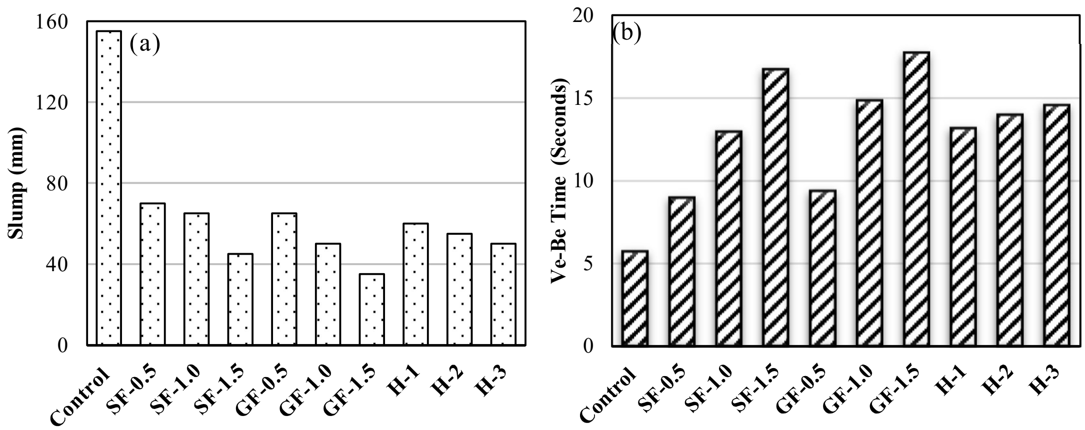

Figure B-4: Workability results obtained in the (a) slump and (b) Ve-Be tests

The effect of chopped fibres dosage and materials on workability measurements is shown in Figure B-5. The results show an inversely proportional relationship between slump results and increasing chopped fibre dosages, so there was a dramatic decrease in workability with increasing fibre content for both slump and Ve-Be time. The slump test is more effective in evaluating the influence of adding fibres, especially glass fibres. The Ve-Be time results also show an inversely proportional trend with increasing the chopped fibres dosages for glass and steel fibres, respectively.

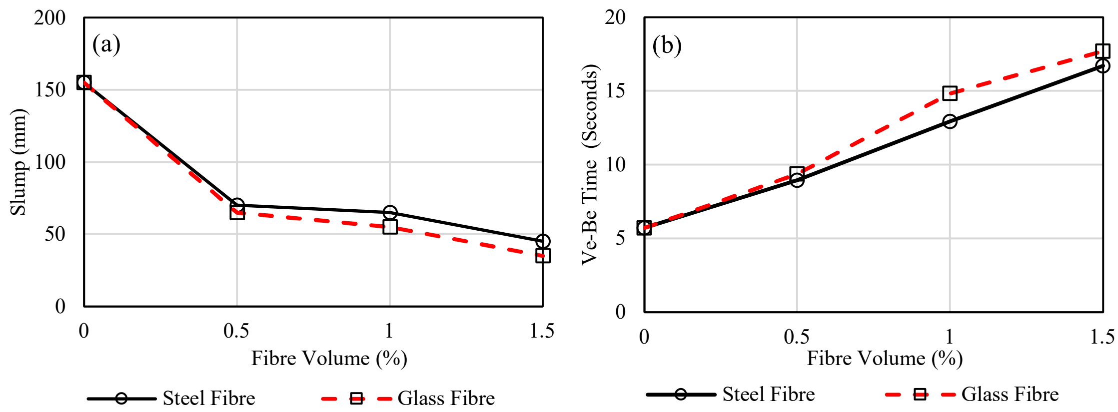

Figure B-5: Effect of the chopped fibre material and dosages on (a) the slump and (b)Ve-Be time results of the CFRC

There was a good correlation between the slump and Ve-Be time results, as shown in Figure B-6. When slump is less than around 70 mm the Ve-Be time increases more rapidly. There is almost no variation in the Ve-Be results when the slump value exceeds 70 mm regardless of fibre type and dosage. This demonstrates that the Ve-Be time test is more suitable for verifying the workability of stiff concretes. In other words, Ve-Be time results may be beneficial and confirm that the slump test has limited effect for evaluating CFRC because non-water-absorbent fibres reduce the stability or cohesion of the mixture under static conditions (the main factor evaluated in slump tests) of the mixture due to their needle like shape and high specific surface area. The Ve-Be test can better evaluate how concrete behaves during compaction where this mechanized action allows fibres to rearrange, thus measuring workability from the perspective of concrete's mobility and compatibility for CFRC. However, the Ve-Be time test is less applicable for conditions in which the concrete is very plastic with slump results (125-190) mm (ACI 211.3R-02 2002).

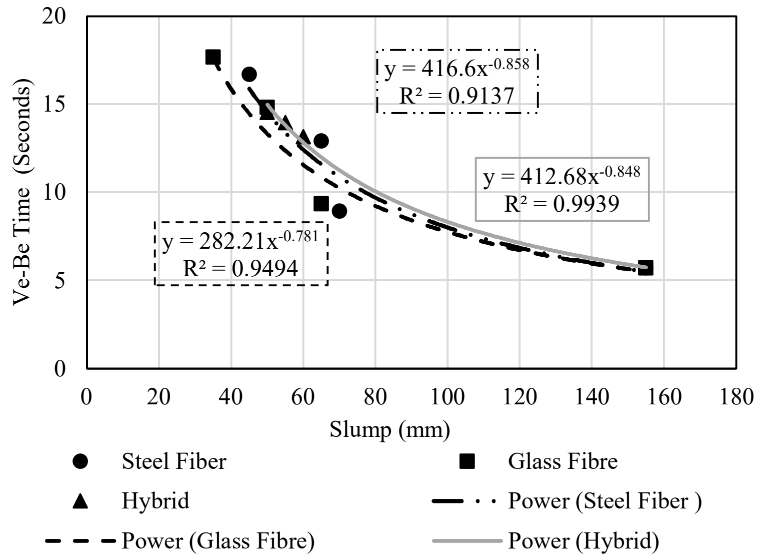

Figure B-6: Correlation between all the slump values and the Ve-Be time.

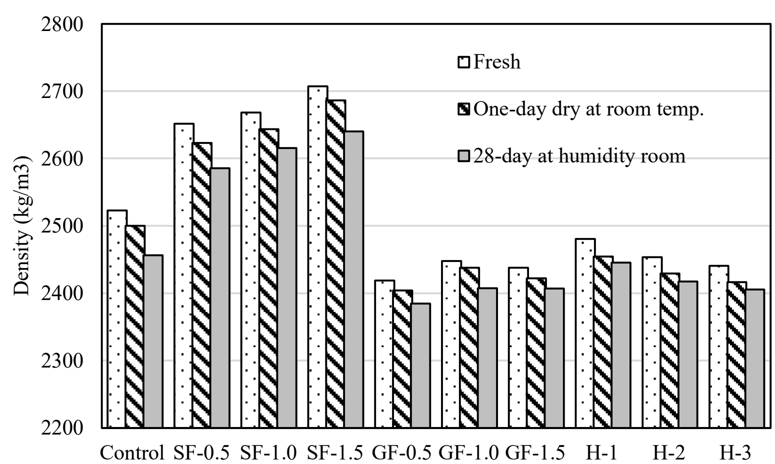

Figure B-7: Fresh, one-day dry at lab room temp., and 28-day at humidity room densities of CFRC cylinders

Figure B-7 shows the fresh, one-day dry, and 28-days at humidity room densities of CFRC cylinders. Adding steel fibres increases concrete densities due to steel's large specific gravity (7.75) g/m3 of steel fibre, which is almost three times the replacement aggregate specific gravity (2.6-2.8) g/m3 in the mixture. There was a minor reduction in the densities of glass fibre reinforced cylinders due to a slight decrease in the specific gravity of glass fibre (2.62) compared to the replacement aggregate specific gravity. This was also observed in the hybrid mixes where the increased ratio of glass fibres, the less the resulting densities. Table B-4 shows the results summary of all cylinders.

B.4 Conclusions and Recommendations

Ten mixtures were prepared to investigate the effect of two fibre types (steel and glass) and a combination of them with volume fractions of 0.5, 1.0, and 1.5% on the fresh concrete's properties, such as workability and densities. Workability was evaluated using both slump and Ve-Be time tests. Three densities (fresh, one-day lab room and 28-day humidity room) of ten samples from each mix were measured. Based on the results reported in this paper, the following conclusions can be drawn:

1. Adding chopped fibres decrees workability remarkably, and there were considerable reductions for all slump values with increased fibre content, and glass fibre mixtures had less workability than steel fibre mixtures. This was further shown in the hybrid mixtures, where workability decreased as the dosage of glass fibres increased.
2. A good correlation between the obtained results between the slump and Ve-Be time can be seen based on this study's data.
3. The Ve-Be time test is more appropriate to evaluate the workability of stiff concretes such as CFRC because it gives an indication about the compatibility and the mobility aspect of freshly mixed concrete while slump tests evaluate mix response in static conditions.
4. The density of CFRC depend on specific gravity and dosage of chopped fibres so adding steel fibres increases concrete density. For this study, this increase ranged between 5.3 and 7.5% (after 28 days) which is enough of an increase that designers should consider the influence of steel fibres on self-weight of concrete elements. That said, there was a minor

reduction in the densities of glass fibre cylinders (<3.0%) which indicates that their effect on member self-weight can be conservatively ignored. This was also shown in the hybrid mixtures, where density decreased as glass fibre dosage increased.

This study used gravel with a maximum size of 20 mm, so the maximum aggregate size and shape effects, which are essential factors that will play the key role in fresh concrete's properties and densities of CFRC should be investigated in future. Studying the influence of the geometric properties of chopped fibres such as aspect ratio and fibre profile (e.g., straight, hooked) as well as other fibre types (e.g., basalt, polypropylene) on concrete's fresh properties should be investigated further.

References

Abbas, A. A., Syed Mohsin, S. M., Cotsovos, D. M., and Ruiz-Teran, A. M. (2014). "Shear behaviour of steel-fibre-reinforced concrete simply supported beams." *Proceedings of the Institution of Civil Engineers-Structures and Buildings*, 167(9), 544-558.

Abdelrazik, A. T., and Khayat, K. H. (2020). "Effect of fiber characteristics on fresh properties of fiber-reinforced concrete with adapted rheology." *Construction and Building Materials*, 230, 116852.

Abousnina, R., Premasiri, S., Anise, V., Lokuge, W., Vimonsatit, V., Ferdous, W., and Alajarmeh, O. (2021). "Mechanical Properties of Macro Polypropylene Fibre-Reinforced Concrete." *Polymers*, 13(23), 4112.

ACI 211.1-91 (1991). "Standard Practice for Selecting Proportions for Normal, Heavyweight, and Mass Concrete (ACI 211.1-91)."

ACI 211.3R-02 (2002). "Guide for Selecting Proportions for No-Slump Concrete Reported by ACI Committee 211." *American Concrete Institute*, 1-26.

Alguhi, H., and Tomlinson, D. (2019). “Evaluation of Proposed Steel Fibre Reinforced Concrete Beams under Ultimate and Serviceability Limit State.” *CSCE Annual Conference.* Laval, Canada.

Altun, F., Haktanir, T., and Ari, K. (2007). “Effects of steel fiber addition on mechanical properties of concrete and RC beams.” *Construction and Building Materials*, 21(3), 654-661.

Bindiganavile, V., Lubell, A. S., and Shoaib, A. (2012). “SER# 294: Shear in Steel Fiber Reinforced Concrete without Stirrups.”

Branston, J., Das, S., Kenno, S. Y., and Taylor, C. (2016). “Mechanical behaviour of basalt fibre reinforced concrete.” *Construction and Building Materials*, 124, 878-886.

Carroll, J. C., and Helminger, N. (2016). “Fresh and hardened properties of fiber-reinforced rubber concrete.” *Journal of Materials in Civil Engineering*, 28(7), 04016027.

Cucchiara, C., La Mendola, L., and Papia, M. (2004). “Effectiveness of stirrups and steel fibres as shear reinforcement.” *Cement and concrete composites*, 26(7), 777-786.

Ding, Y., You, Z., and Jalali, S. (2011). “The composite effect of steel fibres and stirrups on the shear behaviour of beams using self-consolidating concrete.” *Engineering Structures*, 33(1), 107-117.

Gültekin, A., Beycioğlu, A., Arslan, M. E., Serdar, A. H., Dobiszewska, M., and Ramyar, K. (2022). “Fresh Properties and Fracture Energy of Basalt and Glass Fiber–Reinforced Self-Compacting Concrete.” *Journal of Materials in Civil Engineering*, 34(1), 04021406.

Han, J., Zhao, M., Chen, J., and Lan, X. (2019). “Effects of steel fiber length and coarse aggregate maximum size on mechanical properties of steel fiber reinforced concrete.” *Construction and Building Materials*, 209, 577-591.

Johnston, C. D. (1996). “Fly Ash Utilization Bridge Works “The University of Calgay

Johnston, C. D. (2014). *Fiber-reinforced cements and concretes*, Crc Press.

Kabir, A., Hasan, M., and Miah, M. K. "Predicting 28 days compressive strength of concrete from 7 days test result." *Proc., Proceedings of the International Conference on Advances in Design and Construction of Structures*, Citeseer, 18-22.

Liao, L., Zhao, J., Zhang, F., Li, S., and Wang, Z. (2020). "Experimental study on compressive properties of SFRC under high strain rate with different fiber content and aspect ratio." *Construction and Building Materials*, 261, 119906.

Madhkhan, M., and Katirai, R. (2019). "Effect of pozzolanic materials on mechanical properties and aging of glass fiber reinforced concrete." *Construction and Building Materials*, 225, 146-158.

Minelli, F., Conforti, A., Cuenca, E., and Plizzari, G. (2014). "Are steel fibres able to mitigate or eliminate size effect in shear?" *Materials and structures*, 47(3), 459-473.

Voort, T. V., Suleiman, M., and Sritharan, S. (2009). "Characterization of precast UHPC pile drivability." Contemporary Topics in Deep Foundations, 303-310

C NUMERICAL ANALYSIS.

C.1 Verification process.

Remarkably, the L-D response for both the restrained half-beam and the full-beam configurations is identical, as illustrated in Figure C-1 (a and b).

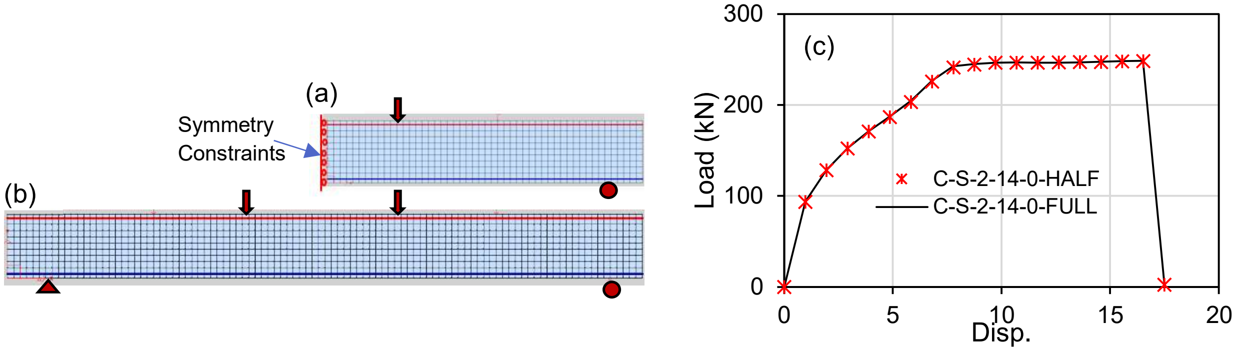

Figure C-1: The symmetry constrains check (a) half-beam with restrains (b) full beam (c) L-D response

C.1.1 Phase-I : Material model (This section is done in 4.5)

C.1.2 Phase-II : Full-Scale-RC

C.1.2.1 Full-Scale GFRP-RC.

Two experimentally tested GFRP-RC beams with simple supports were considered in this phase (Betschoga et al., 2021; El-sayed et al., 2007). Modeling was performed using VecTor2, involving various dimensions: (250 × 400 × 3250 mm) and (170 × 450 × 3900 mm), illustrated in **Figure** C-2 and Figure C-3. The Hybrid rectangular element with size (50 x 50) mm was selected after completing a sensitivity analysis, done by gradually decreasing mesh size till it stopped influencing the results. Results have shown good agreements between modelled and measured L-D responses and failure mode for all tests, as shown **Figure** C-2 (e and d) and Figure C-3 (e and d).

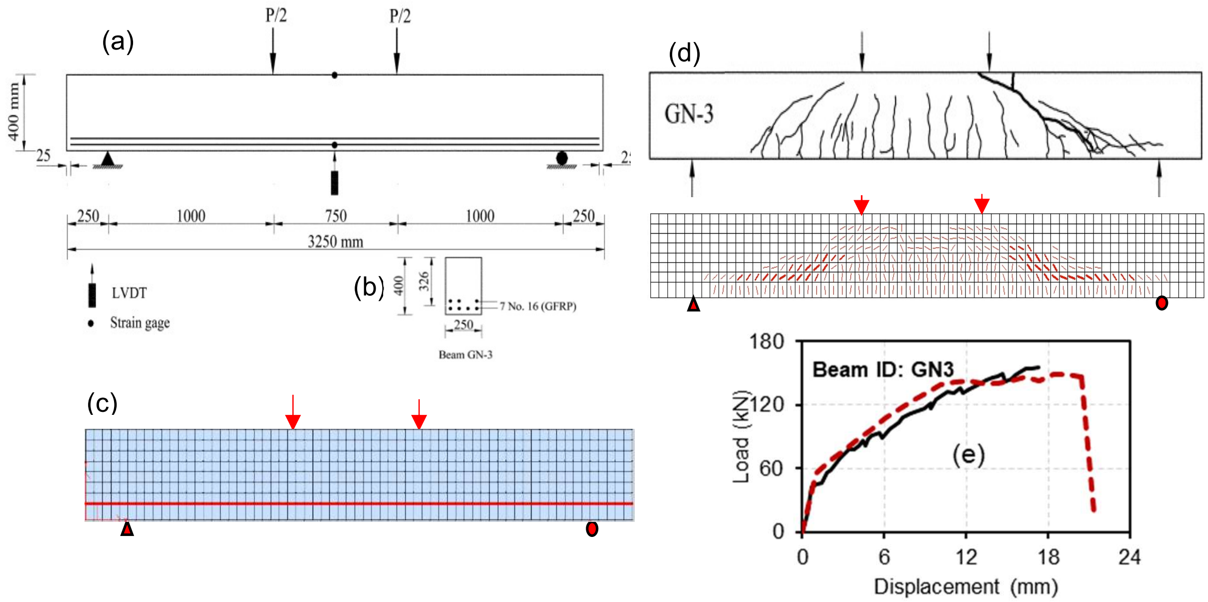

Figure C-2: (a) Test setup and dimensions, (b) cross-sectional details, (c)VecTor2 model, (d) Comparison of modeled and measured L-D responses, and (e) Comparison of modeled and measured failure modes. (El-sayed et al., 2007)

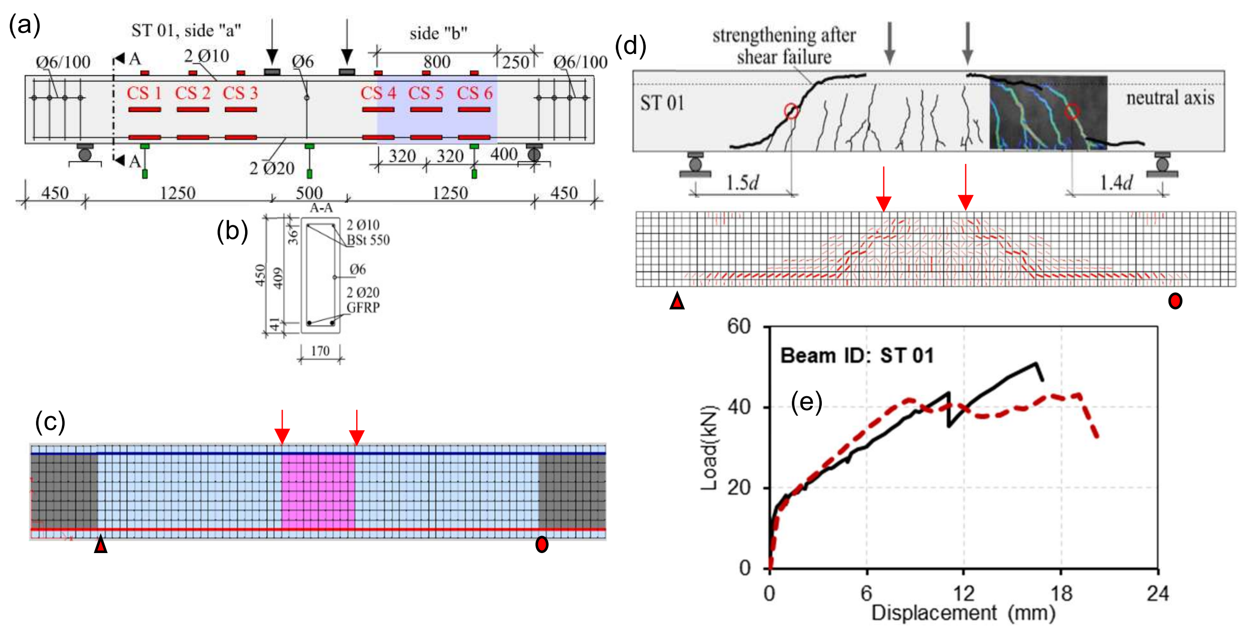

Figure C-3: (a) Test setup and dimensions, (b) cross-sectional details, (c)VecTor2 model, (d) Comparison of modeled and measured L-D responses, and (e) Comparison of modeled and measured failure modes. (Betschoga et al., 2021)

C.1.2.2 Full-Scale Steel-RC

During this stage of verification, the full-scale Steel-RC beam from (Minelli et al., 2014a) is modeled using the VecTor2 model. The comparison between experimental and FEA outcomes indicates good agreement in terms of pre-peak, peak load, and post-peak load-deflection responses, as shown in Figure C-4 (e). Additionally, the failure modes observed in both the experimental and FEA beams are correlated, as evident in Figure C-4 (d).

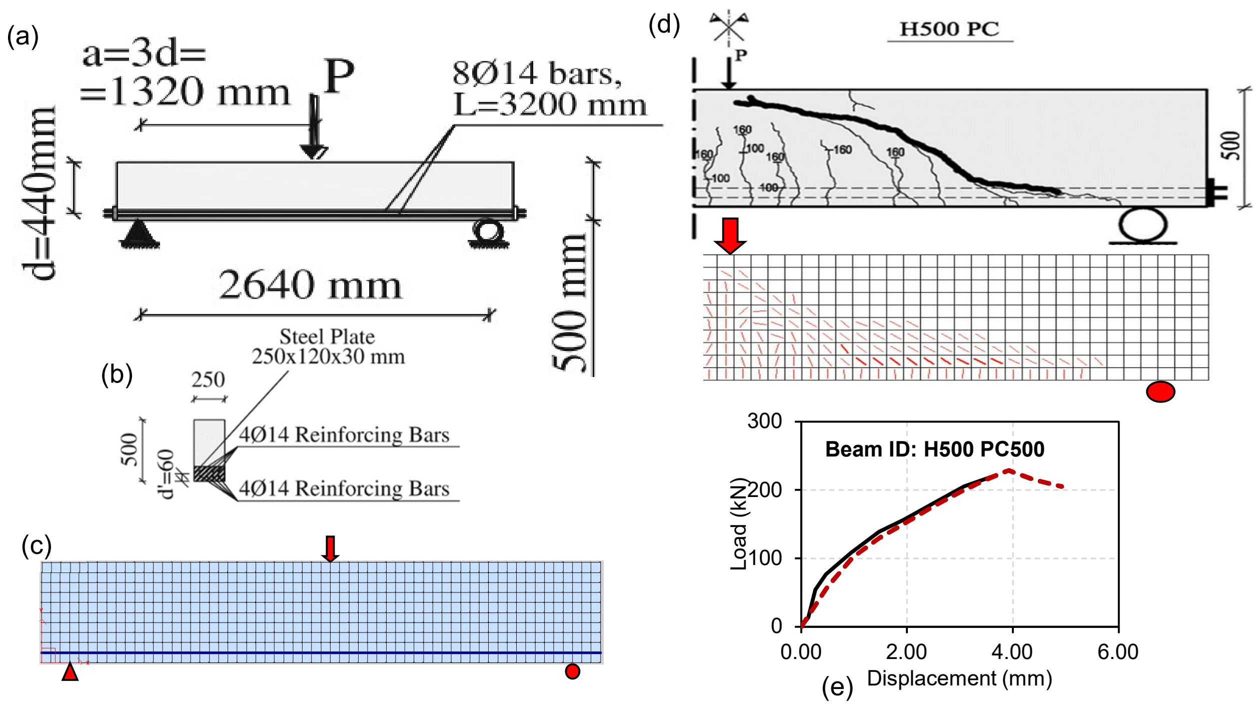

Figure C-4: (a) Test setup and dimensions, (b) cross-sectional details, (c)VecTor2 model, (d) Comparison of modeled and measured L-D responses, and (e) Comparison of modeled and measured failure modes

C.1.3 Phase-III : Full-Scale-RC-FRC.

The third verification level encompasses the evaluation of both primary reinforcement bars (SR and GFRP) and secondary reinforcement fibers (SFs and GFs) as reported in the literature review by (Issa et al., 2011; Minelli et al., 2014).

C.1.3.1 Full-Scale GFRP-GFRC.

An experimental large-scale GFRP beam conducted by (Issa et al., 2011) with dimensions of (150mm x 150mm x 1850mm), was modeled using VecTor2. This beam included 0.5% GFs as secondary reinforcement and featured an 8 mm steel shear stirrup at a spacing of 95 mm, as depicted in Figure C-5. Results indicate a strong correlation between the load-deflection response and failure pattern of both experimental and modeled beams.

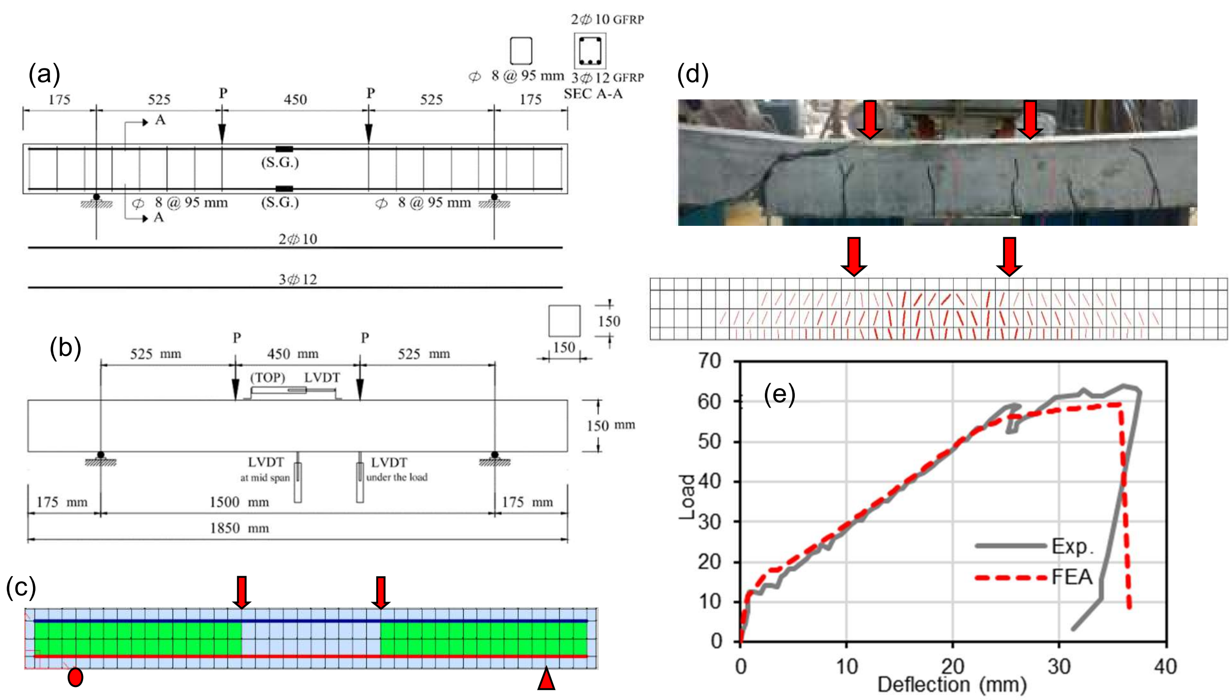

Figure C-5: (a) Test setup and dimensions, (b) cross-sectional details, (c)VecTor2 model, (d) Comparison of modeled and measured L-D responses, and (e) Comparison of modeled and measured failure modes.

C.1.3.1 Full-Scale SR-SFRC

The SR-SFRC full-scale beams (Minelli et al., 2014) were modeled in two different sizes: H500 (250 x 500 x 3200) mm, and H1000 (250 x 1000 x 6100) mm, as shown in Figure C-6 (a and b) and Figure C-8 (a and b), respectively. These beams were reinforced with 0.65% and 1.0% of hooked-end steel fibers, with an aspect ratio of 62.5 and a tensile strength of 1100 MPa. The reinforcement ratios were 1.12 and 1.07 for H500 and H1000, respectively. A comparison between the modeled and experimental results revealed a strong correlation in terms of load-deflection responses and failure patterns, as shown in Figure C-6 (d and e), Figure C-7 (d and e), and Figure C-8 (d and e), for H500 and H1000 beams, respectively.

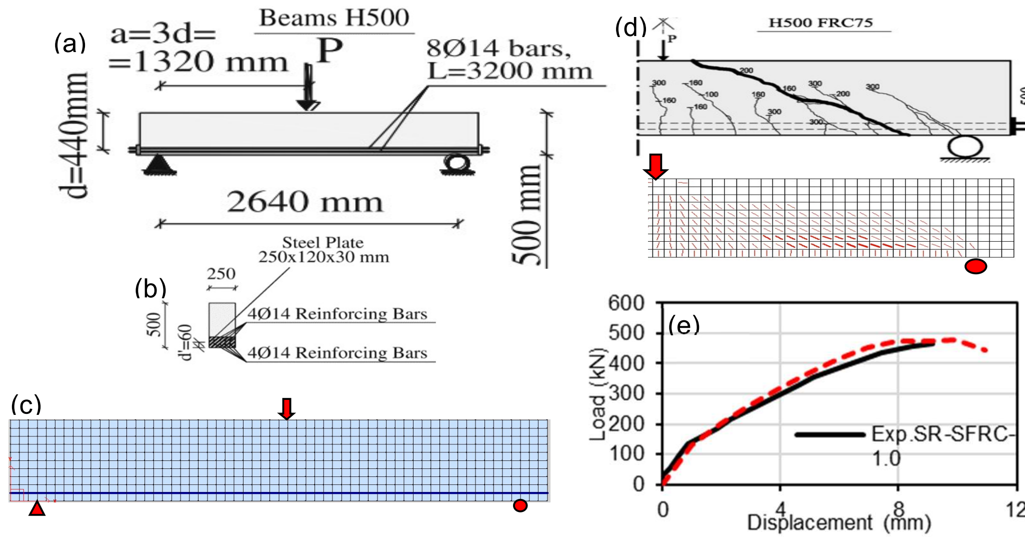

Figure C-6: (a) Test setup and dimensions, (b) cross-sectional details, (c)VecTor2 model, (d) Comparison of modeled and measured L-D responses, and (e) Comparison of modeled and measured failure modes.

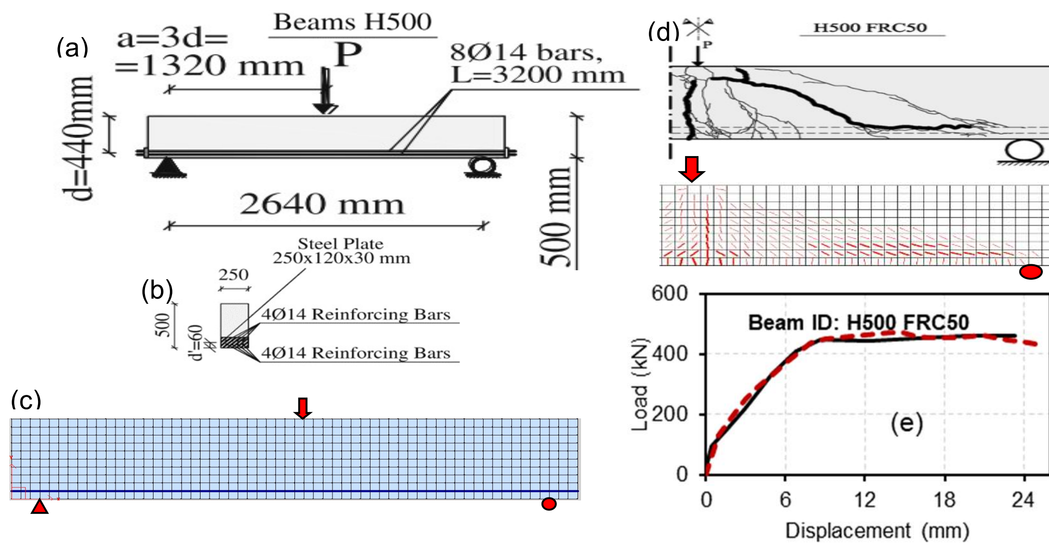

Figure C-7: (a) Test setup and dimensions, (b) cross-sectional details, (c)VecTor2 model, (d) Comparison of modeled and measured L-D responses, and (e) Comparison of modeled and measured failure modes.

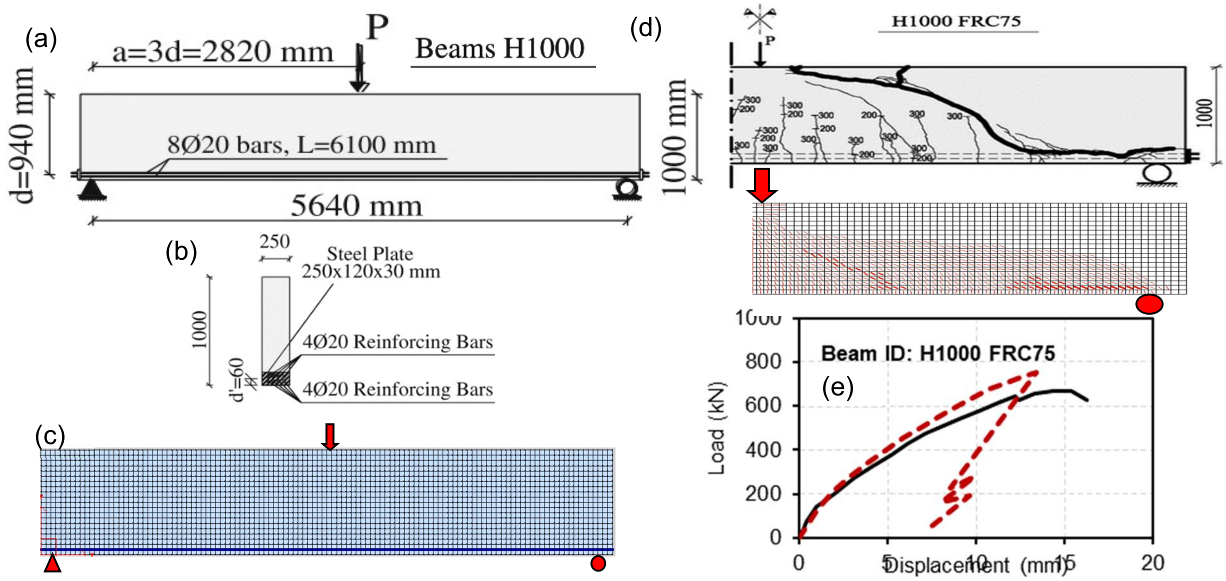

Figure C-8: (a) Test setup and dimensions, (b) cross-sectional details, (c)VecTor2 model, (d) Comparison of modeled and measured L-D responses, and (e) Comparison of modeled and measured failure modes.

C.2 Control Beam Analysis

C.2.1 Peak load of RC beams

Prior to examining influences from fibres, response from parameters investigated with plain (i.e., no fibres) concrete were investigated. Parameters include effects of shear span to depth ratio, *a/d*, reinforcement ratio, ρ, beam hight, h, and the type of reinforcement (steel and GFRP bars).

Figure C-9 shows influences of *a/d*, ρ, d, and reinforcement material on peak load. Generally, increase in peak load with higher ρ is more pronounced in steel-RC beams compared to GFRP beams, and this is attributed to the greater axial stiffness of steel bars, which is nearly three times that of GFRP.

For SR beams, particularly those with lower ρ (e.g., 0.51), stirrups enhance performance, albeit to a lesser extent than increasing the beam depth by 50%. However, for larger ρ (e.g., 1.1 and 2.1) in SR-RC beams, adding stirrups results in a superior increase in the peak load compared to increasing beam depth by 50%. Stirrups play a crucial role in confining the concrete and limiting diagonal cracks, which becomes increasingly important as the shear forces become more significant, which is associated with higher ρ. However, this scenario is different when dealing with GFRP beams, as adding stirrups improves peak load to a greater extent than increasing the beam depth for all ρ ratios, and this may due only one dominate shear failure mode for GFRP beams.

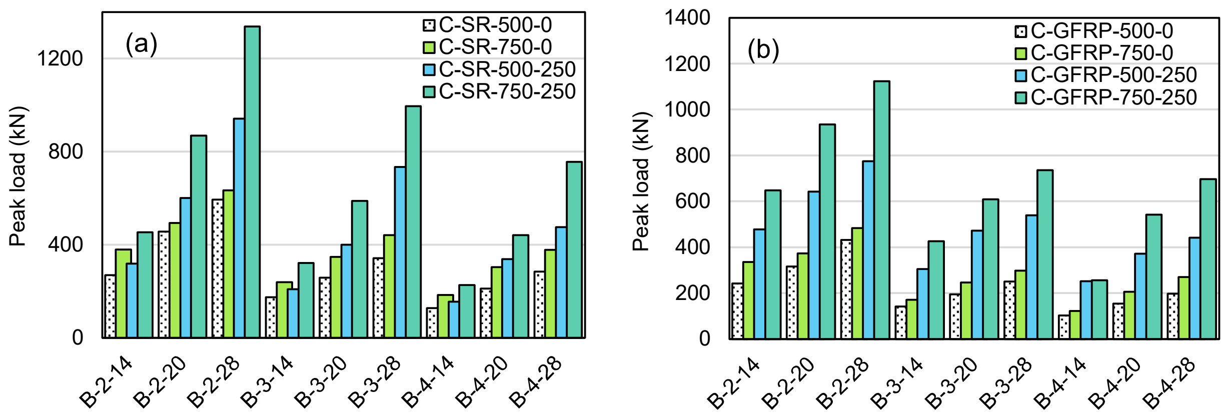

Figure C-9: Effect of a/d, ρ, d, and reinforcement on peak load for (a) SR and (b) GFRP beams.

C.2.2 Serviceability of RC beams

The investigation revolves around how certain parameters, such as the *a/d* ratio, *ρ*, and d, influence serviceability assessments, specifically crack width, deflection, and reinforcement strain affected the beams without fibres.

To explore the impact of *a/d* on serviceability, other parameters were held constant with ρ and *d* set at 1.1% and 500 mm, respectively. Service load was determined based on the most representative beam from this set, where the *a/d* ratio was 4 for both SR and GFRP beams. In Figure C-10, the impact of *a/d* on crack width, deflection, and reinforcement strain is shown. Despite different service loads for Steel-RC and GFRP-RC beams, they have consistent trends of increased crack width, deflection, and reinforcement strain with higher a/d ratios. For SR beams, there is a correlation between crack width and deflection. For instance, increasing *a/d* from 2 to 3 and from 3 to 4 results in a simultaneous increase in all parameters by 130% and 40%, respectively. This can be attributed to the amplified applied moment stemming from the increasing of the shear span (moment arm).

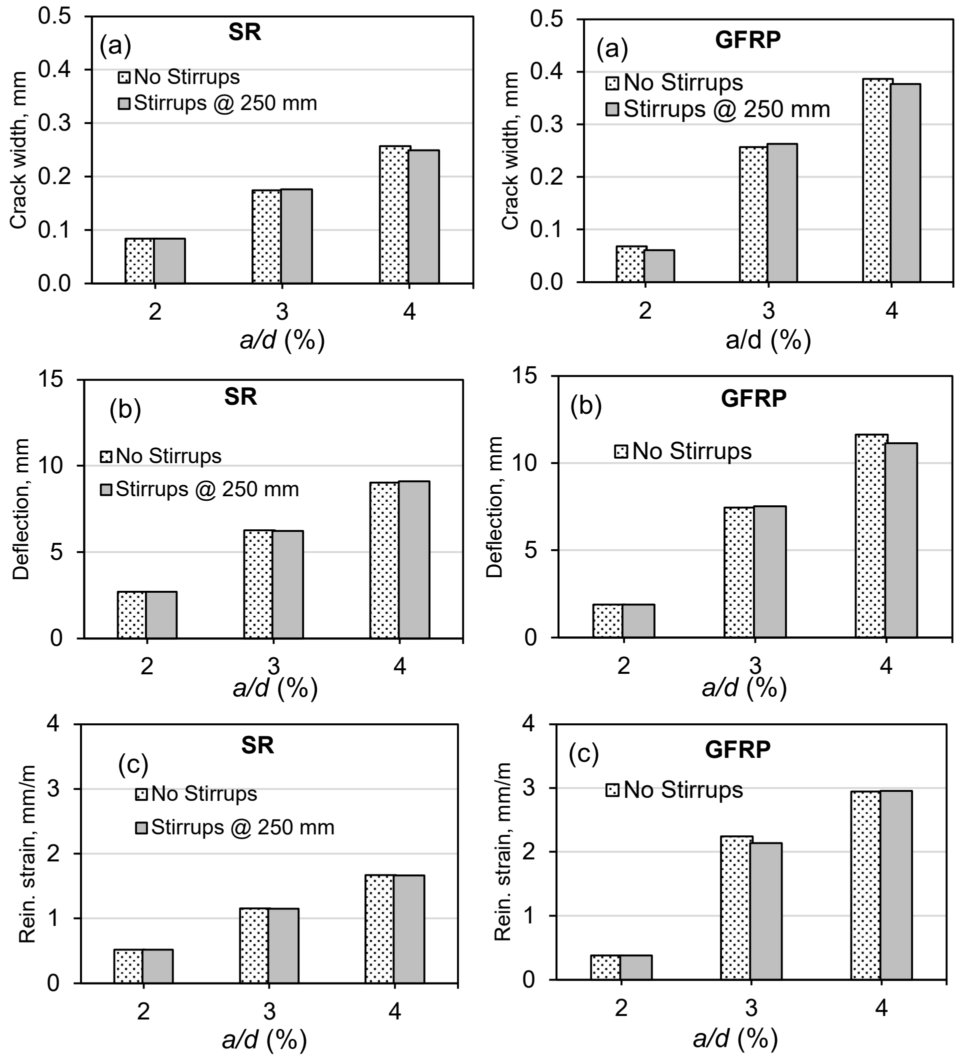

Figure C-10: Effect of the a/d ratio on service checks: (a) crack width, (b) deflection, and (c) reinforcement strain for both SR and GFRP beams

The trend of crack width, deflection, and reinforcement strain increasing is more pronounced in GFRP beams compared to SR beams, with an increase of 330% and 50% when the *a/d* ratio is raised from 2 to 3 and from 3 to 4, respectively. This difference becomes even more significant with higher increases in GFRP beams, due to lower modulus of elasticity of GFRP bars compared with SR bars, as shown in Figure C-10 (a, b, and c).

The percentage increase in all service parameters is more pronounced when the *a/d* ratio is raised from 2 to 3. This shift is primarily due to the potential change in the failure mode, transitioning from shear failure to flexural failure, resulting in higher crack widths. Additionally, when transitioning from an *a/d* ratio of 3 to 4, the failure mode is still likely to be primarily flexural in nature. The contribution of stirrups at service stage on service checks can be negligible and their influence papers at ultimate on beam strength.

The impact of the reinforcement ratio on serviceability checks is a crucial factor under examination. All other parameters, such as *a/d* and d, remain constant with values of 2 and 500 mm, respectively. The service load was determined based on C-SR-500-2-14-250 and C-GFRP-500-14-250 beams for SR and GFRP beams, respectively, which are the most representative beams within this specific group Figure C-11 (a, b, and c).

In Figure C-11, the impact of the ρ on service assessment is illustrated. The results demonstrate a consistent trend where all service checks, including crack width, deflection, and reinforcement strains, decrease as the ρ is increased, for a reason that, the reinforcement ratio ρ increases, there is a corresponding rise in the axial stiffness of both SR and GFRP beams. The reduction is approximately 60% in crack width, deflection, and reinforcement strain when the ρ is doubled, going from 0.55% to 1.1%, for both SR and GFRP beams. However, this reduction diminishes by nearly 15% when the ρ is doubled for SR beams, whereas this trend does not apply to GFRP beams. For GFRP beams, the reduction trend remains consistent as the ρ is increased by an additional 100% in crack width, deflection, and reinforcement strain.

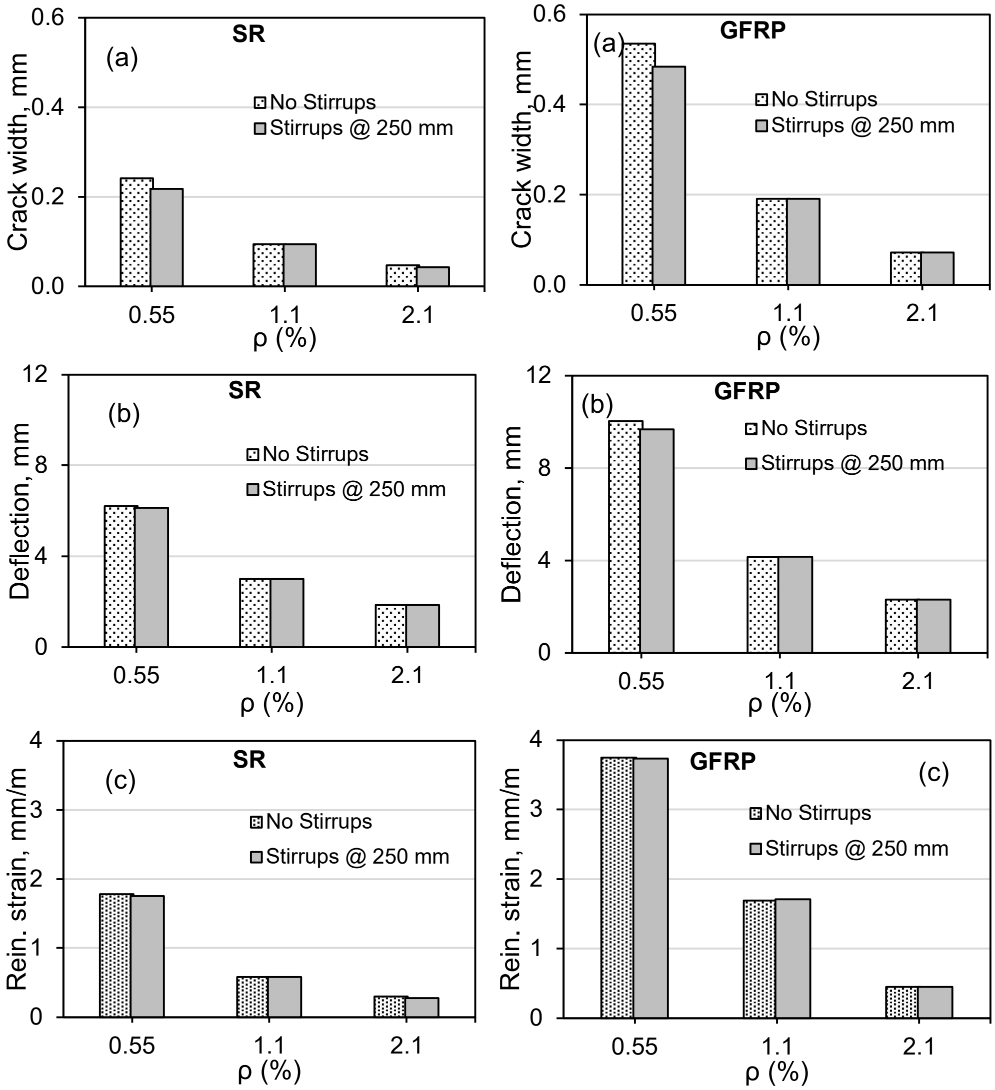

Figure C-11: Effect of the ρ ratio on service checks: (a) crack width, (b) deflection, and (c) reinforcement strain for both SR and GFRP beams.

Another important factor is the impact of beam depth on service checks, as depicted in Figure C-12. As expected, service checks decrease as the beam depth, *d,* increases, attributed to the corresponding increase in sectional flexural stiffness. For SR beams, a 50% increase in beam depth results in an 85% increase in crack width, an 80% increase in deflection, and a 55% increase in reinforcement strain. In contrast, for GFRP beams, the same increase in beam depth leads to larger changes, with an 95% increase in crack width, a 70% increase in deflection, and a significant 88% increase in reinforcement strain. This more pronounced reduction in GFRP beams is primarily due to their lower modulus of elasticity, making the enhancement from increased beam depth more impactful in GFRP beams compared to SR beams, as shown in Figure C-12 (a, b, and c).

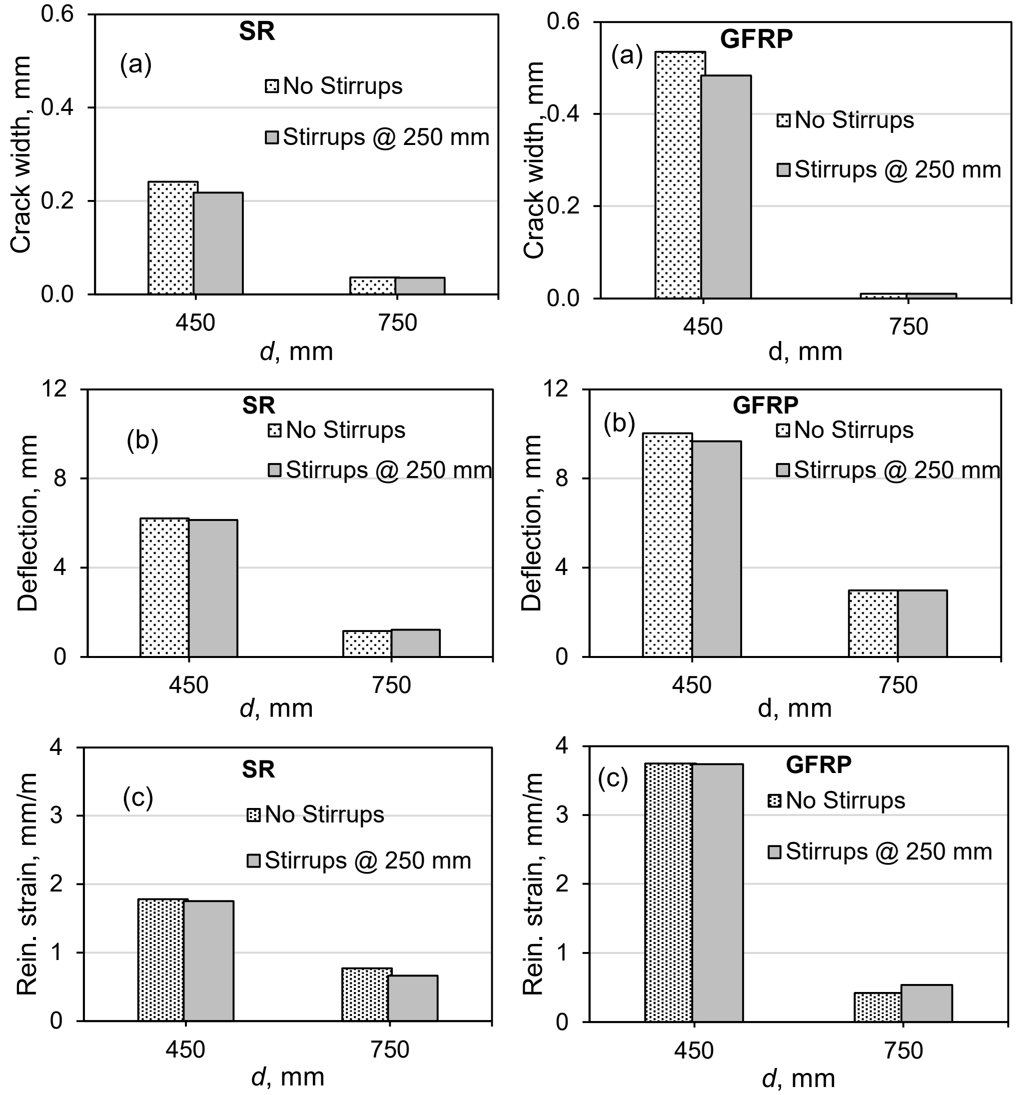

Figure C-12: Effect of *d* on service checks: (a) crack width, (b) deflection, and (c) reinforcement strain for both SR and GFRP beams.

Table C-1: Summary of numerical result

Beam details																	*Service results*				*Ultimate results*		
#	*Beam ID*	*RC*	*Fibre type*	*Stirrups @250 mm*	*Bar diameter mm*	*# of Bars*	*l mm*	*a mm*	*a/d*	A_s mm^2	*b mm*	*h mm*	*d mm*	ρ *%*	*%*	*MPa*	*Service load, kN*	*Maximum deflection at service load, mm*	*Rein. strain, milli strain*	*Maximum crack width at Service, mm*	*Peak load, kN*	$\frac{M_{fib.FEA}}{M_{fib.A}}$	*Failure mode*
1	B-2-14	SR	NO	Yes	14	4	4500	900	2	616	250	500	450	0.55	0.0	41.8	212	6.1	1.75	0.218	318	1.29	*Flexural*
2	B-2-14	SR	SF	Yes	14	4	4500	900	2	616	250	500	450	0.55	0.5	46.2	212	4.7	1.21	0.180	374	1.22	*Flexural*
3	B-2-14	SR	SF	Yes	14	4	4500	900	2	616	250	500	450	0.55	1.0	49.8	212	3.9	0.78	0.121	381	1.15	*Flexural*
4	B-2-14	SR	SF	Yes	14	4	4500	900	2	616	250	500	450	0.55	1.5	52.5	212	3.3	0.62	0.099	398	1.05	*Flexural*
5	B-2-14	SR	GF	Yes	14	4	4500	900	2	616	250	500	450	0.55	0.5	45.6	212	4.7	0.95	0.154	336	1.22	*Flexural*
6	B-2-14	SR	GF	Yes	14	4	4500	900	2	616	250	500	450	0.55	1.0	47.0	212	4.3	0.85	0.136	344	1.22	*Flexural*
7	B-2-14	SR	GF	Yes	14	4	4500	900	2	616	250	500	450	0.55	1.5	47.5	212	4.0	0.76	0.115	348	1.21	*Flexural*
8	B-2-14	SR	H1	Yes	14	4	4500	900	2	616	250	500	450	0.55	1.0	52.7	212	3.0	0.77	0.125	380	0.96	*Flexural*
9	B-2-14	SR	H2	Yes	14	4	4500	900	2	616	250	500	450	0.55	1.0	51.9	212	3.9	0.84	0.131	374	1.00	*Flexural*
10	B-2-14	SR	H3	Yes	14	4	4500	900	2	616	250	500	450	0.55	1.0	47.5	212	4.7	0.97	0.154	371	1.03	*Flexural*
11	B-2-14	SR	NO	Yes	14	6	7000	900	2	924	250	750	700	0.53	0.0	41.8	302	9.9	1.58	0.212	452	1.23	*Flexural*
12	B-2-14	SR	SF	Yes	14	6	7000	900	2	924	250	750	700	0.53	0.5	46.2	302	7.4	1.02	0.134	532	1.17	*Flexural*
13	B-2-14	SR	SF	Yes	14	6	7000	900	2	924	250	750	700	0.53	1.0	49.8	302	6.3	0.75	0.094	551	1.12	*Flexural*
14	B-2-14	SR	SF	Yes	14	6	7000	900	2	924	250	750	700	0.53	1.5	52.5	302	5.3	0.60	0.078	578	1.09	*Flexural*
15	B-2-14	SR	GF	Yes	14	6	7000	900	2	924	250	750	700	0.53	0.5	45.6	302	7.5	0.92	0.119	524	1.28	*Flexural*
16	B-2-14	SR	GF	Yes	14	6	7000	900	2	924	250	750	700	0.53	1.0	47.0	302	6.4	0.78	0.098	523	1.23	*Flexural*
17	B-2-14	SR	GF	Yes	14	6	7000	900	2	924	250	750	700	0.53	1.5	47.5	302	6.2	0.73	0.097	530	1.24	*Flexural*
18	B-2-14	SR	H1	Yes	14	6	7000	900	2	924	250	750	700	0.53	1.0	52.7	302	6.0	0.72	0.089	550	1.01	*Flexural*
19	B-2-14	SR	H2	Yes	14	6	7000	900	2	924	250	750	700	0.53	1.0	51.9	302	6.6	0.81	0.100	558	1.02	*Flexural*
20	B-2-14	SR	H3	Yes	14	6	7000	900	2	924	250	750	700	0.53	1.0	47.5	302	7.5	0.97	0.150	514	1.05	*Flexural*
21	B-2-20	SR	NO	Yes	20	4	4500	900	2	1257	250	500	450	1.12	0.0	41.8	400	7.6	1.67	0.265	600	1.21	*Flexural*
22	B-2-20	SR	SF	Yes	20	4	4500	900	2	1257	250	500	450	1.12	0.5	46.2	400	7.1	1.37	0.227	668	1.19	*Flexural*
23	B-2-20	SR	SF	Yes	20	4	4500	900	2	1257	250	500	450	1.12	1.0	49.8	400	6.5	1.14	0.190	663	1.13	*Flexural*
24	B-2-20	SR	SF	Yes	20	4	4500	900	2	1257	250	500	450	1.12	1.5	52.5	400	5.5	1.05	0.173	695	1.13	*Flexural*
25	B-2-20	SR	GF	Yes	20	4	4500	900	2	1257	250	500	450	1.12	0.5	45.6	400	7.4	1.34	0.246	602	1.13	*Flexural*
26	B-2-20	SR	GF	Yes	20	4	4500	900	2	1257	250	500	450	1.12	1.0	47.0	400	7.0	1.23	0.206	659	1.22	*Flexural*
27	B-2-20	SR	GF	Yes	20	4	4500	900	2	1257	250	500	450	1.12	1.5	47.5	400	6.8	1.13	0.189	632	1.16	*Flexural*
28	B-2-20	SR	H1	Yes	20	4	4500	900	2	1257	250	500	450	1.12	1.0	52.7	400	6.5	1.22	0.199	692	1.00	*Flexural*
29	B-2-20	SR	H2	Yes	20	4	4500	900	2	1257	250	500	450	1.12	1.0	51.9	400	6.8	1.25	0.213	653	1.10	*Flexural*
30	B-2-20	SR	H3	Yes	20	4	4500	900	2	1257	250	500	450	1.12	1.0	47.5	400	7.2	1.30	0.226	639	1.07	*Flexural*
31	B-2-20	SR	NO	Yes	20	6	7000	900	2	1885	250	750	700	1.08	0.0	41.8	579	12.6	1.64	0.210	869	1.17	*Flexural*
32	B-2-20	SR	SF	Yes	20	6	7000	900	2	1885	250	750	700	1.08	0.5	46.2	579	11.8	1.42	0.194	982	1.18	*Flexural*
33	B-2-20	SR	SF	Yes	20	6	7000	900	2	1885	250	750	700	1.08	1.0	49.8	579	9.9	1.19	0.155	959	1.10	*Flexural*
34	B-2-20	SR	SF	Yes	20	6	7000	900	2	1885	250	750	700	1.08	1.5	52.5	579	9.7	1.08	0.141	987	1.08	*Flexural*
35	B-2-20	SR	GF	Yes	20	6	7000	900	2	1885	250	750	700	1.08	0.5	45.6	579	11.9	1.35	0.206	957	1.21	*Flexural*
36	B-2-20	SR	GF	Yes	20	6	7000	900	2	1885	250	750	700	1.08	1.0	47.0	579	10.9	1.22	0.170	967	1.20	*Flexural*
37	B-2-20	SR	GF	Yes	20	6	7000	900	2	1885	250	750	700	1.08	1.5	47.5	579	10.1	1.19	0.154	1010	1.25	*Flexural*
38	B-2-20	SR	H1	Yes	20	6	7000	900	2	1885	250	750	700	1.08	1.0	52.7	579	10.7	1.20	0.166	1002	1.06	*Flexural*
39	B-2-20	SR	H2	Yes	20	6	7000	900	2	1885	250	750	700	1.08	1.0	51.9	579	11.1	1.28	0.171	947	1.08	*Flexural*
40	B-2-20	SR	H3	Yes	20	6	7000	900	2	1885	250	750	700	1.08	1.0	47.5	579	11.7	1.30	0.182	981	1.14	*Flexural*
41	B-2-28	SR	NO	Yes	28	4	4500	900	2	2463	250	500	450	2.19	0.0	41.8	628	7.7	1.34	0.210	942	0.99	*Shear*

42	B-2-28	SR	SF	Yes	28	4	4500	900	2	2463	250	500	450	2.19	0.5	46.2	628	7.5	1.22	0.195	1069	1.03	*Flexural*
43	B-2-28	SR	SF	Yes	28	4	4500	900	2	2463	250	500	450	2.19	1.0	49.8	628	7.1	1.13	0.157	1188	1.12	*Flexural*
44	B-2-28	SR	SF	Yes	28	4	4500	900	2	2463	250	500	450	2.19	1.5	52.5	628	6.9	1.01	0.127	1109	1.02	*Flexural*
45	B-2-28	SR	GF	Yes	28	4	4500	900	2	2463	250	500	450	2.19	0.5	45.6	628	7.7	1.19	0.203	1031	1.02	*Flexural*
46	B-2-28	SR	GF	Yes	28	4	4500	900	2	2463	250	500	450	2.19	1.0	47.0	628	7.3	1.08	0.161	1130	1.11	*Flexural*
47	B-2-28	SR	GF	Yes	28	4	4500	900	2	2463	250	500	450	2.19	1.5	47.5	628	7.1	1.06	0.148	1189	1.16	*Flexural*
48	B-2-28	SR	H1	Yes	28	4	4500	900	2	2463	250	500	450	2.19	1.0	52.7	628	7.2	1.15	0.166	1457	0.96	*Flexural*
49	B-2-28	SR	H2	Yes	28	4	4500	900	2	2463	250	500	450	2.19	1.0	51.9	628	7.3	1.16	0.189	1164	1.05	*Flexural*
50	B-2-28	SR	H3	Yes	28	4	4500	900	2	2463	250	500	450	2.19	1.0	47.5	628	7.7	1.19	0.198	1077	1.11	*Flexural*
51	B-2-28	SR	NO	Yes	28	6	7000	900	2	3695	250	750	700	2.11	0.0	41.8	891	12.5	1.30	0.166	1337	0.93	*Flexural*
52	B-2-28	SR	SF	Yes	28	6	7000	900	2	3695	250	750	700	2.11	0.5	46.2	891	12.1	1.18	0.160	1604	1.05	*Flexural*
53	B-2-28	SR	SF	Yes	28	6	7000	900	2	3695	250	750	700	2.11	1.0	49.8	891	11.4	1.10	0.142	1698	1.08	*Flexural*
54	B-2-28	SR	SF	Yes	28	6	7000	900	2	3695	250	750	700	2.11	1.5	52.5	891	10.8	1.05	0.134	1850	1.15	*Shear*
55	B-2-28	SR	GF	Yes	28	6	7000	900	2	3695	250	750	700	2.11	0.5	45.6	891	12.6	1.16	0.158	1505	1.01	*Flexural*
56	B-2-28	SR	GF	Yes	28	6	7000	900	2	3695	250	750	700	2.11	1.0	47.0	891	11.7	1.12	0.145	1589	1.06	*Flexural*
57	B-2-28	SR	GF	Yes	28	6	7000	900	2	3695	250	750	700	2.11	1.5	47.5	891	11.1	1.10	0.140	1640	1.08	*Flexural*
58	B-2-28	SR	H1	Yes	28	6	7000	900	2	3695	250	750	700	2.11	1.0	52.7	891	11.5	1.10	0.142	1706	0.93	*Flexural*
59	B-2-28	SR	H2	Yes	28	6	7000	900	2	3695	250	750	700	2.11	1.0	51.9	891	11.8	1.28	0.161	1665	0.99	*Flexural*
60	B-2-28	SR	H3	Yes	28	6	7000	900	2	3695	250	750	700	2.11	1.0	47.5	891	12.3	1.15	0.164	1619	1.03	*Flexural*
61	B-3-14	SR	NO	Yes	14	4	4500	1350	3	616	250	500	450	0.55	0.0	41.8	139	7.5	1.68	0.260	208	1.27	*Flexural*
62	B-3-14	SR	SF	Yes	14	4	4500	1350	3	616	250	500	450	0.55	0.5	46.2	139	5.6	1.05	0.155	227	1.11	*Flexural*
63	B-3-14	SR	SF	Yes	14	4	4500	1350	3	616	250	500	450	0.55	1.0	49.8	139	4.7	0.74	0.119	250	1.13	*Flexural*
64	B-3-14	SR	SF	Yes	14	4	4500	1350	3	616	250	500	450	0.55	1.5	52.5	139	3.8	0.56	0.093	265	1.11	*Flexural*
65	B-3-14	SR	GF	Yes	14	4	4500	1350	3	616	250	500	450	0.55	0.5	45.6	139	5.9	1.19	0.164	223	1.22	*Flexural*
66	B-3-14	SR	GF	Yes	14	4	4500	1350	3	616	250	500	450	0.55	1.0	47.0	139	5.1	0.99	0.130	237	1.26	*Flexural*
67	B-3-14	SR	GF	Yes	14	4	4500	1350	3	616	250	500	450	0.55	1.5	47.5	139	4.9	0.90	0.114	237	1.24	*Flexural*
68	B-3-14	SR	H1	Yes	14	4	4500	1350	3	616	250	500	450	0.55	1.0	52.7	139	4.4	0.81	0.110	251	0.96	*Flexural*
69	B-3-14	SR	H2	Yes	14	4	4500	1350	3	616	250	500	450	0.55	1.0	51.9	139	4.8	0.80	0.123	243	1.04	*Flexural*
70	B-3-14	SR	H3	Yes	14	4	4500	1350	3	616	250	500	450	0.55	1.0	47.5	139	5.5	0.90	0.143	240	1.05	*Flexural*
71	B-3-14	SR	NO	Yes	14	6	7000	1350	3	924	250	750	700	0.53	0.0	41.8	214	12.8	1.10	0.245	321	1.31	*Flexural*
72	B-3-14	SR	SF	Yes	14	6	7000	1350	3	924	250	750	700	0.53	0.5	46.2	214	10.0	1.24	0.152	350	1.15	*Flexural*
73	B-3-14	SR	SF	Yes	14	6	7000	1350	3	924	250	750	700	0.53	1.0	49.8	214	8.2	0.85	0.109	358	1.09	*Flexural*
74	B-3-14	SR	SF	Yes	14	6	7000	1350	3	924	250	750	700	0.53	1.5	52.5	214	7.5	0.68	0.084	350	0.99	*Flexural*
75	B-3-14	SR	GF	Yes	14	6	7000	1350	3	924	250	750	700	0.53	0.5	45.6	214	9.8	1.03	0.133	347	1.27	*Flexural*
76	B-3-14	SR	GF	Yes	14	6	7000	1350	3	924	250	750	700	0.53	1.0	47.0	214	8.5	0.89	0.112	347	1.23	*Flexural*
77	B-3-14	SR	GF	Yes	14	6	7000	1350	3	924	250	750	700	0.53	1.5	47.5	214	7.8	0.83	0.111	352	1.23	*Flexural*
78	B-3-14	SR	H1	Yes	14	6	7000	1350	3	924	250	750	700	0.53	1.0	52.7	214	8.0	0.81	0.106	349	1.00	*Flexural*
79	B-3-14	SR	H2	Yes	14	6	7000	1350	3	924	250	750	700	0.53	1.0	51.9	214	8.6	0.90	0.114	350	1.01	*Flexural*
80	B-3-14	SR	H3	Yes	14	6	7000	1350	3	924	250	750	700	0.53	1.0	47.5	214	9.7	1.03	0.131	348	1.05	*Flexural*
81	B-3-20	SR	NO	Yes	20	4	4500	1350	3	1257	250	500	450	1.12	0.0	41.8	267	9.4	1.66	0.250	400	1.21	*Flexural*
82	B-3-20	SR	SF	Yes	20	4	4500	1350	3	1257	250	500	450	1.12	0.5	46.2	267	8.8	1.45	0.227	449	1.20	*Flexural*
83	B-3-20	SR	SF	Yes	20	4	4500	1350	3	1257	250	500	450	1.12	1.0	49.8	267	7.9	1.18	0.187	457	1.17	*Flexural*
84	B-3-20	SR	SF	Yes	20	4	4500	1350	3	1257	250	500	450	1.12	1.5	52.5	267	7.3	1.04	0.172	476	1.16	*Flexural*
85	B-3-20	SR	GF	Yes	20	4	4500	1350	3	1257	250	500	450	1.12	0.5	45.6	267	9.0	1.57	0.236	430	1.21	*Flexural*
86	B-3-20	SR	GF	Yes	20	4	4500	1350	3	1257	250	500	450	1.12	1.0	47.0	267	8.5	1.26	0.199	439	1.22	*Flexural*
87	B-3-20	SR	GF	Yes	20	4	4500	1350	3	1257	250	500	450	1.12	1.5	47.5	267	8.3	1.14	0.194	450	1.24	*Flexural*
88	B-3-20	SR	H1	Yes	20	4	4500	1350	3	1257	250	500	450	1.12	1.0	52.7	267	7.7	1.15	0.189	449	1.07	*Flexural*
89	B-3-20	SR	H2	Yes	20	4	4500	1350	3	1257	250	500	450	1.12	1.0	51.9	267	8.3	1.19	0.202	454	1.10	*Flexural*
90	B-3-20	SR	H3	Yes	20	4	4500	1350	3	1257	250	500	450	1.12	1.0	47.5	267	8.8	1.37	0.232	455	1.14	*Flexural*
91	B-3-20	SR	NO	Yes	20	6	7000	1350	3	1885	250	750	700	1.08	0.0	41.8	392	15.2	1.67	0.221	588	1.19	*Flexural*

92	B-3-20	SR	SF	Yes	20	6	7000	1350	3	1885	250	750	700	1.08	0.5	46.2	392	14.2	1.46	0.196	648	1.17	*Shear*
93	B-3-20	SR	SF	Yes	20	6	7000	1350	3	1885	250	750	700	1.08	1.0	49.8	392	12.8	1.20	0.160	665	1.14	*Flexural*
94	B-3-20	SR	SF	Yes	20	6	7000	1350	3	1885	250	750	700	1.08	1.5	52.5	392	11.7	1.10	0.145	649	1.07	*Flexural*
95	B-3-20	SR	GF	Yes	20	6	7000	1350	3	1885	250	750	700	1.08	0.5	45.6	392	14.4	1.36	0.205	633	1.20	*Flexural*
96	B-3-20	SR	GF	Yes	20	6	7000	1350	3	1885	250	750	700	1.08	1.0	47.0	392	13.1	1.14	0.168	647	1.21	*Flexural*
97	B-3-20	SR	GF	Yes	20	6	7000	1350	3	1885	250	750	700	1.08	1.5	47.5	392	12.4	1.20	0.158	664	1.23	*Flexural*
98	B-3-20	SR	H1	Yes	20	6	7000	1350	3	1885	250	750	700	1.08	1.0	52.7	392	12.9	1.22	0.166	644	1.05	*Flexural*
99	B-3-20	SR	H2	Yes	20	6	7000	1350	3	1885	250	750	700	1.08	1.0	51.9	392	13.4	1.28	0.171	642	1.08	*Flexural*
100	B-3-20	SR	H3	Yes	20	6	7000	1350	3	1885	250	750	700	1.08	1.0	47.5	392	14.1	1.33	0.191	660	1.13	*Flexural*
101	B-3-28	SR	NO	Yes	28	4	4500	1350	3	2463	250	500	450	2.19	0.0	41.8	489	11.5	1.49	0.271	734	1.16	*Flexural*
102	B-3-28	SR	SF	Yes	28	4	4500	1350	3	2463	250	500	450	2.19	0.5	46.2	489	11.1	1.46	0.241	786	1.14	*Shear*
103	B-3-28	SR	SF	Yes	28	4	4500	1350	3	2463	250	500	450	2.19	1.0	49.8	489	10.5	1.33	0.219	820	1.16	*Flexural*
104	B-3-28	SR	SF	Yes	28	4	4500	1350	3	2463	250	500	450	2.19	1.5	52.5	489	10.0	1.31	0.208	804	1.10	*Flexural*
105	B-3-28	SR	GF	Yes	28	4	4500	1350	3	2463	250	500	450	2.19	0.5	45.6	489	11.4	1.42	0.254	753	1.12	*Flexural*
106	B-3-28	SR	GF	Yes	28	4	4500	1350	3	2463	250	500	450	2.19	1.0	47.0	489	11.3	1.39	0.244	769	1.13	*Flexural*
107	B-3-28	SR	GF	Yes	28	4	4500	1350	3	2463	250	500	450	2.19	1.5	47.5	489	11.0	1.36	0.219	790	1.16	*Flexural*
108	B-3-28	SR	H1	Yes	28	4	4500	1350	3	2463	250	500	450	2.19	1.0	52.7	489	10.4	1.33	0.216	795	1.05	*Flexural*
109	B-3-28	SR	H2	Yes	28	4	4500	1350	3	2463	250	500	450	2.19	1.0	51.9	489	11.0	1.42	0.247	817	1.07	*Flexural*
110	B-3-28	SR	H3	Yes	28	4	4500	1350	3	2463	250	500	450	2.19	1.0	47.5	489	11.4	1.41	0.236	800	1.11	*Flexural*
111	B-3-28	SR	NO	Yes	28	6	7000	1350	3	3695	250	750	700	2.11	0.0	41.8	663	16.8	1.41	0.187	995	1.04	*Shear*
112	B-3-28	SR	SF	Yes	28	6	7000	1350	3	3695	250	750	700	2.11	0.5	46.2	663	16.2	1.37	0.176	1065	1.04	*Shear*
113	B-3-28	SR	SF	Yes	28	6	7000	1350	3	3695	250	750	700	2.11	1.0	49.8	663	15.4	1.26	0.163	1119	1.07	*Shear*
114	B-3-28	SR	SF	Yes	28	6	7000	1350	3	3695	250	750	700	2.11	1.5	52.5	663	14.6	1.21	0.155	1146	1.07	*Flexural*
115	B-3-28	SR	GF	Yes	28	6	7000	1350	3	3695	250	750	700	2.11	0.5	45.6	663	16.9	1.30	0.184	1050	1.06	*Flexural*
116	B-3-28	SR	GF	Yes	28	6	7000	1350	3	3695	250	750	700	2.11	1.0	47.0	663	16.7	1.25	0.171	1059	1.06	*Flexural*
117	B-3-28	SR	GF	Yes	28	6	7000	1350	3	3695	250	750	700	2.11	1.5	47.5	663	16.2	1.25	0.162	1084	1.08	*Flexural*
118	B-3-28	SR	H1	Yes	28	6	7000	1350	3	3695	250	750	700	2.11	1.0	52.7	663	15.5	1.27	0.175	1112	0.98	*Flexural*
119	B-3-28	SR	H2	Yes	28	6	7000	1350	3	3695	250	750	700	2.11	1.0	51.9	663	15.9	1.28	0.171	1105	0.99	*Flexural*
120	B-3-28	SR	H3	Yes	28	6	7000	1350	3	3695	250	750	700	2.11	1.0	47.5	663	16.5	1.30	0.180	1088	1.02	*Flexural*
121	B-4-14	SR	NO	Yes	14	4	4500	2100	4	616	250	500	450	0.55	0.0	41.8	103	6.6	1.46	0.338	154	1.25	*Flexural*
122	B-4-14	SR	SF	Yes	14	4	4500	2100	4	616	250	500	450	0.55	0.5	46.2	103	5.0	1.05	0.150	174	1.14	*Flexural*
123	B-4-14	SR	SF	Yes	14	4	4500	2100	4	616	250	500	450	0.55	1.0	49.8	103	4.4	0.81	0.114	193	1.16	*Flexural*
124	B-4-14	SR	SF	Yes	14	4	4500	2100	4	616	250	500	450	0.55	1.5	52.5	103	3.7	0.57	0.091	199	1.11	*Flexural*
125	B-4-14	SR	GF	Yes	14	4	4500	2100	4	616	250	500	450	0.55	0.5	45.6	103	5.2	1.26	0.137	169	1.23	*Flexural*
126	B-4-14	SR	GF	Yes	14	4	4500	2100	4	616	250	500	450	0.55	1.0	47.0	103	4.9	1.11	0.128	174	1.23	*Flexural*
127	B-4-14	SR	GF	Yes	14	4	4500	2100	4	616	250	500	450	0.55	1.5	47.5	103	4.5	0.99	0.117	173	1.21	*Flexural*
128	B-4-14	SR	H1	Yes	14	4	4500	2100	4	616	250	500	450	0.55	1.0	52.7	103	4.1	0.91	0.114	183	0.97	*Flexural*
129	B-4-14	SR	H2	Yes	14	4	4500	2100	4	616	250	500	450	0.55	1.0	51.9	103	4.1	0.95	0.115	181	1.01	*Flexural*
130	B-4-14	SR	H3	Yes	14	4	4500	2100	4	616	250	500	450	0.55	1.0	47.5	103	5.2	0.98	0.130	177	1.03	*Flexural*
131	B-4-14	SR	NO	Yes	14	6	7000	2100	4	924	250	750	700	0.53	0.0	41.8	151	11.7	1.44	0.239	226	1.23	*Flexural*
132	B-4-14	SR	SF	Yes	14	6	7000	2100	4	924	250	750	700	0.53	0.5	46.2	151	8.3	1.05	0.125	267	1.17	*Flexural*
133	B-4-14	SR	SF	Yes	14	6	7000	2100	4	924	250	750	700	0.53	1.0	49.8	151	7.2	0.81	0.096	272	1.10	*Flexural*
134	B-4-14	SR	SF	Yes	14	6	7000	2100	4	924	250	750	700	0.53	1.5	52.5	151	6.0	0.59	0.079	289	1.09	*Flexural*
135	B-4-14	SR	GF	Yes	14	6	7000	2100	4	924	250	750	700	0.53	0.5	45.6	151	8.6	1.24	0.114	261	1.27	*Flexural*
136	B-4-14	SR	GF	Yes	14	6	7000	2100	4	924	250	750	700	0.53	1.0	47.0	151	7.9	1.11	0.102	257	1.22	*Flexural*
137	B-4-14	SR	GF	Yes	14	6	7000	2100	4	924	250	750	700	0.53	1.5	47.5	151	7.5	0.99	0.095	256	1.19	*Flexural*
138	B-4-14	SR	H1	Yes	14	6	7000	2100	4	924	250	750	700	0.53	1.0	52.7	151	6.8	0.91	0.094	266	1.00	*Flexural*
139	B-4-14	SR	H2	Yes	14	6	7000	2100	4	924	250	750	700	0.53	1.0	51.9	151	7.5	0.95	0.104	264	1.00	*Flexural*
140	B-4-14	SR	H3	Yes	14	6	7000	2100	4	924	250	750	700	0.53	1.0	47.5	151	8.5	0.98	0.121	262	1.02	*Flexural*
141	B-4-20	SR	NO	Yes	20	4	4500	2100	4	1257	250	500	450	1.12	0.0	41.8	198	9.2	1.72	0.249	298	1.20	*Flexural*

142	B-4-20	SR	SF	Yes	20	4	4500	2100	4	1257	250	500	450	1.12	0.5	46.2	198	8.5	1.46	0.219	182	0.65	*Flexural*
143	B-4-20	SR	SF	Yes	20	4	4500	2100	4	1257	250	500	450	1.12	1.0	49.8	198	7.8	1.38	0.190	354	1.20	*Flexural*
144	B-4-20	SR	SF	Yes	20	4	4500	2100	4	1257	250	500	450	1.12	1.5	52.5	198	7.1	1.24	0.170	350	1.14	*Flexural*
145	B-4-20	SR	GF	Yes	20	4	4500	2100	4	1257	250	500	450	1.12	0.5	45.6	198	8.8	1.59	0.226	316	1.19	*Flexural*
146	B-4-20	SR	GF	Yes	20	4	4500	2100	4	1257	250	500	450	1.12	1.0	47.0	198	8.3	1.52	0.198	327	1.21	*Flexural*
147	B-4-20	SR	GF	Yes	20	4	4500	2100	4	1257	250	500	450	1.12	1.5	47.5	198	8.1	1.50	0.184	335	1.23	*Flexural*
148	B-4-20	SR	H1	Yes	20	4	4500	2100	4	1257	250	500	450	1.12	1.0	52.7	198	7.7	1.36	0.195	347	1.05	*Flexural*
149	B-4-20	SR	H2	Yes	20	4	4500	2100	4	1257	250	500	450	1.12	1.0	51.9	198	7.8	1.38	0.196	341	1.09	*Flexural*
150	B-4-20	SR	H3	Yes	20	4	4500	2100	4	1257	250	500	450	1.12	1.0	47.5	198	8.6	1.45	0.210	328	1.13	*Flexural*
151	B-4-20	SR	NO	Yes	20	6	7000	2100	4	1885	250	750	700	1.08	0.0	41.8	293	15.1	1.65	0.214	440	1.18	*Flexural*
152	B-4-20	SR	SF	Yes	20	6	7000	2100	4	1885	250	750	700	1.08	0.5	46.2	293	14.1	1.46	0.181	492	1.18	*Flexural*
153	B-4-20	SR	SF	Yes	20	6	7000	2100	4	1885	250	750	700	1.08	1.0	49.8	293	12.7	1.37	0.151	481	1.10	*Flexural*
154	B-4-20	SR	SF	Yes	20	6	7000	2100	4	1885	250	750	700	1.08	1.5	52.5	293	11.6	1.27	0.141	486	1.07	*Flexural*
155	B-4-20	SR	GF	Yes	20	6	7000	2100	4	1885	250	750	700	1.08	0.5	45.6	293	14.4	1.49	0.192	482	1.22	*Flexural*
156	B-4-20	SR	GF	Yes	20	6	7000	2100	4	1885	250	750	700	1.08	1.0	47.0	293	13.0	1.46	0.164	496	1.23	*Flexural*
157	B-4-20	SR	GF	Yes	20	6	7000	2100	4	1885	250	750	700	1.08	1.5	47.5	293	12.7	1.48	0.155	512	1.26	*Flexural*
158	B-4-20	SR	H1	Yes	20	6	7000	2100	4	1885	250	750	700	1.08	1.0	52.7	293	12.7	1.30	0.161	477	1.07	*Flexural*
159	B-4-20	SR	H2	Yes	20	6	7000	2100	4	1885	250	750	700	1.08	1.0	51.9	293	13.3	1.44	0.171	499	1.11	*Flexural*
160	B-4-20	SR	H3	Yes	20	6	7000	2100	4	1885	250	750	700	1.08	1.0	47.5	293	14.0	1.48	0.181	504	1.16	*Flexural*
161	B-4-28	SR	NO	Yes	28	4	4500	2100	4	2463	250	500	450	2.19	0.0	41.8	317	9.6	1.39	0.210	475	1.00	*Shear*
162	B-4-28	SR	SF	Yes	28	4	4500	2100	4	2463	250	500	450	2.19	0.5	46.2	317	9.2	1.37	0.213	588	1.13	*Flexural*
163	B-4-28	SR	SF	Yes	28	4	4500	2100	4	2463	250	500	450	2.19	1.0	49.8	317	8.8	1.24	0.182	616	1.16	*Flexural*
164	B-4-28	SR	SF	Yes	28	4	4500	2100	4	2463	250	500	450	2.19	1.5	52.5	317	8.3	1.26	0.165	622	1.14	*Flexural*
165	B-4-28	SR	GF	Yes	28	4	4500	2100	4	2463	250	500	450	2.19	0.5	45.6	317	9.5	1.42	0.221	583	1.15	*Flexural*
166	B-4-28	SR	GF	Yes	28	4	4500	2100	4	2463	250	500	450	2.19	1.0	47.0	317	9.3	1.62	0.192	584	1.15	*Flexural*
167	B-4-28	SR	GF	Yes	28	4	4500	2100	4	2463	250	500	450	2.19	1.5	47.5	317	9.1	1.41	0.180	580	1.13	*Flexural*
168	B-4-28	SR	H1	Yes	28	4	4500	2100	4	2463	250	500	450	2.19	1.0	52.7	317	8.7	1.48	0.194	614	1.08	*Flexural*
169	B-4-28	SR	H2	Yes	28	4	4500	2100	4	2463	250	500	450	2.19	1.0	51.9	317	8.8	1.51	0.195	586	1.09	*Flexural*
170	B-4-28	SR	H3	Yes	28	4	4500	2100	4	2463	250	500	450	2.19	1.0	47.5	317	9.4	1.29	0.211	598	1.09	*Flexural*
171	B-4-28	SR	NO	Yes	28	6	7000	2100	4	3695	250	750	700	2.11	0.0	41.8	504	17.2	1.53	0.191	756	1.05	*Flexural*
172	B-4-28	SR	SF	Yes	28	6	7000	2100	4	3695	250	750	700	2.11	0.5	46.2	504	16.6	1.44	0.171	801	1.05	*Flexural*
173	B-4-28	SR	SF	Yes	28	6	7000	2100	4	3695	250	750	700	2.11	1.0	49.8	504	15.7	1.37	0.142	853	1.09	*Flexural*
174	B-4-28	SR	SF	Yes	28	6	7000	2100	4	3695	250	750	700	2.11	1.5	52.5	504	14.9	1.35	0.132	857	1.06	*Flexural*
175	B-4-28	SR	GF	Yes	28	6	7000	2100	4	3695	250	750	700	2.11	0.5	45.6	504	17.2	1.46	0.181	796	1.07	*Flexural*
176	B-4-28	SR	GF	Yes	28	6	7000	2100	4	3695	250	750	700	2.11	1.0	47.0	504	16.0	1.44	0.151	802	1.06	*Flexural*
177	B-4-28	SR	GF	Yes	28	6	7000	2100	4	3695	250	750	700	2.11	1.5	47.5	504	15.6	1.66	0.143	832	1.10	*Flexural*
178	B-4-28	SR	H1	Yes	28	6	7000	2100	4	3695	250	750	700	2.11	1.0	52.7	504	15.8	1.32	0.151	848	0.99	*Flexural*
179	B-4-28	SR	H2	Yes	28	6	7000	2100	4	3695	250	750	700	2.11	1.0	51.9	504	16.2	1.45	0.161	841	1.00	*Flexural*
180	B-4-28	SR	H3	Yes	28	6	7000	2100	4	3695	250	750	700	2.11	1.0	47.5	504	16.9	1.38	0.172	820	1.04	*Flexural*
181	B-2-14	GFRP	NO	Yes	14	4	4500	900	2	616	250	500	450	0.55	0.0	41.8	143	9.7	3.43	0.483	478	0.75	*Shear*
182	B-2-14	GFRP	SF	Yes	14	4	4500	900	2	616	250	500	450	0.55	0.5	46.2	143	6.7	2.07	0.345	631	0.97	*Shear*
183	B-2-14	GFRP	SF	Yes	14	4	4500	900	2	616	250	500	450	0.55	1.0	49.8	143	5.9	1.62	0.121	693	0.96	*Shear*
184	B-2-14	GFRP	SF	Yes	14	4	4500	900	2	616	250	500	450	0.55	1.5	52.5	143	5.1	1.19	0.069	706	0.91	*Shear*
185	B-2-14	GFRP	GF	Yes	14	4	4500	900	2	616	250	500	450	0.55	0.5	45.6	143	7.8	2.15	0.193	519	0.53	*Shear*
186	B-2-14	GFRP	GF	Yes	14	4	4500	900	2	616	250	500	450	0.55	1.0	47.0	143	6.5	1.92	0.125	577	0.52	*Shear*
187	B-2-14	GFRP	GF	Yes	14	4	4500	900	2	616	250	500	450	0.55	1.5	47.5	143	7.0	1.69	0.113	706	0.50	*Shear*
188	B-2-14	GFRP	H1	Yes	14	4	4500	900	2	616	250	500	450	0.55	1.0	52.7	143	6.2	1.65	0.087	688	0.48	*Shear*
189	B-2-14	GFRP	H2	Yes	14	4	4500	900	2	616	250	500	450	0.55	1.0	51.9	143	7.3	1.77	0.148	605	0.49	*Shear*
190	B-2-14	GFRP	H3	Yes	14	4	4500	900	2	616	250	500	450	0.55	1.0	47.5	143	7.8	1.91	0.178	687	0.50	*Shear*
191	B-2-14	GFRP	NO	Yes	14	6	7000	900	2	924	250	750	700	0.53	0.0	41.8	194	13.0	2.32	0.381	647	0.50	*Shear*

192	B-2-14	GFRP	SF	Yes	14	6	7000	900	2	924	250	750	700	0.53	0.5	46.2	194	10.2	1.49	0.131	779	0.70	*Shear*
193	B-2-14	GFRP	SF	Yes	14	6	7000	900	2	924	250	750	700	0.53	1.0	49.8	194	9.1	1.36	0.072	789	0.72	*Shear*
194	B-2-14	GFRP	SF	Yes	14	6	7000	900	2	924	250	750	700	0.53	1.5	52.5	194	7.6	0.94	0.048	889	0.77	*Shear*
195	B-2-14	GFRP	GF	Yes	14	6	7000	900	2	924	250	750	700	0.53	0.5	45.6	194	12.4	1.68	0.110	669	0.55	*Shear*
196	B-2-14	GFRP	GF	Yes	14	6	7000	900	2	924	250	750	700	0.53	1.0	47.0	194	11.2	1.61	0.076	754	0.52	*Shear*
197	B-2-14	GFRP	GF	Yes	14	6	7000	900	2	924	250	750	700	0.53	1.5	47.5	194	10.3	1.49	0.063	795	0.50	*Shear*
198	B-2-14	GFRP	H1	Yes	14	6	7000	900	2	924	250	750	700	0.53	1.0	52.7	194	9.5	1.41	0.063	809	0.50	*Shear*
199	B-2-14	GFRP	H2	Yes	14	6	7000	900	2	924	250	750	700	0.53	1.0	51.9	194	10.4	1.57	0.076	783	0.49	*Shear*
200	B-2-14	GFRP	H3	Yes	14	6	7000	900	2	924	250	750	700	0.53	1.0	47.5	194	11.4	1.66	0.110	789	0.50	*Shear*
201	B-2-20	GFRP	NO	Yes	20	4	4500	900	2	1257	250	500	450	1.12	0.0	41.8	192	8.8	2.36	0.319	642	0.71	*Shear*
202	B-2-20	GFRP	SF	Yes	20	4	4500	900	2	1257	250	500	450	1.12	0.5	46.2	192	7.6	1.81	0.264	845	0.93	*Shear*
203	B-2-20	GFRP	SF	Yes	20	4	4500	900	2	1257	250	500	450	1.12	1.0	49.8	192	6.8	1.19	0.147	952	0.94	*Shear*
204	B-2-20	GFRP	SF	Yes	20	4	4500	900	2	1257	250	500	450	1.12	1.5	52.5	192	6.1	0.97	0.106	985	0.89	*Shear*
205	B-2-20	GFRP	GF	Yes	20	4	4500	900	2	1257	250	500	450	1.12	0.5	45.6	192	8.0	1.93	0.301	692	0.68	*Shear*
206	B-2-20	GFRP	GF	Yes	20	4	4500	900	2	1257	250	500	450	1.12	1.0	47.0	192	7.1	1.66	0.169	784	0.71	*Shear*
207	B-2-20	GFRP	GF	Yes	20	4	4500	900	2	1257	250	500	450	1.12	1.5	47.5	192	6.6	1.59	0.148	787	0.65	*Shear*
208	B-2-20	GFRP	H1	Yes	20	4	4500	900	2	1257	250	500	450	1.12	1.0	52.7	192	6.9	1.59	0.148	879	0.62	*Shear*
209	B-2-20	GFRP	H2	Yes	20	4	4500	900	2	1257	250	500	450	1.12	1.0	51.9	192	7.6	1.75	0.172	757	0.68	*Shear*
210	B-2-20	GFRP	H3	Yes	20	4	4500	900	2	1257	250	500	450	1.12	1.0	47.5	192	8.0	1.90	0.207	757	0.65	*Shear*
211	B-2-20	GFRP	NO	Yes	20	6	7000	900	2	1885	250	750	700	1.08	0.0	41.8	280	13.1	2.26	0.287	935	0.66	*Shear*
212	B-2-20	GFRP	SF	Yes	20	6	7000	900	2	1885	250	750	700	1.08	0.5	46.2	280	12.4	1.68	0.232	1063	0.78	*Shear*
213	B-2-20	GFRP	SF	Yes	20	6	7000	900	2	1885	250	750	700	1.08	1.0	49.8	280	10.9	1.12	0.123	1263	0.83	*Shear*
214	B-2-20	GFRP	SF	Yes	20	6	7000	900	2	1885	250	750	700	1.08	1.5	52.5	280	10.2	0.98	0.094	1335	0.81	*Shear*
215	B-2-20	GFRP	GF	Yes	20	6	7000	900	2	1885	250	750	700	1.08	0.5	45.6	280	12.7	1.74	0.269	878	0.72	*Shear*
216	B-2-20	GFRP	GF	Yes	20	6	7000	900	2	1885	250	750	700	1.08	1.0	47.0	280	11.4	1.57	0.137	911	0.69	*Shear*
217	B-2-20	GFRP	GF	Yes	20	6	7000	900	2	1885	250	750	700	1.08	1.5	47.5	280	10.8	1.39	0.120	997	0.69	*Shear*
218	B-2-20	GFRP	H1	Yes	20	6	7000	900	2	1885	250	750	700	1.08	1.0	52.7	280	11.2	1.29	0.123	1260	0.66	*Shear*
219	B-2-20	GFRP	H2	Yes	20	6	7000	900	2	1885	250	750	700	1.08	1.0	51.9	280	12.0	1.37	0.141	1049	0.66	*Shear*
220	B-2-20	GFRP	H3	Yes	20	6	7000	900	2	1885	250	750	700	1.08	1.0	47.5	280	12.5	1.51	0.160	1144	0.69	*Shear*
221	B-2-28	GFRP	NO	Yes	28	4	4500	900	2	2463	250	500	450	2.19	0.0	41.8	232	5.5	1.43	0.190	774	0.60	*Shear*
222	B-2-28	GFRP	SF	Yes	28	4	4500	900	2	2463	250	500	450	2.19	0.5	46.2	232	4.8	0.95	0.159	1076	0.86	*Shear*
223	B-2-28	GFRP	SF	Yes	28	4	4500	900	2	2463	250	500	450	2.19	1.0	49.8	232	4.3	0.81	0.126	1258	0.91	*Shear*
224	B-2-28	GFRP	SF	Yes	28	4	4500	900	2	2463	250	500	450	2.19	1.5	52.5	232	3.6	0.65	0.102	1301	0.86	*Shear*
225	B-2-28	GFRP	GF	Yes	28	4	4500	900	2	2463	250	500	450	2.19	0.5	45.6	232	5.0	0.96	0.174	817	0.85	*Shear*
226	B-2-28	GFRP	GF	Yes	28	4	4500	900	2	2463	250	500	450	2.19	1.0	47.0	232	4.7	0.87	0.135	919	0.88	*Shear*
227	B-2-28	GFRP	GF	Yes	28	4	4500	900	2	2463	250	500	450	2.19	1.5	47.5	232	4.5	0.79	0.128	1072	0.89	*Shear*
228	B-2-28	GFRP	H1	Yes	28	4	4500	900	2	2463	250	500	450	2.19	1.0	52.7	232	4.1	0.78	0.128	1186	0.78	*Shear*
229	B-2-28	GFRP	H2	Yes	28	4	4500	900	2	2463	250	500	450	2.19	1.0	51.9	232	4.5	0.86	0.137	944	0.85	*Shear*
230	B-2-28	GFRP	H3	Yes	28	4	4500	900	2	2463	250	500	450	2.19	1.0	47.5	232	4.9	0.96	0.152	944	0.90	*Shear*
231	B-2-28	GFRP	NO	Yes	28	6	7000	900	2	3695	250	750	700	2.11	0.0	41.8	337	9.3	1.35	0.168	1123	0.66	*Shear*
232	B-2-28	GFRP	SF	Yes	28	6	7000	900	2	3695	250	750	700	2.11	0.5	46.2	337	7.9	0.95	0.135	1445	0.78	*Shear*
233	B-2-28	GFRP	SF	Yes	28	6	7000	900	2	3695	250	750	700	2.11	1.0	49.8	337	7.2	0.84	0.111	1695	0.82	*Shear*
234	B-2-28	GFRP	SF	Yes	28	6	7000	900	2	3695	250	750	700	2.11	1.5	52.5	337	6.0	0.66	0.088	1788	0.79	*Shear*
235	B-2-28	GFRP	GF	Yes	28	6	7000	900	2	3695	250	750	700	2.11	0.5	45.6	337	8.1	1.25	0.151	1199	0.84	*Shear*
236	B-2-28	GFRP	GF	Yes	28	6	7000	900	2	3695	250	750	700	2.11	1.0	47.0	337	7.6	1.06	0.135	1253	0.84	*Shear*
237	B-2-28	GFRP	GF	Yes	28	6	7000	900	2	3695	250	750	700	2.11	1.5	47.5	337	7.3	0.80	0.099	1329	0.83	*Shear*
238	B-2-28	GFRP	H1	Yes	28	6	7000	900	2	3695	250	750	700	2.11	1.0	52.7	337	6.8	0.88	0.100	1499	0.77	*Shear*
239	B-2-28	GFRP	H2	Yes	28	6	7000	900	2	3695	250	750	700	2.11	1.0	51.9	337	7.2	0.95	0.107	1516	0.81	*Shear*
240	B-2-28	GFRP	H3	Yes	28	6	7000	900	2	3695	250	750	700	2.11	1.0	47.5	337	8.1	1.07	0.130	1425	0.84	*Shear*
241	B-3-14	GFRP	NO	Yes	14	4	4500	1350	3	616	250	500	450	0.55	0.0	41.8	91	7.8	2.38	0.464	305	0.72	*Shear*

242	B-3-14	GFRP	SF	Yes	14	4	4500	1350	3	616	250	500	450	0.55	0.5	46.2	91	6.0	1.38	0.130	387	0.89	*Shear*
243	B-3-14	GFRP	SF	Yes	14	4	4500	1350	3	616	250	500	450	0.55	1.0	49.8	91	5.3	1.19	0.080	401	0.83	*Shear*
244	B-3-14	GFRP	SF	Yes	14	4	4500	1350	3	616	250	500	450	0.55	1.5	52.5	91	4.7	0.80	0.052	473	0.91	*Shear*
245	B-3-14	GFRP	GF	Yes	14	4	4500	1350	3	616	250	500	450	0.55	0.5	45.6	91	6.7	1.69	0.145	362	0.53	*Shear*
246	B-3-14	GFRP	GF	Yes	14	4	4500	1350	3	616	250	500	450	0.55	1.0	47.0	91	5.7	1.56	0.099	394	0.53	*Shear*
247	B-3-14	GFRP	GF	Yes	14	4	4500	1350	3	616	250	500	450	0.55	1.5	47.5	91	5.0	1.45	0.077	404	0.51	*Shear*
248	B-3-14	GFRP	H1	Yes	14	4	4500	1350	3	616	250	500	450	0.55	1.0	52.7	91	5.8	1.15	0.072	462	0.48	*Shear*
249	B-3-14	GFRP	H2	Yes	14	4	4500	1350	3	616	250	500	450	0.55	1.0	51.9	91	6.3	1.16	0.092	460	0.51	*Shear*
250	B-3-14	GFRP	H3	Yes	14	4	4500	1350	3	616	250	500	450	0.55	1.0	47.5	91	6.9	1.26	0.148	452	0.51	*Shear*
251	B-3-14	GFRP	NO	Yes	14	6	7000	1350	3	924	250	750	700	0.53	0.0	41.8	128	11.1	2.08	0.403	426	0.56	*Shear*
252	B-3-14	GFRP	SF	Yes	14	6	7000	1350	3	924	250	750	700	0.53	0.5	46.2	128	10.2	1.25	0.098	579	0.88	*Shear*
253	B-3-14	GFRP	SF	Yes	14	6	7000	1350	3	924	250	750	700	0.53	1.0	49.8	128	8.6	0.98	0.062	620	0.85	*Shear*
254	B-3-14	GFRP	SF	Yes	14	6	7000	1350	3	924	250	750	700	0.53	1.5	52.5	128	7.6	0.63	0.043	666	0.86	*Shear*
255	B-3-14	GFRP	GF	Yes	14	6	7000	1350	3	924	250	750	700	0.53	0.5	45.6	128	10.6	1.58	0.101	548	0.54	*Shear*
256	B-3-14	GFRP	GF	Yes	14	6	7000	1350	3	924	250	750	700	0.53	1.0	47.0	128	9.4	1.40	0.070	595	0.51	*Shear*
257	B-3-14	GFRP	GF	Yes	14	6	7000	1350	3	924	250	750	700	0.53	1.5	47.5	128	8.8	1.45	0.062	615	0.50	*Shear*
258	B-3-14	GFRP	H1	Yes	14	6	7000	1350	3	924	250	750	700	0.53	1.0	52.7	128	9.0	1.14	0.049	647	0.49	*Shear*
259	B-3-14	GFRP	H2	Yes	14	6	7000	1350	3	924	250	750	700	0.53	1.0	51.9	128	9.9	1.25	0.067	631	0.49	*Shear*
260	B-3-14	GFRP	H3	Yes	14	6	7000	1350	3	924	250	750	700	0.53	1.0	47.5	128	9.7	1.27	0.103	615	0.50	*Shear*
261	B-3-20	GFRP	NO	Yes	20	4	4500	1350	3	1257	250	500	450	1.12	0.0	41.8	142	10.9	2.82	0.371	472	0.52	*Shear*
262	B-3-20	GFRP	SF	Yes	20	4	4500	1350	3	1257	250	500	450	1.12	0.5	46.2	142	8.0	1.86	0.335	491	0.81	*Shear*
263	B-3-20	GFRP	SF	Yes	20	4	4500	1350	3	1257	250	500	450	1.12	1.0	49.8	142	7.7	1.53	0.200	526	0.78	*Shear*
264	B-3-20	GFRP	SF	Yes	20	4	4500	1350	3	1257	250	500	450	1.12	1.5	52.5	142	6.9	1.35	0.132	748	1.02	*Shear*
265	B-3-20	GFRP	GF	Yes	20	4	4500	1350	3	1257	250	500	450	1.12	0.5	45.6	142	8.8	2.07	0.310	511	0.73	*Shear*
266	B-3-20	GFRP	GF	Yes	20	4	4500	1350	3	1257	250	500	450	1.12	1.0	47.0	142	8.0	1.98	0.244	521	0.71	*Shear*
267	B-3-20	GFRP	GF	Yes	20	4	4500	1350	3	1257	250	500	450	1.12	1.5	47.5	142	7.8	1.85	0.183	560	0.70	*Shear*
268	B-3-20	GFRP	H1	Yes	20	4	4500	1350	3	1257	250	500	450	1.12	1.0	52.7	142	7.9	1.68	0.230	683	0.67	*Shear*
269	B-3-20	GFRP	H2	Yes	20	4	4500	1350	3	1257	250	500	450	1.12	1.0	51.9	142	8.3	1.88	0.251	721	0.68	*Shear*
270	B-3-20	GFRP	H3	Yes	20	4	4500	1350	3	1257	250	500	450	1.12	1.0	47.5	142	9.4	2.02	0.323	662	0.70	*Shear*
271	B-3-20	GFRP	NO	Yes	20	6	7000	1350	3	1885	250	750	700	1.08	0.0	41.8	182	15.3	2.20	0.270	608	0.65	*Shear*
272	B-3-20	GFRP	SF	Yes	20	6	7000	1350	3	1885	250	750	700	1.08	0.5	46.2	182	12.6	1.70	0.225	801	0.88	*Shear*
273	B-3-20	GFRP	SF	Yes	20	6	7000	1350	3	1885	250	750	700	1.08	1.0	49.8	182	9.1	1.19	0.111	889	0.88	*Shear*
274	B-3-20	GFRP	SF	Yes	20	6	7000	1350	3	1885	250	750	700	1.08	1.5	52.5	182	8.3	0.94	0.084	928	0.84	*Shear*
275	B-3-20	GFRP	GF	Yes	20	6	7000	1350	3	1885	250	750	700	1.08	0.5	45.6	182	11.3	1.92	0.216	756	0.71	*Shear*
276	B-3-20	GFRP	GF	Yes	20	6	7000	1350	3	1885	250	750	700	1.08	1.0	47.0	182	10.3	1.60	0.128	816	0.69	*Shear*
277	B-3-20	GFRP	GF	Yes	20	6	7000	1350	3	1885	250	750	700	1.08	1.5	47.5	182	9.3	1.76	0.114	822	0.68	*Shear*
278	B-3-20	GFRP	H1	Yes	20	6	7000	1350	3	1885	250	750	700	1.08	1.0	52.7	182	8.1	1.46	0.115	887	0.66	*Shear*
279	B-3-20	GFRP	H2	Yes	20	6	7000	1350	3	1885	250	750	700	1.08	1.0	51.9	182	8.9	1.62	0.136	876	0.66	*Shear*
280	B-3-20	GFRP	H3	Yes	20	6	7000	1350	3	1885	250	750	700	1.08	1.0	47.5	182	10.7	1.74	0.175	838	0.69	*Shear*
281	B-3-28	GFRP	NO	Yes	28	4	4500	1350	3	2463	250	500	450	2.19	0.0	41.8	162	7.0	1.56	0.208	539	0.55	*Shear*
282	B-3-28	GFRP	SF	Yes	28	4	4500	1350	3	2463	250	500	450	2.19	0.5	46.2	162	6.6	1.29	0.186	600	0.72	*Shear*
283	B-3-28	GFRP	SF	Yes	28	4	4500	1350	3	2463	250	500	450	2.19	1.0	49.8	162	5.1	1.12	0.142	667	0.72	*Shear*
284	B-3-28	GFRP	SF	Yes	28	4	4500	1350	3	2463	250	500	450	2.19	1.5	52.5	162	4.8	1.00	0.112	923	0.92	*Shear*
285	B-3-28	GFRP	GF	Yes	28	4	4500	1350	3	2463	250	500	450	2.19	0.5	45.6	162	6.7	1.34	0.204	682	0.93	*Shear*
286	B-3-28	GFRP	GF	Yes	28	4	4500	1350	3	2463	250	500	450	2.19	1.0	47.0	162	6.2	1.23	0.153	672	0.90	*Shear*
287	B-3-28	GFRP	GF	Yes	28	4	4500	1350	3	2463	250	500	450	2.19	1.5	47.5	162	5.9	1.19	0.134	738	0.89	*Shear*
288	B-3-28	GFRP	H1	Yes	28	4	4500	1350	3	2463	250	500	450	2.19	1.0	52.7	162	5.5	1.11	0.142	904	0.86	*Shear*
289	B-3-28	GFRP	H2	Yes	28	4	4500	1350	3	2463	250	500	450	2.19	1.0	51.9	162	5.6	1.17	0.150	989	0.87	*Shear*
290	B-3-28	GFRP	H3	Yes	28	4	4500	1350	3	2463	250	500	450	2.19	1.0	47.5	162	5.9	1.35	0.162	924	0.90	*Shear*
291	B-3-28	GFRP	NO	Yes	28	6	7000	1350	3	3695	250	750	700	2.11	0.0	41.8	221	11.0	1.40	0.178	736	0.65	*Shear*

292	B-3-28	GFRP	SF	Yes	28	6	7000	1350	3	3695	250	750	700	2.11	0.5	46.2	221	8.9	1.10	0.131	1026	0.83	*Shear*
293	B-3-28	GFRP	SF	Yes	28	6	7000	1350	3	3695	250	750	700	2.11	1.0	49.8	221	7.9	0.98	0.098	1140	0.83	*Shear*
294	B-3-28	GFRP	SF	Yes	28	6	7000	1350	3	3695	250	750	700	2.11	1.5	52.5	221	7.3	0.74	0.082	1133	0.75	*Shear*
295	B-3-28	GFRP	GF	Yes	28	6	7000	1350	3	3695	250	750	700	2.11	0.5	45.6	221	9.2	1.19	0.118	998	0.87	*Shear*
296	B-3-28	GFRP	GF	Yes	28	6	7000	1350	3	3695	250	750	700	2.11	1.0	47.0	221	8.7	1.09	0.107	1030	0.84	*Shear*
297	B-3-28	GFRP	GF	Yes	28	6	7000	1350	3	3695	250	750	700	2.11	1.5	47.5	221	8.3	0.87	0.093	1133	0.82	*Shear*
298	B-3-28	GFRP	H1	Yes	28	6	7000	1350	3	3695	250	750	700	2.11	1.0	52.7	221	8.0	1.01	0.094	1205	0.81	*Shear*
299	B-3-28	GFRP	H2	Yes	28	6	7000	1350	3	3695	250	750	700	2.11	1.0	51.9	221	8.6	1.11	0.102	1105	0.81	*Shear*
300	B-3-28	GFRP	H3	Yes	28	6	7000	1350	3	3695	250	750	700	2.11	1.0	47.5	221	9.1	1.29	0.116	1092	0.83	*Shear*
301	B-4-14	GFRP	NO	Yes	14	4	4500	2100	4	616	250	500	450	0.55	0.0	41.8	75	12.0	2.80	0.560	252	0.79	*Shear*
302	B-4-14	GFRP	SF	Yes	14	4	4500	2100	4	616	250	500	450	0.55	0.5	46.2	75	8.5	1.89	0.375	340	1.04	*Shear*
303	B-4-14	GFRP	SF	Yes	14	4	4500	2100	4	616	250	500	450	0.55	1.0	49.8	75	7.0	1.33	0.114	351	0.97	*Shear*
304	B-4-14	GFRP	SF	Yes	14	4	4500	2100	4	616	250	500	450	0.55	1.5	52.5	75	5.0	0.83	0.051	354	0.91	*Shear*
305	B-4-14	GFRP	GF	Yes	14	4	4500	2100	4	616	250	500	450	0.55	0.5	45.6	75	9.4	2.46	0.447	330	0.53	*Shear*
306	B-4-14	GFRP	GF	Yes	14	4	4500	2100	4	616	250	500	450	0.55	1.0	47.0	75	8.8	1.99	0.144	336	0.52	*Shear*
307	B-4-14	GFRP	GF	Yes	14	4	4500	2100	4	616	250	500	450	0.55	1.5	47.5	75	7.5	1.87	0.105	340	0.50	*Shear*
308	B-4-14	GFRP	H1	Yes	14	4	4500	2100	4	616	250	500	450	0.55	1.0	52.7	75	7.8	1.67	0.109	345	0.48	*Shear*
309	B-4-14	GFRP	H2	Yes	14	4	4500	2100	4	616	250	500	450	0.55	1.0	51.9	75	8.5	1.90	0.143	344	0.50	*Shear*
310	B-4-14	GFRP	H3	Yes	14	4	4500	2100	4	616	250	500	450	0.55	1.0	47.5	75	9.0	2.15	0.188	343	0.50	*Shear*
311	B-4-14	GFRP	NO	Yes	14	6	7000	2100	4	924	250	750	700	0.53	0.0	41.8	99	13.2	2.47	0.393	330	0.55	*Shear*
312	B-4-14	GFRP	SF	Yes	14	6	7000	2100	4	924	250	750	700	0.53	0.5	46.2	99	9.9	1.67	0.115	441	0.89	*Shear*
313	B-4-14	GFRP	SF	Yes	14	6	7000	2100	4	924	250	750	700	0.53	1.0	49.8	99	7.8	1.15	0.067	470	0.86	*Shear*
314	B-4-14	GFRP	SF	Yes	14	6	7000	2100	4	924	250	750	700	0.53	1.5	52.5	99	6.7	0.46	0.046	508	0.88	*Shear*
315	B-4-14	GFRP	GF	Yes	14	6	7000	2100	4	924	250	750	700	0.53	0.5	45.6	99	10.9	1.90	0.118	318	0.54	*Shear*
316	B-4-14	GFRP	GF	Yes	14	6	7000	2100	4	924	250	750	700	0.53	1.0	47.0	99	9.5	1.63	0.082	366	0.51	*Shear*
317	B-4-14	GFRP	GF	Yes	14	6	7000	2100	4	924	250	750	700	0.53	1.5	47.5	99	8.5	1.51	0.066	403	0.49	*Shear*
318	B-4-14	GFRP	H1	Yes	14	6	7000	2100	4	924	250	750	700	0.53	1.0	52.7	99	8.5	1.15	0.054	464	0.50	*Shear*
319	B-4-14	GFRP	H2	Yes	14	6	7000	2100	4	924	250	750	700	0.53	1.0	51.9	99	9.1	1.30	0.082	412	0.49	*Shear*
320	B-4-14	GFRP	H3	Yes	14	6	7000	2100	4	924	250	750	700	0.53	1.0	47.5	99	9.9	1.41	0.118	445	0.49	*Shear*
321	B-4-20	GFRP	NO	Yes	20	4	4500	2100	4	1257	250	500	450	1.12	0.0	41.8	111	11.1	2.47	0.511	372	0.82	*Shear*
322	B-4-20	GFRP	SF	Yes	20	4	4500	2100	4	1257	250	500	450	1.12	0.5	46.2	111	9.8	2.00	0.341	501	1.10	*Shear*
323	B-4-20	GFRP	SF	Yes	20	4	4500	2100	4	1257	250	500	450	1.12	1.0	49.8	111	7.9	1.85	0.091	549	1.09	*Shear*
324	B-4-20	GFRP	SF	Yes	20	4	4500	2100	4	1257	250	500	450	1.12	1.5	52.5	111	7.2	1.54	0.041	578	1.05	*Shear*
325	B-4-20	GFRP	GF	Yes	20	4	4500	2100	4	1257	250	500	450	1.12	0.5	45.6	111	10.5	2.40	0.421	388	0.71	*Shear*
326	B-4-20	GFRP	GF	Yes	20	4	4500	2100	4	1257	250	500	450	1.12	1.0	47.0	111	8.8	2.13	0.121	462	0.70	*Shear*
327	B-4-20	GFRP	GF	Yes	20	4	4500	2100	4	1257	250	500	450	1.12	1.5	47.5	111	8.1	2.22	0.091	478	0.69	*Shear*
328	B-4-20	GFRP	H1	Yes	20	4	4500	2100	4	1257	250	500	450	1.12	1.0	52.7	111	8.6	1.81	0.092	525	0.66	*Shear*
329	B-4-20	GFRP	H2	Yes	20	4	4500	2100	4	1257	250	500	450	1.12	1.0	51.9	111	9.7	1.93	0.134	543	0.67	*Shear*
330	B-4-20	GFRP	H3	Yes	20	4	4500	2100	4	1257	250	500	450	1.12	1.0	47.5	111	9.9	2.02	0.181	525	0.69	*Shear*
331	B-4-20	GFRP	NO	Yes	20	6	7000	2100	4	1885	250	750	700	1.08	0.0	41.8	163	18.7	2.53	0.345	542	0.93	*Shear*
332	B-4-20	GFRP	SF	Yes	20	6	7000	2100	4	1885	250	750	700	1.08	0.5	46.2	163	16.3	2.10	0.091	626	0.92	*Shear*
333	B-4-20	GFRP	SF	Yes	20	6	7000	2100	4	1885	250	750	700	1.08	1.0	49.8	163	13.3	2.09	0.062	697	0.92	*Shear*
334	B-4-20	GFRP	SF	Yes	20	6	7000	2100	4	1885	250	750	700	1.08	1.5	52.5	163	11.1	1.84	0.044	726	0.88	*Shear*
335	B-4-20	GFRP	GF	Yes	20	6	7000	2100	4	1885	250	750	700	1.08	0.5	45.6	163	17.6	2.32	0.112	527	0.73	*Shear*
336	B-4-20	GFRP	GF	Yes	20	6	7000	2100	4	1885	250	750	700	1.08	1.0	47.0	163	15.3	2.57	0.076	528	0.71	*Shear*
337	B-4-20	GFRP	GF	Yes	20	6	7000	2100	4	1885	250	750	700	1.08	1.5	47.5	163	11.5	2.10	0.062	619	0.70	*Shear*
338	B-4-20	GFRP	H1	Yes	20	6	7000	2100	4	1885	250	750	700	1.08	1.0	52.7	163	13.5	1.91	0.042	678	0.67	*Shear*
339	B-4-20	GFRP	H2	Yes	20	6	7000	2100	4	1885	250	750	700	1.08	1.0	51.9	163	14.7	1.95	0.095	667	0.68	*Shear*
340	B-4-20	GFRP	H3	Yes	20	6	7000	2100	4	1885	250	750	700	1.08	1.0	47.5	163	16.3	1.87	0.092	660	0.70	*Shear*
341	B-4-28	GFRP	NO	Yes	28	4	4500	2100	4	2463	250	500	450	2.19	0.0	41.8	133	8.1	1.62	0.423	442	0.69	*Shear*

342	B-4-28	GFRP	SF	Yes	28	4	4500	2100	4	2463	250	500	450	2.19	0.5	46.2	133	7.3	1.38	0.312	603	0.97	*Shear*
343	B-4-28	GFRP	SF	Yes	28	4	4500	2100	4	2463	250	500	450	2.19	1.0	49.8	133	6.3	1.30	0.082	681	0.99	*Shear*
344	B-4-28	GFRP	SF	Yes	28	4	4500	2100	4	2463	250	500	450	2.19	1.5	52.5	133	5.4	1.12	0.032	715	0.95	*Shear*
345	B-4-28	GFRP	GF	Yes	28	4	4500	2100	4	2463	250	500	450	2.19	0.5	45.6	133	8.2	1.61	0.402	530	0.96	*Shear*
346	B-4-28	GFRP	GF	Yes	28	4	4500	2100	4	2463	250	500	450	2.19	1.0	47.0	133	6.9	1.44	0.100	551	0.91	*Shear*
347	B-4-28	GFRP	GF	Yes	28	4	4500	2100	4	2463	250	500	450	2.19	1.5	47.5	133	6.6	1.51	0.078	651	0.87	*Shear*
348	B-4-28	GFRP	H1	Yes	28	4	4500	2100	4	2463	250	500	450	2.19	1.0	52.7	133	6.2	1.27	0.081	635	0.89	*Shear*
349	B-4-28	GFRP	H2	Yes	28	4	4500	2100	4	2463	250	500	450	2.19	1.0	51.9	133	6.5	1.34	0.111	687	0.88	*Shear*
350	B-4-28	GFRP	H3	Yes	28	4	4500	2100	4	2463	250	500	450	2.19	1.0	47.5	133	7.3	1.39	0.175	631	0.88	*Shear*
351	B-4-28	GFRP	NO	Yes	28	6	7000	2100	4	3695	250	750	700	2.11	0.0	41.8	209	14.7	1.82	0.313	696	0.77	*Shear*
352	B-4-28	GFRP	SF	Yes	28	6	7000	2100	4	3695	250	750	700	2.11	0.5	46.2	209	13.5	1.60	0.081	794	0.86	*Shear*
353	B-4-28	GFRP	SF	Yes	28	6	7000	2100	4	3695	250	750	700	2.11	1.0	49.8	209	11.3	1.64	0.051	943	0.92	*Shear*
354	B-4-28	GFRP	SF	Yes	28	6	7000	2100	4	3695	250	750	700	2.11	1.5	52.5	209	9.8	1.50	0.032	1006	0.89	*Shear*
355	B-4-28	GFRP	GF	Yes	28	6	7000	2100	4	3695	250	750	700	2.11	0.5	45.6	209	13.7	1.71	0.091	739	0.88	*Shear*
356	B-4-28	GFRP	GF	Yes	28	6	7000	2100	4	3695	250	750	700	2.11	1.0	47.0	209	12.5	1.91	0.072	801	0.84	*Shear*
357	B-4-28	GFRP	GF	Yes	28	6	7000	2100	4	3695	250	750	700	2.11	1.5	47.5	209	11.9	1.57	0.053	832	0.84	*Shear*
358	B-4-28	GFRP	H1	Yes	28	6	7000	2100	4	3695	250	750	700	2.11	1.0	52.7	209	11.5	1.49	0.031	943	0.81	*Shear*
359	B-4-28	GFRP	H2	Yes	28	6	7000	2100	4	3695	250	750	700	2.11	1.0	51.9	209	11.9	1.50	0.092	938	0.81	*Shear*
360	B-4-28	GFRP	H3	Yes	28	6	7000	2100	4	3695	250	750	700	2.11	1.0	47.5	209	13.2	1.43	0.102	887	0.85	*Shear*
361	B-2-14	SR	NO	No	14	4	4500	900	2	616	250	500	450	0.55	0.0	41.8	----	----	----	----	269	1.12	*Flexural*
362	B-2-14	SR	SF	No	14	4	4500	900	2	616	250	500	450	0.55	0.5	46.2	----	----	----	----	301	0.98	*Flexural*
363	B-2-14	SR	SF	No	14	4	4500	900	2	616	250	500	450	0.55	1.0	49.8	----	----	----	----	361	1.09	*Flexural*
364	B-2-14	SR	SF	No	14	4	4500	900	2	616	250	500	450	0.55	1.5	52.5	----	----	----	----	398	1.11	*Flexural*
365	B-2-14	SR	GF	No	14	4	4500	900	2	616	250	500	450	0.55	0.5	45.6	----	----	----	----	301	1.10	*Flexural*
366	B-2-14	SR	GF	No	14	4	4500	900	2	616	250	500	450	0.55	1.0	47.0	----	----	----	----	297	1.05	*Flexural*
367	B-2-14	SR	GF	No	14	4	4500	900	2	616	250	500	450	0.55	1.5	47.5	----	----	----	----	323	1.13	*Flexural*
368	B-2-14	SR	H1	No	14	4	4500	900	2	616	250	500	450	0.55	1.0	52.7	----	----	----	----	332	0.86	*Flexural*
369	B-2-14	SR	H2	No	14	4	4500	900	2	616	250	500	450	0.55	1.0	51.9	----	----	----	----	327	0.86	*Flexural*
370	B-2-14	SR	H3	No	14	4	4500	900	2	616	250	500	450	0.55	1.0	47.5	----	----	----	----	310	0.96	*Shear*
371	B-2-14	SR	NO	No	14	6	7000	900	2	924	250	750	700	0.53	0.0	41.8	----	----	----	----	379	1.03	*Flexural*
372	B-2-14	SR	SF	No	14	6	7000	900	2	924	250	750	700	0.53	0.5	46.2	----	----	----	----	430	0.83	*Shear*
373	B-2-14	SR	SF	No	14	6	7000	900	2	924	250	750	700	0.53	1.0	49.8	----	----	----	----	523	0.90	*Flexural*
374	B-2-14	SR	SF	No	14	6	7000	900	2	924	250	750	700	0.53	1.5	52.5	----	----	----	----	653	1.02	*Flexural*
375	B-2-14	SR	GF	No	14	6	7000	900	2	924	250	750	700	0.53	0.5	45.6	----	----	----	----	402	0.90	*Shear*
376	B-2-14	SR	GF	No	14	6	7000	900	2	924	250	750	700	0.53	1.0	47.0	----	----	----	----	421	0.90	*Shear*
377	B-2-14	SR	GF	No	14	6	7000	900	2	924	250	750	700	0.53	1.5	47.5	----	----	----	----	489	1.03	*Flexural*
378	B-2-14	SR	H1	No	14	6	7000	900	2	924	250	750	700	0.53	1.0	52.7	----	----	----	----	463	0.65	*Shear*
379	B-2-14	SR	H2	No	14	6	7000	900	2	924	250	750	700	0.53	1.0	51.9	----	----	----	----	456	0.69	*Shear*
380	B-2-14	SR	H3	No	14	6	7000	900	2	924	250	750	700	0.53	1.0	47.5	----	----	----	----	434	0.83	*Shear*
381	B-2-20	SR	NO	No	20	4	4500	900	2	1257	250	500	450	1.12	0.0	41.8	----	----	----	----	455	0.92	*Shear*
382	B-2-20	SR	SF	No	20	4	4500	900	2	1257	250	500	450	1.12	0.5	46.2	----	----	----	----	563	1.00	*Shear*
383	B-2-20	SR	SF	No	20	4	4500	900	2	1257	250	500	450	1.12	1.0	49.8	----	----	----	----	615	1.05	*Flexural*
384	B-2-20	SR	SF	No	20	4	4500	900	2	1257	250	500	450	1.12	1.5	52.5	----	----	----	----	636	1.04	*Flexural*
385	B-2-20	SR	GF	No	20	4	4500	900	2	1257	250	500	450	1.12	0.5	45.6	----	----	----	----	526	0.99	*Shear*
386	B-2-20	SR	GF	No	20	4	4500	900	2	1257	250	500	450	1.12	1.0	47.0	----	----	----	----	549	1.01	*Flexural*
387	B-2-20	SR	GF	No	20	4	4500	900	2	1257	250	500	450	1.12	1.5	47.5	----	----	----	----	570	1.05	*Flexural*
388	B-2-20	SR	H1	No	20	4	4500	900	2	1257	250	500	450	1.12	1.0	52.7	----	----	----	----	593	0.87	*Flexural*
389	B-2-20	SR	H2	No	20	4	4500	900	2	1257	250	500	450	1.12	1.0	51.9	----	----	----	----	596	0.92	*Flexural*
390	B-2-20	SR	H3	No	20	4	4500	900	2	1257	250	500	450	1.12	1.0	47.5	----	----	----	----	580	0.96	*Flexural*
391	B-2-20	SR	NO	No	20	6	7000	900	2	1885	250	750	700	1.08	0.0	41.8	----	----	----	----	493	0.66	*Flexural*

392	B-2-20	SR	SF	No	20	6	7000	900	2	1885	250	750	700	1.08	0.5	46.2	----	----	----	----	797	0.87	*Shear*
393	B-2-20	SR	SF	No	20	6	7000	900	2	1885	250	750	700	1.08	1.0	49.8	----	----	----	----	1007	1.03	*Shear*
394	B-2-20	SR	SF	No	20	6	7000	900	2	1885	250	750	700	1.08	1.5	52.5	----	----	----	----	1054	1.02	*Flexural*
395	B-2-20	SR	GF	No	20	6	7000	900	2	1885	250	750	700	1.08	0.5	45.6	----	----	----	----	647	0.76	*Shear*
396	B-2-20	SR	GF	No	20	6	7000	900	2	1885	250	750	700	1.08	1.0	47.0	----	----	----	----	758	0.87	*Shear*
397	B-2-20	SR	GF	No	20	6	7000	900	2	1885	250	750	700	1.08	1.5	47.5	----	----	----	----	813	0.93	*Shear*
398	B-2-20	SR	H1	No	20	6	7000	900	2	1885	250	750	700	1.08	1.0	52.7	----	----	----	----	828	0.64	*Shear*
399	B-2-20	SR	H2	No	20	6	7000	900	2	1885	250	750	700	1.08	1.0	51.9	----	----	----	----	828	0.76	*Shear*
400	B-2-20	SR	H3	No	20	6	7000	900	2	1885	250	750	700	1.08	1.0	47.5	----	----	----	----	825	0.82	*Shear*
401	B-2-28	SR	NO	No	28	4	4500	900	2	2463	250	500	450	2.19	0.0	41.8	----	----	----	----	593	0.62	*Shear*
402	B-2-28	SR	SF	No	28	4	4500	900	2	2463	250	500	450	2.19	0.5	46.2	----	----	----	----	903	0.87	*Shear*
403	B-2-28	SR	SF	No	28	4	4500	900	2	2463	250	500	450	2.19	1.0	49.8	----	----	----	----	1087	1.02	*Flexural*
404	B-2-28	SR	SF	No	28	4	4500	900	2	2463	250	500	450	2.19	1.5	52.5	----	----	----	----	1169	1.07	*Flexural*
405	B-2-28	SR	GF	No	28	4	4500	900	2	2463	250	500	450	2.19	0.5	45.6	----	----	----	----	706	0.70	*Shear*
406	B-2-28	SR	GF	No	28	4	4500	900	2	2463	250	500	450	2.19	1.0	47.0	----	----	----	----	805	0.79	*Shear*
407	B-2-28	SR	GF	No	28	4	4500	900	2	2463	250	500	450	2.19	1.5	47.5	----	----	----	----	934	0.91	*Shear*
408	B-2-28	SR	H1	No	28	4	4500	900	2	2463	250	500	450	2.19	1.0	52.7	----	----	----	----	1081	0.66	*Flexural*
409	B-2-28	SR	H2	No	28	4	4500	900	2	2463	250	500	450	2.19	1.0	51.9	----	----	----	----	1052	0.75	*Shear*
410	B-2-28	SR	H3	No	28	4	4500	900	2	2463	250	500	450	2.19	1.0	47.5	----	----	----	----	1000	0.88	*Shear*
411	B-2-28	SR	NO	No	28	6	7000	900	2	3695	250	750	700	2.11	0.0	41.8	----	----	----	----	633	0.44	*Shear*
412	B-2-28	SR	SF	No	28	6	7000	900	2	3695	250	750	700	2.11	0.5	46.2	----	----	----	----	1015	0.61	*Shear*
413	B-2-28	SR	SF	No	28	6	7000	900	2	3695	250	750	700	2.11	1.0	49.8	----	----	----	----	1577	0.92	*Shear*
414	B-2-28	SR	SF	No	28	6	7000	900	2	3695	250	750	700	2.11	1.5	52.5	----	----	----	----	1626	0.92	*Shear*
415	B-2-28	SR	GF	No	28	6	7000	900	2	3695	250	750	700	2.11	0.5	45.6	----	----	----	----	839	0.53	*Shear*
416	B-2-28	SR	GF	No	28	6	7000	900	2	3695	250	750	700	2.11	1.0	47.0	----	----	----	----	935	0.58	*Shear*
417	B-2-28	SR	GF	No	28	6	7000	900	2	3695	250	750	700	2.11	1.5	47.5	----	----	----	----	1056	0.65	*Shear*
418	B-2-28	SR	H1	No	28	6	7000	900	2	3695	250	750	700	2.11	1.0	52.7	----	----	----	----	1336	0.48	*Shear*
419	B-2-28	SR	H2	No	28	6	7000	900	2	3695	250	750	700	2.11	1.0	51.9	----	----	----	----	1300	0.54	*Shear*
420	B-2-28	SR	H3	No	28	6	7000	900	2	3695	250	750	700	2.11	1.0	47.5	----	----	----	----	1106	0.61	*Shear*
421	B-3-14	SR	NO	No	14	4	4500	1350	3	616	250	500	450	0.55	0.0	41.8	----	----	----	----	174	1.06	*Flexural*
422	B-3-14	SR	SF	No	14	4	4500	1350	3	616	250	500	450	0.55	0.5	46.2	----	----	----	----	202	0.99	*Flexural*
423	B-3-14	SR	SF	No	14	4	4500	1350	3	616	250	500	450	0.55	1.0	49.8	----	----	----	----	239	1.08	*Flexural*
424	B-3-14	SR	SF	No	14	4	4500	1350	3	616	250	500	450	0.55	1.5	52.5	----	----	----	----	265	1.10	*Flexural*
425	B-3-14	SR	GF	No	14	4	4500	1350	3	616	250	500	450	0.55	0.5	45.6	----	----	----	----	183	1.00	*Flexural*
426	B-3-14	SR	GF	No	14	4	4500	1350	3	616	250	500	450	0.55	1.0	47.0	----	----	----	----	210	1.11	*Flexural*
427	B-3-14	SR	GF	No	14	4	4500	1350	3	616	250	500	450	0.55	1.5	47.5	----	----	----	----	236	1.23	*Flexural*
428	B-3-14	SR	H1	No	14	4	4500	1350	3	616	250	500	450	0.55	1.0	52.7	----	----	----	----	220	0.79	*Flexural*
429	B-3-14	SR	H2	No	14	4	4500	1350	3	616	250	500	450	0.55	1.0	51.9	----	----	----	----	219	0.92	*Flexural*
430	B-3-14	SR	H3	No	14	4	4500	1350	3	616	250	500	450	0.55	1.0	47.5	----	----	----	----	208	1.05	*Shear*
431	B-3-14	SR	NO	No	14	6	7000	1350	3	924	250	750	700	0.53	0.0	41.8	----	----	----	----	239	0.97	*Flexural*
432	B-3-14	SR	SF	No	14	6	7000	1350	3	924	250	750	700	0.53	0.5	46.2	----	----	----	----	290	0.84	*Flexural*
433	B-3-14	SR	SF	No	14	6	7000	1350	3	924	250	750	700	0.53	1.0	49.8	----	----	----	----	349	0.91	*Flexural*
434	B-3-14	SR	SF	No	14	6	7000	1350	3	924	250	750	700	0.53	1.5	52.5	----	----	----	----	385	0.90	*Flexural*
435	B-3-14	SR	GF	No	14	6	7000	1350	3	924	250	750	700	0.53	0.5	45.6	----	----	----	----	262	0.88	*Shear*
436	B-3-14	SR	GF	No	14	6	7000	1350	3	924	250	750	700	0.53	1.0	47.0	----	----	----	----	283	0.91	*Shear*
437	B-3-14	SR	GF	No	14	6	7000	1350	3	924	250	750	700	0.53	1.5	47.5	----	----	----	----	318	1.00	*Flexural*
438	B-3-14	SR	H1	No	14	6	7000	1350	3	924	250	750	700	0.53	1.0	52.7	----	----	----	----	309	0.64	*Shear*
439	B-3-14	SR	H2	No	14	6	7000	1350	3	924	250	750	700	0.53	1.0	51.9	----	----	----	----	304	0.70	*Shear*
440	B-3-14	SR	H3	No	14	6	7000	1350	3	924	250	750	700	0.53	1.0	47.5	----	----	----	----	292	0.81	*Shear*
441	B-3-20	SR	NO	No	20	4	4500	1350	3	1257	250	500	450	1.12	0.0	41.8	----	----	----	----	258	0.78	*Shear*

442	B-3-20	SR	SF	No	20	4	4500	1350	3	1257	250	500	450	1.12	0.5	46.2	----	----	----	----	374	1.00	*Flexural*
443	B-3-20	SR	SF	No	20	4	4500	1350	3	1257	250	500	450	1.12	1.0	49.8	----	----	----	----	415	1.06	*Flexural*
444	B-3-20	SR	SF	No	20	4	4500	1350	3	1257	250	500	450	1.12	1.5	52.5	----	----	----	----	421	1.03	*Flexural*
445	B-3-20	SR	GF	No	20	4	4500	1350	3	1257	250	500	450	1.12	0.5	45.6	----	----	----	----	316	0.89	*Shear*
446	B-3-20	SR	GF	No	20	4	4500	1350	3	1257	250	500	450	1.12	1.0	47.0	----	----	----	----	362	1.00	*Shear*
447	B-3-20	SR	GF	No	20	4	4500	1350	3	1257	250	500	450	1.12	1.5	47.5	----	----	----	----	381	1.05	*Flexural*
448	B-3-20	SR	H1	No	20	4	4500	1350	3	1257	250	500	450	1.12	1.0	52.7	----	----	----	----	395	0.78	*Flexural*
449	B-3-20	SR	H2	No	20	4	4500	1350	3	1257	250	500	450	1.12	1.0	51.9	----	----	----	----	395	0.91	*Shear*
450	B-3-20	SR	H3	No	20	4	4500	1350	3	1257	250	500	450	1.12	1.0	47.5	----	----	----	----	387	0.96	*Flexural*
451	B-3-20	SR	NO	No	20	6	7000	1350	3	1885	250	750	700	1.08	0.0	41.8	----	----	----	----	347	0.70	*Flexural*
452	B-3-20	SR	SF	No	20	6	7000	1350	3	1885	250	750	700	1.08	0.5	46.2	----	----	----	----	541	0.89	*Shear*
453	B-3-20	SR	SF	No	20	6	7000	1350	3	1885	250	750	700	1.08	1.0	49.8	----	----	----	----	578	0.89	*Flexural*
454	B-3-20	SR	SF	No	20	6	7000	1350	3	1885	250	750	700	1.08	1.5	52.5	----	----	----	----	618	0.89	*Flexural*
455	B-3-20	SR	GF	No	20	6	7000	1350	3	1885	250	750	700	1.08	0.5	45.6	----	----	----	----	444	0.79	*Shear*
456	B-3-20	SR	GF	No	20	6	7000	1350	3	1885	250	750	700	1.08	1.0	47.0	----	----	----	----	489	0.85	*Shear*
457	B-3-20	SR	GF	No	20	6	7000	1350	3	1885	250	750	700	1.08	1.5	47.5	----	----	----	----	540	0.93	*Shear*
458	B-3-20	SR	H1	No	20	6	7000	1350	3	1885	250	750	700	1.08	1.0	52.7	----	----	----	----	564	0.66	*Shear*
459	B-3-20	SR	H2	No	20	6	7000	1350	3	1885	250	750	700	1.08	1.0	51.9	----	----	----	----	560	0.73	*Shear*
460	B-3-20	SR	H3	No	20	6	7000	1350	3	1885	250	750	700	1.08	1.0	47.5	----	----	----	----	412	0.82	*Shear*
461	B-3-28	SR	NO	No	28	4	4500	1350	3	2463	250	500	450	2.19	0.0	41.8	----	----	----	----	342	0.54	*Shear*
462	B-3-28	SR	SF	No	28	4	4500	1350	3	2463	250	500	450	2.19	0.5	46.2	----	----	----	----	543	0.79	*Shear*
463	B-3-28	SR	SF	No	28	4	4500	1350	3	2463	250	500	450	2.19	1.0	49.8	----	----	----	----	747	1.05	*Flexural*
464	B-3-28	SR	SF	No	28	4	4500	1350	3	2463	250	500	450	2.19	1.5	52.5	----	----	----	----	790	1.09	*Flexural*
465	B-3-28	SR	GF	No	28	4	4500	1350	3	2463	250	500	450	2.19	0.5	45.6	----	----	----	----	409	0.61	*Shear*
466	B-3-28	SR	GF	No	28	4	4500	1350	3	2463	250	500	450	2.19	1.0	47.0	----	----	----	----	466	0.69	*Shear*
467	B-3-28	SR	GF	No	28	4	4500	1350	3	2463	250	500	450	2.19	1.5	47.5	----	----	----	----	567	0.83	*Shear*
468	B-3-28	SR	H1	No	28	4	4500	1350	3	2463	250	500	450	2.19	1.0	52.7	----	----	----	----	732	0.57	*Flexural*
469	B-3-28	SR	H2	No	28	4	4500	1350	3	2463	250	500	450	2.19	1.0	51.9	----	----	----	----	736	0.65	*Flexural*
470	B-3-28	SR	H3	No	28	4	4500	1350	3	2463	250	500	450	2.19	1.0	47.5	----	----	----	----	637	0.80	*Shear*
471	B-3-28	SR	NO	No	28	6	7000	1350	3	3695	250	750	700	2.11	0.0	41.8	----	----	----	----	440	0.46	*Flexural*
472	B-3-28	SR	SF	No	28	6	7000	1350	3	3695	250	750	700	2.11	0.5	46.2	----	----	----	----	676	0.61	*Shear*
473	B-3-28	SR	SF	No	28	6	7000	1350	3	3695	250	750	700	2.11	1.0	49.8	----	----	----	----	1061	0.93	*Shear*
474	B-3-28	SR	SF	No	28	6	7000	1350	3	3695	250	750	700	2.11	1.5	52.5	----	----	----	----	1088	0.92	*Flexural*
475	B-3-28	SR	GF	No	28	6	7000	1350	3	3695	250	750	700	2.11	0.5	45.6	----	----	----	----	594	0.56	*Shear*
476	B-3-28	SR	GF	No	28	6	7000	1350	3	3695	250	750	700	2.11	1.0	47.0	----	----	----	----	677	0.63	*Shear*
477	B-3-28	SR	GF	No	28	6	7000	1350	3	3695	250	750	700	2.11	1.5	47.5	----	----	----	----	785	0.73	*Shear*
478	B-3-28	SR	H1	No	28	6	7000	1350	3	3695	250	750	700	2.11	1.0	52.7	----	----	----	----	930	0.51	*Shear*
479	B-3-28	SR	H2	No	28	6	7000	1350	3	3695	250	750	700	2.11	1.0	51.9	----	----	----	----	842	0.58	*Shear*
480	B-3-28	SR	H3	No	28	6	7000	1350	3	3695	250	750	700	2.11	1.0	47.5	----	----	----	----	711	0.68	*Shear*
481	B-4-14	SR	NO	No	14	4	4500	2100	4	616	250	500	450	0.55	0.0	41.8	----	----	----	----	128	1.04	*Flexural*
482	B-4-14	SR	SF	No	14	4	4500	2100	4	616	250	500	450	0.55	0.5	46.2	----	----	----	----	150	0.98	*Flexural*
483	B-4-14	SR	SF	No	14	4	4500	2100	4	616	250	500	450	0.55	1.0	49.8	----	----	----	----	180	1.09	*Flexural*
484	B-4-14	SR	SF	No	14	4	4500	2100	4	616	250	500	450	0.55	1.5	52.5	----	----	----	----	200	1.11	*Flexural*
485	B-4-14	SR	GF	No	14	4	4500	2100	4	616	250	500	450	0.55	0.5	45.6	----	----	----	----	140	1.02	*Flexural*
486	B-4-14	SR	GF	No	14	4	4500	2100	4	616	250	500	450	0.55	1.0	47.0	----	----	----	----	153	1.08	*Flexural*
487	B-4-14	SR	GF	No	14	4	4500	2100	4	616	250	500	450	0.55	1.5	47.5	----	----	----	----	173	1.21	*Flexural*
488	B-4-14	SR	H1	No	14	4	4500	2100	4	616	250	500	450	0.55	1.0	52.7	----	----	----	----	165	0.80	*Flexural*
489	B-4-14	SR	H2	No	14	4	4500	2100	4	616	250	500	450	0.55	1.0	51.9	----	----	----	----	159	0.89	*Shear*
490	B-4-14	SR	H3	No	14	4	4500	2100	4	616	250	500	450	0.55	1.0	47.5	----	----	----	----	155	1.03	*Shear*
491	B-4-14	SR	NO	No	14	6	7000	2100	4	924	250	750	700	0.53	0.0	41.8	----	----	----	----	183	1.00	*Flexural*

492	B-4-14	SR	SF	No	14	6	7000	2100	4	924	250	750	700	0.53	0.5	46.2	----	----	----	----	216	0.83	*Flexural*
493	B-4-14	SR	SF	No	14	6	7000	2100	4	924	250	750	700	0.53	1.0	49.8	----	----	----	----	262	0.91	*Flexural*
494	B-4-14	SR	SF	No	14	6	7000	2100	4	924	250	750	700	0.53	1.5	52.5	----	----	----	----	289	0.90	*Flexural*
495	B-4-14	SR	GF	No	14	6	7000	2100	4	924	250	750	700	0.53	0.5	45.6	----	----	----	----	198	0.89	*Flexural*
496	B-4-14	SR	GF	No	14	6	7000	2100	4	924	250	750	700	0.53	1.0	47.0	----	----	----	----	216	0.92	*Flexural*
497	B-4-14	SR	GF	No	14	6	7000	2100	4	924	250	750	700	0.53	1.5	47.5	----	----	----	----	250	1.05	*Flexural*
498	B-4-14	SR	H1	No	14	6	7000	2100	4	924	250	750	700	0.53	1.0	52.7	----	----	----	----	234	0.64	*Flexural*
499	B-4-14	SR	H2	No	14	6	7000	2100	4	924	250	750	700	0.53	1.0	51.9	----	----	----	----	231	0.71	*Flexural*
500	B-4-14	SR	H3	No	14	6	7000	2100	4	924	250	750	700	0.53	1.0	47.5	----	----	----	----	219	0.85	*Shear*
501	B-4-20	SR	NO	No	20	4	4500	2100	4	1257	250	500	450	1.12	0.0	41.8	----	----	----	----	211	0.85	*Shear*
502	B-4-20	SR	SF	No	20	4	4500	2100	4	1257	250	500	450	1.12	0.5	46.2	----	----	----	----	280	1.00	*Flexural*
503	B-4-20	SR	SF	No	20	4	4500	2100	4	1257	250	500	450	1.12	1.0	49.8	----	----	----	----	316	1.08	*Flexural*
504	B-4-20	SR	SF	No	20	4	4500	2100	4	1257	250	500	450	1.12	1.5	52.5	----	----	----	----	323	1.05	*Flexural*
505	B-4-20	SR	GF	No	20	4	4500	2100	4	1257	250	500	450	1.12	0.5	45.6	----	----	----	----	249	0.94	*Shear*
506	B-4-20	SR	GF	No	20	4	4500	2100	4	1257	250	500	450	1.12	1.0	47.0	----	----	----	----	261	0.97	*Shear*
507	B-4-20	SR	GF	No	20	4	4500	2100	4	1257	250	500	450	1.12	1.5	47.5	----	----	----	----	282	1.03	*Flexural*
508	B-4-20	SR	H1	No	20	4	4500	2100	4	1257	250	500	450	1.12	1.0	52.7	----	----	----	----	292	0.83	*Flexural*
509	B-4-20	SR	H2	No	20	4	4500	2100	4	1257	250	500	450	1.12	1.0	51.9	----	----	----	----	301	0.87	*Flexural*
510	B-4-20	SR	H3	No	20	4	4500	2100	4	1257	250	500	450	1.12	1.0	47.5	----	----	----	----	290	0.95	*Flexural*
511	B-4-20	SR	NO	No	20	6	7000	2100	4	1885	250	750	700	1.08	0.0	41.8	----	----	----	----	303	0.82	*Flexural*
512	B-4-20	SR	SF	No	20	6	7000	2100	4	1885	250	750	700	1.08	0.5	46.2	----	----	----	----	401	0.87	*Flexural*
513	B-4-20	SR	SF	No	20	6	7000	2100	4	1885	250	750	700	1.08	1.0	49.8	----	----	----	----	433	0.89	*Flexural*
514	B-4-20	SR	SF	No	20	6	7000	2100	4	1885	250	750	700	1.08	1.5	52.5	----	----	----	----	463	0.89	*Flexural*
515	B-4-20	SR	GF	No	20	6	7000	2100	4	1885	250	750	700	1.08	0.5	45.6	----	----	----	----	363	0.86	*Shear*
516	B-4-20	SR	GF	No	20	6	7000	2100	4	1885	250	750	700	1.08	1.0	47.0	----	----	----	----	381	0.88	*Shear*
517	B-4-20	SR	GF	No	20	6	7000	2100	4	1885	250	750	700	1.08	1.5	47.5	----	----	----	----	405	0.93	*Shear*
518	B-4-20	SR	H1	No	20	6	7000	2100	4	1885	250	750	700	1.08	1.0	52.7	----	----	----	----	418	0.72	*Shear*
519	B-4-20	SR	H2	No	20	6	7000	2100	4	1885	250	750	700	1.08	1.0	51.9	----	----	----	----	419	0.76	*Shear*
520	B-4-20	SR	H3	No	20	6	7000	2100	4	1885	250	750	700	1.08	1.0	47.5	----	----	----	----	404	0.82	*Shear*
521	B-4-28	SR	NO	No	28	4	4500	2100	4	2463	250	500	450	2.19	0.0	41.8	----	----	----	----	284	0.60	*Shear*
522	B-4-28	SR	SF	No	28	4	4500	2100	4	2463	250	500	450	2.19	0.5	46.2	----	----	----	----	406	0.78	*Shear*
523	B-4-28	SR	SF	No	28	4	4500	2100	4	2463	250	500	450	2.19	1.0	49.8	----	----	----	----	551	1.04	*Flexural*
524	B-4-28	SR	SF	No	28	4	4500	2100	4	2463	250	500	450	2.19	1.5	52.5	----	----	----	----	577	1.06	*Flexural*
525	B-4-28	SR	GF	No	28	4	4500	2100	4	2463	250	500	450	2.19	0.5	45.6	----	----	----	----	343	0.68	*Shear*
526	B-4-28	SR	GF	No	28	4	4500	2100	4	2463	250	500	450	2.19	1.0	47.0	----	----	----	----	387	0.76	*Shear*
527	B-4-28	SR	GF	No	28	4	4500	2100	4	2463	250	500	450	2.19	1.5	47.5	----	----	----	----	453	0.89	*Shear*
528	B-4-28	SR	H1	No	28	4	4500	2100	4	2463	250	500	450	2.19	1.0	52.7	----	----	----	----	545	0.64	*Flexural*
529	B-4-28	SR	H2	No	28	4	4500	2100	4	2463	250	500	450	2.19	1.0	51.9	----	----	----	----	522	0.72	*Shear*
530	B-4-28	SR	H3	No	28	4	4500	2100	4	2463	250	500	450	2.19	1.0	47.5	----	----	----	----	469	0.85	*Shear*
531	B-4-28	SR	NO	No	28	6	7000	2100	4	3695	250	750	700	2.11	0.0	41.8	----	----	----	----	377	0.53	*Flexural*
532	B-4-28	SR	SF	No	28	6	7000	2100	4	3695	250	750	700	2.11	0.5	46.2	----	----	----	----	520	0.63	*Shear*
533	B-4-28	SR	SF	No	28	6	7000	2100	4	3695	250	750	700	2.11	1.0	49.8	----	----	----	----	797	0.93	*Shear*
534	B-4-28	SR	SF	No	28	6	7000	2100	4	3695	250	750	700	2.11	1.5	52.5	----	----	----	----	824	0.93	*Flexural*
535	B-4-28	SR	GF	No	28	6	7000	2100	4	3695	250	750	700	2.11	0.5	45.6	----	----	----	----	505	0.63	*Shear*
536	B-4-28	SR	GF	No	28	6	7000	2100	4	3695	250	750	700	2.11	1.0	47.0	----	----	----	----	571	0.71	*Shear*
537	B-4-28	SR	GF	No	28	6	7000	2100	4	3695	250	750	700	2.11	1.5	47.5	----	----	----	----	658	0.81	*Shear*
538	B-4-28	SR	H1	No	28	6	7000	2100	4	3695	250	750	700	2.11	1.0	52.7	----	----	----	----	773	0.58	*Shear*
539	B-4-28	SR	H2	No	28	6	7000	2100	4	3695	250	750	700	2.11	1.0	51.9	----	----	----	----	758	0.66	*Shear*
540	B-4-28	SR	H3	No	28	6	7000	2100	4	3695	250	750	700	2.11	1.0	47.5	----	----	----	----	609	0.76	*Shear*
541	B-2-14	GFRP	NO	No	14	4	4500	900	2	616	250	500	450	0.55	0.0	41.8	----	----	----	----	242	0.38	*Shear*

542	B-2-14	GFRP	SF	No	14	4	4500	900	2	616	250	500	450	0.55	0.5	46.2	----	----	----	----	433	0.67	*Shear*
543	B-2-14	GFRP	SF	No	14	4	4500	900	2	616	250	500	450	0.55	1.0	49.8	----	----	----	----	554	0.77	*Shear*
544	B-2-14	GFRP	SF	No	14	4	4500	900	2	616	250	500	450	0.55	1.5	52.5	----	----	----	----	560	0.72	*Shear*
545	B-2-14	GFRP	GF	No	14	4	4500	900	2	616	250	500	450	0.55	0.5	45.6	----	----	----	----	294	0.47	*Shear*
546	B-2-14	GFRP	GF	No	14	4	4500	900	2	616	250	500	450	0.55	1.0	47.0	----	----	----	----	341	0.45	*Shear*
547	B-2-14	GFRP	GF	No	14	4	4500	900	2	616	250	500	450	0.55	1.5	47.5	----	----	----	----	454	0.47	*Shear*
548	B-2-14	GFRP	H1	No	14	4	4500	900	2	616	250	500	450	0.55	1.0	52.7	----	----	----	----	505	0.43	*Shear*
549	B-2-14	GFRP	H2	No	14	4	4500	900	2	616	250	500	450	0.55	1.0	51.9	----	----	----	----	466	0.42	*Shear*
550	B-2-14	GFRP	H3	No	14	4	4500	900	2	616	250	500	450	0.55	1.0	47.5	----	----	----	----	411	0.46	*Shear*
551	B-2-14	GFRP	NO	No	14	6	7000	900	2	924	250	750	700	0.53	0.0	41.8	----	----	----	----	336	0.34	*Shear*
552	B-2-14	GFRP	SF	No	14	6	7000	900	2	924	250	750	700	0.53	0.5	46.2	----	----	----	----	540	0.46	*Shear*
553	B-2-14	GFRP	SF	No	14	6	7000	900	2	924	250	750	700	0.53	1.0	49.8	----	----	----	----	698	0.57	*Shear*
554	B-2-14	GFRP	SF	No	14	6	7000	900	2	924	250	750	700	0.53	1.5	52.5	----	----	----	----	850	0.66	*Shear*
555	B-2-14	GFRP	GF	No	14	6	7000	900	2	924	250	750	700	0.53	0.5	45.6	----	----	----	----	400	0.36	*Shear*
556	B-2-14	GFRP	GF	No	14	6	7000	900	2	924	250	750	700	0.53	1.0	47.0	----	----	----	----	442	0.37	*Shear*
557	B-2-14	GFRP	GF	No	14	6	7000	900	2	924	250	750	700	0.53	1.5	47.5	----	----	----	----	564	0.43	*Shear*
558	B-2-14	GFRP	H1	No	14	6	7000	900	2	924	250	750	700	0.53	1.0	52.7	----	----	----	----	650		*Shear*
559	B-2-14	GFRP	H2	No	14	6	7000	900	2	924	250	750	700	0.53	1.0	51.9	----	----	----	----	631	0.39	*Shear*
560	B-2-14	GFRP	H3	No	14	6	7000	900	2	924	250	750	700	0.53	1.0	47.5	----	----	----	----	560	0.44	*Shear*
561	B-2-20	GFRP	NO	No	20	4	4500	900	2	1257	250	500	450	1.12	0.0	41.8	----	----	----	----	315	0.35	*Shear*
562	B-2-20	GFRP	SF	No	20	4	4500	900	2	1257	250	500	450	1.12	0.5	46.2	----	----	----	----	527	0.58	*Shear*
563	B-2-20	GFRP	SF	No	20	4	4500	900	2	1257	250	500	450	1.12	1.0	49.8	----	----	----	----	707	0.70	*Shear*
564	B-2-20	GFRP	SF	No	20	4	4500	900	2	1257	250	500	450	1.12	1.5	52.5	----	----	----	----	772	0.70	*Shear*
565	B-2-20	GFRP	GF	No	20	4	4500	900	2	1257	250	500	450	1.12	0.5	45.6	----	----	----	----	349	0.59	*Shear*
566	B-2-20	GFRP	GF	No	20	4	4500	900	2	1257	250	500	450	1.12	1.0	47.0	----	----	----	----	405	0.59	*Shear*
567	B-2-20	GFRP	GF	No	20	4	4500	900	2	1257	250	500	450	1.12	1.5	47.5	----	----	----	----	568	0.59	*Shear*
568	B-2-20	GFRP	H1	No	20	4	4500	900	2	1257	250	500	450	1.12	1.0	52.7	----	----	----	----	692	0.55	*Shear*
569	B-2-20	GFRP	H2	No	20	4	4500	900	2	1257	250	500	450	1.12	1.0	51.9	----	----	----	----	648	0.56	*Shear*
570	B-2-20	GFRP	H3	No	20	4	4500	900	2	1257	250	500	450	1.12	1.0	47.5	----	----	----	----	584	0.59	*Shear*
571	B-2-20	GFRP	NO	No	20	6	7000	900	2	1885	250	750	700	1.08	0.0	41.8	----	----	----	----	373	0.26	*Shear*
572	B-2-20	GFRP	SF	No	20	6	7000	900	2	1885	250	750	700	1.08	0.5	46.2	----	----	----	----	657	0.37	*Shear*
573	B-2-20	GFRP	SF	No	20	6	7000	900	2	1885	250	750	700	1.08	1.0	49.8	----	----	----	----	1007	0.51	*Shear*
574	B-2-20	GFRP	SF	No	20	6	7000	900	2	1885	250	750	700	1.08	1.5	52.5	----	----	----	----	1193	0.55	*Shear*
575	B-2-20	GFRP	GF	No	20	6	7000	900	2	1885	250	750	700	1.08	0.5	45.6	----	----	----	----	492	0.37	*Shear*
576	B-2-20	GFRP	GF	No	20	6	7000	900	2	1885	250	750	700	1.08	1.0	47.0	----	----	----	----	566	0.41	*Shear*
577	B-2-20	GFRP	GF	No	20	6	7000	900	2	1885	250	750	700	1.08	1.5	47.5	----	----	----	----	651	0.43	*Shear*
578	B-2-20	GFRP	H1	No	20	6	7000	900	2	1885	250	750	700	1.08	1.0	52.7	----	----	----	----	796	0.32	*Shear*
579	B-2-20	GFRP	H2	No	20	6	7000	900	2	1885	250	750	700	1.08	1.0	51.9	----	----	----	----	762	0.34	*Shear*
580	B-2-20	GFRP	H3	No	20	6	7000	900	2	1885	250	750	700	1.08	1.0	47.5	----	----	----	----	730	0.39	*Shear*
581	B-2-28	GFRP	NO	No	28	4	4500	900	2	2463	250	500	450	2.19	0.0	41.8	----	----	----	----	432	0.34	*Shear*
582	B-2-28	GFRP	SF	No	28	4	4500	900	2	2463	250	500	450	2.19	0.5	46.2	----	----	----	----	654	0.52	*Shear*
583	B-2-28	GFRP	SF	No	28	4	4500	900	2	2463	250	500	450	2.19	1.0	49.8	----	----	----	----	938	0.68	*Shear*
584	B-2-28	GFRP	SF	No	28	4	4500	900	2	2463	250	500	450	2.19	1.5	52.5	----	----	----	----	996	0.66	*Shear*
585	B-2-28	GFRP	GF	No	28	4	4500	900	2	2463	250	500	450	2.19	0.5	45.6	----	----	----	----	436	0.58	*Shear*
586	B-2-28	GFRP	GF	No	28	4	4500	900	2	2463	250	500	450	2.19	1.0	47.0	----	----	----	----	537	0.63	*Shear*
587	B-2-28	GFRP	GF	No	28	4	4500	900	2	2463	250	500	450	2.19	1.5	47.5	----	----	----	----	707	0.70	*Shear*
588	B-2-28	GFRP	H1	No	28	4	4500	900	2	2463	250	500	450	2.19	1.0	52.7	----	----	----	----	835	0.54	*Shear*
589	B-2-28	GFRP	H2	No	28	4	4500	900	2	2463	250	500	450	2.19	1.0	51.9	----	----	----	----	730	0.61	*Shear*
590	B-2-28	GFRP	H3	No	28	4	4500	900	2	2463	250	500	450	2.19	1.0	47.5	----	----	----	----	730	0.71	*Shear*
591	B-2-28	GFRP	NO	No	28	6	7000	900	2	3695	250	750	700	2.11	0.0	41.8	----	----	----	----	483	0.24	*Shear*

592	B-2-28	GFRP	SF	No	28	6	7000	900	2	3695	250	750	700	2.11	0.5	46.2	----	----	----	----	766	0.31	*Shear*
593	B-2-28	GFRP	SF	No	28	6	7000	900	2	3695	250	750	700	2.11	1.0	49.8	----	----	----	----	1127	0.41	*Shear*
594	B-2-28	GFRP	SF	No	28	6	7000	900	2	3695	250	750	700	2.11	1.5	52.5	----	----	----	----	1353	0.46	*Shear*
595	B-2-28	GFRP	GF	No	28	6	7000	900	2	3695	250	750	700	2.11	0.5	45.6	----	----	----	----	610	0.35	*Shear*
596	B-2-28	GFRP	GF	No	28	6	7000	900	2	3695	250	750	700	2.11	1.0	47.0	----	----	----	----	673	0.37	*Shear*
597	B-2-28	GFRP	GF	No	28	6	7000	900	2	3695	250	750	700	2.11	1.5	47.5	----	----	----	----	803	0.40	*Shear*
598	B-2-28	GFRP	H1	No	28	6	7000	900	2	3695	250	750	700	2.11	1.0	52.7	----	----	----	----	927	0.34	*Shear*
599	B-2-28	GFRP	H2	No	28	6	7000	900	2	3695	250	750	700	2.11	1.0	51.9	----	----	----	----	825	0.39	*Shear*
600	B-2-28	GFRP	H3	No	28	6	7000	900	2	3695	250	750	700	2.11	1.0	47.5	----	----	----	----	790	0.42	*Shear*
601	B-3-14	GFRP	NO	No	14	4	4500	1350	3	616	250	500	450	0.55	0.0	41.8	----	----	----	----	141	0.33	*Shear*
602	B-3-14	GFRP	SF	No	14	4	4500	1350	3	616	250	500	450	0.55	0.5	46.2	----	----	----	----	244	0.56	*Shear*
603	B-3-14	GFRP	SF	No	14	4	4500	1350	3	616	250	500	450	0.55	1.0	49.8	----	----	----	----	361	0.75	*Shear*
604	B-3-14	GFRP	SF	No	14	4	4500	1350	3	616	250	500	450	0.55	1.5	52.5	----	----	----	----	391	0.75	*Shear*
605	B-3-14	GFRP	GF	No	14	4	4500	1350	3	616	250	500	450	0.55	0.5	45.6	----	----	----	----	168	0.43	*Shear*
606	B-3-14	GFRP	GF	No	14	4	4500	1350	3	616	250	500	450	0.55	1.0	47.0	----	----	----	----	188	0.47	*Shear*
607	B-3-14	GFRP	GF	No	14	4	4500	1350	3	616	250	500	450	0.55	1.5	47.5	----	----	----	----	208	0.51	*Shear*
608	B-3-14	GFRP	H1	No	14	4	4500	1350	3	616	250	500	450	0.55	1.0	52.7	----	----	----	----	298	0.39	*Shear*
609	B-3-14	GFRP	H2	No	14	4	4500	1350	3	616	250	500	450	0.55	1.0	51.9	----	----	----	----	277	0.45	*Shear*
610	B-3-14	GFRP	H3	No	14	4	4500	1350	3	616	250	500	450	0.55	1.0	47.5	----	----	----	----	300	0.51	*Shear*
611	B-3-14	GFRP	NO	No	14	6	7000	1350	3	924	250	750	700	0.53	0.0	41.8	----	----	----	----	171	0.26	*Shear*
612	B-3-14	GFRP	SF	No	14	6	7000	1350	3	924	250	750	700	0.53	0.5	46.2	----	----	----	----	284	0.36	*Shear*
613	B-3-14	GFRP	SF	No	14	6	7000	1350	3	924	250	750	700	0.53	1.0	49.8	----	----	----	----	408	0.50	*Shear*
614	B-3-14	GFRP	SF	No	14	6	7000	1350	3	924	250	750	700	0.53	1.5	52.5	----	----	----	----	488	0.57	*Shear*
615	B-3-14	GFRP	GF	No	14	6	7000	1350	3	924	250	750	700	0.53	0.5	45.6	----	----	----	----	189	0.35	*Shear*
616	B-3-14	GFRP	GF	No	14	6	7000	1350	3	924	250	750	700	0.53	1.0	47.0	----	----	----	----	222	0.38	*Shear*
617	B-3-14	GFRP	GF	No	14	6	7000	1350	3	924	250	750	700	0.53	1.5	47.5	----	----	----	----	275	0.42	*Shear*
618	B-3-14	GFRP	H1	No	14	6	7000	1350	3	924	250	750	700	0.53	1.0	52.7	----	----	----	----	339	0.32	*Shear*
619	B-3-14	GFRP	H2	No	14	6	7000	1350	3	924	250	750	700	0.53	1.0	51.9	----	----	----	----	340	0.36	*Shear*
620	B-3-14	GFRP	H3	No	14	6	7000	1350	3	924	250	750	700	0.53	1.0	47.5	----	----	----	----	288	0.40	*Shear*
621	B-3-20	GFRP	NO	No	20	4	4500	1350	3	1257	250	500	450	1.12	0.0	41.8	----	----	----	----	195	0.32	*Shear*
622	B-3-20	GFRP	SF	No	20	4	4500	1350	3	1257	250	500	450	1.12	0.5	46.2	----	----	----	----	301	0.50	*Shear*
623	B-3-20	GFRP	SF	No	20	4	4500	1350	3	1257	250	500	450	1.12	1.0	49.8	----	----	----	----	415	0.62	*Shear*
624	B-3-20	GFRP	SF	No	20	4	4500	1350	3	1257	250	500	450	1.12	1.5	52.5	----	----	----	----	421	0.57	*Shear*
625	B-3-20	GFRP	GF	No	20	4	4500	1350	3	1257	250	500	450	1.12	0.5	45.6	----	----	----	----	204	0.53	*Shear*
626	B-3-20	GFRP	GF	No	20	4	4500	1350	3	1257	250	500	450	1.12	1.0	47.0	----	----	----	----	243	0.58	*Shear*
627	B-3-20	GFRP	GF	No	20	4	4500	1350	3	1257	250	500	450	1.12	1.5	47.5	----	----	----	----	295	0.59	*Shear*
628	B-3-20	GFRP	H1	No	20	4	4500	1350	3	1257	250	500	450	1.12	1.0	52.7	----	----	----	----	397	0.49	*Shear*
629	B-3-20	GFRP	H2	No	20	4	4500	1350	3	1257	250	500	450	1.12	1.0	51.9	----	----	----	----	381	0.56	*Shear*
630	B-3-20	GFRP	H3	No	20	4	4500	1350	3	1257	250	500	450	1.12	1.0	47.5	----	----	----	----	413	0.59	*Shear*
631	B-3-20	GFRP	NO	No	20	6	7000	1350	3	1885	250	750	700	1.08	0.0	41.8	----	----	----	----	246	0.21	*Shear*
632	B-3-20	GFRP	SF	No	20	6	7000	1350	3	1885	250	750	700	1.08	0.5	46.2	----	----	----	----	373	0.31	*Shear*
633	B-3-20	GFRP	SF	No	20	6	7000	1350	3	1885	250	750	700	1.08	1.0	49.8	----	----	----	----	582	0.44	*Shear*
634	B-3-20	GFRP	SF	No	20	6	7000	1350	3	1885	250	750	700	1.08	1.5	52.5	----	----	----	----	669	0.46	*Shear*
635	B-3-20	GFRP	GF	No	20	6	7000	1350	3	1885	250	750	700	1.08	0.5	45.6	----	----	----	----	246	0.38	*Shear*
636	B-3-20	GFRP	GF	No	20	6	7000	1350	3	1885	250	750	700	1.08	1.0	47.0	----	----	----	----	280	0.40	*Shear*
637	B-3-20	GFRP	GF	No	20	6	7000	1350	3	1885	250	750	700	1.08	1.5	47.5	----	----	----	----	344	0.42	*Shear*
638	B-3-20	GFRP	H1	No	20	6	7000	1350	3	1885	250	750	700	1.08	1.0	52.7	----	----	----	----	518	0.31	*Shear*
639	B-3-20	GFRP	H2	No	20	6	7000	1350	3	1885	250	750	700	1.08	1.0	51.9	----	----	----	----	480	0.34	*Shear*
640	B-3-20	GFRP	H3	No	20	6	7000	1350	3	1885	250	750	700	1.08	1.0	47.5	----	----	----	----	412	0.38	*Shear*
641	B-3-28	GFRP	NO	No	28	4	4500	1350	3	2463	250	500	450	2.19	0.0	41.8	----	----	----	----	250	0.29	*Shear*

642	B-3-28	GFRP	SF	No	28	4	4500	1350	3	2463	250	500	450	2.19	0.5	46.2	----	----	----	----	369	0.44	*Shear*
643	B-3-28	GFRP	SF	No	28	4	4500	1350	3	2463	250	500	450	2.19	1.0	49.8	----	----	----	----	640	0.70	*Shear*
644	B-3-28	GFRP	SF	No	28	4	4500	1350	3	2463	250	500	450	2.19	1.5	52.5	----	----	----	----	697	0.69	*Shear*
645	B-3-28	GFRP	GF	No	28	4	4500	1350	3	2463	250	500	450	2.19	0.5	45.6	----	----	----	----	262	0.51	*Shear*
646	B-3-28	GFRP	GF	No	28	4	4500	1350	3	2463	250	500	450	2.19	1.0	47.0	----	----	----	----	323	0.55	*Shear*
647	B-3-28	GFRP	GF	No	28	4	4500	1350	3	2463	250	500	450	2.19	1.5	47.5	----	----	----	----	368	0.64	*Shear*
648	B-3-28	GFRP	H1	No	28	4	4500	1350	3	2463	250	500	450	2.19	1.0	52.7	----	----	----	----	512	0.47	*Shear*
649	B-3-28	GFRP	H2	No	28	4	4500	1350	3	2463	250	500	450	2.19	1.0	51.9	----	----	----	----	469	0.53	*Shear*
650	B-3-28	GFRP	H3	No	28	4	4500	1350	3	2463	250	500	450	2.19	1.0	47.5	----	----	----	----	550	0.64	*Shear*
651	B-3-28	GFRP	NO	No	28	6	7000	1350	3	3695	250	750	700	2.11	0.0	41.8	----	----	----	----	298	0.22	*Shear*
652	B-3-28	GFRP	SF	No	28	6	7000	1350	3	3695	250	750	700	2.11	0.5	46.2	----	----	----	----	488	0.30	*Shear*
653	B-3-28	GFRP	SF	No	28	6	7000	1350	3	3695	250	750	700	2.11	1.0	49.8	----	----	----	----	765	0.42	*Shear*
654	B-3-28	GFRP	SF	No	28	6	7000	1350	3	3695	250	750	700	2.11	1.5	52.5	----	----	----	----	923	0.47	*Shear*
655	B-3-28	GFRP	GF	No	28	6	7000	1350	3	3695	250	750	700	2.11	0.5	45.6	----	----	----	----	329	0.37	*Shear*
656	B-3-28	GFRP	GF	No	28	6	7000	1350	3	3695	250	750	700	2.11	1.0	47.0	----	----	----	----	374	0.40	*Shear*
657	B-3-28	GFRP	GF	No	28	6	7000	1350	3	3695	250	750	700	2.11	1.5	47.5	----	----	----	----	452	0.45	*Shear*
658	B-3-28	GFRP	H1	No	28	6	7000	1350	3	3695	250	750	700	2.11	1.0	52.7	----	----	----	----	656	0.35	*Shear*
659	B-3-28	GFRP	H2	No	28	6	7000	1350	3	3695	250	750	700	2.11	1.0	51.9	----	----	----	----	608	0.38	*Shear*
660	B-3-28	GFRP	H3	No	28	6	7000	1350	3	3695	250	750	700	2.11	1.0	47.5	----	----	----	----	502	0.42	*Shear*
661	B-4-14	GFRP	NO	No	14	4	4500	2100	4	616	250	500	450	0.55	0.0	41.8	----	----	----	----	103	0.32	*Shear*
662	B-4-14	GFRP	SF	No	14	4	4500	2100	4	616	250	500	450	0.55	0.5	46.2	----	----	----	----	208	0.64	*Shear*
663	B-4-14	GFRP	SF	No	14	4	4500	2100	4	616	250	500	450	0.55	1.0	49.8	----	----	----	----	293	0.81	*Shear*
664	B-4-14	GFRP	SF	No	14	4	4500	2100	4	616	250	500	450	0.55	1.5	52.5	----	----	----	----	296	0.76	*Shear*
665	B-4-14	GFRP	GF	No	14	4	4500	2100	4	616	250	500	450	0.55	0.5	45.6	----	----	----	----	117	0.44	*Shear*
666	B-4-14	GFRP	GF	No	14	4	4500	2100	4	616	250	500	450	0.55	1.0	47.0	----	----	----	----	131	0.46	*Shear*
667	B-4-14	GFRP	GF	No	14	4	4500	2100	4	616	250	500	450	0.55	1.5	47.5	----	----	----	----	163	0.50	*Shear*
668	B-4-14	GFRP	H1	No	14	4	4500	2100	4	616	250	500	450	0.55	1.0	52.7	----	----	----	----	248	0.40	*Shear*
669	B-4-14	GFRP	H2	No	14	4	4500	2100	4	616	250	500	450	0.55	1.0	51.9	----	----	----	----	228	0.44	*Shear*
670	B-4-14	GFRP	H3	No	14	4	4500	2100	4	616	250	500	450	0.55	1.0	47.5	----	----	----	----	221	0.50	*Shear*
671	B-4-14	GFRP	NO	No	14	6	7000	2100	4	924	250	750	700	0.53	0.0	41.8	----	----	----	----	122	0.25	*Shear*
672	B-4-14	GFRP	SF	No	14	6	7000	2100	4	924	250	750	700	0.53	0.5	46.2	----	----	----	----	244	0.42	*Shear*
673	B-4-14	GFRP	SF	No	14	6	7000	2100	4	924	250	750	700	0.53	1.0	49.8	----	----	----	----	345	0.56	*Shear*
674	B-4-14	GFRP	SF	No	14	6	7000	2100	4	924	250	750	700	0.53	1.5	52.5	----	----	----	----	391	0.61	*Shear*
675	B-4-14	GFRP	GF	No	14	6	7000	2100	4	924	250	750	700	0.53	0.5	45.6	----	----	----	----	145	0.36	*Shear*
676	B-4-14	GFRP	GF	No	14	6	7000	2100	4	924	250	750	700	0.53	1.0	47.0	----	----	----	----	181	0.38	*Shear*
677	B-4-14	GFRP	GF	No	14	6	7000	2100	4	924	250	750	700	0.53	1.5	47.5	----	----	----	----	223	0.44	*Shear*
678	B-4-14	GFRP	H1	No	14	6	7000	2100	4	924	250	750	700	0.53	1.0	52.7	----	----	----	----	303	0.34	*Shear*
679	B-4-14	GFRP	H2	No	14	6	7000	2100	4	924	250	750	700	0.53	1.0	51.9	----	----	----	----	272	0.39	*Shear*
680	B-4-14	GFRP	H3	No	14	6	7000	2100	4	924	250	750	700	0.53	1.0	47.5	----	----	----	----	261	0.45	*Shear*
681	B-4-20	GFRP	NO	No	20	4	4500	2100	4	1257	250	500	450	1.12	0.0	41.8	----	----	----	----	154	0.34	*Shear*
682	B-4-20	GFRP	SF	No	20	4	4500	2100	4	1257	250	500	450	1.12	0.5	46.2	----	----	----	----	280	0.62	*Shear*
683	B-4-20	GFRP	SF	No	20	4	4500	2100	4	1257	250	500	450	1.12	1.0	49.8	----	----	----	----	428	0.85	*Shear*
684	B-4-20	GFRP	SF	No	20	4	4500	2100	4	1257	250	500	450	1.12	1.5	52.5	----	----	----	----	476	0.87	*Shear*
685	B-4-20	GFRP	GF	No	20	4	4500	2100	4	1257	250	500	450	1.12	0.5	45.6	----	----	----	----	162	0.56	*Shear*
686	B-4-20	GFRP	GF	No	20	4	4500	2100	4	1257	250	500	450	1.12	1.0	47.0	----	----	----	----	186	0.56	*Shear*
687	B-4-20	GFRP	GF	No	20	4	4500	2100	4	1257	250	500	450	1.12	1.5	47.5	----	----	----	----	221	0.58	*Shear*
688	B-4-20	GFRP	H1	No	20	4	4500	2100	4	1257	250	500	450	1.12	1.0	52.7	----	----	----	----	335	0.52	*Shear*
689	B-4-20	GFRP	H2	No	20	4	4500	2100	4	1257	250	500	450	1.12	1.0	51.9	----	----	----	----	301	0.54	*Shear*
690	B-4-20	GFRP	H3	No	20	4	4500	2100	4	1257	250	500	450	1.12	1.0	47.5	----	----	----	----	313	0.58	*Shear*
691	B-4-20	GFRP	NO	No	20	6	7000	2100	4	1885	250	750	700	1.08	0.0	41.8	----	----	----	----	205	0.29	*Shear*

692	B-4-20	GFRP	SF	No	20	6	7000	2100	4	1885	250	750	700	1.08	0.5	46.2	----	----	----	----	327	0.36	*Shear*
693	B-4-20	GFRP	SF	No	20	6	7000	2100	4	1885	250	750	700	1.08	1.0	49.8	----	----	----	----	543	0.55	*Shear*
694	B-4-20	GFRP	SF	No	20	6	7000	2100	4	1885	250	750	700	1.08	1.5	52.5	----	----	----	----	603	0.56	*Shear*
695	B-4-20	GFRP	GF	No	20	6	7000	2100	4	1885	250	750	700	1.08	0.5	45.6	----	----	----	----	216	0.42	*Shear*
696	B-4-20	GFRP	GF	No	20	6	7000	2100	4	1885	250	750	700	1.08	1.0	47.0	----	----	----	----	247	0.41	*Shear*
697	B-4-20	GFRP	GF	No	20	6	7000	2100	4	1885	250	750	700	1.08	1.5	47.5	----	----	----	----	320	0.42	*Shear*
698	B-4-20	GFRP	H1	No	20	6	7000	2100	4	1885	250	750	700	1.08	1.0	52.7	----	----	----	----	433	0.31	*Shear*
699	B-4-20	GFRP	H2	No	20	6	7000	2100	4	1885	250	750	700	1.08	1.0	51.9	----	----	----	----	404	0.34	*Shear*
700	B-4-20	GFRP	H3	No	20	6	7000	2100	4	1885	250	750	700	1.08	1.0	47.5	----	----	----	----	386	0.40	*Shear*
701	B-4-28	GFRP	NO	No	28	4	4500	2100	4	2463	250	500	450	2.19	0.0	41.8	----	----	----	----	198	0.31	*Shear*
702	B-4-28	GFRP	SF	No	28	4	4500	2100	4	2463	250	500	450	2.19	0.5	46.2	----	----	----	----	315	0.51	*Shear*
703	B-4-28	GFRP	SF	No	28	4	4500	2100	4	2463	250	500	450	2.19	1.0	49.8	----	----	----	----	539	0.78	*Shear*
704	B-4-28	GFRP	SF	No	28	4	4500	2100	4	2463	250	500	450	2.19	1.5	52.5	----	----	----	----	629	0.83	*Shear*
705	B-4-28	GFRP	GF	No	28	4	4500	2100	4	2463	250	500	450	2.19	0.5	45.6	----	----	----	----	213	0.56	*Shear*
706	B-4-28	GFRP	GF	No	28	4	4500	2100	4	2463	250	500	450	2.19	1.0	47.0	----	----	----	----	234	0.61	*Shear*
707	B-4-28	GFRP	GF	No	28	4	4500	2100	4	2463	250	500	450	2.19	1.5	47.5	----	----	----	----	290	0.68	*Shear*
708	B-4-28	GFRP	H1	No	28	4	4500	2100	4	2463	250	500	450	2.19	1.0	52.7	----	----	----	----	434	0.52	*Shear*
709	B-4-28	GFRP	H2	No	28	4	4500	2100	4	2463	250	500	450	2.19	1.0	51.9	----	----	----	----	412	0.58	*Shear*
710	B-4-28	GFRP	H3	No	28	4	4500	2100	4	2463	250	500	450	2.19	1.0	47.5	----	----	----	----	369	0.69	*Shear*
711	B-4-28	GFRP	NO	No	28	6	7000	2100	4	3695	250	750	700	2.11	0.0	41.8	----	----	----	----	270	0.27	*Shear*
712	B-4-28	GFRP	SF	No	28	6	7000	2100	4	3695	250	750	700	2.11	0.5	46.2	----	----	----	----	444	0.36	*Shear*
713	B-4-28	GFRP	SF	No	28	6	7000	2100	4	3695	250	750	700	2.11	1.0	49.8	----	----	----	----	739	0.54	*Shear*
714	B-4-28	GFRP	SF	No	28	6	7000	2100	4	3695	250	750	700	2.11	1.5	52.5	----	----	----	----	829	0.56	*Shear*
715	B-4-28	GFRP	GF	No	28	6	7000	2100	4	3695	250	750	700	2.11	0.5	45.6	----	----	----	----	294	0.42	*Shear*
716	B-4-28	GFRP	GF	No	28	6	7000	2100	4	3695	250	750	700	2.11	1.0	47.0	----	----	----	----	346	0.45	*Shear*
717	B-4-28	GFRP	GF	No	28	6	7000	2100	4	3695	250	750	700	2.11	1.5	47.5	----	----	----	----	389	0.50	*Shear*
718	B-4-28	GFRP	H1	No	28	6	7000	2100	4	3695	250	750	700	2.11	1.0	52.7	----	----	----	----	604	0.38	*Shear*
719	B-4-28	GFRP	H2	No	28	6	7000	2100	4	3695	250	750	700	2.11	1.0	51.9	----	----	----	----	558	0.40	*Shear*
720	B-4-28	GFRP	H3	No	28	6	7000	2100	4	3695	250	750	700	2.11	1.0	47.5	----	----	----	----	483	0.42	*Shear*